DIPEPTIDES AS POTENTIAL ANTI-INFLAMMATORY DRUGS FOR RHEUMATOID ARTHRITIS

A thesis submitted to the

UNIVERSITY OF CAPE TOWN

In fulfillment of the requirements for the degree of

DOCTOR OF PHILOSOPHY

By

'MAMOHALE MOHAJANE

MSc (University of Cape Town)

Supervisor: Prof. Graham E. Jackson

DEPARTMENT OF CHEMISTRY

UNIVERSITY OF CAPE TOWN

RONDEBOSCH 7701

CAPE TOWN

SOUTH AFRICA

JUNE 2013

In loving memory of my mother 'Mantholeng Mohajane

(15 May 1959 - 04 January 2013)

DECLARATION

I, 'Mamohale Mohajane, declare that **Dipeptides as potential anti-inflammatory drugs for rheumatoid arthritis** is my own unaided work both in concept and execution, and that all sources that I have used and quoted have been indicated and acknowledged by means of complete and clear references. This thesis is submitted for the Doctor of Philosophy (PhD) degree, to the Department of Chemistry, Faculty of Science, University of Cape Town, it has not been submitted before for any degree or any examination at the University of Cape Town or any other university.

Signed by candidate

'Mamohale Mohajane

June 2013

ACKNOWLEDGEMENTS

- My supervisor Professor Graham Jackson for guidance and support throughout the research,
- My colleagues in the research group for their contribution and discussion,
- Members of staff and fellow students in the Department of Chemistry UCT for the contributions, seminars, symposia and conferences,
- Mr. Hesselink Gerald and Mr. Peter de Cork for technical support,
- Mr. Hendricks Noel and Peter Roberts for running the NMR experiments,
- Stephanie Snoek and co-workers in the Department of Chemical Engineering UCT (analytical group) for running the AAS experiments, and
- My family for moral and financial support

CONFERENCES AND PROCEEDINGS

Part of the results was presented in the following conferences and symposia;

- Inorganic Symposium; October 2008 at Business School, University of Cape Town; *Design and synthesis of the ligand; protonation and complexation of glycine with Cu(II)*
- South African Chemical Institute Conference; November/December 2008 at main Campus Stellenbosch University; *Protonation of glycyl-L-histidine, complexes of glycyl-L-histidine with Cu(II), Ni(II) and Zn (II)*
- Inorganic 2009 Conference; September 2009 at University of the Free State; *Development of copper based anti-inflammatory drugs, histidine derivatives.*
- South African Chemical Institute Conference; January 2011 at Wits University; *Dipeptides as potential anti-inflammatory drugs for rheumatoid arthritis.*

ABSTRACT

The H^+ and Cu^{2+} equilibria of four glycine peptides (glycyl-glycine, glycyl-L-leucine, glycyl-L-phenylalanine and glycyl-L-histidine) and four sarcosine peptides (sarcosyl-glycine, sarcosyl-L-leucine, sarcosyl-L-phenylalanine and sarcosyl-L-histidine) have been studied using glass electrode potentiometry and isothermal titration calorimetry at 25 ^{0}C and an ionic strength 0.15 M (NaCl). The terminal amine of the sarcosine peptides is more basic than the glycine analogues. The methyl group on the terminal amine (for sarcosine peptides) does not affect the stability constants of the ML species, significantly. Log K for ML species for all the Cu(II)/peptides complexes ranged between 5.79 and 6.54, except for glycyl-L-histidine that showed log K_{ML} = 9.16. Heat accompanying the formation of ML for all the species ranged between -5.1 kcal mol^{-1} and -6.6 kcal mol^{-1}, except for glycyl-L-histidine that showed ΔH_{ML} = -3.6 kcal.mol^{-1}.

Structures for the different species in solution were postulated based on nuclear magnetic resonance and ultraviolet-visible spectrophotometry data. Molecular mechanics was used to investigate the possible structures. The minimum energy of the *trans* form of most the complexes was less than the *cis* form of the complexes.

Octanol/water partition coefficients (log P_{ow}) were determined as a measure of the tissue permeability of the complexes. All the log P_{ow} values were negative indicating that the complexes would be poorly absorbed through the skin. A computer model of blood plasma (ECCLES) was used to assess the speciation *in vivo* of the copper complexes. Glycyl-L-phenylalanine had the highest mobilization of Cu(II), with a log (p.m.i) of 4.44 at a pL of 0.13.

LIST OF ABBREVIATIONS AND SYMBOLS

RA	- Rheumatoid arthritis
RF	- Rheumatoid factor
SLE	- Systematic lupus erythematosus
Anti-CCP	- Anticitrullinated cyclic protein
NSAIDs	- Non-steroidal anti-inflammatory drugs
COX	- Cyclooxygenase
DMARD	- Disease modifying anti-rheumatic drugs
SOD	- Superoxide dismutase
HSA	- Human serum albumin
GLY	- Glycine
SAR	- Sarcosine
GLY-GLY	- Glycyl-glycine
SAR-GLY	- Sarcosyl-glycine
GLY-LEU	- Glycyl-leucine
SAR-LEU	- Sarcosyl-leucine
GLY-PHE	- Glycyl-L-phenylalanine
SAR-PHE	- Sarcosyl-L-phenylalanine
GLY-HIS	- Glycyl-L-histidine
SAR-HIS	- Sarcosyl-L-histidine
EDTA	- ethylenediaminetetraacetic acid
ESTA	- Equilibrium Simulations for Titration Analysis
Log β	- Logarithm (to base 10) of the cumulative equilibrium constants
Log K	- Logarithm (to base 10) of the equilibrium constants
Z_H-bar	- The protonation function
Z_M-bar	- The metal formation function
Q_M-bar	- The deprotonation function
n-bar	- The formation function
σ	- Standard deviation

R^H	- The Hamiltonian R- factor
R^H_{lim}	- R_{lim} is the Hamiltonian R-limit
nT	- Number of titrations
nP	- Number of titration points
ITC	-Isothermal titration calorimetry
T	- Temperature
N	- Number of binding sides on the ligand
K	- Equilibrium constant
ΔH	- Enthalpy change
ΔS	- Entropy change
ΔG	- Gibb's free energy change
UV-Vis	- Ultraviolet-Visible
NMR	- nuclear magnetic resonance
ECCLES	- Evaluation of Constituent Concentrations in Large Equilibrium Systems
UFF	- Universal force field
U_{tot}	-Total strain energy
U_b	- The total bond deformation strain
U_s	- The total steric strain/van der Waals strain (U_s)
U_a	- The angle strain
U_t	- The torsional strain
D_{ow}	-Distribution coefficient
P_{ow}	-Partition coefficeint
p.m.i	- Plasma mobilizing indices

LIST OF FIGURES

LIST OF TABLES

TABLE OF CONTENTS

1. RHEUMATOID ARTHRITIS

1.1 INTRODUCTION

Rheumatoid arthritis (RA) is an autoimmune disease that causes systematic and chronic inflammation of the joints and other parts of the body [1, 9, 14-16]. RA is progressive disease. At an early stage, the body produces an antibody that attacks healthy body tissues resulting in excessive production of cytokines [14-18]. These cytokines cause changes in the synovial membrane, as a result the body produces excessive amounts of synovium fluid. Excessive amounts of synovial fluid around the joints can lead to mild loss of functioning and mobility of the joints [14-18]. If this condition is not treated the synovial membrane might swell off and cause the cartilage to wear off. This may cause the synonium fluid to thicken. The thickening of the synovium fluid leads to growth and division of pannus (second stage). This can lead to cartilage and bones being eroded which may cause severe loss of mobility (final stage) [14-18].

Rheumatoid arthritis affects 1 to 3 % of the world population [1]. Early symptoms are common in persons between 30 and 50 years of age [1]. RA affects more women than men, with a ratio of 3:1 women to men reported in 2008 [1].

Morning stiffness, joint pain, swelling and tenderness around the joints, and loss of functioning and mobility of joints are the symptoms of RA [11-13].

The exact cause of rheumatoid arthritis is not yet known. It is however believed that a combination of factors may cause this condition. These include;

1. Genetic susceptibility: human leukocyte antigen (HLA) is believed to increase the progression of RA. Most individuals with HLA-DR1 and HLA-DR4 genes have been reported to be at risk of developing RA [1-3].
2. Hormonal factors: scientists think certain hormones may cause RA. This is due to the fact that RA affects more women than men, and RA may progress after pregnancy [1-3].

3. Environmental factors: some authors believe certain bacteria and virus may cause RA. Other authors [32, 33] believe smoking may trigger rheumatoid arthritis.

The direct connection between these factors and RA has not been completely established. Patients with rheumatoid arthritis have been reported to have elevated amounts serum copper and synovium fluid copper than people who do not have RA [5-8]. It is believed that this is a result of homeostasis. A precise correlation has not been established.

1.2 THERAPY FOR RHEUMATOID ARTHRITIS

There is no cure for RA, however symptoms and progression can be treated. The traditional method is by wearing copper bracelets [4, 19-21]. It is believed that the copper in the bracelets and sweat form chelates that permeate through the skin into the bloodstream where they will be transported to the affected areas [4]. Copper-sweat chelates are less toxic than drugs which, in most cases are associated with side effects. There are limitations. The efficiency of the chelates depends on amount of copper in the bracelet and the rate at with these chelates permeates through the skin [4, 19-21]. Another traditional treatment, but less common, is by wearing stainless steel bracelets with neodymium magnets encapsulated in them. These bracelets do not provide with useful chelates (for treatment of RA) but the magnetic field accelerates the circulation of blood to all parts of the body [22, 23], and thus distributing copper evenly throughout the body.

A copper enriched diet has also been reported to be useful in alleviating RA symptoms. This includes a diet that consists of animal liver, cereals, legumes, crustacean, shell fish, dried fruits, nuts and chocolate [24-26].

Pharmaceutical treatment includes the use of non-steroidal anti-inflammatory drugs (NSAID's), disease modifying anti-rheumatic drugs (DMARD's) and glucocorticoids. Surgical treatment (joint replacement) is done if the joints have been severely deformed (27, 28).

1.2.1 Non-steroidal anti-inflammatory drugs

NSAID's are used to alleviate inflammation and to treat mild to moderate pain. Examples of these are aspirin, ibuprofen and naproxen (chemical structures are given in Figure 1.1). Non-steroidal anti-inflammatory drugs alleviate inflammation and pain by blocking cyclooxygenase (COX) which is an enzyme that is responsible for the production of prostaglandins [34, 35]. Prostaglandins activate inflammation, pain and fever. NSAID's are effective but they are associated with side effects: nausea, loss of appetite, vomiting, diarrhea, constipation, rash, dizziness, drowsiness and headache. They can also cause ulcers, renal impairment, gastrointestinal irritation and sometimes bleeding if used for a long period of time. NSAIDS's do not reduce/stop the progression of the disease [34, 35].

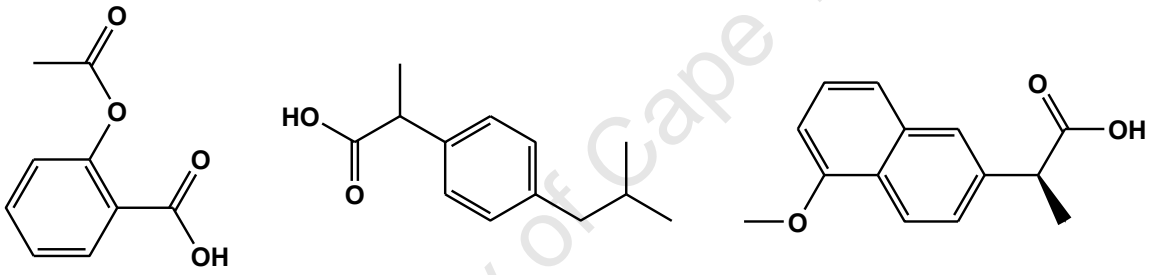

aspirin ibuprofen naproxen

Figure 1.1: Examples of NSAID's (structural representation)

1.2.2 Disease modifying anti-rheumatic drugs

DMARD's reduce the progression of RA and prevent bone damage. [36] Hydroxychloroquinone, methotreane and auranofin are examples of disease modifying anti-rheumatic drugs. The structures of these are given in Figure 1.2. The mechanism through which these drugs work has not been fully established. The use of DMARD's is also associated with some side effects. These include upset stomach, sore and dry mouth, nausea, skin rash. Prolonged usage may lead to gastrointestinal irritation, renal and liver toxicity [36, 37].

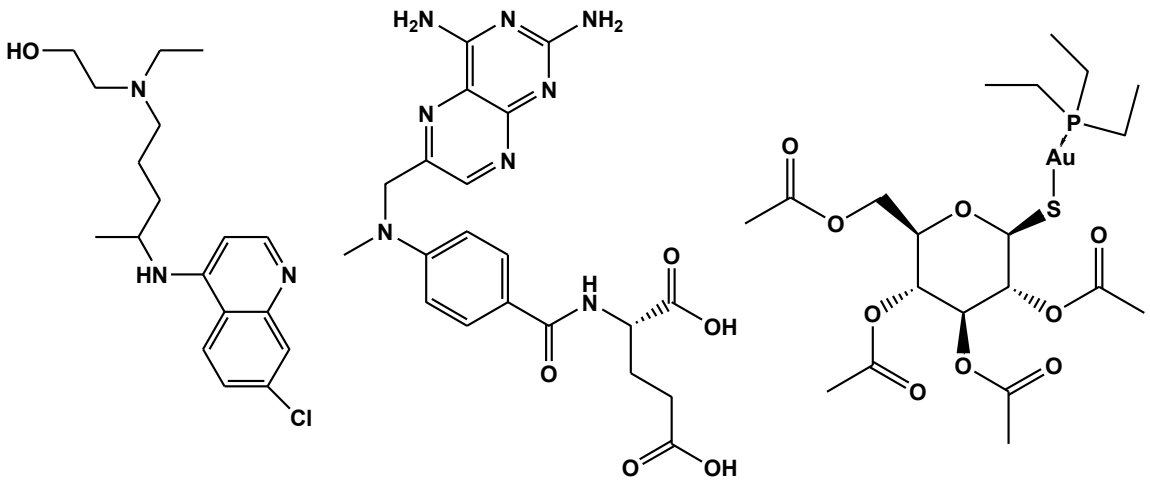

hydroxychloroquinone methotrexate auranofin

Figure 1.2: Examples of DMARD's (structural representation)

1.2.3 Corticosteroids (Glucocorticoids)

These can be taken during the final stage of RA. These drugs suppress inflammation and they have a high potency compared to NSAID's and DMARD's but they can make the immune system to be less resistant to infections [38, 39]. An example of corticosteroids is prednisone. Side effects include a puffy face, a sharp appetite, weight gain, mood swings, water retentions and fractures [38, 39].

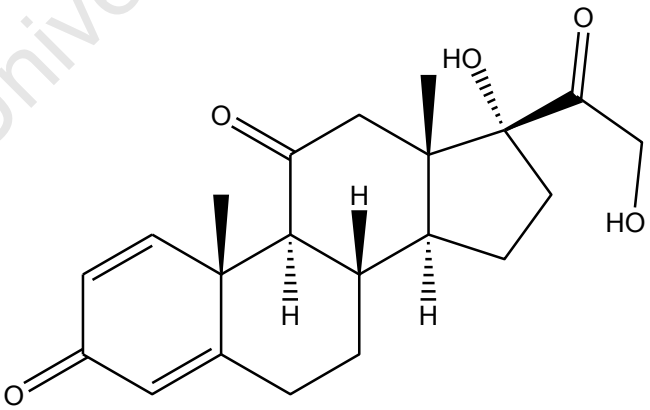

prednisone

Figure 1.3: An examples of corticosteroids (structural representation)

1.3 COPPER AND RHEUMATOID ARTHRITIS

Copper salts and organic salts have been reported to play an important role in reducing inflammation [29-31]. The most common copper salts are copper salicylate and copper aspirinate, A precise mechanism on how this is achieved has not been established however, it is believed that copper may;

1. reduce the production or activity of prostaglandins which stimulate pain and inflammation [9],
2. increase the production or activity of lysyl oxidase. Lysyl oxidase is a copper-containing enzyme that is responsible for the protection of connective in tissues [7].
3. boost the production of histidine which regulates the response of inflammation,
4. increase the production or the activity of superoxide dismutase (SD) which is an enzyme responsible for repairing cells [10],
5. reduce the production or the activity of lysosomes [17-18].

1.4 AIM

The main aim of this study is to alleviate the inflammation associated with RA by developing a dermally absorbable, copper complex that will elevate the bioavailable pool of copper *in vivo*. These ligands should;

1. be more selective for Cu (II) than for other cations found in high concentrations in blood plasma,
2. form thermodynamically stable complexes with Cu (II). These complexes should however be kinetically labile so that the copper is at the biological sites where it is needed,
3. promote dermal absorption as this is the preferred route of administration. Anti-inflammatory drugs that are administered orally are accompanied by side effect. Side effects like ulcers, renal impairment, and gastrointestinal irritation may be avoided if the drugs are administered trans-dermally.

1.5 OBJECTIVES

1. Design new ligands (drugs) that fulfill the aims.
2. Determine the thermodynamic properties of these ligands and their complexes with Cu (II) using;
    a) Glass electrode potentiometry, and
    b) Isothermal titration calorimetry
3. Predict the structures of the complex species using;
    a) UV-Vis spectrophotometry,
    b) ^{1}H NMR, and
    c) Molecular mechanics
4. Determine the lipophilicity/hydrophilicity of the complexes using octanol/water distribution coefficients, and evaluate the ligand *in silica* (via computer simulation) using a computer model of blood plasma.

REFERENCES

[1] Richmond, S. J. *Trials.* **(2008)**; 9(53): 953-960.

[2] Weyand, C. M and Goronzy, J. J. *Arthritis Research and Therapy* **(2011);** 2(3): 231-239.

[3] Kapitány A., et al. *Annals of the New York Academy of Sciences.* **(2005);** 1051: 263-270

[4] Dollwet, H. H. A. and Sorenson, J. R. J. *The Copper Bracelet and Arthritis* **(1985)**; 2(2): 80-87.

[5] Svenson, K. L. G. et al. *Inflammation.* **(1985)**; 9:189-199.

[6] Mahmood, A. and Shukri, M. *Journal of College of Dentistry***. (2012)**; 24(3): 87-92.

[7] Çaglayan, O. and Aydog, Y. S. *Journal of Islamic Academy of Sciences.* **(1997)**; 10(1): 19-24

[8] Lorber, A., Cutler, L. S., and Chang, C. C. *Arthritis and Rheumatism.* **(1969)**; 11(1): 65–071

[9] Katz, J. M., Skinner, S. J. M., Wilson, T. and Grayi, D. H. *Annals of the Rheumatic Disease.* (**1984**); 43, 841-846

[10] Upadhyaya, I., Agrawal, J. K., Dubey G. P. and Udupa, K. N. *European Journal of Endocrinology*. (**1992**); 126(4): 315-318

[11] Pincus, T., Callahan, L. F., Sale, W.G., Brooks, A. L., Payne, L. E., Vaughn, W. *Arthritis and Rheumatism.* **(1984)**; 27:864-72.

[12] Gabriel, S. E. and Crowson CS, O'Fallon, W. M. *.Journal of Rheumatology.* **(1999)**; 26: 2529-2533

[13] Suresh, E. *Journal of Royal Society of Medicine.* **(2004)**; 97(9): 421–424

[14] Scott, I. C., Tan, R., Stahl, D., Steer, S., Lewis, C. M. and Cope, A. P. *Rheumatology*. (**2013**); 52: 856-867

[15] Plantinga, T. S. et al. *Rheumatology.* (**2013**); 52: 806-814

[16] Gaby, A. R. *Alternative Medicine Review*. (**1999**); 4(6): 392-402.

[17] Clarris, B. J., Fraser, J. R., Muirden, K. D., Malcolm, L. P., Holmes, M, W. and Rogers, K. *Annals of the Rheumatic Diseases*. (**1984);** 43(2): 313–319.

[18] Sohar, N., Hammer, H. and Sohar, I. *Journal of Biological Chemistry*. (**2002**): 383(5): 865-9

[19] Cerhan, J. R., et al. *American Journal of Epidemiology*. (**2003**); 157(4): 345-354.

[20] Steven, J., Weiss, M. D., Kevin, M., Takakuwa, M. D. Amy, A. and Ernst, M. D. *Academic Emergency Medicine.* 2001);8(1): 41-47

[21] Walker, W. R. and Keats, D. M. *Agents Actions*. (**1976);** 6(4): 454-459.

[22] Østergaard, M., Hansen, M., Stoltenberg, M., Gideon, P., Klarlund, M., Jensen, K. E. and Lorenzen, I. B. *Arthritis and Rheumatism.* 42(5): (**1999**); 918–929

[23] Quinn, M. A., Conaghan, P. G., O'Connor, P. J. Karim, Z., Greenstein, A., Brown, A., Brown, C., Fraser, A., Jarret, S., and Emery, P. *Arthritis and Rheumatism*. (**2005**); 52(1): 27–35.

[24] Nelson, S. K., Huang, C. J., Mathias, M. M. and Allen, K. G. *Journal of Nutrition*. (**1992**); 122(11): 2101-8.

[25] Willet, W. C. *Science.* **(1994)**; 264: 532–537.

[26] Hafström, I., Ringertz, B., Spångberg, A., von Zweigbergk, L., Brannemark, S., Nylander, I., Rönnelid, I., Laasonen, L. and Klareskog, L. *Rheumatology.* **(2001);** 40(10): 1175-1179.

[27] Morrey, B.F. and Adams, R. A. *Journal of Bone and Joint Surgery.* (**1995**); 77(1): 67-72

[28] Wolfe1,F. and Zwillich, S. H. *Arthritis and Rheumatism*. (**1998**); 41(6): 1072-1082.

[29] Duncan, C. and White, A. R. *Metallomics.* (**2012**);4(2): 127-38

[30] Cooper, G. J. *Drugs*. (**2011)**; 71(10):1281-1320

[31] Paterson, B.M. and Donnelly, P. S. *Journal of Chemical Society.* (**2011**); 40(5): 1460-4744

[32] Baka, Z., Buzás, E. and Nagy, G. *Arthritis Research & Therapy*. (**2009**); 11(4): 238-441

[33] Másdóttir, B., Jónsson, T., Manfreðsdóttir, V., Víkingsson, A., Brekkan, A. and Valdimarsson, H. *Rheumatology.* (**2000**); 39 (11): 1202-1205.

[34] Schnitzer, T. J. *The American Journal of Medicine*. (**1998**);105: 45–52

[35] Bergh, M. S. and Budsberg, S.C. *Journal of Veterinary Internal Medicine*. (**2005**); 19(5): 633–643,

[36] Amrutkar, R. D., Khairnar, P. S. and Bhambar1, R. S. *International Journal of*

Pharmaceutical Research and Development. (**2010**); 2(10): 138-146

[37] Grove, M. L., Hassell, A. B., Hay, E. M. and Shadforth, M. F. An *International Journal of Medicine.* (**2001**); 94 (6): 309-319

[38] Nieminen, S., Rämö, M. P., Viitasalo, M., Heikkilä, P., Karjalainen, J., Mäntysaari, M. and Heikkila, J. *European Heart Journal*. (**1996**); 17(10): 1576-1583.

[39] Stanbury, R. M. and Graham, E. M. *British Journal of Ophthalmology.* (**1998**): 82:704-708

2. LIGAND DESIGN

2.1 INTRODUCTION

The aim of this study was to develop ligands which are able to increase the bio-available pool of copper *in vivo*. The hypothesis being that an increase in this pool of copper would have an anti-inflammatory effect in diseases like rheumatoid arthritis. The design of a drug/ligand depends on a number of factors. It depends on;

1. Knowledge of the biological sites (active sites) of ligands: if the active sites of the ligands are known it is easy to predict whether the ligands and the target molecule (or metal ion) will actually bind. The species that will form when the ligands bind to the target molecule or metal ion, and their stabilities can be predicted based on previous studies.

2. Prediction of stability of drugs (affinity and selectivity to the metal ion of interest): this is necessary in predicting whether the ligands will be effective in transporting the metal ion of interest and whether the ligands are selective for a specific ion or not. It is also important in predicting the dosage. High affinity/highly selective ligands can be effective even with small doses. Selective ligands will not chelate and remove essential metal ions from the blood plasma [5-6]

3. Prediction of the potency /efficacy of the drugs: this factor is important in predicting whether the ligands are capable of producing a biological response once they have binded with the target molecule (or metal ion). This is also important in predicting whether the ligands will transport and deliver the molecules or metal ions of interest to the parts of the body where they are needed.

4. Prediction of the aqueous solubility of drugs: this factor affects the bioavailability of the drug [1]. This is therefore necessary in predicting the route of administration, orally or trans-dermally.

5. Knowledge of the toxicity of drugs and target metabolites. This factor is important limiting the dosage and predicting possible side effects.

2.2 LIGAND SELECTION

In blood plasma, copper is transported by proteins; human serum albumin (HSA) being the most effective protein [10-12]. Cu(II) binding sites of HSA are shown in Figure 2.1. Amine and amide N-donors of HSA are the main transport binding sites for Cu(II). N-donors have been reported to be more selective for Cu(II) than other metal ions found in high concentrations in blood plasma [11-14]. This however, makes complexes of Cu(II) and HSA very stable and thus less bioavailable. A chelate sequence 5, 5, 6 (Cu-NH_2-CH-CO-N; Cu-N-CH-CO-N; Cu-N-CH-CH2-CH rings) is observed for Cu(II)-HSA (Figure 2.1).

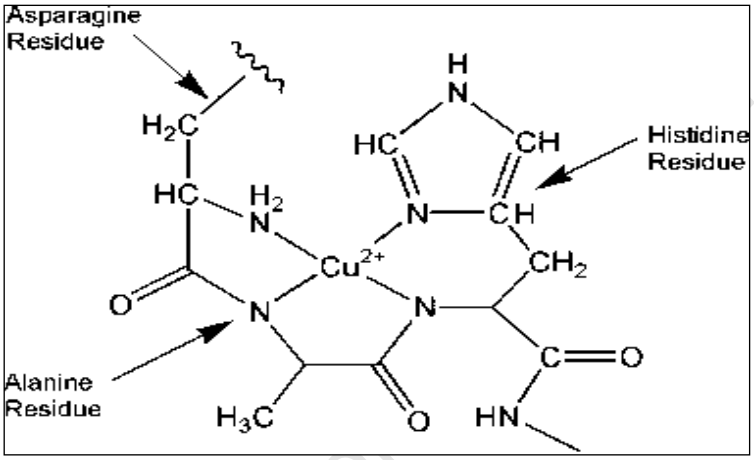

Figure 2.1: Structure of Cu(II)-human serum albumin [18].

The design of the ligands was based on the structure of HSA. The designed ligands each have three active Cu(II) binding sites: an amine N-donor, an amide N-donor and a carboxylate O-donor. Glycyl-L-histidine and sarcosyl-L-histidine each has two additional N-donor atoms on the imidazole ring. The structures of these are given in Figure 2.2. The amine and the amide N-donor groups will make the ligands to be more selective for Cu(II) than for Ca (II), Ni (II) and Zn (II) which are found in high concentrations in blood plasma. Cu(II) complexes of these ligands should be less stable than Cu(II)-HSA complexes and so release the their copper in plasma. Cu-O bond is not as strong as Cu-N [2, 17] and thus complexes formed between these ligands and Cu(II) will not be as strong as the Cu(II)-HSA complexes which has Cu(II) coordinating on four N-donors. This may improve the liability/bioavailability of the complexes of Cu(II) with these ligands.

Two series of ligands have been chosen; glycine dipeptides and sarcosine dipeptides. This was based on the fact that methylated N-terminals of amines are more lipophilic than their

non-methylated analogues [15, 16]. N-methylated peptides are also less susceptible to metabolism [19]. Drugs that will be administered trans-dermally are preferred over drugs that will be administered orally therefore the ligands have to be slightly lipophilic. This however, has to be achieved without compromising the stability of the Cu(II) complexes. Thermodynamic, permeation and solubility properties of complexes of Cu(II) with these two series of ligands are therefore compared. The length of the peptides between the C-terminal and the N-terminal is the same for all the ligands because the length of the chain may also affect the solubility of organic compounds. The group on the α-carbon of the C-terminal may also have an effect not only on the stability of the complexes but also on the solubility of complexes in water and in organic phase.

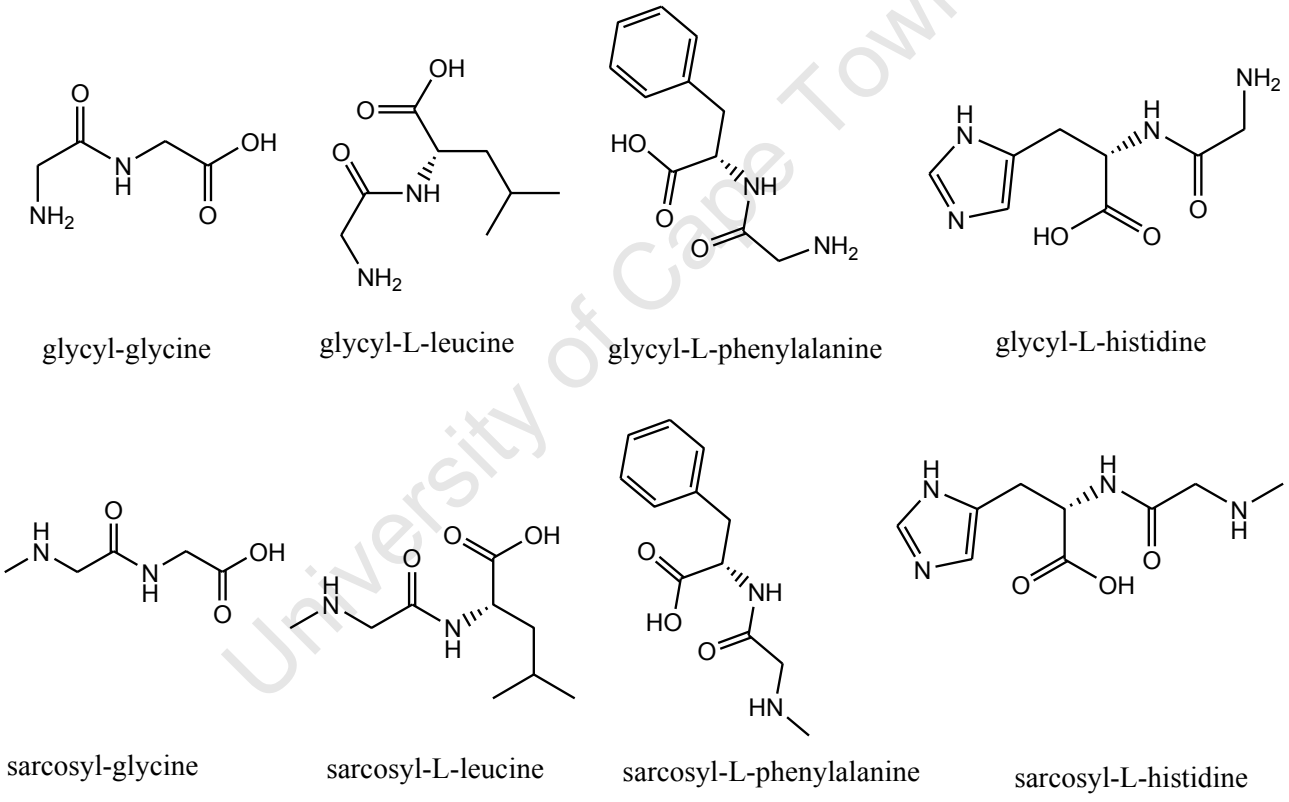

Figure 2.2: Structures of proposed glycine and sarcosine dipeptides

Even though a trans-dermal route of administration is preferred over oral, all experiments are run in water therefore all the ligands have to be soluble in water. Proposed ligands all have two amino acid residues therefore they are generally soluble in water [4, 7-9] and generally have low toxicity [3].

REFERENCES

[1] Jorgensen, W. L. and Duffy, E. M. *Advanced Drug Delivery Reviews.* **(2002)**; 54(3): 355-366

[2] Odisitse, S., Jackson, G. E., Govender, T., Krugerb, G. H. and Singhb, A. *Journal of Chemical Society.* **(2007)**; 1140–1149

[3] Smith, M. E. and Smith, L. B. *The Biological Bulletin.* **(1949)**; 96(3): 233-237

[4] Breil, M. P., Mollerup, J. M., Rudolph, E. S. Ottens, M. and Van der Wielen L. A. M. *Fluid Phase Equilibria.* **(2004)**; 215(2):221-225

[5] Miller, M. J. *Chemical Reviews* **(1989)**; 89(7): 1563-1579

[6] Chouhan, G and James, K. *Organic Letters* **(2011)**; 13(10): 2754-2757

[7] Sheehan, J. C and Hlavka, J. J. *Journal of Organic Chemistry.* **(1956)**; 21(4): 439–441

[8] Mavropoulou, I. P. and Kosikowsk, F. V. *Journal of Dairy Science,* **(1973);** 56(12): 1610-1613

[9] Toniolo, C., Bonora, G. M. and Schaaper, W.M.M. *International Journal of Peptide and Protein Research*. **(1984)**;23(4): 389–393

[10] Goode, C. A., Dinh, C. T. and Linder, M. C. *Copper Bioavailability and Metabolism* **(1990)**; 131-144

[11] Perrone, L., Mothes, E., Vignes, M., Mockel, A., Figueroa, C., Miquel, M. C., Maddelein, M. L., and Faller, P. *European Journal of Chemical Biology*. **(2010)**; 11(1): 110-118

[12] Neumann, P. Z. and Kortsa, -S.A. *Journal of Clinical Investigation*. **(1967)**; 46(4): 646–658.

[15] Uhlmann, T., Geoghegan, V. L., Thomas, B., Ridlova, G., Trudgian, C., and Acuto, O. *American Society for Biochemistry and Molecular Biology* **(2012)**; 12(4): 1489-1499

[16] Andrzejewski, M., Olejniczaka, A. and Katrusiak, A. *Journal of Crystal Engineering Communications*. **(2012)**; 14: 6374-6376

[17] Aliyu, H. N. and Bello, I. *Biokemistri* **(2010)**; 22,(2): 100-104

[18] Zvimba, J. N. and Jackson, G. E. *Polyhedron*. (**2007**); 26(12): 2395-2404.

[19] Biron, E., et al. *Angewandte Chemie. International Edition.* (**2008**); 47: 2595–2599

[20] Ovadia ,O., Greenberg, S., Laufer, B., Gilon, C., Hoffman, A. and Kessler, H. *Drug Discovery*. (**2010**); 5: 655–671

3. GLASS ELECTRODE POTENTIOMETRY

3.1 INTRODUCTION

Potentiometry is a technique used to study chemical interactions of substances in solution [2]. The titration vessel is filled with analyte solutions of known concentration and volume. Standard solutions of the titrant are injected into the titration vessel, and the potential difference between the glass electrode and the reference electrode is measured. These are direct measurements since indicators are not used. The output is therefore not corrected.

Data is reported in millivolts per unit volume of injection. The output basically depends on the concentrations of the analyte solution and the titrant solution. From the output, equilibrium constants of species are calculated. The effect of temperature and ionic strength on equilibrium constants have been reported [4-6]. The titrations are therefore run at a fixed temperature and a fixed ionic strength.

In pH glass electrode potentiometry, the sensor (pH electrode) consists of a reference electrode, a glass electrode and a salt bridge. Each of these components has its own potential. A reference electrode potential (E_{ref}) is the potential of the internal reference solution. It has fixed value and is not affected by the concentration of the analyte solution. This is however affected by temperature and thus has to be determined before running the titrations [36]. The potential of the glass electrode (E_g) depends on the concentration of the analyte solution. The liquid junction potential (E_j) is the difference between the potential of the internal reference solution and the potential of the analyte solution. These components are arranged in this fashion:

reference electrode || salt bridge || analyte solution || glass electrode

The observed potential (E_{cell}) is the sum of all three;

$$E_{cell} = E_{ref} + E_j + E_g \tag{3.1}$$

E_g depends on the activity of H^+ ions ($\{H^+\}$). E_g can be expressed in terms of the standard electrode potential (E^0_g) and the concentration of H^+ ions;

$$E_g = E_g^0 + \frac{RT\ln\{H\}}{F} \tag{3.2}$$

R is the universal gas constant, T is the temperature and F is Faraday's constant. Substituting Equation 3.2 into 3.1 yields;

$$E_{cell} = E_{ref} + E_j + \left(E_g^0 + \frac{RT\ln\{H\}}{F}\right) \tag{3.3}$$

E_g depends on the pH of the analyte solution therefore it depends on the activity of H^+ {H} ions can be expressed as;

$$\{H\} = \Upsilon_H[H] \tag{3.4}$$

Where Υ_H is the activity coefficient and [H] is the concentration of H^+ ions. The charge has been omitted for simplicity.

E_g also depends on the ionic strength (I) of the analyte solution.

$$I = \frac{1}{2}\sum(C_i Z_i)^2 \tag{3.5}$$

Where C_i is the concentration of species i and Z_i is the charge of species i.

If I is constant then Equation 3.3 can be written as;

$$E_{cell} = E_{constant} + \frac{RT\ln[H]}{F} \tag{3.6}$$

R and F are constants. If T is also constant, the slope (s) of the electrode can be expressed as;

$$s = \frac{2.30RT}{F} \tag{3.7}$$

The dependence of potentials on pH (or –log [H]) yields a linear curve. Putting Equation 3.7 into 3.6 yields;

$$E_{cell} = E_{constant} + s \log[H] \tag{3.8}$$

Calibration of the electrode requires the determination of $E_{constant}$ and s.

3.2 THEORY

From the self ionisation of water; $H_2O \rightleftharpoons OH + H$

The charges have been omitted for simplicity,

$$OH = \frac{K_W}{H} \tag{3.9}$$

Where OH is the initial concentration of the hydroxide ions, H is the initial concentration of H^+ ions and K_w is the dissociation constant of water.

For a ligand L being protonated into LH by the reaction; $L + H \rightleftharpoons LH$

The thermodynamic protonation constant for LH, ${}^TK_{LH}$ can be expressed as;

$${}^TK_{LH} = \frac{\{LH\}}{\{L\}\{H\}} \tag{3.10}$$

Where {LH} is the activity of LH, {L} is the activity of L and {H} is the activity of H. The activity of a species X can be expressed in terms of its concentration [12] and the activity coefficient Υ_X as given in Equation 3.11;

$$\{X\} = \Upsilon_X [X] \tag{3.11}$$

Similarly;

$$ {}^{T}K_{LH} = \frac{(\gamma_{LH}\,[LH])}{(\gamma_{L}\,[L])\,(\gamma_{H}\,[H])} \tag{3.12} $$

Equation 3.12 can be rearranged;

$$ {}^{T}K_{LH} = \left(\frac{\gamma_{LH}}{\gamma_{L}\ \gamma_{H}}\right)\left(\frac{[LH]}{[L]\,[H]}\right) \tag{3.13} $$

At constant ionic strength $\left(\frac{\gamma_{LH}}{\gamma_{L}\ \gamma_{H}}\right)$ is constant therefore the concentration binding affinity K_{LH} can be expressed as;

$$ K_{LH} = \frac{[LH]}{[L][H]} \tag{3.14} $$

For a ligand that has two dissociable protons;

$LH + H \rightleftharpoons LH_2$

K_{LH2} can be expressed as;

$$ K_{LH2} = \frac{[LH_2]}{[LH][H]} \tag{3.15} $$

For a ligand that has multiple dissociable protons;

$LH_{n-1} + H \rightleftharpoons LH_n$

K_{LHn} can be expressed as;

$$ K_{LHn} = \frac{[LH_n]}{[LH_{n-1}][H]} \tag{3.16} $$

Cumulative protonation/deprotonation constants (β's) can be expressed as;

$L + H \rightleftharpoons LH$ $\qquad \beta_{LH} = K_{LH} = \frac{[LH]}{[L][H]}$

(3.17)

$LH + H \rightleftharpoons LH_2$ $\qquad \beta_{LH2} = K_{LH} K_{LH2} = \frac{[LH_2]}{[L][H]^2}$

(3.18)

$LH_2 + H \rightleftharpoons LH_3$ $\qquad \beta_{LH3} = K_{LH} K_{LH2} K_{LH3} = \frac{[LH_3]}{[L][H]^3}$

(3.19)

$LH_{n-1} + H \rightleftharpoons LH_n$ $\qquad \beta_{LHn} = K_{LH} K_{LH2} K_{LH3} \ldots K_{LHn} = \frac{[LH_n]}{[LK_{n-1}][H]^n}$

(3.20)

For a metal M and a ligand L forming a complex ML by;

$M + L \rightleftharpoons ML$

The concentration equilibrium constant for ML can be expressed as

$$K_{ML} = \frac{[ML]}{[M][L]}$$

(3.21)

And for;

$ML_{n-1} + L \rightleftharpoons ML_n$

The concentration equilibrium constant can be expressed as;

$$K_{MLn} = \frac{[ML_n]}{[ML_{n-1}][L]}$$

(3.22)

Log K's for other species MLH_{-1}, MLH_{-2} do not have a definite meaning. For a reaction;

$ML \rightleftharpoons MLH_{-1} + H$

$$K_{MLH-1} = \frac{[MLH_{-1}][H]}{[ML]}$$

(3.23)

Log K for more complicated species ML_2H_{-1}, ML_2H_{-2} depend of the pathway of the reaction. There are two (or more) possible routes for the formation of these species. ML_2H_{-1} can be formed by;

$ML_2 \rightleftharpoons ML_2H_{-1} + H$

$$K_{ML2H-1} = \frac{[ML_2H_{-1}][H]}{[ML_2]} \tag{3.24}$$

Or;

$MLH_{-1} + L \rightleftharpoons ML_2H_{-1}$

$$K_{ML2H-1} = \frac{[ML_2H_{-1}]}{[MLH_{-1}][L]} \tag{3.25}$$

Similarly, log K_{ML2H-2} from different routes;

$ML_2 \rightleftharpoons ML_2H_{-2} + 2H$

$MLH_{-2} + L \rightleftharpoons ML_2H_{-2}$

$ML_2H_{-1} \rightleftharpoons ML_2H_{-2} + H$

The stability of these species is therefore better described by the cumulative stability constants, log β's.

Cumulative equilibrium constants can be calculated;

$M + L \rightleftharpoons ML$ $\qquad \beta_{ML} = K_{ML} = \frac{[ML]}{[M][L]}$ (3.26)

$ML + L \rightleftharpoons ML_2$ $\qquad \beta_{ML2} = K_{ML} K_{ML2} = \frac{[ML_2]}{[M][L]^2}$ (3.27)

$ML_2 + L \rightleftharpoons ML_3$ $\qquad \beta_{ML3} = K_{ML} K_{ML2} K_{ML3} = \frac{[ML_3]}{[M][L]^3}$ (3.28)

$ML_{n-1} + L \rightleftharpoons ML_n$ $\qquad \beta_{MLn} = K_{ML} K_{ML2} K_{ML3} \ldots K_{MLn} = \frac{[ML_n]}{[ML_{n-1}][L]^n}$ (3.29)

For the reaction;

$pM + qL + rH \rightleftharpoons M_pL_qH_r$

Where p, q and r are stoichiometric coefficients,

$$\beta_{MpLqHr} = \frac{[M_p\, L_q\, H_r\,]}{[M]^p[L]^q[H]^r} \tag{3.30}$$

3.3 EXPERIMENTAL

3.3.1 Sample preparation

Sodium chloride granules, potassium hydrogen phthalate, and sodium hydroxide and hydrochloric acid ampoules were purchased from Merck. They were of analytical grade and were used without further purification. Glycine, glycyl-glycine, glycyl-L-leucine, glycyl-L-phenylalanine, glycyl-L-histidine and sarcosine were purchased from Sigma-Aldrich. Sarcosyl-glycine, sarcosyl-L-leucine, sarcosyl-L-phenylalanine and sarcosyl-L-histidine were purchased from GL Biochem (Shanghai).

NaOH ampoules were diluted with distilled/de-ionized water as described on the ampoule box. All weighing was done to 5 decimal places on an A&D GH-202 analytical scale balance. NaOH was standardized against standard potassium hydrogen phthalate [28, 29]. HCl ampoules were also diluted with distilled deionised water as described on the ampoule box. HCl solutions were standardized by titration against NaOH and borax, and the end point was determined with the Gran method [3, 18].

Ligand solutions were prepared in standard HCl solutions. Metal ion solutions were prepared and standardized as described [20, 21].

3.3.2 Potentiometric measurements

Ω Metrohm glass electrodes were used to measure the electrode potentials. These potentials were monitored with 848 Titrino plus autotitrator from Ω Metrohm. A double walled titration vessel (with water at 25 ^{0}C circulating between the walls) was used. All titrations were run at 25 ^{0}C and 0.15 M ionic strength (NaCl) in an inert atmosphere of nitrogen. The slope of the glass electrode was calibrated using three pH buffer solutions of different pH's (pH 3.994, pH 7.001 and pH 9.012). The slope ranged between 58.92 and 59.18. The

standard electrode potential (E^0) and pKw were calculated from NaOH/HCl titrations. E^0 ranged between 402.97 and 416.03 milivolts, pKw ranged between 13.76 and 13.79. Metal titrations were performed using 1:2 metal/ligand concentrations

3.3.3 Data handling

Potentiometric data is reported in potential difference (in millivolts) per unit volume of injection. Stability constants are calculated from this data. In this study the computer program, Equilibrium Simulations for Titration Analysis (ESTA) was used to analyse the raw potentiometric data. ESTA has a number of tasks. In this study ZBAR, QBAR and OBJE tasks were used.

ZBAR task is a simulation unit that uses mass balance equations to characterise the system on point by point basis [1]. This task plots curves, Z_H-bar curve for ligand protonation and Z_M-bar curve for complex formation titrations. The protonation/deprotonation formation function (Z_H-bar) is expressed as;

$$Z_{H-bar} = \frac{T_H - H + OH}{T_{lig}} \tag{3.31}$$

Where T_H is the total concentration of hydronium ions, T_{lig} is the total concentration of the ligand and OH.

A typical Z_H-bar curve is given in Figure 3.0A. If a ligand has two dissociable protons, Z_H-bar levels off at two and at one. The pka values can also be estimated from Z_H-bar curves. The pka's are given by the pH that makes the mid-point of the steepest slope; log K_{LH} = 7.8 and log K_{LH2} = 3.4.

Complex formation function (Z_M-bar) depends on the cumulative protonation/deprotonation constants of the ligand to which the metal ion is binding to. This can be expressed as;

$$Z_{M-bar} = \frac{T_L - A(1 + \sum_n \beta_{LHn} H^n)}{T_M} \tag{3.32}$$

Where T_M is the total metal concentration, and;

$$A = \frac{T_H - H + OH}{\sum_n (\beta_{LHn} H^n)} \tag{3.33}$$

ESTA calculates the residual;

$$Z_{-bar}\text{residual} = Z^{o}{}_{-bar} - Z^{c}{}_{-bar} \tag{3.34}$$

Where Z^0-bar is the observed and Z^C-bar is the calculated Z-bar. A good agreement is observed if the observed and calculated Z-bar curves are superimposable.

Z_M-bar works for ML, ML_2, ML_3…ML_n species. A typical Z_M curve is given in Figure 3.0B. If ML is the most predominant species in solution, Z_M-bar levels off at 1. Log K_{ML} can be estimated from the pL that makes the mid-point of the steepest slope; log K_{ML} = 8.9. If ML_n (n = 1, 2, 3…) is not the most predominant species in solution, the Z_M-bar fails. Typical graphs are given in Figure 3.0C. The curling of the plots indicates the formation of hydroxo species. From Z_M-bar graphs, the model of Cu(II)/ligand species can be predicted. Looking at the black plot (Figure 3.0C), the graph levels off at 1 indicating formation of ML, then curls back at low pL's indicating the formation of MLH_{-1}. The pink plot of Figure 3.0 indicates that hydroxo species begin to form at very low pH's.

It is also important to know how many protons have been lost upon complexation with a metal ion. A deprotonation function (Q_M-bar) is calculated;

$$Q_{M-BAR} = \frac{T_H^* - T_H}{T_M} \tag{3.35}$$

Where T^*_H is total concentration or H^+ ions in solution at the observed pH. The mass balance equations for T^*_H and T_L can be expressed as;

$$T_H^* = H - OH + \sum_{J=1}^{NJ} r\,[M_p\,L_q\,H_r\,]$$

$$T_L = L + H - OH + \sum_{J=1}^{NJ} q\,[M_p\,L_q\,H_r\,] \tag{3.36}$$

Once Q_M-bar has been calculated, it can be plotted as a function of pH. ESTA plots Q_M-bar on the same graph with n-bar. The latter estimates the total number of dissociable protons on the ligand.

$$n_{-bar} = \frac{T_H^* - H + OH}{T_L^r} \tag{3.37}$$

A typical Q_M-bar graph is given in Figure 3.0D. The pink plot is the n-bar. The blue plot is Q_M-bar. N-bar levels off at 1 indicating there is one dissociable proton on the ligand. At pH 3.9 there is an intersection between n-bar and Q_M-bar. This indicates that the proton on the ligand has been displaced due to complexation; therefore the species formed is ML. At pH 6.4, the ligand has lost two protons due to complexation (Q_M-bar = 2), the complex species forming here is the MLH_{-1}. Between pH 6.4 and pH 8.9, n-bar and Q_M-bar parallel indicating that there are no more protons being displaced by the metal ion. At pH 8.9, the curve increases indicating the formation of hydroxo species.

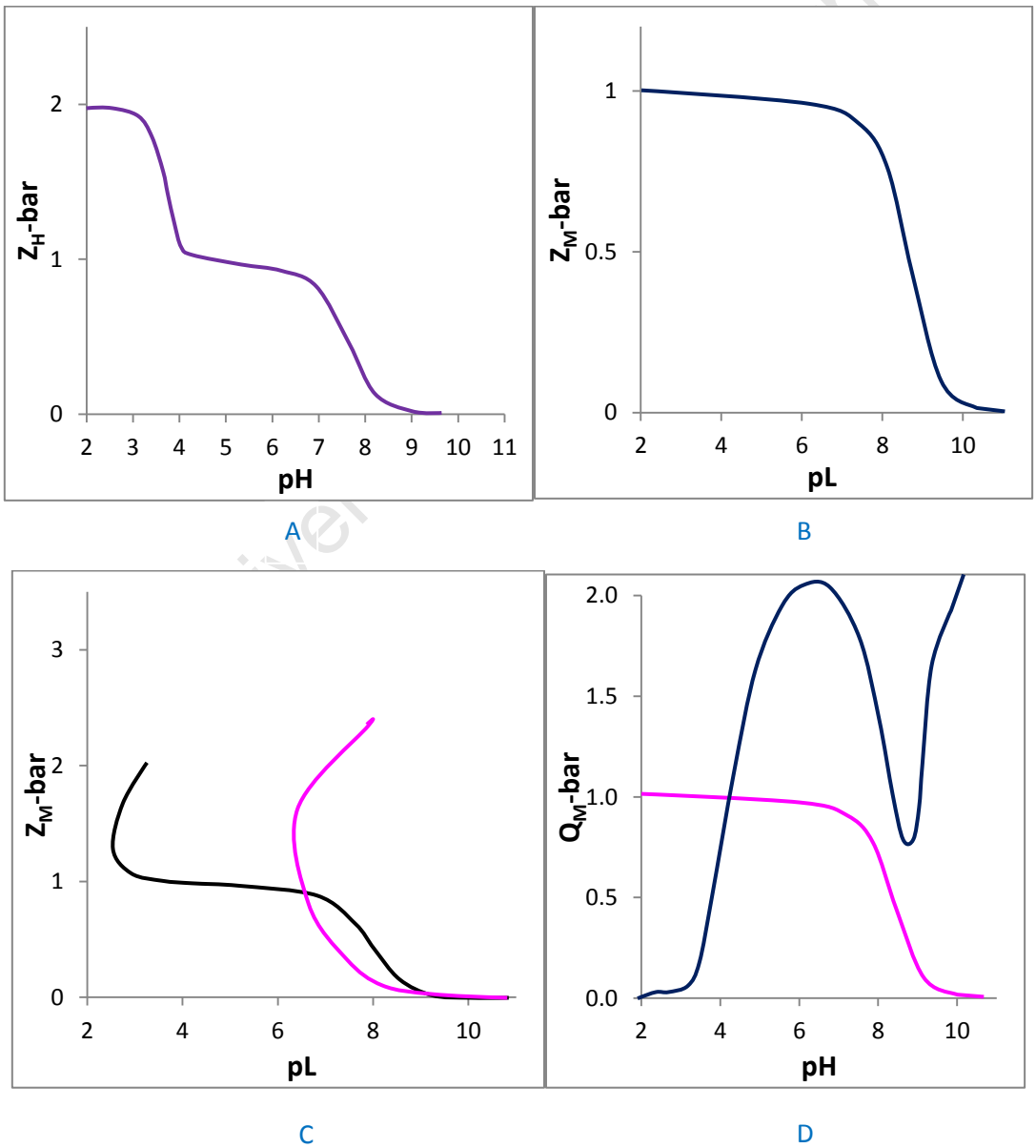

Figure 3.0: Typical Z_H-bar , Z_M-bar and Q_M-bar curves

Once the models have been chosen (for both the protonation titrations and the complex formation titrations and log K's have been estimated, cumulative equilibrium constants (log β's) can be put into OBJE task. OBJE task of ESTA optimises titration parameters using the weighted or unweighted least squares. The optimisation is based on the residuals of the electrode potential and the objective function (U_{obj}). U_{obj} is expressed as;

$$U_{obj} = (N - n_p)^{-1} \sum_{n=1}^{N} {n_e}^{-1} \sum_{q=1}^{n_e} W_{nq} ({Y_{nq}}^{obs} - {Y_{nq}}^{calc})^2$$

(3.38)

Where N is the number of experimental titration points, n_p is the total number of points being optimised, ne is the total number of electrodes, w_{nq} of the q^{th} residual at the n^{th} titration point, ${y_n}^{calc}$ is the calculated variable of the q^{th} residual at the n^{th} titration point and ${y_n}^{obs}$ is the observed variable of the q^{th} residual at the n^{th} titration point.

Using Gauss-Newton methods [10], Equation 3.38 can be expressed as a quadratic;

$$U_{obj} = a + {p^t}b + \frac{{p^t}H_p}{2}$$

(3.39)

Where a and b are Gauss-Newton quadratic parameter vectors, p is the optimization parameter vector and p^t is the rearranged form of Equation 3.39 (Hessian method);

$$H_{sr} = \frac{d^2 U_{obj}}{dp_s dp_r}$$

(3.40)

OBJE optimizes the titration parameters and calculates the standard deviations (δ) by;

$$\delta = \left(\frac{U_{obj} G_{rr}}{N - n_p} \right)^{1/2}$$

(3.41)

OBJE also optimizes the Hamilton R-factor (R^H) to check if the model is accurate. R^H is expressed as;

$$R^H = \left(\frac{U_{obj}}{\sum n_e{}^{-1} \sum W_{nq} \, (Y_{nq}{}^{obs})^2} \right)^{1/2}$$

(3.42)

R^H depends on random errors and the number of variables optimised. If R^H is less than R^H_{lim} then the model is accurate. R^H_{lim} is expressed as;

$$R^H_{lim} = \left(\frac{N}{\sum n_e{}^{-1} \sum W_{nq} \, (Y_{nq}{}^{obs})^2} \right)^{1/2}$$

(3.43)

Once the titration variables have been optimised and the program has converged, the speciation graph can be plotted from the initial concentrations of the analyte and the titrant. Accuracy, precision and reproducibility are achieved by having a large data population (n_p), and doing the same titration twice or more than two times (n_T) and comparing the results with the literature if the titrations have been published before.

3.4 RESULTS

3.4.1 Protonation titrations

3.4.1.1 Protonation of glycine

Glycine protonation has been reported before [11-14]. This system is used to check the reliability of the method and that of the operator. Glycine peptides (GLY-GLY, GLY-LEU, GLY-PHE and GLY-HIS) are compounds of interest and thus the study of glycine would provide a useful reference.

Figure 3.1 shows Z_H-bar as a function of pH for the protonation of glycine. For clarity, a selected number of data points was plotted. The blue markers represent the experimental plot and the solid line is the theoretical curve calculated using the model given in Table 3.1. The experimental and the theoretical plots are on top of each other. This leads to confidence in the model. At pH 11.0, Z_H-bar is 0, therefore glycine exists as a free ligand and no protonation has occurred. Z_H-bar rises from pH 10.8 to pH 8.2, where it levels off at Z_H-bar = 1. In this pH range, glycine is being protonated from the L-form to the LH-form. Log K_{LH} can be estimated from the half Z_H-bar value to be 9.5. From pH 8.2 to pH 3.5, Z_H-bar

was fairly constant (Z_H-bar ≈ 1) indicating that no further protonation was occurring. From pH 3.5, Z_H-bar rises from 1 to 1.5, as a result of the protonation of the second site. This indicates that glycine has two dissociable protons. Complete protonation of LH to LH_2 occurs at very low pH's (pH < 2). Titrations were not performed pH 2 because the electrode response was no longer linear.

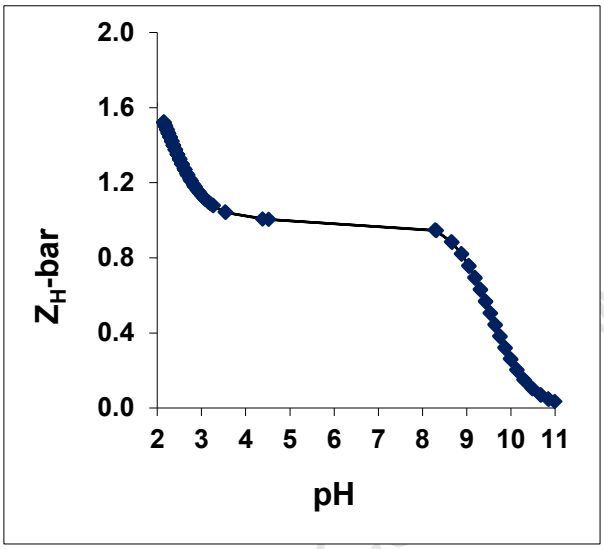

Figure 3.1: Z_H-bar as a function of pH for the protonation of glycine

Even though the protonation constants could be estimated from Z_H-bar graph, they were calculated and optimized using the OBJE function of ESTA. Log K_{LH} = 9.53 and log K_{LH2} = 2.29 (Table 3.1). These values agree well with the literature (K_{LH} = 9.50 and log K_{LH2} = 2.34) [11-14, 17]. The standard deviations $\sigma_{p\,q\,r}$ were small, R^H was less than R^H_{lim} therefore the model was within the allowed maximum error.

Table 3.1: Calculated protonation constants of glycine and the standard deviations

p q r	Log β	$\sigma_{p\,q\,r}$	R^H	R^H_{lim}	nT(nP)	Log K_{exp}	Log K_{lit} [17]
0 1 1	9.53	0.01	0.003	0.01	4(204)	9.53	9.50
0 1 2	11.8	0.02				2.29	2.34

Figure 3.2 shows the speciation of glycine in its three forms from pH 2 to pH 11. At pH's above pH 9.57, the most predominant species was L. Between pH 9.57 and pH 2.35, the most predominant species was LH. LH_2 was the most predominant species at pH's below pH 2.35.

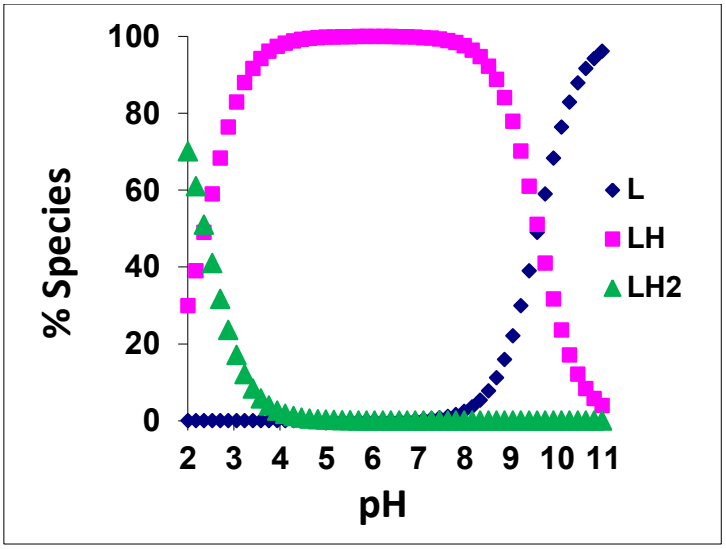

Figure 3.2: Speciation for the protonation of glycine

3.4.1.2 Protonation of sarcosine

Studies on the protonation of sarcosine have also been done extensively [7-9]. Sarcosine was also used to test the reliability of the method and that of the operator. Four sarcosine peptides (SAR-GLY, SAR-LEU, SAR-PHE and SAR-HIS) were also compounds of interest in this study thus sarcosine was used as a reference.

Figure 3.3 shows Z_H-bar as a function of pH for the protonation of sarcosine Complete deprotonation of sarcosine occurs at very high pH's (pH's above 11). Titrations could only be done between pH 2 and pH 11 because pH's outside this pH range the electrode response is not linear. Z_H-bar rises from pH 11.0 to pH 8.5 where it levels off at Z_H-bar = 1. At this pH range the ligand was going from the L-form to the LH form. The graph was extrapolated and the first protonation constant was estimated, log K_{LH} = 10.0. Between pH 8.5 and pH 3.5 Z_H-bar was not changing much (Z_H-bar ≈ 1). From pH 3.5 to pH 2, the graph rises to Z_H-bar = 1.4. At this pH range, sarcosine was going from the LH form to the LH_2 form. Complete protonation to LH to LH_2 occurs at very low pH's. When the graph was extrapolated, log K_{LH2} was estimated log K_{LH2} = 2.0).

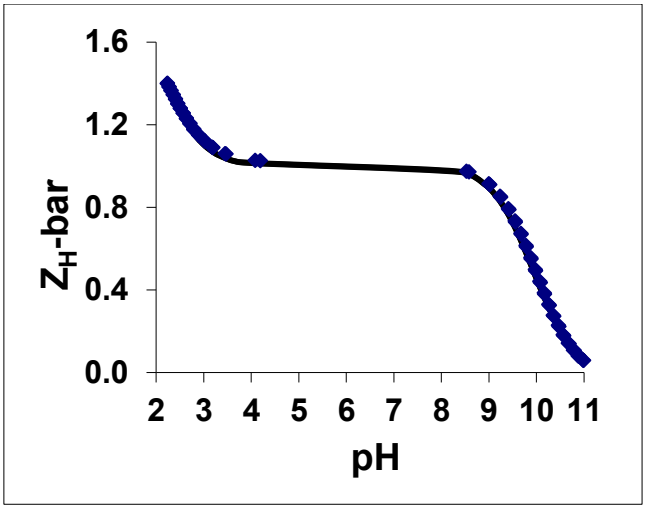

Figure 3.3: Z_H-bar as a function of pH for the protonation of sarcosine

The pKa values are given in Table 3.2. The standard deviations σ_{pqr} are small, R^H was less than R^H_{lim} therefore the model was within the allowed maximum error.

Table 3.2: Calculated protonation constants of sarcosine and the standard deviations

p q r	Log β	σ_{pqr}	R^H	R^H_{lim}	nT(nP)	Log K_{exp}	Log K_{lit}[17]
0 1 1	10.0	0.005	0.007	0.01	3(133)	10.0	10.0
0 1 2	12.1	0.01				2.10	2.12

Figure 3.2 shows the speciation of sarcosine from pH 2 to pH 11. At pH's above pH 9.57, the most predominant species was L. Between pH 9.57 and pH 2.35, the most predominant species was LH. LH_2 was the most predominant species at pH's below pH 2.35.

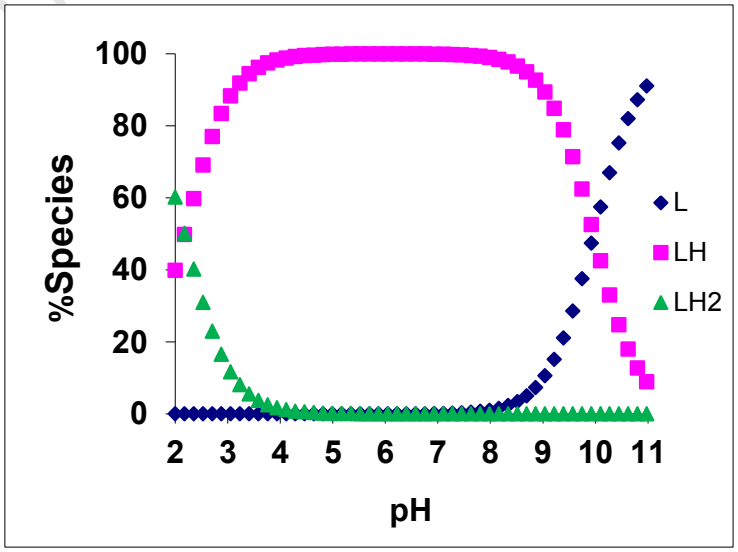

Figure 3.4: Speciation for the protonation of sarcosine

3.4.1.3 Protonation of glycyl-glycine

Figure 3.5 shows Z_H-bar as a function of pH for the protonation of GLY-GLY. GLY-GLY was completely deprotonated from pH 10.0. Z_H-bar rises up from pH 9.9 to pH 7.0 indicating protonation of GLY-GLY from L to LH. The mid-point of this slope is equivalent to log K_{LH} (log K_{LH} = 8.2). The graph levels off at Z_H-bar = 1 from pH 7.1 to pH 4.4. From pH 4.4 the graph rises up until it reaches Z_H-bar = 1.88. Log K_{LH2} = 3.2.

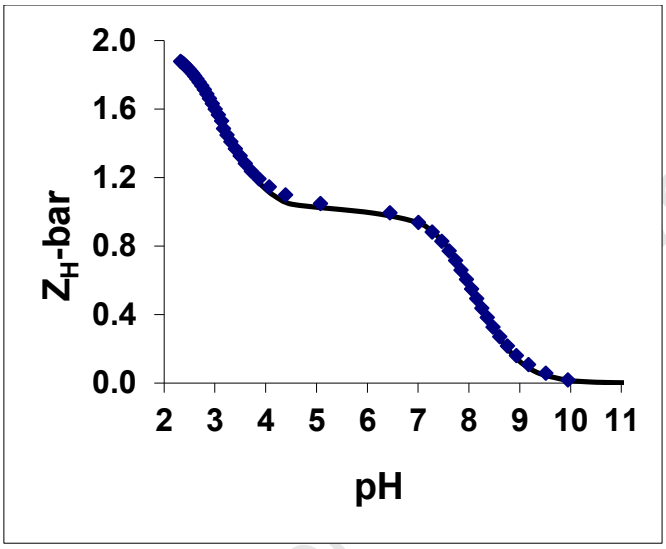

Figure 3.5: Z_H-bar as a function of pH for the protonation of GLY-GLY

Optimised pKa's are given in Table 3.3.

Table 3.3: Calculated protonation constants of GLY-GLY and the standard deviations

p q r	Log β	σ_{pqr}	R^H	R^H_{lim}	nT(nP)	Log K_{exp}	Log K_{lit}[17]
0 1 1	8.16	0.01	0.01	0.1	2(65)	8.16	8.10
0 1 2	11.3	0.01				3.18	2.54

Figure 3.6 shows the distribution of species from pH 2 to pH 11 for GLY-GLY protonation. At pH 8.68 there was already more L than LH in solution. From pH 8.33 to pH 3.04, the most predominant species was LH. At low pH's, the most predominant species was LH_2.

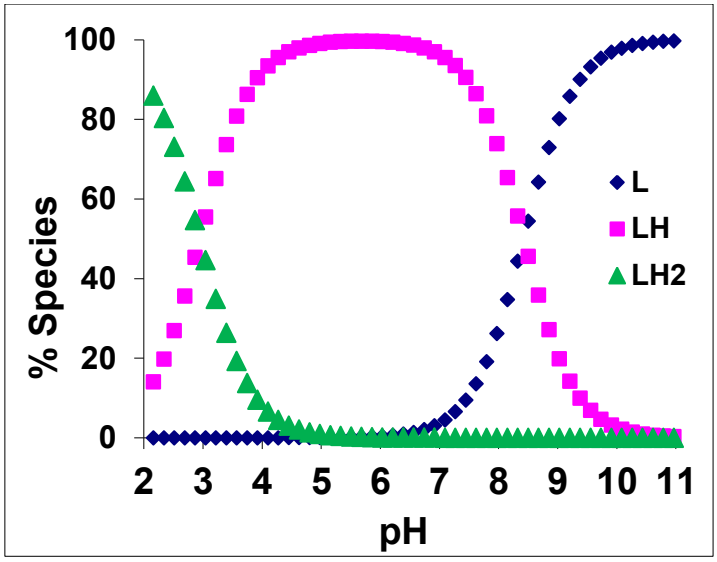

Figure 3.6: Speciation for the protonation of GLY-GLY

3.4.1.4 Protonation of sarcosyl-glycine

Figure 3.7 shows Z_H-bar as a function of pH for the protonation of SAR-GLY. SAR-GLY was completely deprotonated from pH 10.0 (Z_H-bar is zero). From pH 9.9 to pH 7.4 the graph rises then levels off at Z_H-bar = 1. Mid-point of this slope is 8.4, therefore log K_{LH} = 8.4. From pH 7.4 to pH 4.7 Z_H-bar does not change therefore the reactants and the products for this reaction were at equilibrium; $LH + H \rightleftharpoons LH_2$

The second protonation constant was estimated by extrapolating the graph, log K_{LH2} = 3.

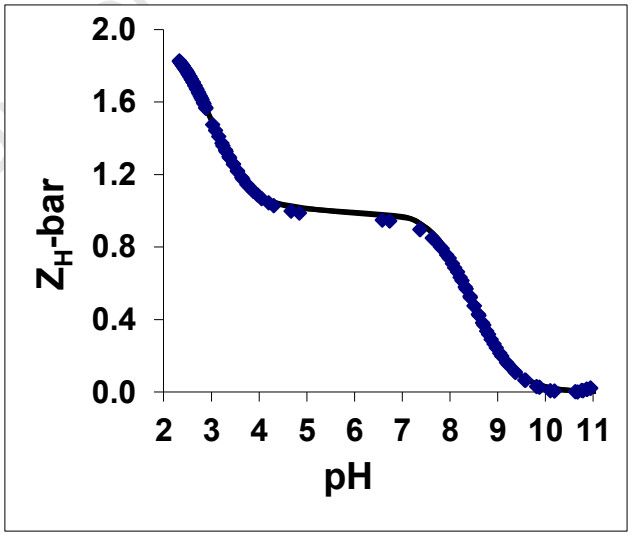

Figure 3.7: Z_H-bar as a function of pH for the protonation of SAR-GLY

Log K values are given in Table 3.4.

Table 3.4: Calculated protonation constants of SAR-GLY and the standard deviations

p q r	Log β	σ_{pqr}	R^H	R^H_{lim}	nT(nP)	Log K_{exp}	Log K_{lit}[17]
0 1 1	8.43	0.007	0.009	0.01	2(153)	8.43	8.44
0 1 2	11.4	0.01				2.95	3.00

Figure 3.8 shows the distribution of species from pH 2.0 to pH 11.0 for SAR-GLY protonation. From pH 11.0 to pH 8.6 L was the predominant species in solution. From pH 8.3 to pH 2.9, LH was the most predominant species in solution. From pH 2.7 to pH 2.0, LH_2 was predominant in solution.

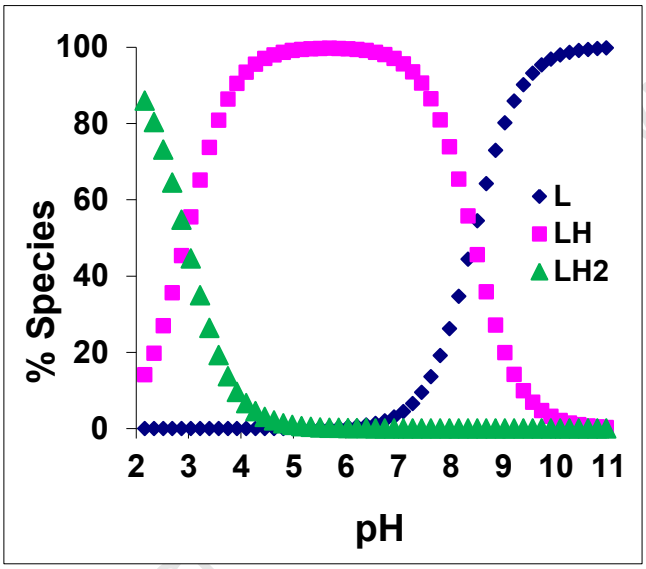

Figure 3.8: Speciation for the protonation of SAR-GLY

3.4.1.5 Protonation of glycyl-L-leucine

Figure 3.9 shows Z_H-bar as a function of pH for the protonation of GLY-LEU. From pH 11.0 to pH 10.0, Z is zero. From pH 9.8 the graph rises until it gets to pH 7.1 where is levels off at Z_H-bar = 1. The first protonation constant was estimated from the slope, log K_{LH} = 8.2. From pH 7.2 to pH 4.6, the height of the graph does not change much. From pH 4.2, the graph rises until Z_H-bar = 1.7 is achieved at pH 2.6. The second protonation constant was estimated by extrapolation, log K_{LH2} = 3.1.

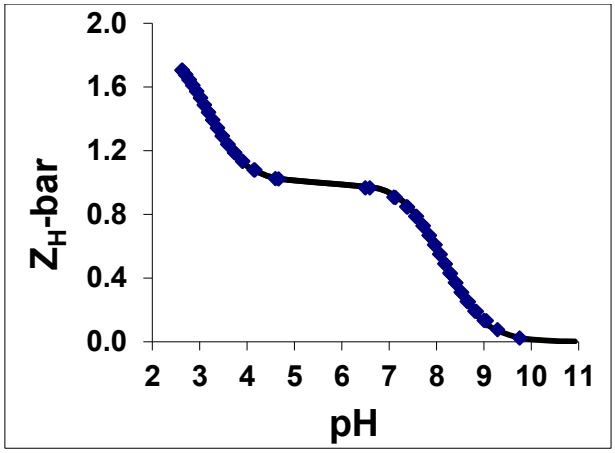

Figure 3.9: Z_H-bar as a function of pH for the protonation of GLY-LEU

Table 3.5 shows calculated log K's for the protonation of GLY-LEU. The experimental values are in good agreement with the literature values.

Table 3.5: Calculated protonation constants of GLY-LEU and the standard deviations

p q r	Log β	σ_{pqr}	R^H	R^H_{lim}	nT(nP)	Log K_{exp}	Log K_{lit}[17]
0 1 1	8.20	0.004	0.01	0.02	2(67)	8.20	8.18
0 1 2	11.3	0.009				3.14	3.10

Figure 3.10 shows the distribution of GLY-LEU species from pH 2.0 to pH 11.0. From pH 11.0 to pH 8.3 the most predominant species is L. From pH 8.0 to pH 3.2, the most predominant species is LH. From pH 2.9 to pH 2.0 the most predominant species is LH_2.

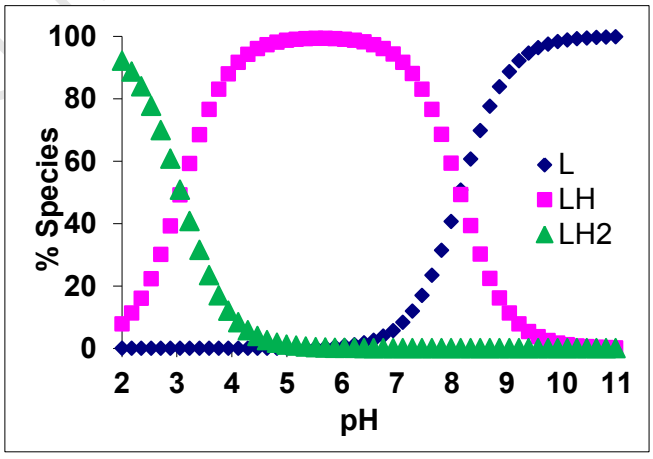

Figure 3.10: Speciation for the protonation of GLY-LEU

3.4.1.6 Protonation of sarcosyl-L-leucine

Figure 3.11 shows Z_H-bar as a function of pH for the protonation of SAR-LEU. From pH 11.0 to pH 10.5, the SAR-LEU was completely deprotonated (Z_H-bar is zero). The graph rises up from pH 10.5 to pH 7.4. Log K_{LH} = 8.4. From pH 7.4 to pH 5.1 the ZH-bar ≈ 1 was maintained. The graph rises from pH 5.1 to pH 2.0 where Z_H-bar = 2 was reached. This indicates that SAR-LEU has two dissociable protons (log K_{LH2} = 3.5).

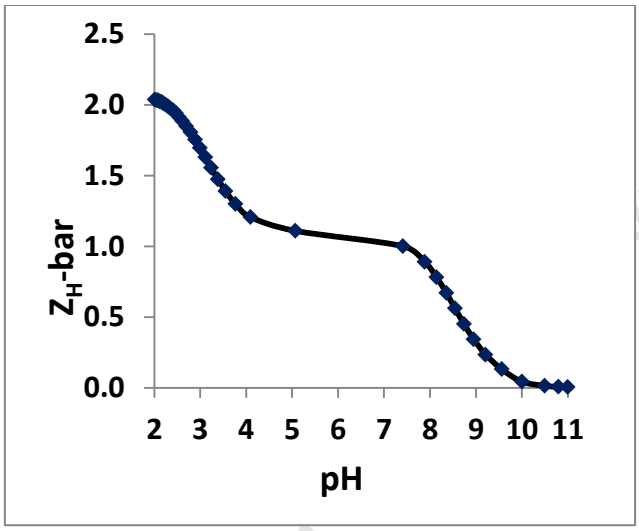

Figure 3.11: Z_H-bar as a function of pH for the protonation of SAR-LEU

Table 3.6 shows calculated log K's for the protonation of SAR-LEU. The first protonation constant agrees well with the literature [15] and the second protonation is slightly higher than the literature [15]. The slight difference in log K_{LH2} could be due to the differences in the ionic strength.

Table 3.6: Calculated protonation constants of SAR-LEU and the standard deviations

p q r	Log β	σ_{pqr}	R^H	R^H_{lim}	nT(nP)	Log K_{exp}	Log K_{lit}[17]
0 1 1	8.69	0.02	0.009	0.02	2(51)	8.69	8.64
0 1 2	12.2	0.04				3.48	2.61

Figure 3.12 shows the speciation of SAR-LEU as a function of pH. SAR-LEU exists in its L form from pH 11.0 to pH 8.5. From pH 8.5 to pH 3.6, SAR-LEU exists in its LH form. LH_2 is the most predominant species from pH 4.1 to pH 2.0.

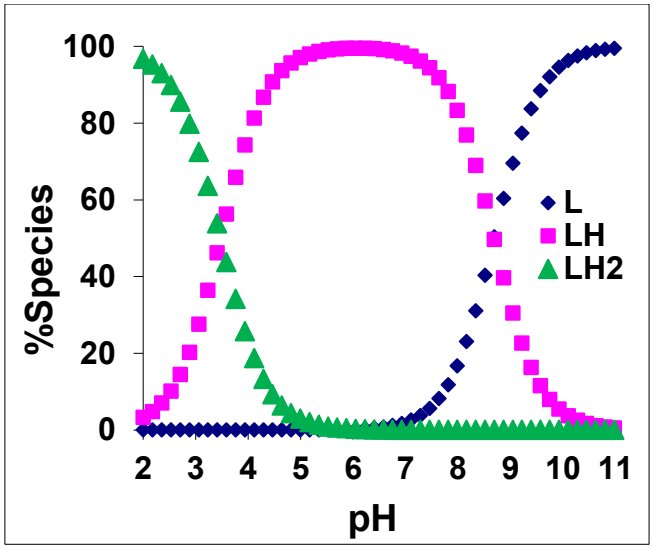

Figure 3.12: Speciation for the protonation of SAR-LEU

3.4.1.7 Protonation of glycyl-L-phenylalanine

Z_H-bar for the protonation of GLY-PHE is given in Figure 3.13. The graph levels off between pH 11.0 ant pH 9.8 where it rises until it reaches Z_H-bar = 1 (between pH 6.8 and pH 4.4). The graph rises again from pH 4.4 to pH 2.2. Protonation constants of GLY-PHE were estimated from the slopes; log K_{LH} = 8.2 and log K_{LH2} = 2.9.

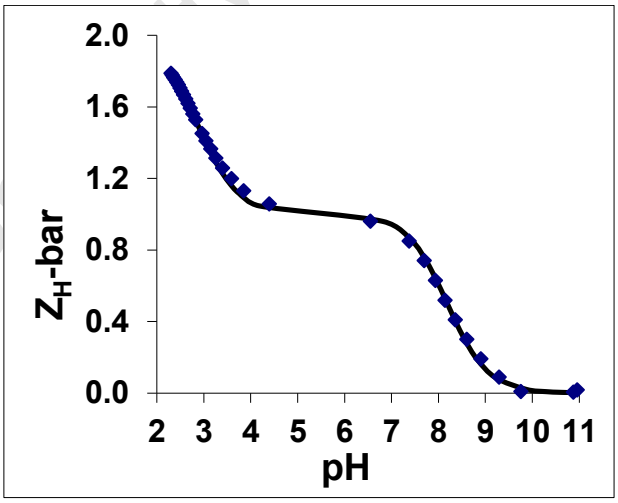

Figure 3.13: Z_H-bar as a function of pH for the protonation of GLY-PHE

Optimized log K's are given in Table 3.7. Log K's for the protonation of GLY-PHE agree well with literature [8, 9]. The standard deviations are small and the model is accurate since R^H is less than R^H_{lim}. This gives confidence in the results.

Table 3.7: Calculated protonation constants of GLY-PHE and the standard deviations

p q r	Log β	$\sigma_{p\,q\,r}$	R^H	R^H_{lim}	nT(nP)	Log K_{exp}	Log K_{lit}[17]
0 1 1	8.20	0.01	0.009	0.01	2(60)	8.20	8.11
0 1 2	11.1	0.02				2.91	3.00

Speciation for GLY-PHE protonation titrations is given in Figure 3.14. From pH 11.0 to pH 8.3 the most predominate species in solution is L. From pH 8.0 to pH 3.1 the most predominate species in solution is LH and from pH 2.7 to pH 2.0 the most predominate species is LH_2.

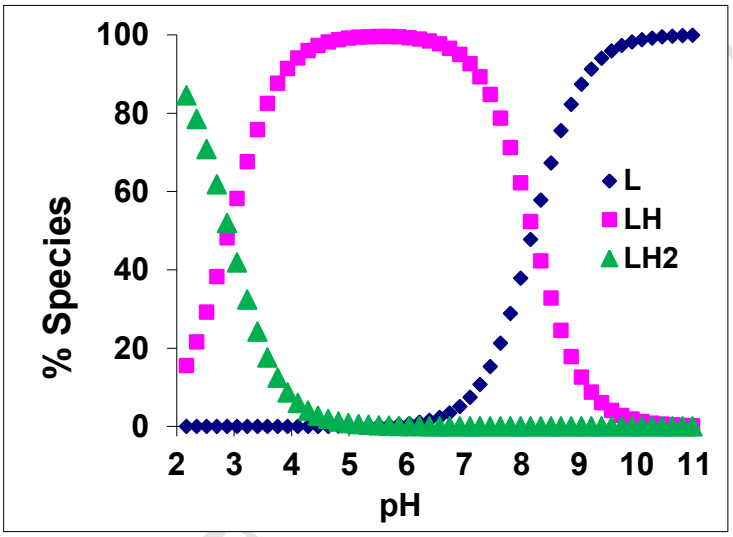

Figure 3.14: Speciation for the protonation of GLY-PHE

3.4.1.8 Protonation of sarcosyl-L-phenylalanine

Z_H-bar for the protonation of SAR-PHE is given in Figure 3.15. Equilibrium is observed between pH 11.0 and pH 9.6 for $L + H \rightleftharpoons LH$. The equilibrium constant for this reaction from the graph, log K_{LH} = 8.5. The second equilibrium was observed between pH 7.4 and pH 4.0 for $LH + H \rightleftharpoons LH_2$. Log K_{LH} = 3.0 from the graph.

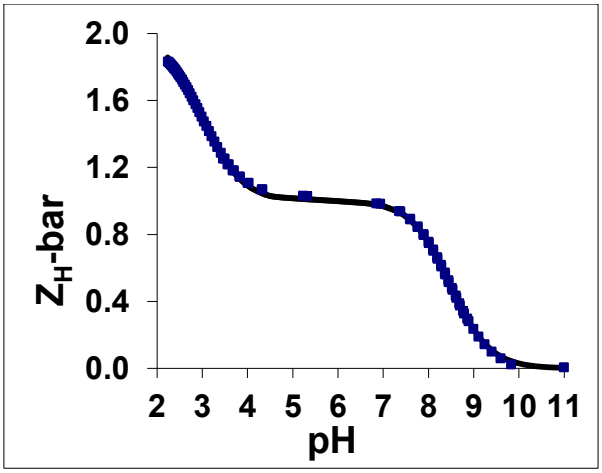

Figure 3.15: Z_H-bar as a function of pH for the protonation of SAR-PHE

Log K_{LH} and log K_{LH2} were calculated and optimized. These are given in Table 3.8. Protonation of SAR-PHE has not been reported before however the results obtained are comparable with the results obtained for GLY-PHE protonation. The errors for log β's are small and R^H is less than R^H_{lim}. This gives confidence in the results.

Table 3.8: Calculated protonation constants of SAR-PHE and the standard deviations

p q r	Log β	σ_{pqr}	R^H	R^H_{lim}	nT(nP)	Log K_{exp}
0 1 1	8.48	0.01	0.001	0.03	2(118)	8.48
0 1 2	11.5	0.03				3.05

The speciation for the protonaion of SAR-PHE is given in Figure 3.16. The L form of SAR-PHE is most predominat from pH 11.0 to pH 8.7. LH is most predominat from pH 8.3 to pH 2.9, and LH_2 is most predominant from pH 2.8 to pH 2.0

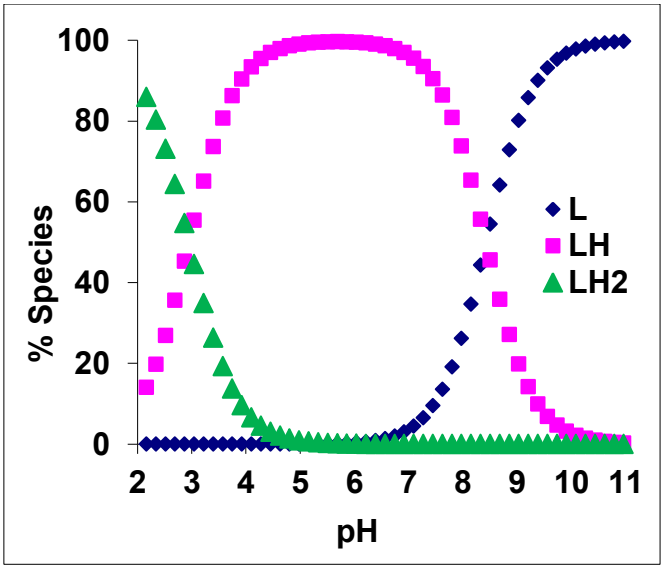

Figure 3.16: Speciation for the protonation of SAR-PHE

3.4.1.9 Protonation of glycyl-L-histidine

GLY-HIS titrations have been reported elsewhere [11]. The same media, titrations conditions and instrumentation were used, therefore these titrations were not repeated. The first and the second protonation occur around the same pH region (log K_{LH} = 8.34 and log K_{LH2} = 6.61). Log K_{LH3} = 2.29. The first protonation occurs on the amine terminal, the second protonation occurs on -atom of the imidazole ring and the third protonation occurs on the carboxylate terminal [11, 22-23].

3.4.1.10 Protonation of sarcosyl-L-histidine

Due to solubility problems, studies on SAR-HIS could not be done. The order of protonation is expected to be the same as the order of protonation in GLY-HIS.

3.4.2 Complex formation titrations

3.4.2.1 Glycine complexes

3.4.2.1.1 GLY / Cu(II)

Z_M-BAR for Cu(II)/GLY is given in Figure 3.17. The blue markers are the experimental data points, the solid line is the theoretical plot. For clarity not all the data points have been plotted. Z_M-bar is zero from pL 9.4 to pL 8.6. Z_M-bar rises from pL 8.6 to pL 5.0. From pH 5.0 to pH 2.0, Z_M bar = 2. This indicates the formation of the ML_2, and that there are no hydroxo species forming in solution since the plot does not fan back at low pL's.

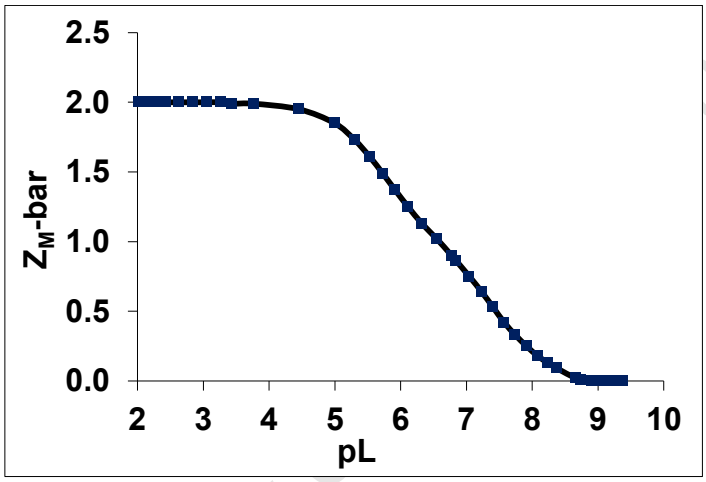

Figure 3.17: Z_M-bar as a function of pL for the Cu(II)/GLY titrations

Optimised log K's are given in Table 3.9. Log K_{ML} = 8.09 and log K_{ML2} = 7.02. These agree with the literature [13-14]. The standard deviations are small and R^H is less than R^H_{lim}. This shows that the model is accurate.

Table 3.9: Calculated equilibrium constants for Cu(II)/GLY complexes

Metal	p q r	Log β	σ_{pqr}	R^H	R^H_{lim}	nT(nP)	Log K_{exp}	Log K_{lit}[17]
Cu(II)	1 1 0 1 2 0	8.09 15.1	0.004 0.006	0.003	0.01	4(216)	8.09 7.02	8.15 6.85

The total number of dissociable protons on the ligand (n-bar) and the total number of lost protons upon complexation of Cu(II) with GLY (Q_M-bar) are shown in Figure 3.18. The solid line is the experimental plot. N-Bar (pink markers) rises from pH 11 to pH 9.1 where it levels off at Q_M-bar = 1. The graph rises again from pH 3.3 to pH 2.0 where Q_M-bar = 1.7 is observed. This shows that there are two dissociable protons on GLY (n-bar is the same as

Z_M-bar as a function of pH in protonation titrations). The blue markers (Q_M-bar) shows the number of protons lost upon complexation of Cu(II) with GLY. Q_M-bar rises from pH 11.0 until it reaches a maximum value (Q_M-bar = 2 at pH 7.0), then drops until Q_M-bar is zero. This shows that all two dissociable protons are lost upon complexation of Cu(II) with GLY. The solid line is the experimental plot. The theoretical plot and the experimental plot are superimposable; this gives confidence in the results.

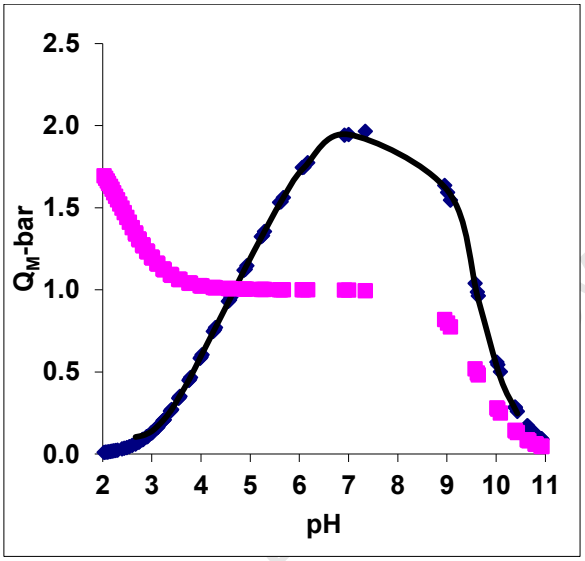

Figure 3.18: Q_M-bar as a function of pH for the Cu(II)/GLY titrations. Pink curve is n-bar, blue curve is experimental Q-bar and the solid line is the theoretical plot.

Figure 3.19 shows the speciation for 1:2 Cu(II)/GLY from pH 2.0 to pH 11.0. The ML species starts to form from pH 2.7 and the amount of this species increases until about 78 % (at pH 4.6) of it is formed, and the then starts decrease from pH 4.6 to pH 9.0 where it is converted to ML_2.

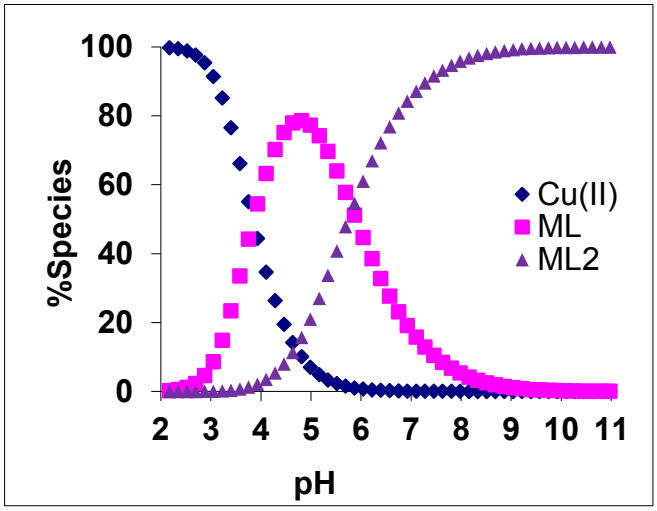

Figure 3.19: Speciation for complex formation titrations of Cu(II)/GLY, 1:2 ratio. [GLY] = 0.006279 M.

3.4.2.2 Sarcosine complexes

3.4.2.2.1 SAR / Cu(II)

Z_M-bar for Cu(II)/SAR titrations is shown in Figure 3.20. Z_M-bar is zero from pL 10.0 to pL 9.4. From pL 9.4 the graph rises then levels off between pL 5.0 to pL 3.1 (Z_M-bar = 2). This indicates the formation of ML_2. The graph then fans back at pL 3.1. This indicates the formation of hydroxo species.

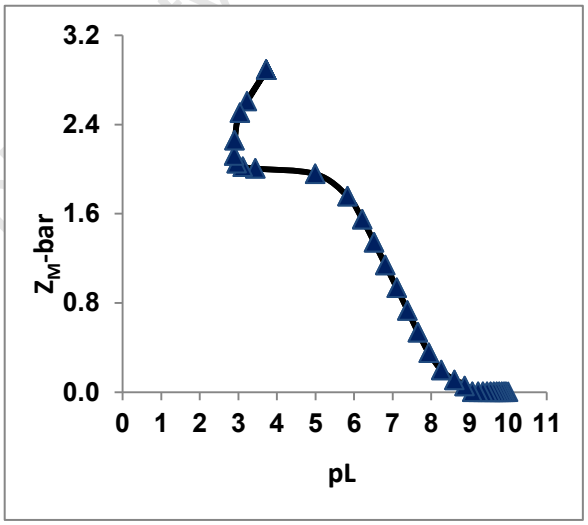

Figure 3.20: Z_M-bar as a function of pL for the Cu(II)/SAR titrations

Equilibrium constants for species formed between Cu(II) and SAR from pH 2.0 to pH 11.0 are given in Table 3.10. The standard deviations are small and R^H is less than R^H_{lim}. This

shows that the model is accurate. With the exception of log K_2 the experimental equilibrium constants agree well with the literature [7, 8]. ML_3 was not observed.

Table 3.10: Calculated equilibrium constants for Cu(II)/SAR complexes

Metal	p q r	Log β	σ_{pqr}	R^H	R^H_{lim}	nT(nP)	Log K_{exp}	Log K_{lit}[17]
Cu(II)	1 1 0	7.89	0.02	0.09	0.1	2(68)	7.89	7.83
	1 2 0	14.2	0.06				6.31	6.74
	1 1 1	12.0	0.20				4.09	-
	1 3 0	-	-				-	0.77
	1 2 -1	2.66	0.07				11.6	11.3

Q_M-bar as a function of pH for Cu(II)/SAR titrations is shown in Figure 3.21. SAR has two dissociable protons and it loses two protons upon complexation with Cu(II). Q_M-bar does not touch the baseline (X-axis) at pH 11.0. This indicates the formation of hydroxo species at high pH's.

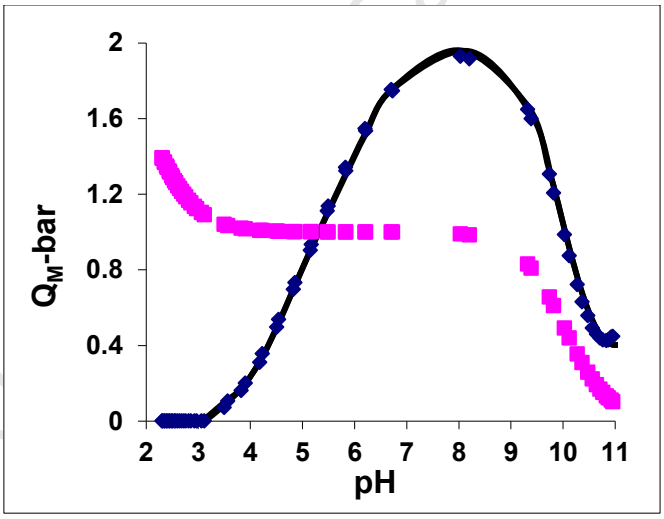

Figure 3.21: Q_M-bar as a function of pH for the Cu(II)/SAR titrations. Pink curve is n-bar, blue curve is experimental Q-bar and the solid line is the theoretical plot.

The speciation graph for Cu(II)/SAR is given in Figure 3.22.

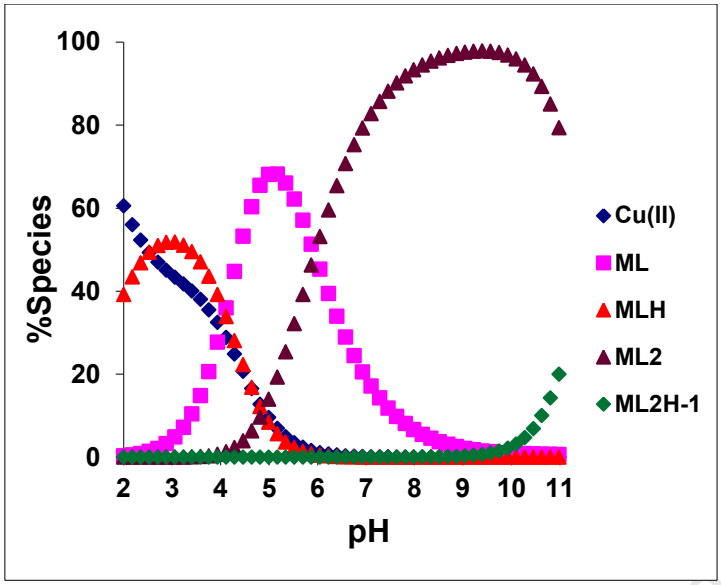

Figure 3.22: Speciation for complex formation titrations of Cu(II)/SAR, 1:2 ratio. [SAR] = 0.002098 M.

3.4.2.3 Glycyl-glycine complexes

3.4.2.3.1 GLY-GLY / Cu(II)

Z_M-bar for Cu(II)/GLY-GLY is given in Figure 3.23. Z_M-bar levels off at 1.5. At pH 4.5, Z_M-bar flags back indicating the formation of hydroxo species.

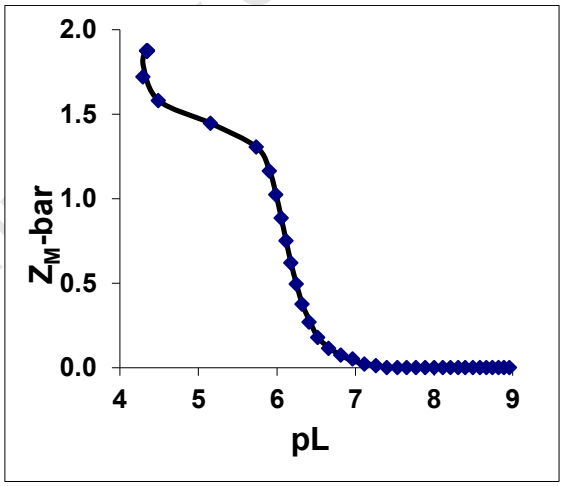

Figure 3.23: Z_M-bar as a function of pL for the Cu(II)/GLY-GLY titrations

Species formed between Cu(II) and GLY-GLY and their equilibrium constants are given in Table 3.11. The results are slightly higher than the literature [17, 24]. The slight difference is due to the difference in ionic strength.

Table 3.11: Calculated equilibrium constants for Cu(II)/GLY-GLY complexes

p q r	Log β	σ_{pqr}	R^H	R^H_{lim}	nT(nP)	Log K_{exp}	Log K_{lit}[17]
1 1 0	6.33	0.06				6.33	5.55
1 2 0	11.0	0.09				4.67	-
1 1 -1	-0.121	0.08				6.45	4.15
1 1 -2	-10.6	0.1	0.01	0.03	2(71)	10.5	9.31
1 2 -1	-	-				-	3.10
1 2 -2	-	-				-	12.5
2 2 -3	-	-				-	2.10

GLY-GLY has two dissociable protons and about two protons were lost upon complexation of GLY-GLY with Cu(II) (Figure 3.24). Between pH 7.1 and pH 8.9, Q_M-bar runs parallel to n-bar. This indicates that complexation is complete. The graph (Q_M-bar however rises from pH 8.9 to pH 11.0. This indicates the formation of the hydroxo species.

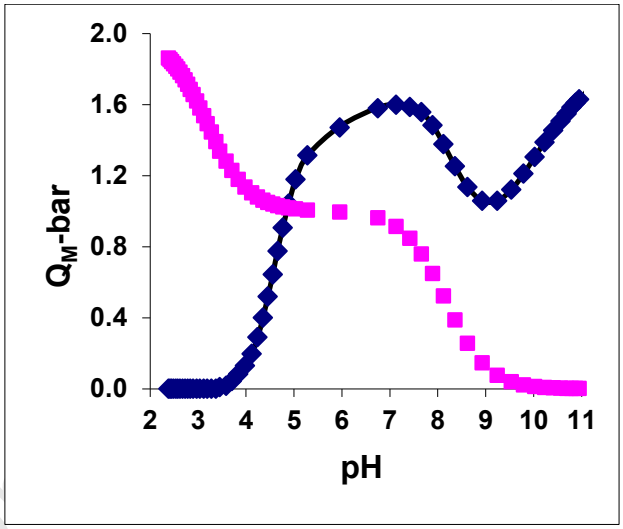

Figure 3.24: Q_M-bar as a function of pH for the Cu(II)/GLY-GLY titrations. Pink curve is n-bar, blue curve is experimental Q-bar and the solid line is the theoretical plot.

Figure 3.25 shows the speciation graph for 1:2 Cu(II)/GLY-GLY between pH 2.0 and pH 11.0. ML species forms between pH 2.8 and pH 7.4. ML_2 forms between pH 4.2 and pH 9.9. MLH_{-1} form between pH 4.6 and starts to deplete from pH 9.4. MLH_{-2} starts to form at pH 8.5.

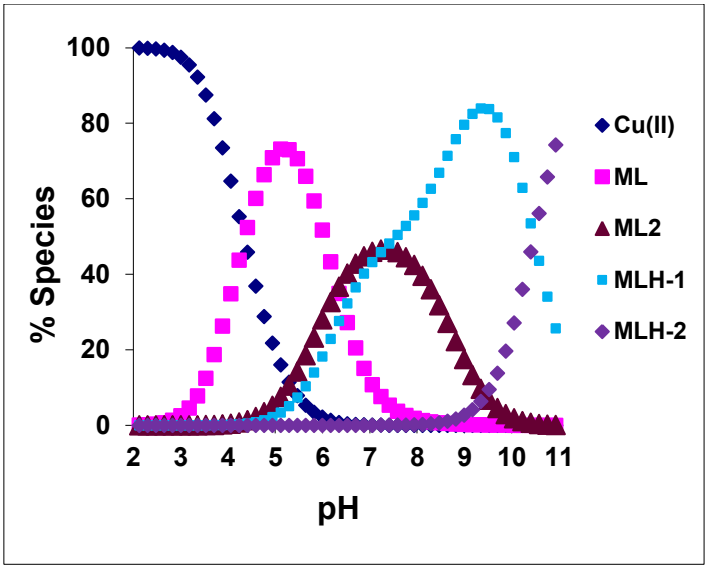

Figure 3.25: Speciation for complex formation titrations of Cu(II)/GLY-GLY, 1:2 ratio. [GLY-GLY] = 0.004345 M.

3.4.2.3.2 GLY-GLY / Ni(II)

Z_M-bar for Ni(II) GLY-GLY is given in Figure 3.26. At pH 5.8 the graph rises and fans back at pH 3.3 indicating the formation of hydroxo species.

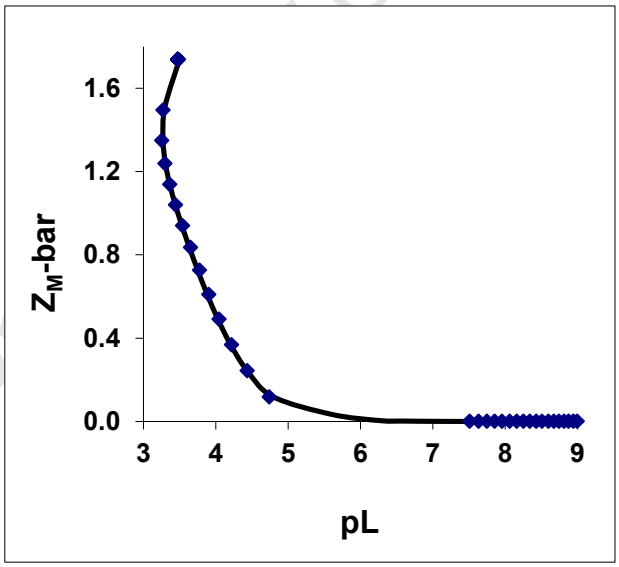

Figure 3.26: Z_M-bar as a function of pL for the Ni(II)/GLY-GLY titrations

Species formed between Ni(II) and GLY-GLY and their stability constants are given in Table 3.12. ML and ML_2 species have very low log K values.

Table 3.12: Calculated equilibrium constants for Ni(II)/GLY-GLY complexes.

p q r	Log β	$\sigma_{p\,q\,r}$	R^H	R^H_{lim}	nT(nP)	Log K_{exp}	Log K_{lit}[17]
1 1 0	3.91	0.02				3.91	4.05
1 2 0	6.90	0.04				2.99	3.20
1 3 0	-	-	0.01	0.01	2(61)	-	9.40
1 1 1	-	-				-	6.29
1 2 -1	-1.93	0.02				8.84	9.00
1 2 -2	-12.1	0.02				10.2	9.70

Figure 3.27 shows the Q_M-bar for Ni(II)/GLY-GLY titrations. GLY-GLY has two dissociable protons and it loses one proton upon complexation with Ni(II). The system consists mostly of hydroxo species from pH 8.8 to pH 11.0

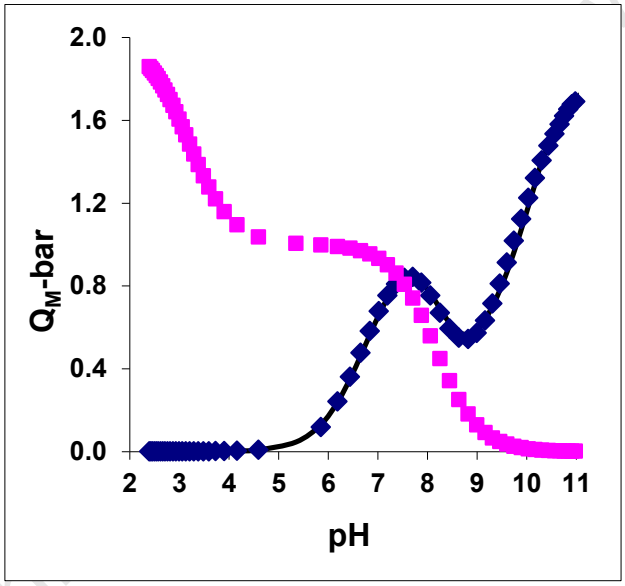

Figure 3.27: Q_M-bar as a function of pH for the Ni(II)/GLY-GLY titrations. Pink curve is n-bar, blue curve is experimental Q-bar and the solid line is the theoretical plot.

The distribution graph for 1:2 Ni(II)/GLY-GLY titrations is shown in Figure 3.28. Complexation occurs from pH 4.4 to pH 11.0.

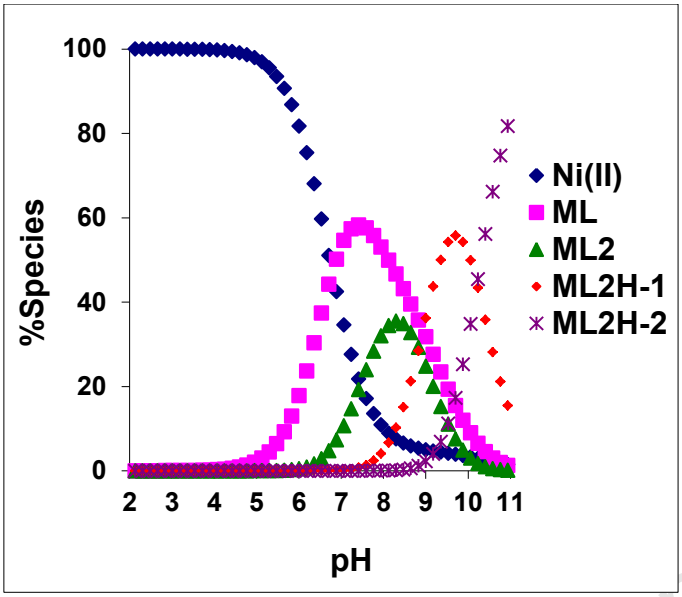

Figure 3.28: Speciation for complex formation titrations of Ni(II)/GLY-GLY, 1:2 ratio. [GLY-GLY] = 0.004258 M.

3.4.2.3.3 GLY-GLY / Zn(II)

Z_M-bar for Zn(II)/GLY-GLY is given in Figure 3.29. The graph flags back at low pL's indicating the formation of hydroxo species.

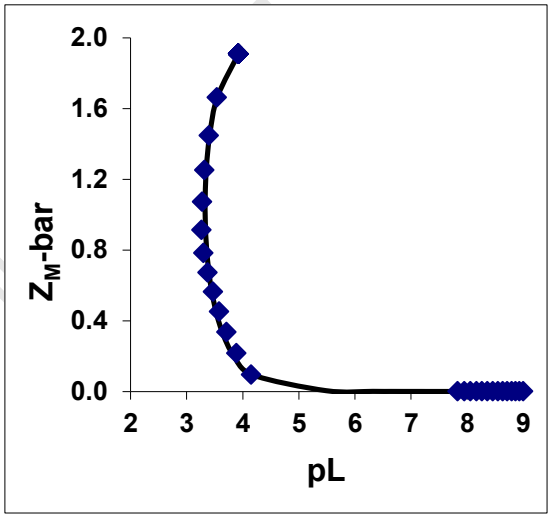

Figure 3.29: Z_M-bar as a function of pL for the Zn(II)/GLY-GLY titrations

Log K_{ML} = 3.14, this agrees with the literature [17], log K_{MLH-1} = 8.18, this agrees well with the literature, log K_{MLH-2} = 9.98 (Table 3.13).

Table 3.13: Calculated equilibrium constants for Zn(II)/GLY-GLY complexes

p q r	Log β	$\sigma_{p\,q\,r}$	R^H	R^H_{lim}	nT(nP)	Log K_{exp}	Log K_{lit}[17]
1 1 0	3.14	0.02				3.14	3.44
1 2 0	-	-				-	6.31
1 1 1	-	-	0.01	0.02	2(63)	-	5.60
1 1 -1	-4.60	0.03				8.18	8.24
1 1 -2	-13.8	0.05				9.98	-

Q_M-bar for this titration is given in Figure 3.30. Q_M-bar rises at pH 5.9. The slope of this curve changes (but it does not level off) between pH 8.2 and pH 9.0. The slope of the graph changes again from pH 9.0 to pH 11.0. This shows that complexation starts at pH 5.9 and stops at pH 8.2. However the production of the hydroxo species is rapid and the distribution curve for MLH_{-1} almost overlaps that of ML, therefore Q_M-bar does not level off as an indication that ML has finished forming, before rising again as an indication that hydroxo species have begun to form. One proton was lost upon complexation with Cu(II).

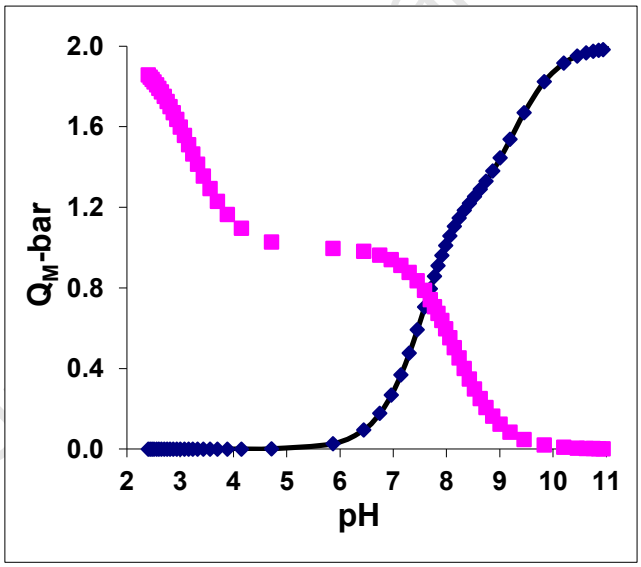

Figure 3.30: Q_M-bar as a function of pH for the Zn(II)/GLY-GLY titrations. Pink curve is n-bar, blue curve is experimental Q-bar and the solid line is the theoretical plot.

Speciation for Zn(II)/GLY-GLY is given in Figure 3.31. The gap between ML distribution curve and MLH_{-1} distribution curve is very small (0.70 pH units apart). At pH 7.8 where ML stops forming, the amount of ML is equal to the amount of MLH_{-1} present in solution. The production of MLH_{-1} stops at pH 8.5.

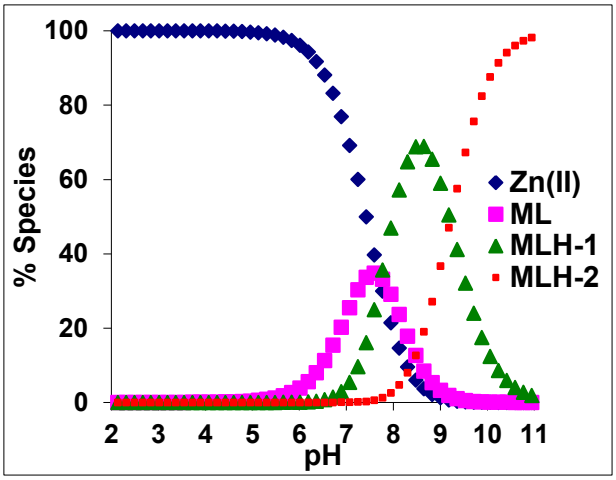

Figure 3.31: Speciation for complex formation titrations of Zn(II)/GLY-GLY, 1:2 ratio. [GLY-GLY] = 0.004192 M.

3.4.2.4 Sarcosyl-glycine complexes

3.4.2.4.1 SAR-GLY / Cu(II)

Z_M-bar levels off at 1.5. Hydroxo species start to form at pL 4.1 where the curve flags back.

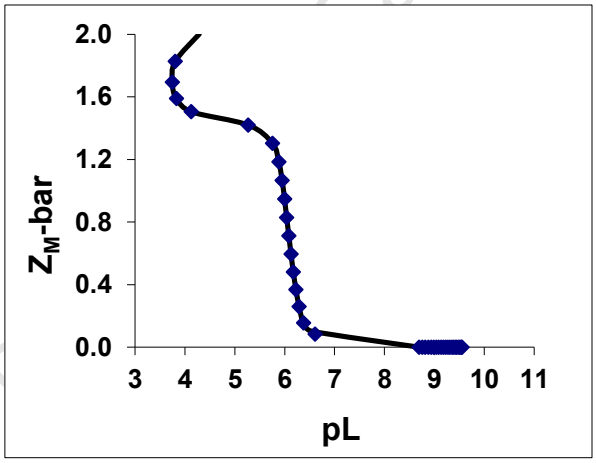

Figure 3.32: Z_M-bar as a function of pL for the Cu(II)/SAR-GLY titrations

Log K_{ML} = 6.15, this is slightly higher than the literature [17, 25]. Log K's are affected by the ionic strength, the difference between the experimental and the literature is due to the differences in ionic strength.

Table 3.14: Calculated equilibrium constants for Cu(II)/SAR-GLY complexes

p q r	Log β	σ_{pqr}	R^H	R^H_{lim}	nT(nP)	Log K_{exp}	Log K_{lit}[17]
1 1 0 1 2 0 1 2 -1 1 2 -2	6.15 11.1 2.12 -8.77	0.08 0.09 0.10 0.10	0.01	0.05	2(81)	6.15 4.45 8.35 11.5	5.32 3.96 - -

SAR-GLY lost two protons upon complexation with Cu(II) (Figure 3.33). Between pH 7.7 and pH 8.7 complexation was complete. Hydroxo species started to form from pH 8.7.

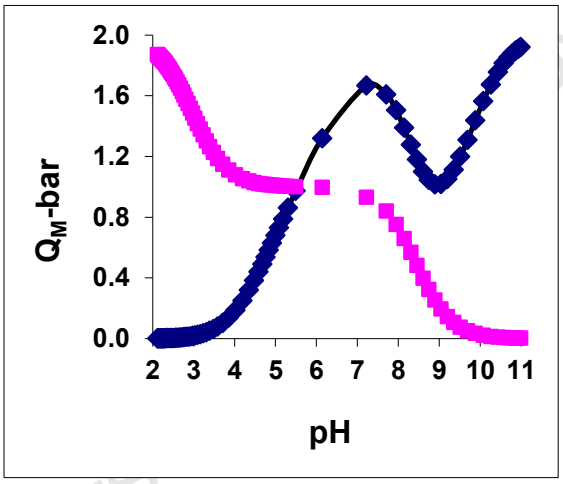

Figure 3.33: Q_M-bar as a function of pH for the Cu(II)/SAR-GLY titrations. Pink curve is n-bar, blue curve is experimental Q-bar and the solid line is the theoretical plot.

The speciation for Cu(II)/SAR-GLY is shown in Figure 3.34.

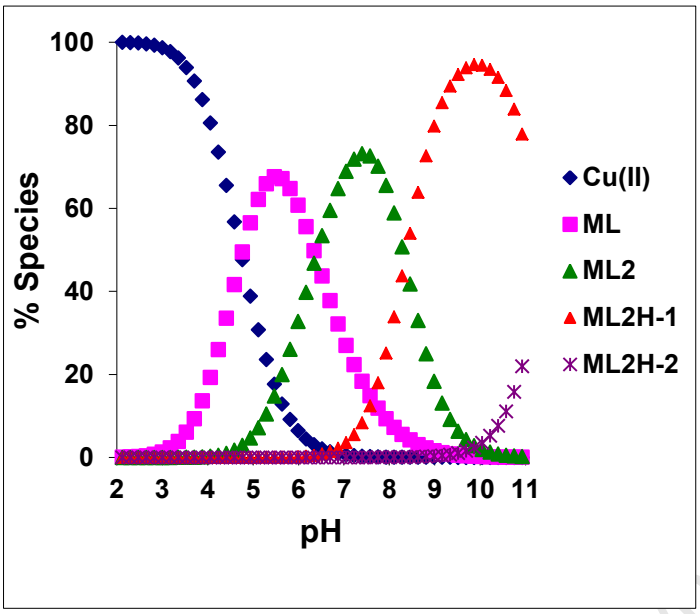

Figure 3.34: Speciation for complex formation titrations of Cu(II)/SAR-GLY, 1:2 ratio. [SAR-GLY] = 0.004649 M.

3.4.2.4.2 SAR-GLY / Ni(II)

Z_M-bar for Ni(II)/SAR-GLY is given in Figure 3.35.

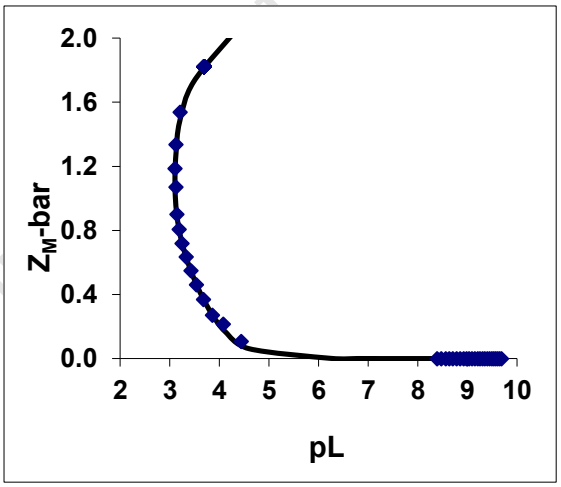

Figure 3.35: Z_M-bar as a function of pL for the Ni(II)/SAR-GLY titrations

Log K_{ML} = 3.41, log K_{MLH-1} = 8.79 and log K_{MLH-2} = 10.5 (Table 3.15). This titration has not been reported before, however the standard deviations are small and R^H is less than R^H_{lim}. This gives confidence in the model.

Table 3.15: Calculated equilibrium constants for Ni(II)/SAR-GLY complexes

p q r	Log β	$\sigma_{p\,q\,r}$	R^H	R^H_{lim}	nT(nP)	Log K_{exp}
1 1 0	3.41	0.04				3.41
1 1 -1	-5.38	0.03	0.01	0.03	2(81)	8.79
1 1 -2	-15.9	0.06				10.5

SAR-GLY has two dissociable protons and it loses one proton upon complexation with Ni(II) (Figure 3.36). Complexation was complete at pH 8.5 and hydroxo species formed between pH 8.5 and pH 11.0.

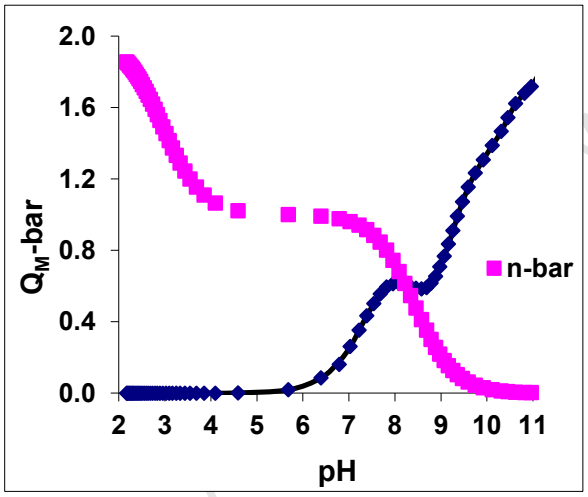

Figure 3.36: Q_M-bar as a function of pH for the Ni(II)/SAR-GLY titrations. Pink curve is n-bar, blue curve is experimental Q-bar and the solid line is the theoretical plot.

The distribution graph for Ni(II)/SAR-GLY is given in Figure 3.37. There was no chemical change from pH 2 to pH 5.1. The base of ML distribution is 5.1 pH units long (from pH 5.1 to pH 10.2). MLH_{-1} exists between pH 7.2 and pH 11.0 and MLH_{-2} begins to form at pH 8.6.

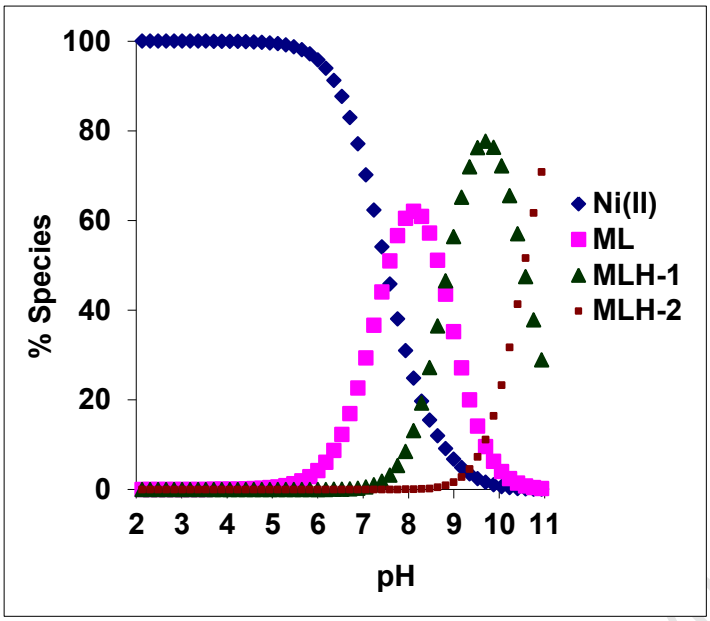

Figure 3.37: Speciation for complex formation titrations of Ni(II)/SAR-GLY, 1:2 ratio. [SAR-GLY] = 0.004585 M.

3.4.2.4.3 SAR-GLY / Zn(II)

Z_M-bar for Zn(II)/SAR-GLY is given in Figure 3.38.

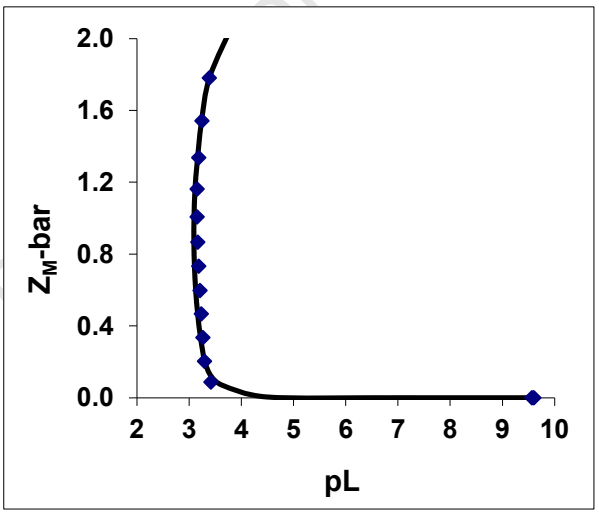

Figure 3.38: Z_M-bar as a function of pL for the Zn(II)/SAR-GLY titrations

ML species formed between Zn(II) and SAR-GLY are very unstable since log K_{ML} is very small (log K_{ML} = 2.08). Only two species formed in this titration, ML and MLH_{-1}. The most predominant species is MLH_{-1} (log K = 7.53). There is no published data on this titration, $R^H \approx R^H_{lim}$ therefore the model could not be modified to any further extent.

Table 3.16: Calculated equilibrium constants for Zn(II)/SAR-GLY complexes

p q r	Log β	σ_{pqr}	R^H	R^H_{lim}	nT(nP)	Log K_{exp}
1 1 0 1 1 -1	2.08 -5.45	0.9 0.3	0.09	0.1	2(81)	2.08 7.53

SAR-GLY loses one proton upon complexation with Zn(II) (Figure 3.39). Q_M-bar rises from pH 7.0 and levels off between pH 8.8 and pH 11.0. There is a small depression between pH 9.3 and pH 9.9. This shows that ML forms between pH 7.0 and pH 9.3. The depression is due to the formation of hydroxo (MLH_{-1}) species.

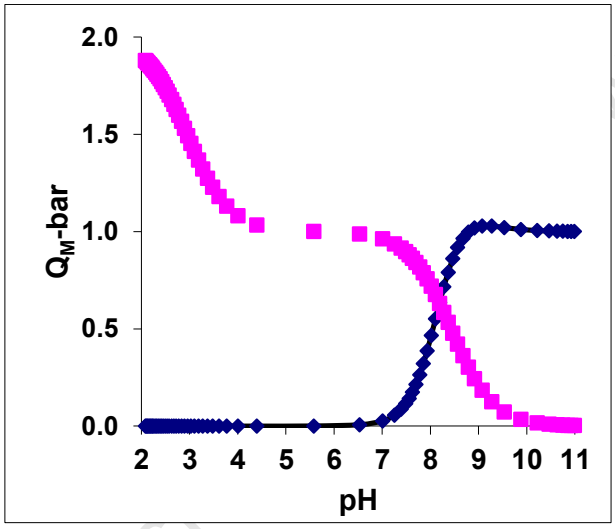

Figure 3.39: Q_M-bar as a function of pH for the Zn(II)/SAR-GLY titrations. Pink curve is n-bar, blue curve is experimental Q-bar and the solid line is the theoretical plot.

The distribution graph for Zn(II)/SAR-GLY is given in Figure 3.40. A very small amount of Cu(II) existed in ML form. ML and MLH_{-1} started forming around the same pH (pH 7.2).

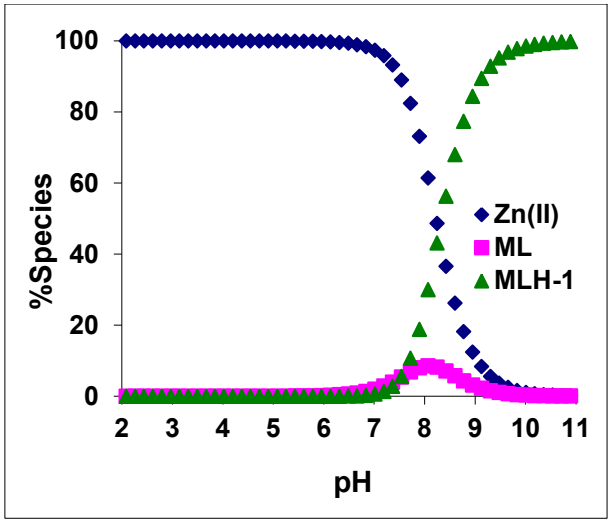

Figure 3.40: Speciation for complex formation titrations of Zn(II)/SAR-GLY, 1:2 ratio. [SAR-GLY] = 0.004564 M.

3.4.2.5 Glycyl-L-leucine complexes

3.4.2.5.1 GLY-LEU / Cu(II)

Z_M-bar for Cu(II)/GLY-LEU t is given in Figure 3.41.

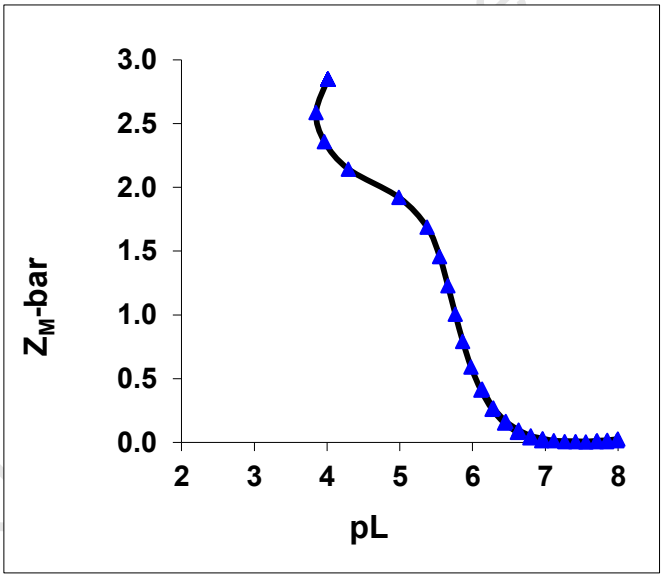

Figure 3.41: Z_M-bar as a function of pL for the Cu(II)/GLY-LEU titrations

Log K's for complexes formed between Cu(II) and GLY-LEU are given in Table 4.17. These agree with the literature [17, 26-27].

Table 3.17: Calculated equilibrium constants for Cu(II)/GLY-LEU complexes

p q r	Log β	$\sigma_{p\,q\,r}$	R^H	R^H_{lim}	nT(nP)	Log K_{exp}	Log K_{lit}[17]
1 1 0	5.79	0.02				5.79	5.93
1 1 -1	1.08	0.05				4.71	4.70
1 1 -2	-	-	0.01	0.04	2(72)	-	9.50
1 2 -1	4.19	0.08				3.57	3.56
2 2 -3	-3.03	0.16				1.78	2.27

Q_M-bar is given in Figure 3.42. Complexation starts at very low pH's (from pH 2.6) for Cu(II)/GLY-LEU titrations. Complexation was complete between pH 7.0 and pH 9.4 where hydroxo species began to form. Two protons were lost upon complexation of GLY-LEU with Cu(II).

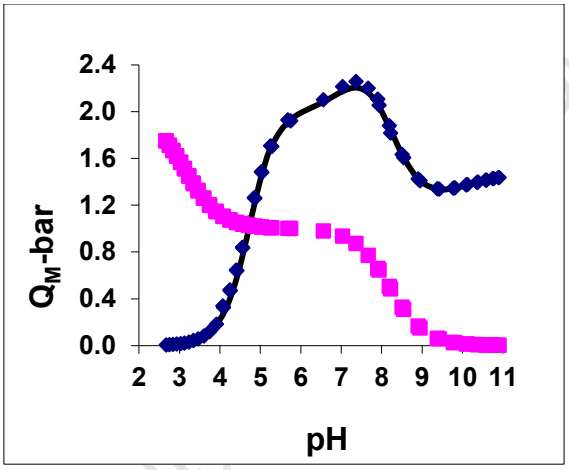

Figure 3.42: Q_M-bar as a function of pH for the Cu(II)/GLY-LEU titrations. Pink curve is n-bar, blue curve is experimental Q-bar and the solid line is the theoretical plot.

The speciation for Cu(II)/GLY-LEU titrations is given in Figure 3.43. Mixed species were observed at all pH's except at pH's below 2.6 where there was about 100 % Cu(II) in solution, and at pH's above 11.6 where almost all Cu(II) ion in solution existed in $M_2L_2H_{-3}$ form.

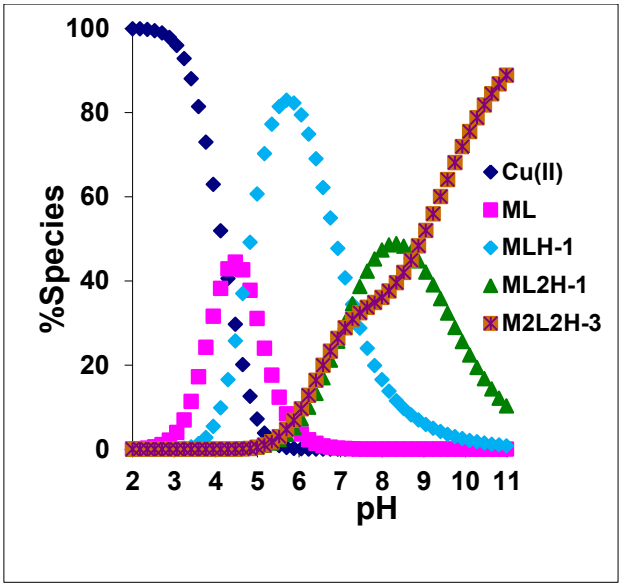

Figure 3.43: Speciation for complex formation titrations of Cu(II)/GLY-LEU, 1:2 ratio. [GLY-LEU] = 0.009143 M.

3.4.2.5.2 GLY-LEU / Ni(II)

Z_M-bar for Ni(II)/GLY-LEU titrations is given in Figure 3.44.

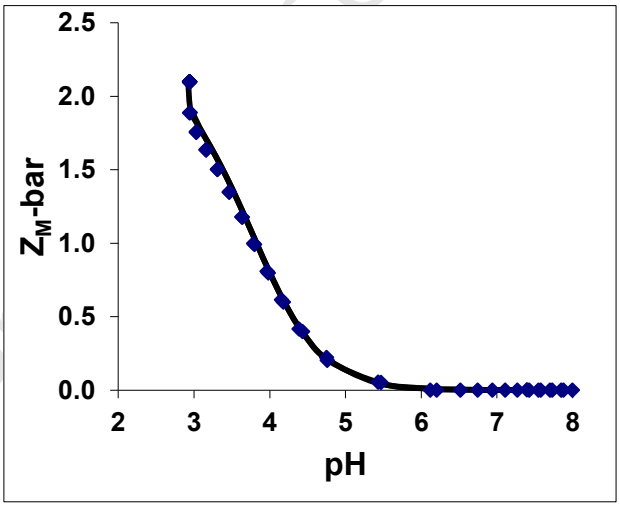

Figure 3.44: Z_M-bar as a function of pL for the Ni(II)/GLY-LEU titrations

Equilibrium constants for Ni(II)/GLY-LEU titrations are given in Table 3.18. These agree with the literature [17]. Log K_{ML} (Cu(II)/GLY-LEU) is 1.61 log larger than log K_{ML} (Ni(II)/GLY-LEU). ML species of Cu(II) and GLY-LEU are therefore more stable than ML species of Ni(II) and GLY-LEU.

Table 3.18: Calculated equilibrium constants for Ni(II)/GLY-LEU complexes

p q r	Log β	σ_{pqr}	R^H	R^H_{lim}	nT(nP)	$LogK_{exp}$	Log K_{lit}[17]
1 1 0	4.18	0.04	0.03	0.01	2(68)	4.18	4.24
1 2 0	7.56	0.06				3.38	3.43
1 3 0	9.64	0.30				2.08	2.80
1 2 -1	-2.25	0.05				9.81	9.90

One proton is lost when GLY-LEU forms complexes with Ni(II) (Figure 4.5). Complexation stopped bewteen pH 7.4 and pH 9.1 where hydroxo species began to form.

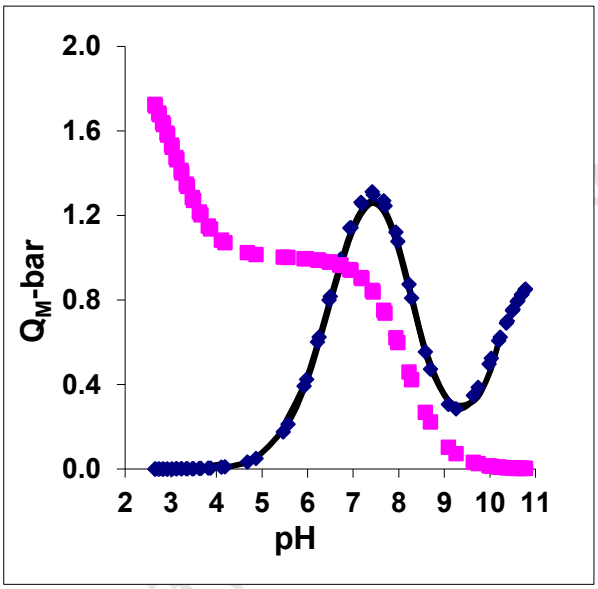

Figure 3.45: Q_M-bar as a function of pH for the Zn(II)/GLY-LEU titrations. Pink curve is n-bar, blue curve is experimental Q-bar and the solid line is the theoretical plot.

The distribution curve for this titration is given in Figure 3.46. ML_2H_{-1} species is the most predominant species in solution; however this forms at high pH's (from pH 7.8). ML_3 is the least predominant species.

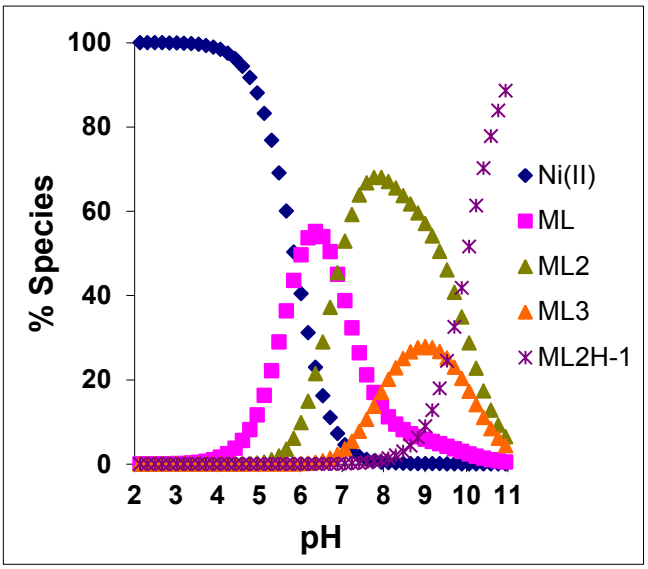

Figure 3.46: Speciation for complex formation titrations of Ni(II)/GLY-LEU, 1:2 ratio. [GLY-LEU] = 0.016101 M.

3.4.2.5.3 GLY-LEU / Zn(II)

Z_M-bar for Ni(II)/GLY-LEU titrations is shown in Figure 3.47.

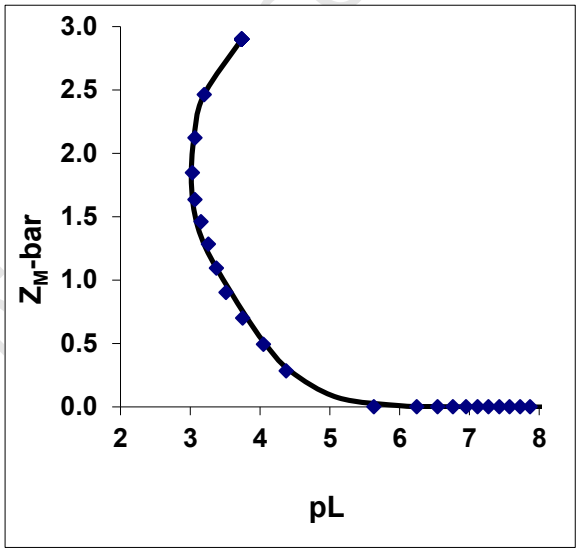

Figure 3.47: Z_M-bar as a function of pL for the Zn(II)/GLY-LEU titrations

Four species were observed for this titration and the equilibrium constants are given in Table 3.19. These agree with the literature [17]. Log K_{ML} (Zn(II)/GLY-LEU) < Log K_{ML} (Ni(II)/GLY-LEU) < Log K_{ML} (Cu(II)/GLY-LEU). GLY-LEU is therefore more selective of Cu(II) than Ni(II) and Zn(II).

Table 3.19: Calculated equilibrium constants for Zn(II)/GLY-LEU complexes

p q r	Log β	σ_{pqr}	R^H	R^H_{lim}	nT(nP)	Log K_{exp}	Log K_{lit}[17]
1 1 0	3.93	0.02	0.01	0.03	2(34)	3.93	3.86
1 2 0	6.79	0.10				2.86	2.89
1 1 -1	-4.22	0.10				8.15	-
1 1 -2	-12.5	0.08				8.31	-

Q_M-bar for Cu(II)/GLY-LEU titrations is given in Figure 4.48. Complexation begins at pH 4.7 and stops between pH 7.7 and pH 8.2. Hydroxo species form from pH 8.2. GLY-LEU lost one proton upon complexation with Zn(II).

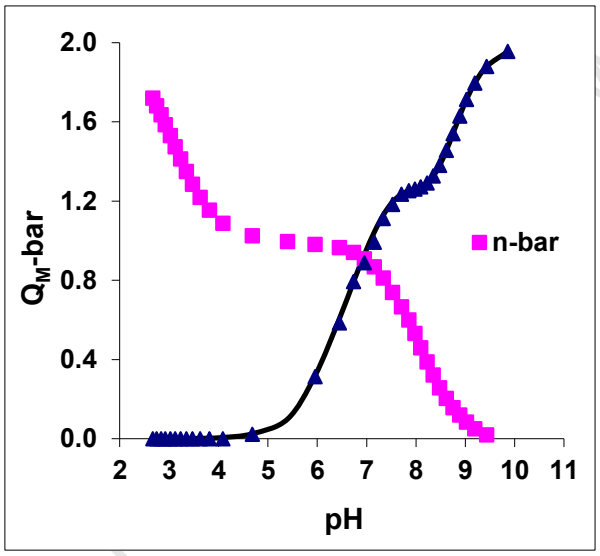

Figure 3.48: Q_M-bar as a function of pH for the Zn(II)/GLY-LEU titrations. Pink curve is n-bar, blue curve is experimental Q-bar and the solid line is the theoretical plot.

The distribution curve for Zn(II)/GLY-LEU is given in Figure 3.49. From pH 2.0 to pH 6.2 zinc mostly exists as free ions. From pH 6.5 to pH 7.7, zinc exists as ML. Between pH 7.9 and pH 8.5 zinc mostly exists in its ML_2 form and from pH 8.6 to pH 11.0, zinc exists mostly in its MLH_{-2} form. MLH_{-1} was observed but at low concentrations.

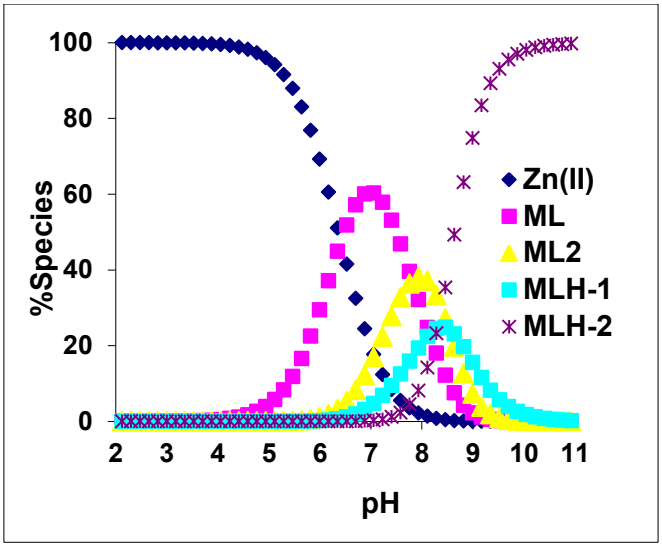

Figure 3.49: Speciation for complex formation titrations of Zn(II)/GLY-LEU, 1:2 ratio. [GLY-LEU] = 0.008003 M.

3.4.2.6 Sarcosyl-L-leucine complexes

3.4.2.6.1 SAR-LEU / Cu(II)

Z_M-bar for Cu(II)/SAR-LEU titrations is shown in Figure 3.50. The graph flags back at low pL's indicating the formation of hydroxo species.

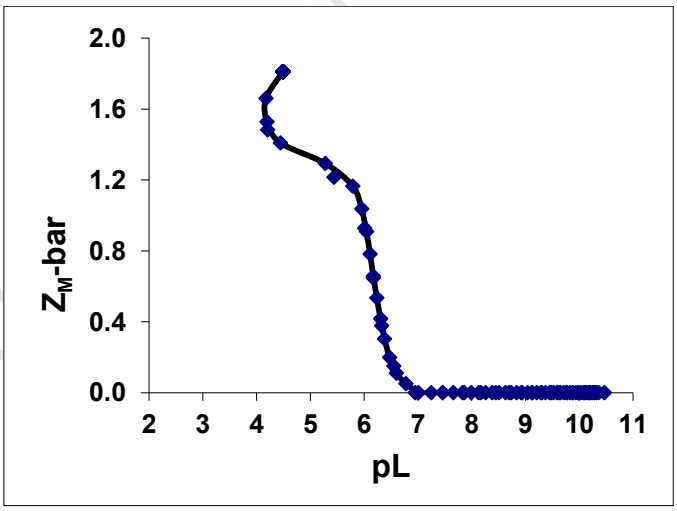

Figure 3.50: Z_M-bar as a function of pL for the Cu(II)/SAR-LEU titrations

Stability constants for complexes formed between Cu(II) and SAR-LEU are given in Table 3.20. Log K_{ML} is 1.00 log units larger than the literature [15]. The difference in these values is due to the fact that Datta and co-workers [15] used zero ionic strength and 0.15 M ionic strength was used in this study. Log K_{ML2} compares well with the literature [15].

Table 3.20: Calculated equilibrium constants for Cu(II)/SAR-LEU complexes

p q r	Log β	σ_{pqr}	R^H	R^H_{lim}	nT(nP)	Log K_{exp}	Log K_{lit}[17]
1 1 0	6.32	0.04	0.03	0.009	3(194)	6.32	5.32
1 2 0	10.3	0.07				4.01	4.35
1 1 -1	-1.25	0.06				7.57	-
1 1 -2	-11.6	0.06				10.3	-

Q_M-bar for this titration is given in Figure 4.51. SAR-LEU loses one protons upon complexation with Cu(II). From pH 8.1 to pH 9.2 Q_M-bar runs parallel n-bar therefore complexation was complete at this pH range. Q_M-bar rises from pH 9.2 indicating the formation of hydroxo species.

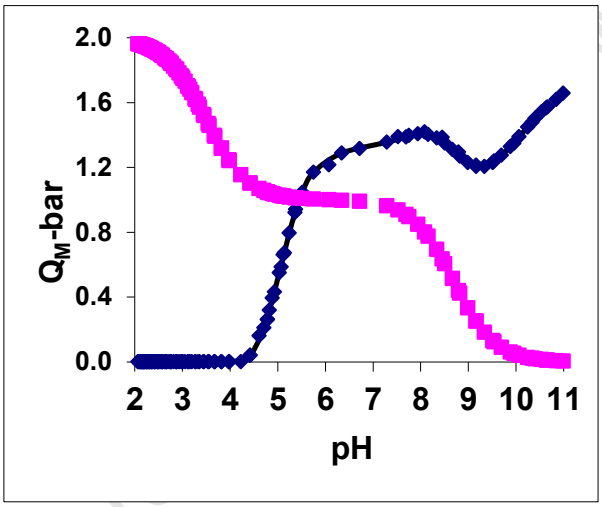

Figure 3.51: Q_M-bar as a function of pH for the Cu(II)/SAR-LEU titrations. Pink curve is n-bar, blue curve is experimental Q-bar and the solid line is the theoretical plot.

The distribution curve for Cu(II)/SAR-LEU titrations is given in Figure 3.52. Complexation starts at pH 2.8.

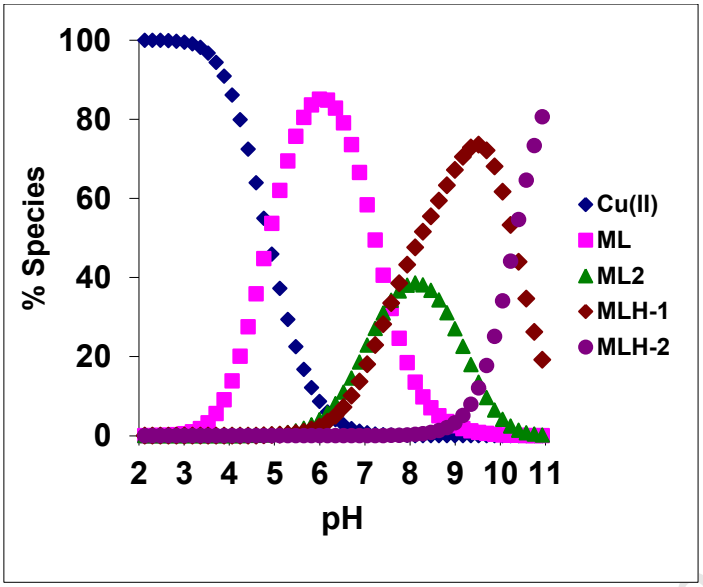

Figure 3.52: Speciation for complex formation titrations of Cu(II)/SAR-LEU, 1:2 ratio. [SAR-LEU] = 0.004366 M.

3.4.2.6.2 SAR-LEU / Ni(II)

The results are given in Figure 3.53.. Hydroxo species form at pL's where the graph flags back.

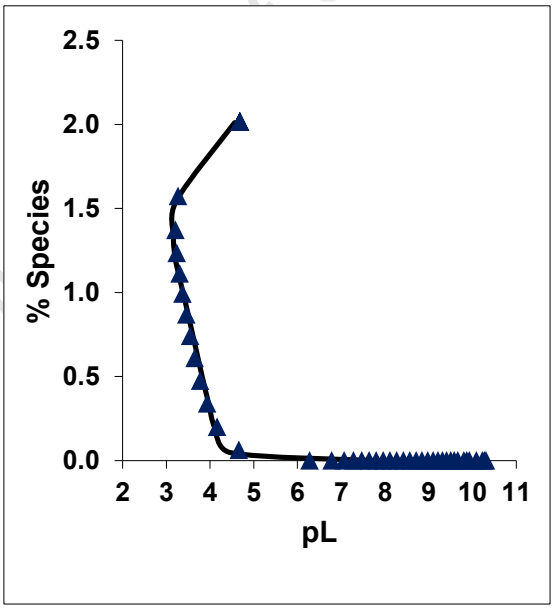

Figure 3.53: Z_M-bar as a function of pL for the Ni(II)/SAR-LEU titrations

Stability constants for Ni(II)/SAR-LEU are given in Table 3.21. There is no published data on this titration however the standard deviations are small and R^H is less than R^H_{lim}. The model is accurate.

Table 3.21: Calculated equilibrium constants for Ni(II)/SAR-LEU complexes

p q r	Log β	σ_{pqr}	R^H	R^H_{lim}	nT(nP)	Log K_{exp}
1 1 0	3.85	0.05	0.009	0.03	2(77)	3.85
1 2 0	6.69	0.03				2.84
1 1 -1	-5.94	0.03				9.52
1 1 -2	-16.9	0.07				10.7

Q_M-bar is given in Figure 3.54. Complexation begins at pH 5.8 and stops between pH 8.1 and pH 9.2. SAR-LEU loses one proton upon complexation with Ni(II).

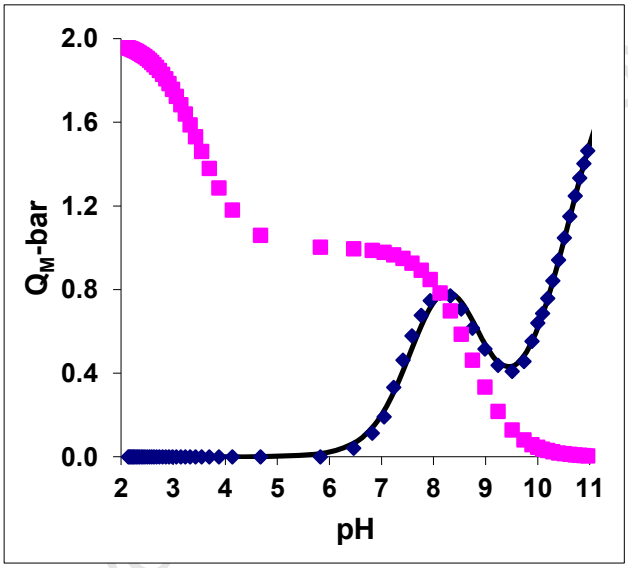

Figure 3.54: Q_M-bar as a function of pH for the Ni(II)/SAR-LEU titrations. Pink curve is n-bar, blue curve is experimental Q-bar and the solid line is the theoretical plot.

The speciation graph for this titration is given in Figure 3.55. From pH 2.0 to pH 7.8 the system consists mostly of Ni(II).

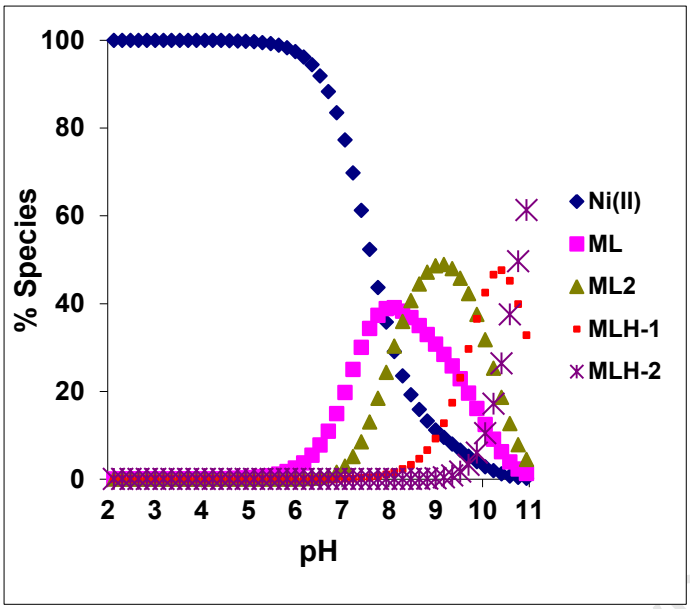

Figure 3.55: Speciation for complex formation titrations of Ni(II)/SAR-LEU, 1:2 ratio. [SAR-LEU] = 0.004306 M.

3.4.2.6.3 SAR-LEU / Zn(II)

Z_M-bar for Zn(II)/SAR-LEU titrations is shown in Figure 3.56.

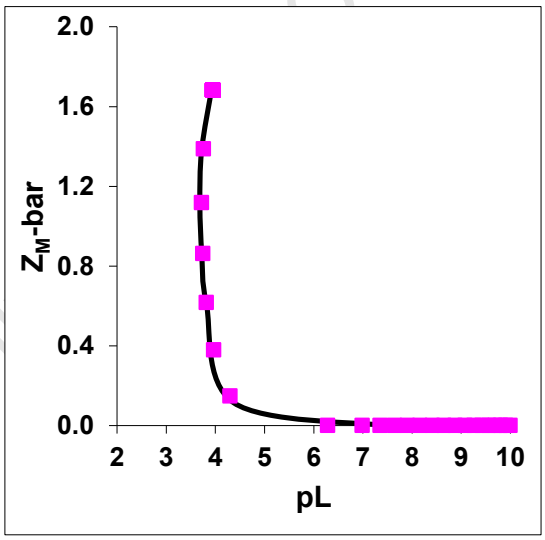

Figure 3.56: Z_M-bar as a function of pL for the Zn(II)/SAR-LEU titrations

Equilibrium constants for complexes formed between Zn(II) and SAR-LEU are given in Table 3.22. SAR-LEU is more selective for Cu(II) than for Ni(II) and Zn(II).

Table 3.22: Calculated equilibrium constants for Zn(II)/SAR-LEU complexes

p q r	Log β	σ_{pqr}	R^H	R^H_{lim}	nT(nP)	Log K_{exp}
1 1 0	3.40	0.1				3.40
1 1 -1	-4.25	0.06	0.009	0.02	2(51)	7.65
1 1 -2	-13.7	0.07				9.45

Q_M-bar (Figure 3.57) rises at pH 5.8 and levels off at Q_M-bar = 1.7 between pH 8.6 and pH 9.8. It does not drop before it rises again. This indicates that SAR-LEU loses two protons upon complexation with Zn(II), and ML species and MLH_{-1} species form at about the same pH.

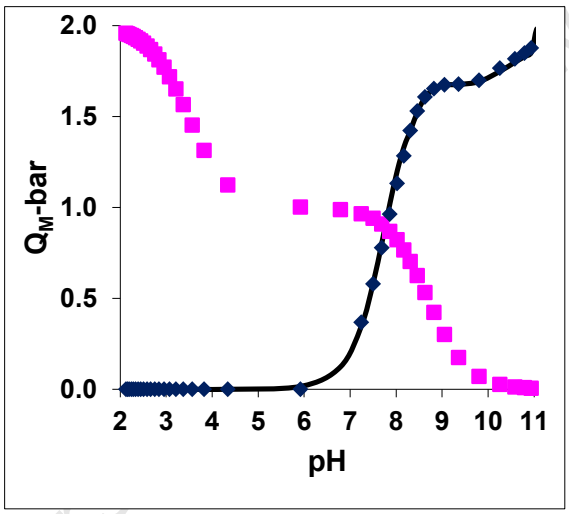

Figure 3.57: Q_M-bar as a function of pH for the Zn(II)/SAR-LEU titrations. Pink curve is n-bar, blue curve is experimental Q-bar and the solid line is the theoretical plot.

Speciation graph for Zn(II)/SAR-LEU titrations is given in Figure 3.58. ML is mostly predominant in solution between pH 6.7 and pH 7.4. MLH_{-1} is mostly predominant in solution between pH 7.8 and pH 9.2. MLH_{-2} is predominant from pH 9.6 to pH 11.0.

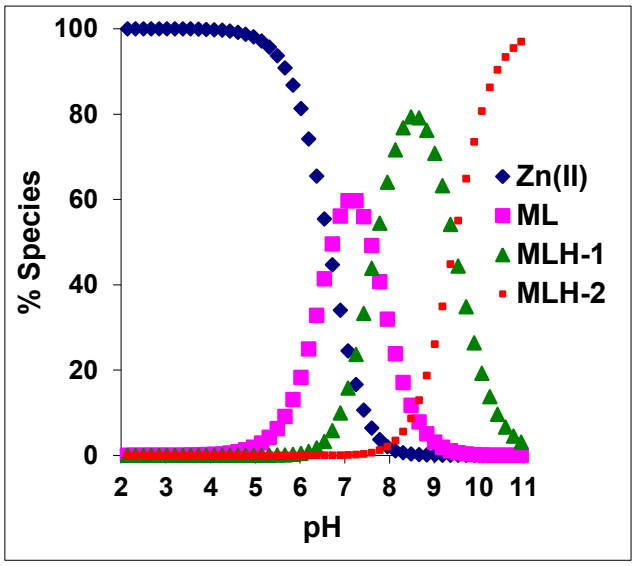

Figure 3.58: Speciation for complex formation titrations of Zn(II)/SAR-LEU, 1:2 ratio. [SAR-LEU] = 0.004191 M.

3.4.2.7 Glycyl-L-phenylalanine complexes

3.4.2.7.1 GLY-PHE / Cu(II)

Z_M-bar for Cu(II)/GLY-PHE is given in Figure 4.59.

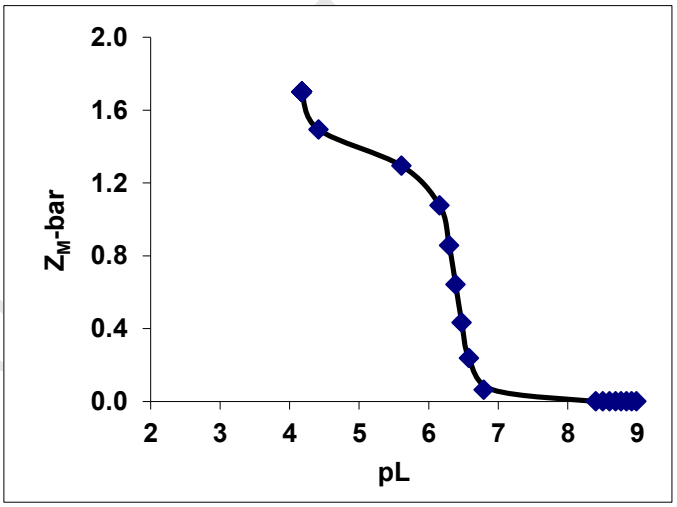

Figure 3.59: Z_M-bar as a function of pL for the Cu(II)/GLY-PHE titrations

Equilibrium constants for these titrations are given in Table 3.23. Only four species were observed (ML, ML_2, MLH_{-1} and MLH_{-2}). The equilibrium constants for these species are comparable with the literature [16, 17, 19], except for ML_2 which was not observed in the literature. The standard deviations are small and R^H is less than R^H_{lim} therefore the model is accurate.

Table 3.23: Calculated equilibrium constants for Cu(II)/GLY-PHE complexes

p q r	Log β	$\sigma_{p\,q\,r}$	R^H	R^H_{lim}	nT(nP)	Log K_{exp}	Log K_{lit}[17]
1 1 0	6.37	0.04				6.37	5.70
1 2 0	11.5	0.08				5.16	-
1 1 -1	-	-				-	3.87
1 1 -2	-	-	0.009	0.01	2(61)	-	9.37
1 2 -1	2.59	0.1				3.78	3.22
1 2 -2	-8.18	0.1				10.8	12.5
2 2 -3	-	-				-	2.38

Two protons were lost upon complexation of GLY-PHE with Cu(II) (Figure 3.60). Complexation was complete between pH 7.1 and pH 8.6. Hydroxo formed from pH 8.6.

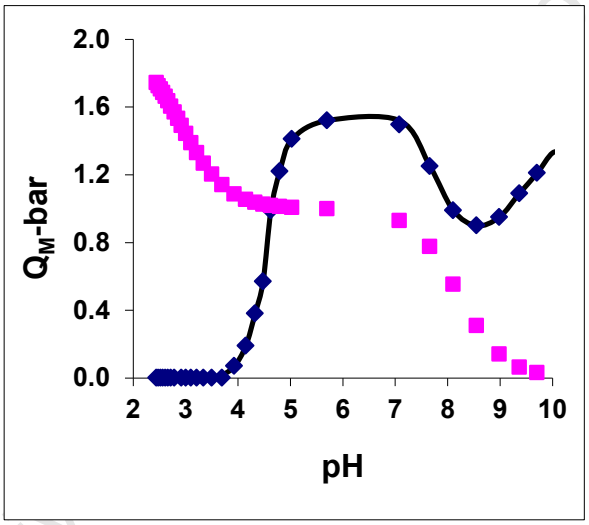

Figure 3.60: Q_M-bar as a function of pH for the Cu(II)/GLY-PHE titrations. Pink curve is n-bar, blue curve is experimental Q-bar and the solid line is the theoretical plot.

The speciation graph for Cu(II)/GLY-PHE is given in Figure 3.61. Complexation begins at pH 2.2 and ML species exist for quite a wide range (from H 2.2 to pH 11.0). ML is most predominant in solution between pH's 4.7 and 6.1. ML_2 is most predominant in solution from pH 6.5 to pH 8.8. MLH_{-1} is mostly predominant in solution between pH's 9.1 and 10.5. MLH_{-2} species is most predominant from pH 10.9 to pH 11.0.

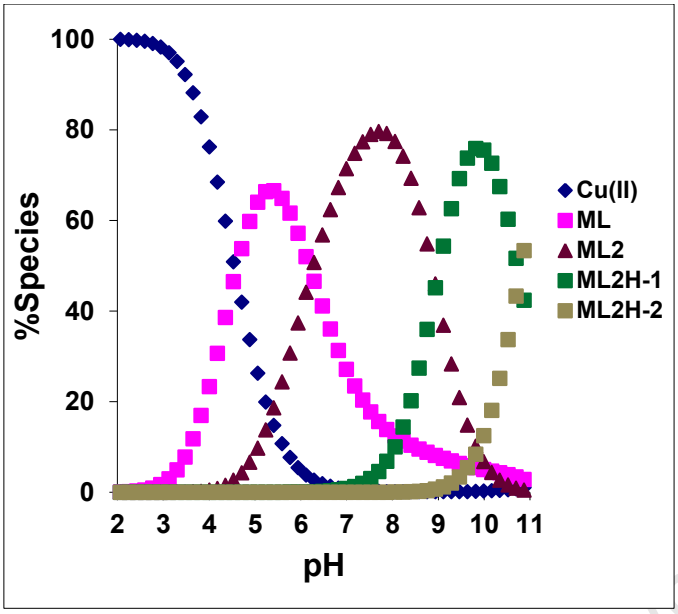

Figure 3.61: Speciation for complex formation titrations of Cu(II)/GLY-PHE, 1:2 ratio. [GLY-PHE] = 0.004542 M.

3.4.2.7.2 GLY-PHE / Ni(II)

Z_M-bar for Ni(II)/GLY-PHE titrations is given in Figure 3.62.

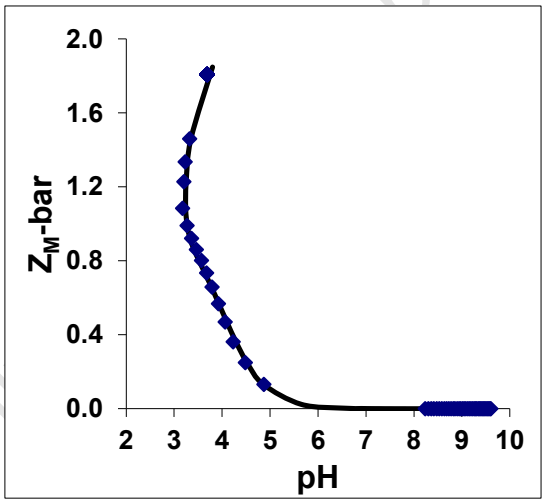

Figure 3.62: Z_M-bar as a function of pL for the Ni(II)/GLY-PHE titrations

Species formed between Ni(II) and GLY-PHE and their stability constants are given in Table 3.24. Only three species were observed (ML, MLH_{-1} and MLH_{-2}).

Table 3.24: Calculated equilibrium constants for Ni(II)/GLY-PHE complexes

p q r	Log β	σ_{pqr}	R^H	R^H_{lim}	nT(nP)	Log K_{exp}	Log K_{lit}
1 1 0	3.75	0.03				3.75	4.03
1 2 0	-	-				-	7.49
1 3 0	-	-	0.008	0.02	2(121)	-	9.80
1 1 -1	-5.40	0.06				9.14	8.59
1 1 -2	-15.6	0.06				10.2	-
1 2 -2	-	-				-	18.3

Q_M-bar is given in Figure 3.63. Q_M-bar rises from pH 5.4, levels off at Q_M-bar = 0.6 (between pH 7.2 and pH 8.0). This indicates that GLY-PHE lost one proton upon complexation with Ni(II). Q_M-bar drops from pH 8.0 to pH 8.4, and rises again at pH 8.4 indicating the formation of hydroxo species.

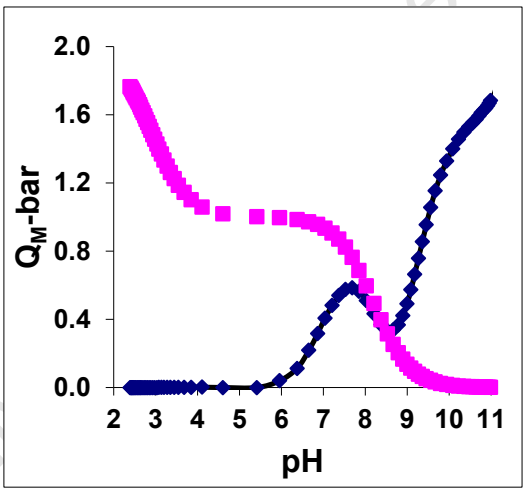

Figure 3.63: Q_M-bar as a function of pH for the Ni(II)/GLY-PHE titrations. Pink curve is n-bar, blue curve is experimental Q-bar and the solid line is the theoretical plot.

The distribution graph (Figure 3.64) shows that there was free Ni(II) in solution from pH 2.0 to pH 10.3. ML species exist between pH 5.4 and pH 10.3, MLH_{-1} occurs between pH 7.2 and pH 11.0 and MLH_{-2} occurs from pH 8.1.

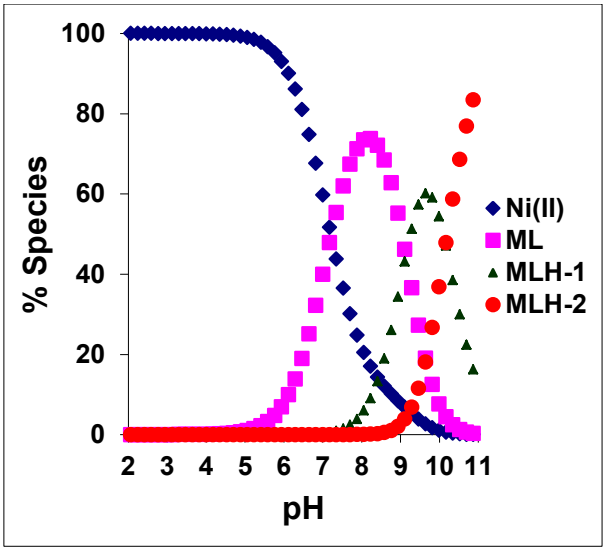

Figure 3.64: Speciation for complex formation titrations of Ni(II)/GLY-PHE, 1:2 ratio. [GLY-PHE] = 0.004529 M.

3.4.2.7.3 GLY-PHE / Zn(II)

Z_M-bar for complex formation titrations between Zn(II) and GLY-PHE are given in Figure 3.65.

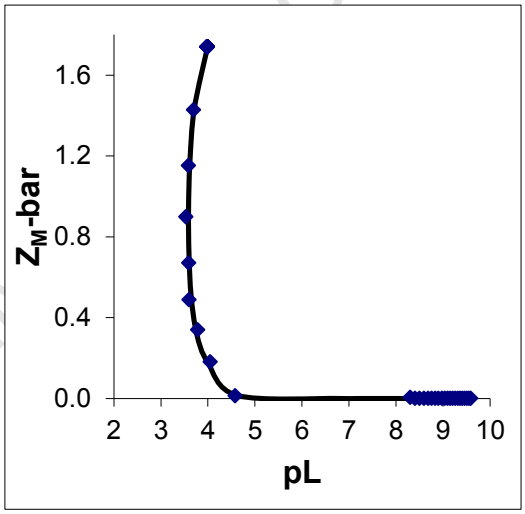

Figure 3.65: Z_M-bar as a function of pL for the Zn(II)/GLY-PHE titrations

Zn(II) and GLY-PHE form three species in solution (ML, MLH_{-1} and MLH_{-2}). Equilibrium constants for these species are given in Table 3.25.

Table 3.25: Calculated equilibrium constants for Zn(II)/GLY-PHE complexes

p q r	Log β	σ_{pqr}	R^H	R^H_{lim}	nT(nP)	Log K_{exp}
1 1 0	2.70	0.03				2.70
1 1 -1	-4.39	0.06	0.006	0.03	2(71)	7.51
1 1 -2	-14.0	0.08				9.22

Q_M-bar for this titration is given in Figure 3.66. Q_M-bar rises at pH 6.2 and levels off between pH 8.1 and pH 8.6. The graph does not drop, it rises instead. This shows that ML and MLH_{-1} begin form around the same pH.

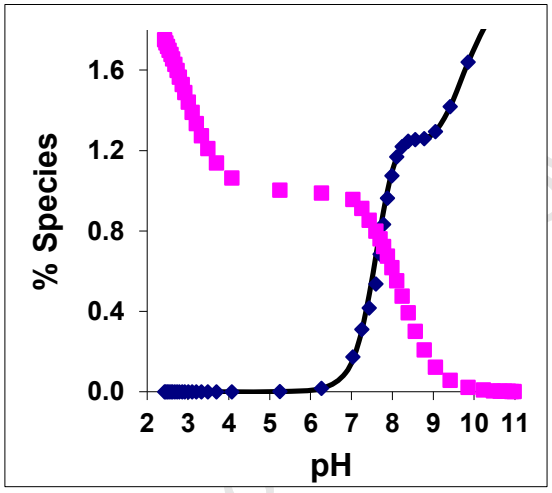

Figure 3.66: Q_M-bar as a function of pH for the Zn(II)/GLY-PHE titrations. Pink curve is n-bar, blue curve is experimental Q-bar and the solid line is the theoretical plot.

The speciation graph for Zn(II)/GLY-PHE is given in Figure 3.67.

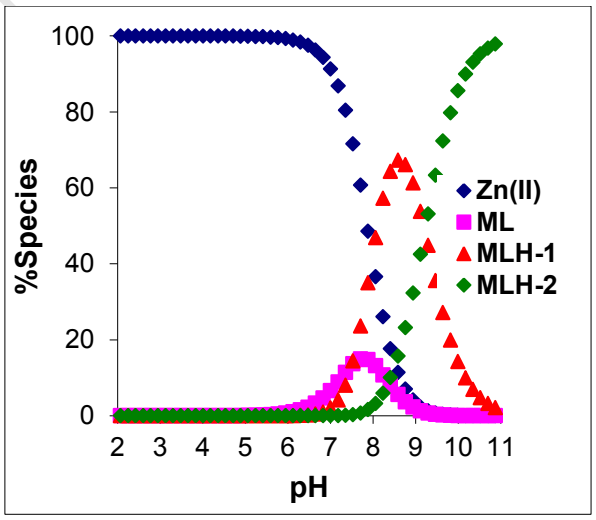

Figure 3.67: Speciation for complex formation titrations of Zn(II)/GLY-PHE, 1:2 ratio. [GLY-PHE] = 0.004482 M.

3.4.2.8 Sarcosyl-L-phenylalanine complexes

3.4.2.8.1 SAR-PHE / Cu(II)

Z_M-bar for titrations between Cu(II) and SAR-PHE is given in Figure 3.68.

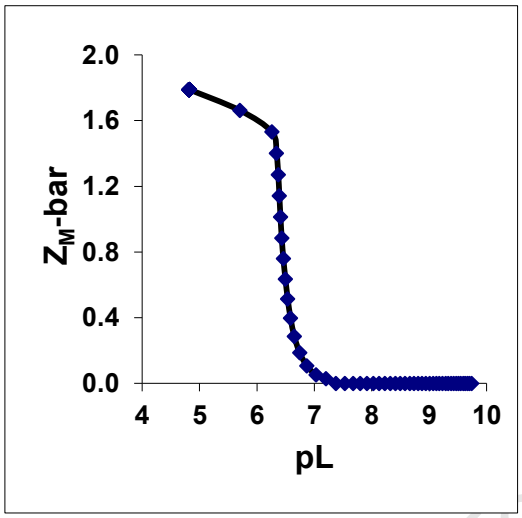

Figure 3.68: Z_M-bar as a function of pL for the Cu(II)/SAR-PHE titrations

There are three species formed between Cu(II) and SAR-PHE. The species and their equilibrium constants are given in Table 3.26. There is no published data on these titrations to compare with, however the errors a small and R^H is less than R^H_{lim}. This gives confidence in the model.

Table 3.26: Calculated equilibrium constants for Cu(II)/SAR-PHE complexes

p q r	Log β	σ p q r	R^H	R^H_{lim}	nT(nP)	Log K_{exp}
1 1 0 1 1 -1 1 1 -2	6.54 1.03 -8.89	0.03 0.07 0.10	0.01	0.04	2(81)	6.54 5.51 9.92

Q_M-bar is given in Figure 3.69. SAR-LEU loses two protons upon complexation with Cu(II).

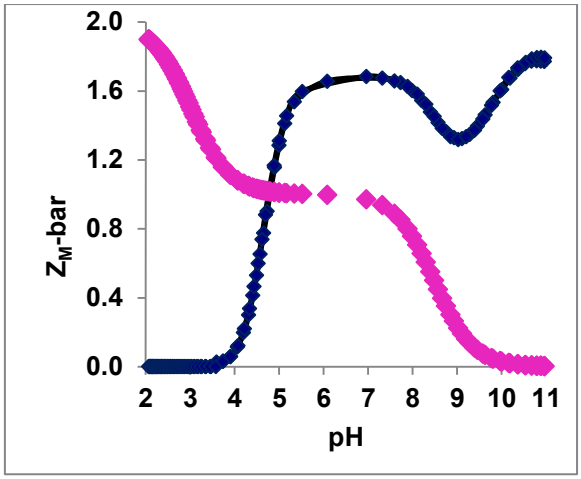

Figure 3.69: Q_M-bar as a function of pH for the Cu(II)/SAR-PHE titrations. Pink curve is n-bar, blue curve is experimental Q-bar and the solid line is the theoretical plot.

The distribution curve for this titration is given in Figure 3.70. ML occurs between pH 2.5 and pH 7.4. MLH_{-1} occurs between pH 4.0 and pH 11.0. MLH_{-2} occurs from pH 7.8.

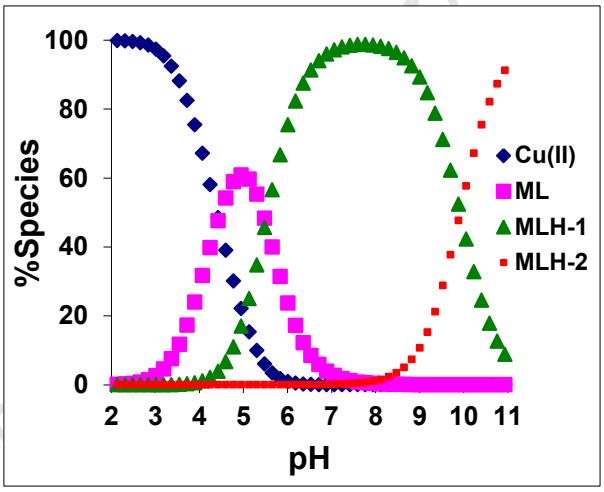

Figure 3.70: Speciation for complex formation titrations of Cu(II)/SAR-PHE, 1:2 ratio. [SAR-PHE] = 0.004533 M.

3.4.2.8.2 SAR-PHE / Ni(II)

Z_M-bar for Ni(II)/SAR-PHE titrations is given in Figure 3.71.

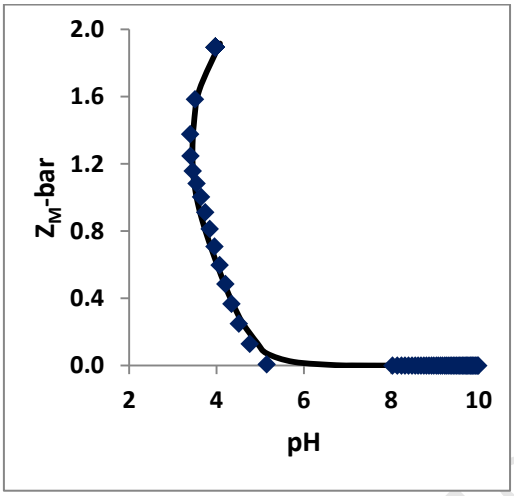

Figure 3.71: Z_M-bar as a function of pL for the Ni(II)/SAR-PHE titrations

Equilibrium constants for Ni(II)/SAR-PHE are given in Table 3.27. Four species were observed; ML, ML_2, MLH_{-1} and MLH_{-2} (K_{ML} = 4.12, K_{ML2} = 2.46, K_{MLH-1} = 8.97 and K_{MLH-2} = 10.2).

Table 3.27: Calculated equilibrium constants for Ni(II)/SAR-PHE complexes

p q r	Log β	σ_{pqr}	R^H	R^H_{lim}	nT(nP)	Log K_{exp}
1 1 0	4.12	0.02	0.009	0.02	2(121)	4.12
1 2 0	6.58	0.04				2.46
1 1 -1	-4.82	0.05				8.97
1 1 -2	-15.0	0.06				10.2

SAR-PHE loses one proton upon complexation with Ni(II) (Figure 3.72). Compleation begins at pH 5.2. Hydroxo species form from pH 8.7.

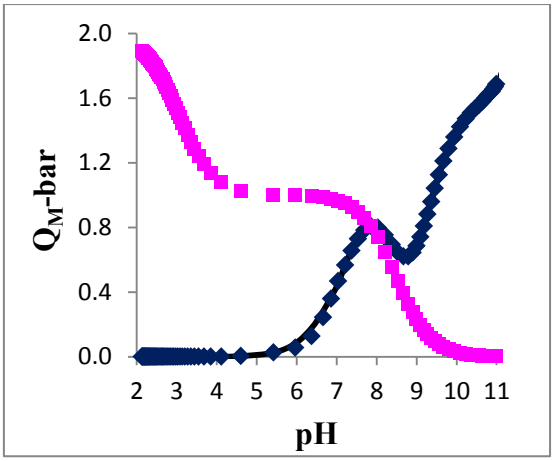

Figure 3.72: Q_M-bar as a function of pH for the Ni(II)/SAR-PHE titrations. Pink curve is n-bar, blue curve is experimental Q-bar and the solid line is the theoretical plot.

The distribution for Ni(II)/SAR-PHE titrations is given in Figure 3.73.

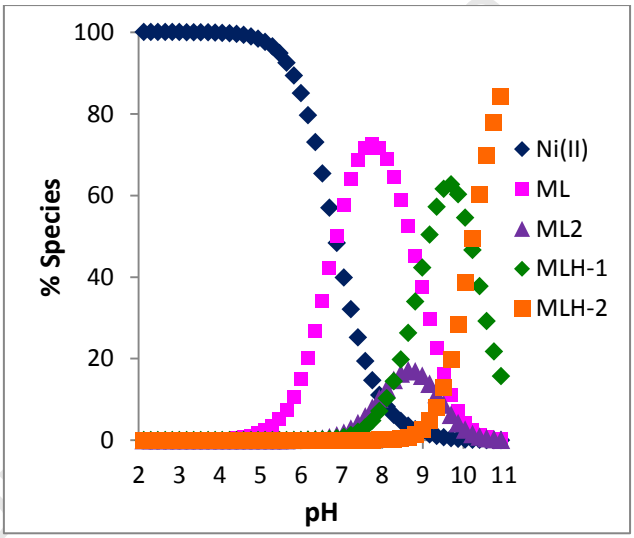

Figure 3.73: Speciation for complex formation titrations of Ni(II)/SAR-PHE, 1:2 ratio. [SAR-PHE] = 0.004287 M.

3.4.2.8.3 SAR-PHE / Zn(II)

Z_M-bar for Zn(II)/SAR-PHE titrations is given in Figure 3.74.

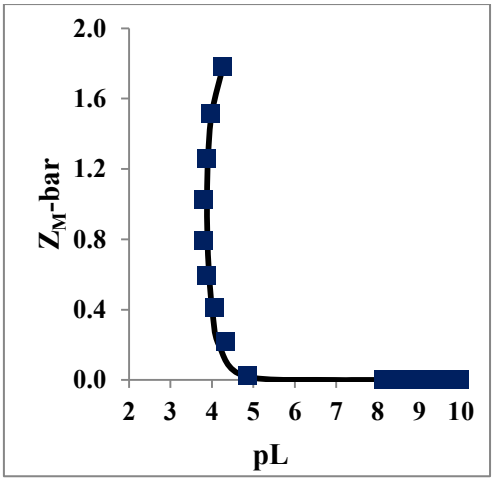

Figure 3.74: Z_M-bar as a function of pL for the Zn(II)/SAR-PHE titrations

Stability constants for species formed between Zn(II) and SAR-PHE are given in Table 3.28. Three species formed in solution. ML for Zn(II) is less stable than ML for Ni(II) and Cu(II) of the same ligand.

Table 3.28: Calculated equilibrium constants for Zn(II)/SAR-PHE complexes

p q r	Log β	σ_{pqr}	R^H	R^H_{lim}	nT(nP)	Log K_{exp}
1 1 0	2.96	0.01				2.96
1 1 -1	-3.96	0.03	0.006	0.02	2(711)	6.92
1 1 -2	-13.5	0.06				9.52

Q_M-bar is shown in Figure 3.75. SAR-PHE has two dissociable protons and it losses both protons upon complexation with Zn(II). ML and MLH_{-1} for start forming around the same pH does not drop (at pH 9.1) before rising again.

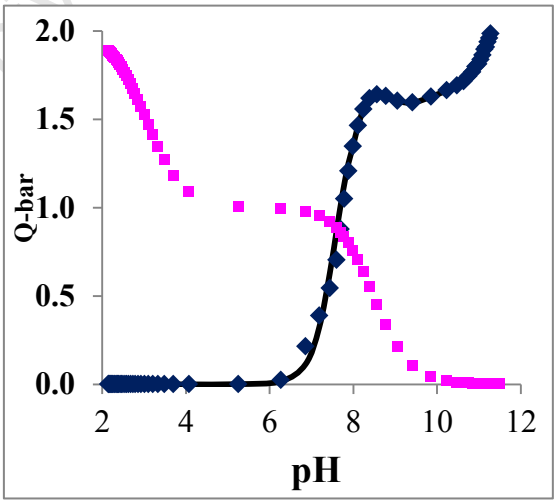

Figure 3.75: Q_M-bar as a function of pH for the Zn(II)/SAR-PHE titrations. Pink curve is n-bar, blue curve is experimental Q-bar and the solid line is the theoretical plot.

The speciation graph for this titration is given in Figure 3.76. Complexation begins at pH 5.0.

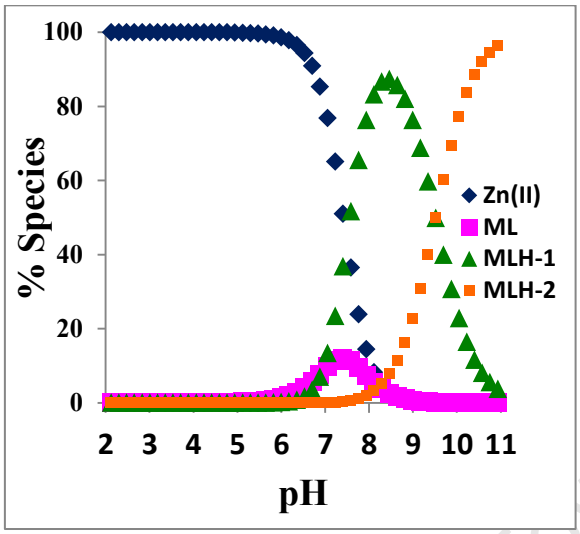

Figure 3.76: Speciation for complex formation titrations of Zn(II)/SAR-PHE, 1:2 ratio. [SAR-PHE] = 0.004513 M.

3.5 DISCUSSIONS

A summary table for the protonation constants is given in Table 3.29. The presence of the methyl group could have an inductive and steric effect. Comparing the amine protonation (log K_{LH}; GLY = 9.53; SAR = 10.0) it was observed that indeed the methyl group does have an inductive effect making the SAR amine 0.47 log units more basic. A similar effect is seen with the dipeptides, thus SAR-GLY is 0.27 log units more basic than GLY-GLY; SAR-LEU is 0.49 more basic than GLY-LEU; and SAR-PHE is 0.28 log units more basic than GLY-PHE.

The N-methyl substituent increases log K_{LH} by 0.47 log units and it decreases log K_{LH2} by 0.18 log units (pKa_1 SAR minus pKa_1 GLY; and pKa_2 SAR minus pKa_2 GLY). The peptide bond decreases log K_{LH} by 1.37 log units for GLY-GLY and decreased by 1.33 log units for GLY-LEU and GLY-PHE. The peptide bond therefore decreases log K_{LH} in glycine peptides by 1.37 log units, and the 2-methyl propyl of GLY-LEU and the methyl benzyl substituents increases log K_{LH} by 0.04 log units. Similarly, log K_{LH2} increased (from 2.29) by 0.84 (GLY-GLY), 0.85 (GLY-LEU) and 0.62 (GLY-PHE). The peptide bond increases log K_{LH2} by 0.84 log units, the 2-methyl propyl on the α-carbon of the C-terminal decreases log K_{LH2} by 0.01 and the benzyl methyl increases log K_{LH} by 0.22 log units. In sarcosine peptides, the peptide bond decreases log K_{LH} by 1.37 log units; the 2-methyl propyl decreases

log K_{LH2} by 0.06 and the benzyl methyl increases log K_{LH2} by 0.15 log units. The peptide bond increases log K_{LH2} by 0.84 log units; 2-methyl propyl decreases log K_{LH2} by 0.53 log units and the benzyl methyl increases log K_{LH} by 0.48 log units. The effect of the second amino acid on the log values is not the same in sarcosine peptides as in glycine peptides due to the inductive effect possessed by the methyl substituent.

Table 3.29: A summary table for protonation constants

Ligand	p q r	Log K_{exp}
GLY	0 1 1 0 1 2	9.53 2.29
SAR	0 1 1 0 1 2	10.0 2.11
GLY-GLY	0 1 1 0 1 2	8.16 3.18
SAR-GLY	0 1 1 0 1 2	8.43 2.95
GLY-LEU	0 1 1 0 1 2	8.20 3.14
SAR-LEU	0 1 1 0 1 2	8.69 3.48
GLY-PHE	0 1 1 0 1 2	8.20 2.91
SAR-PHE	0 1 1 0 1 2	8.48 3.05

SAR and GLY differ only by a methyl substituent on the amine, thus their metal complexes are likely to be very similar. The inductive effect of the methyl group is expected to increase the stability of the SAR complex. In fact the Cu-GLY complexes are slightly more stable than the Cu-SAR complex (0.16 log units) which means that the methyl group must have some steric effect as well. It may be possible to clarify this point using enthalpy and entropy measurements (see Chapter 4).

Since a major fraction of copper in plasma is bound to serum albumin it is important to study the effect peptide formation has on the stability of amino acid complexes. To this end a series of dipeptides were studied. With dipeptides, in addition to the two terminal groups, there is also the possibility of coordination to the central amide, either through the carbonyl group or the deprotonated amide nitrogen. A summary table for the equilibrium constants of complexes of these ligands with Cu(II) is given in Table 3.30.

Table 3.30: A summary table of equilibrium constants

Ligand	p q r	Log K_{exp}
GLY	1 1 0	8.09
	1 2 0	7.02
SAR	1 1 0	7.89
	1 2 0	6.31
	1 1 1	4.09
	1 2 -1	11.6
GLY-GLY	1 1 0	6.33
	1 2 0	4.67
	1 1 -1	6.45
	1 1 -2	10.5
SAR-GLY	1 1 0	6.15
	1 2 0	4.45
	1 2 -1	8.35
	1 2 -2	11.5
GLY-LEU	1 1 0	5.79
	1 1 -1	4.71
	1 2 -1	3.57
	2 2 -3	1.78
SAR-LEU	1 1 0	6.32
	1 2 0	4.01
	1 1 -1	7.57
	1 1 -2	10.3
GLY-PHE	1 1 0	6.37
	1 2 0	5.16
	1 2 -1	3.78
	1 2 -2	10.8
SAR-PHE	1 1 0	6.54
	1 1 -1	5.51
	1 1 -2	9.92

Although thermodynamics does not give information about species structure it is possible to infer something about the structure of the different species formed by comparing results from different ligands. The crystal structure of Cu-GLY shows that the metal ion is coordinated to both the amine and carboxyl group [33, 35]. While solution and solid state structures are not always the same it is generally accepted that this is the mode of coordination of GLY. Log K_{ML} (GLY) is 1.44 log units less than log K_{LH} (GLY). Previous studies [35] show that Cu(II) coordinates to the amine N and the carboxylate O when the ML forms. From this information the structure of the ML species that form between Cu(II) and the ligands can be predicted. Log K_{ML} (GLY-GLY) is 1.83 log units less than log K_{LH} (GLY-GLY); log K_{ML} (GLY-LEU) is 2.41 log units less than log K_{LH} (GLY); and log K_{ML} (GLY-PHE) is 1.83 units less than log K_{LH} (GLY-PHE). Log K_{LH} (GLY-GLY) and log K_{LH} (GLY-PHE) dropped by

0.39 log units more less than log K_{LH} (GLY). It is possible than Cu(II) could be coordinating on the same sites as Cu-GLY. Cu(II) could be coordinating to the Carbonyl O and the carboxylate O when ML-GLY-LEU forms. A small decrease in log K_{LH} (GLY-LEU) may mean that the amine terminal is still protonated.

Similarly, log K_{LH}(SAR) decreased by 2.11 log units when ML forms, log K_{LH}(SAR-GLY) decreased by 2.28 log units, log K_{LH}(SAR-LEU) decreased by 2.37 long units and log K_{LH}(SAR-PHE) decreased by 1.94. ML(SAR), ML(SAR-GLY), ML(SAR-LEU) and ML(SAR-PHE) all have the same structure. Cu(II) binds to the amine N and the carboxylate O when this species forms.

All ligands are more selective for Cu(II) than they are for Ni(II) and Zn(II). All ligands are more selective for Ni(II) than they are for Zn(II). This trend obeys Irving-Williams stability series [30].

3.6 CONCLUSIONS

The aim of this study was to develop lipophilic copper complexes, which could possibly be used to increase the *in vivo* bioavailable pool of copper. The idea is that methyl group on the amine terminal may would increase the lipophilicity of the ligands without compromising the stability of Cu(II) complexes. The results shown here confirm that the complexation of SAR dipeptides and GLY dipeptides are comparable and so the metal complex stability has not been compromised. In Chapter 6, lipophilicity studies are reported.

RERERENCES

[1] Murray, K and May, M. P. Equilibrium Simulations for Titration Analysis. Version 3.0 for Windows. (**1989**).

[2] Hamza1, S. M., Rizk, N. M. H and Matter, H. A. B. *International Journal of Pharmaceutical Research and Development.* (**2010**); 2(6);

[3] Gran, G., Johansson, A. and Johansson, S. *Analyst*. (**1981**);106: 1109-1118.

[4] Majlesi, K., Rezaienejad, S., Mehnatfarsa, S. and Zare, K. *Journal of Solution Chemistry.* (**2011**); 40(3):545-560.

[5] Jensen, J. H. *Current Pharmaceutical Biotechnology*. (**2008**); 9(2): 96-102.

[6] Zhao, Q., Jayawardhana, D. A. and Guan, X. *Biophysical Journal*. (**2008**); 94(4): 1267-1275

[7] Hamborg, E. S, Niederer, J. P. M and Versteeg, G. F. *Journal of Chemical and Engineering Data*. (**2007**); 52: 2491-2502

[8] Tewari, B. B. *Journal of the Chilean Chemical Society.* (**2012**); 57(1): 995-998.

[9] Datta, S. P and Grzybowski, A. K. *Transactions of the Faraday Society*. (**1958**); 54:1179-1187

[10] Wedderburn, R. W. M. *Biometrika*. (**1974**); 61(3): 439-447

[11] Mohajane, M. *MSc. Thesis*. University of Cape Town. (**2010**).

[12] Odisitse, S. *PhD Thesis*. University of Cape Town. (**2007**).

[13] Syme, C. D., Nadal, R. C., Rigby, S. E. J. and Viles, J. H. *Journal of Biological Chemistry*. (**2004**); 279: 18169-18177

[14] Cukrowski, I., Marques, H. M., Mkwizua, T. S., Magampaa, P. P and Serge, C. *Analytica Chimica Acta*. (**2007**); 590: 203–216

[15] Datta, S. P., Lebermaann, A. R. and Rabin B. R. *Transactions of the Faraday Society*. (**1959**); 55:2141-2151

[16] Aihara, M., Tanaka, F., Fujimoto, M. and Takehara, K. *Analytical Sciences*. (**1992**); 8: 755-759

[17] Smith, R. M. and Martell, A. E. NIST Critically Selected Stability Constants of Metal Complexes Database. (**1994**). Version 8.0 for Windows.

[18] Gran, G. *Analyst.* (**1952**); 77: 661-671.

[19] Kiss, T and Szucs, Z. *Journal of the Chemical Society*. (**1986**); 92(49): 2443-2447.

[20] http://www.titrations.info/EDTA-titration-nickel

[21] http://www.titrations.info/EDTA-titration-zinc

[22] Tanakana, H., Yokoyama, A. and Aiba, H. *Bulletin of the Chemical Society of Japan*. (**1974**); 47(6): 1437-1441

[23] Rabenstein , D. L., Daignault , S. A.,. Isab ,A. A., Arnold , A/ P and Shoukry, M. M. *Journal of American Society of Chemistry.* (**1985**); 107 (23): 6435–6439

[24] Monk, C. B. *Transactions of the Faraday Society*: (**1951**); 47: 297-302.

[25] Reddy, V. K., Jen-Jin, S. Arora, P. K. Sfeir, D. S., Maloney, S. C. F., Urbach , F. L. and Sayre, L. M. *Journal of American Chemical Society.* (**1990**); 112(6): 2332–2340

[26] Pasternack, R. F., Gipp, L. and Sigel, H. *Journal of American Chemical Society* (**1972**); 94(23): 8031–8038

[27] Perkins, D. J. *Biochemical Journal*. (**1954**); 57(4): 702–704.

[28] Oxtoby, G. W. and Nachtrieb, N. H. *Principles of Modern Chemistry*, Saunders College Publishing, (**1990**); 2 ed.

[29] http://www.chem.queensu.ca/Courses/Labs/Year1/apsc100/titrimetric_analysis.htm

[30] Irving, H. M. N. H., Williams, R. J. P. *Journal of Chemical Society.* (**1953);** 637: 3192-3210

[31] Galijasevic, S., Krylova, K. Koenigbauer, M. J., Jaeger, G. S. Bushendorf, J. D. Heeg, M. J. Ochrymowycz, L. A., Taschnerc M. J. and Rorabacher, D. B. *Royal Society of Chemistry*. (**2003**);12(5): 1577-1586

[32] Stadlbauer ,S., Riechers, A., Späth, A. and König, B. *Chemistry - A European Journal.* (**2008)**;14(8): 2536-2541

[33] Temitayo, A., Issac, O. and Olugbenga, A. *International Journal of Chemistry.*(**2012**);

4(2): 49-59.

[34] Hancock, R. D. *Pure and Applied Chemistry*. (**1986**); 58(11): 1445-1452.

[35] Colaneri, M. J., Vitali, J. and Peisach, *Journal of Physical Chemistry*. (**2009**); 113(19): 5700–5709.

[36] Santini, A. O., Pezza, H. R., de Oliveira, J. E. and Pezza, L. *Journal of the Brazilian Chemical Society.*(**2008**); 19(10): 162-168.

4. ISOTHERMAL TITRATION CALORIMETRY

4.1 INTRODUCTION

Isothermal titration calorimetry (ITC) is used to determine the thermodynamic properties of substances in solution [6]. A typical isothermal titration calorimeter has a reference cell and a sample cell [1, 6, 7]. The sample cell is filled with the analyte solution and the reference cell is filled with solvent, water if the analyte is in water or a buffer solution if the analyte is in a buffer solution or a mixture of solvents if the analyte is in a mixture of solvents [1, 6, 7]. The titrations are run at a fixed temperature and the amount of heat transfer between the sample cell and the surroundings upon injection of titrant solutions into the sample cell is monitored by temperature sensors [6, 7]. The same volume should be used from the beginning of the titration to the end. The signals are reported as heat units per mole of injection [1], therefore the amount of heat evolved/absorbed depends on the concentration of the titrant and as well as the volume of the titrant: a 2 µm injection gives twice the heat per injection as the heat produced by 1 µm of the same concentration.

The sensors of the calorimeter measure the amount of power used to maintain the temperature between the reference cell and the sample cell after every injection. The power is measured in $\mu cal.sec^{-1}$. This power has to be within the dynamic range of 0-12.25 $\mu cal.sec^{-1}$. If the power used to maintain the temperature of the sample cell the same as that of the reference cell does not fall within this range, the sensors overreact and give incorrect results. The amount to power depends mostly on the concentrations of the titrant solutions and injection volume. Since the heats measured between injections are given in heat units per mol of injection, it is wise to use dilute titrant solutions. It is also wise to control the injection volumes.

Using the mass balance equations, ITC data is then reported in heat units per mol of injection as a function of molar ratio of the amount of the titrant to the amount of analyte [6, 7]. Thermodynamic parameters can then be generated from this data by model fitting. These parameters are basically N the equivalence point, K the binding constant, ΔH the enthalpy change and ΔS the entropy change. There are different programs used to fit the ITC data, the most common one being Origin (by OriginLab). This program has five fitting modes;

i. One set of sets of sites model

ii. Two set of sets of sites model,
iii. Sequential binding model,
iv. Competitive binding model, and
v. Dissociation fitting mode.

All five model fitting modes have been described fully in the user manual [1].

To make sure that the results are accurate, prior to fitting data the background heats of dilution for both the analyte and the titrant solutions have to be determined [6]. The easiest way is by running control experiments for both the analyte and the titrant. A control experiment for the analyte is done by injecting a solvent (water if the analyte is in water, a buffer solution if the analyte is in a buffer solution or a mixture of solvents if the analyte is in a mixture of solvents) into the analyte solution and measure the heat transfer between the sample cell and the reference cell. It is possible to get non-zero background heats if the analyte hydrolyses in solution, there is heat accompanying that process, and if the analyte forms aggregates, or foam. There is heat accompanying all those processes. If the backgrounds heats are non-zero heats then the ITC data have to be corrected by subtracting data obtained from the control [1, 6, 13, 14].

A control experiment for the titrant is done by injecting the titrant into a sample cell filled with the solvent. In this control experiment, the sample cell and the reference cell are filled with the same substance. There should not be any heat transfer between the sample cell and the reference cell if the titrate does not hydrolyse, or form aggregates, or forms lather. If non-zero heats are obtained in this control the control data has to be corrected from the actual titration [1, 6, 14]. Once data has been corrected then all four thermodynamic parameters (N, K, ΔH and ΔH) can be calculated from a single titration.

Kasimova [18] has discussed how to diagnose errors on ITC data. Some of the things they discussed are the drifting baseline, overlapping power signals, oscillating signals, square signals and unevenly distributed data points. It is important that cells and the syringe are clean and that the ionic strength of analyte and that of the titrant should match to avoid the baseline from drifting. The titrant solutions should also be at the same temperature as the analyte solution. If the titrant is at lower (or higher) temperatures than the analyte, upon injection into the sample cell the temperature of the analyte will be lower than the set cell

temperature. This will cause the baseline to drift and the results will be affected [18]. To avoid the power signals from overlapping, enough retention time should be set to allow all the analyte that has been injected into the sample cell to react [1, 7, 18]. Enough reference power should be set to avoid the power signals from oscillating [1, 8]. If square power signals are observed, then the titrant solutions are too concentrated and have to be diluted, and if the data points are not evenly distributed then the injection volume may not be properly edited. The same injection volume should be used throughout the titration; if 1.0 µL are used, 1.0 µL should be used from the first point of the titration to the last point of the titration [18].

4.2 THEORY

The sample cell of the ITC instrument has a fixed volume V_0. This cell is shaped like a lollipop. When an analyte solution of concentration M^0_t is titrated with a ligand of concentration X^0_t and the injection volume of the ligand is ΔV_i per injection, some of the solution in the sample cell will be pushed out of the cell into the overflow tubing. The total volume of the solution that has been pushed into the dead volume at n^{th} titration point is ΔV. Since some of the analyte will be pushed into the dead volume, its concentration in the sample cell will not be the same from titration point to titration point.

If the concentration of the analyte at the n^{th} titration point is M_t, mass balance equation requires that;

$$M^0{}_t V_0 = M_t V_0 \frac{1}{2} (M_t + M^0{}_t) \Delta V \tag{4.0}$$

The concentration of the analyte solution at the n^{th} titration point M_t can be calculated by re-arranging Equation 4.0;

$$M_t = M^0{}_t \frac{1 - (\Delta V/2V_0)}{1 + (\Delta V/2V_0)} \tag{4.1}$$

The total amount of the titrant after the n^{th} titration point differs from titration point to titration point. If the total concentration of the titrant in the sample cell after the n^{th} titration is X_t, the mass balance equation can be expressed as;

$$X^0{}_t V_0 = X_t V_0 + \frac{1}{2} X_t \Delta V$$

(4.3)

Re-arranging Equation 4.3 gives;

$$X_t = X^0{}_t \left(1 - \frac{\Delta V}{2V_0}\right)$$

(4.4)

Origin calculate M_t and X_t from titration point to titration point, and measures the amount of heat transfer between the sample cell and the reference cell from point to point. Origin calculates four thermodynamic parameters from a single titration by model fitting. These parameters are n the number of binding sites, K the binding constant, ΔH the enthalpy change and ΔS the entropy change.

The value of n depends mostly on the shape of the titration curve. A single S-curve is observed for substances that have one biding site. However, a single S-curve can be observed for a substance that has identical multiple sites. The model used to fit the data depends on the type of distribution curve obtained during the titration. Origin provides with five model fitting modes. Only three of these modes were used in this study. These being;

i. One set of sites fitting mode,
ii. Two set sites model, and
iii. Competitive binding mode.

For a single set of identical sites, the binding constant K can be expressed as;

$$K = \left(\frac{\Theta}{(1 - \Theta)[X]}\right)$$

(4.5)

Where [X] is the concentration of the free titrant solution and Θ is the fraction of sites occupied by the titrant X.

The concentration of the titrant solution X_t at the n^{th} titration point can be expressed in terms of [X] the concentration of the free titrant, Θ the fraction of sites occupied by titrant X, the number of binding sites n, and Mt the concentration of the analyte at the n^{th} titration point as;

$$X_t = [X] + n\Theta M_t$$

(4.6)

Adding Equations 4.5 and 4.6 yields;

$$\Theta^2 - \Theta\left[1 + \frac{X_t}{nM_t} + \frac{1}{nKM_t}\right] + \frac{X_t}{nM_t} = 0$$

(4.7)

Q total heat per in the sample cell of volume V_0 at fractional saturation Θ is expressed as;

$$Q = n\Theta M_t \Delta H V_0$$

(4.8)

Where ΔH is the heat in heat unit per mole of injection of the titrant. Substituting Θ in equation 4.8 with Equation 4.7 yields;

$$Q = \frac{nM_t\Delta HV_0}{2}\left[1 + \frac{X_t}{nM_t} + \frac{1}{nKM_t} - \sqrt{\left(1 + \frac{X_t}{nM_t} + \frac{1}{nKM_t}\right)^2}\right] + \frac{4X_t}{nM_t}$$

(4.9)

Calculations for Q are done at any point of the titration for any value of n, K and ΔH. The parameter of interest however is the change in heat (ΔQ) between injections. Since after every injection some of the sample cell contents are being pushed into the dead volume and the amount that goes into the dead volume outflows with some heat quantity, about 50 % of the heat is lost when the solution is pushed into the dead volume and about 50 % of the heat remains in the sample cell. Origin takes into account the amount of heat lost and the change in heat between injections (Q_i) at the n^{th} titration point can be expressed as;

$$\Delta Q_i = Q_i + \frac{dV_i}{V_0}\left[\frac{Q_i + Q_{i-1}}{2}\right] - Q_{i-1}$$

(4.10)

When the titration is done, the output is the concentration of the analyte at every titration point, the concentration of the titrant at every titration point, the volume of the titrant injected at every titration point, the ratio of the concentrations of titrant/concentrations of the analyte at every titration point and the change in heat measure between injections. To fit the data,

all four thermodynamic parameters (n, K, ΔH and ΔS) are optimised by Levenberg-Marquandt methods for nonlinear least squares [19, 20].

For a two sets of sites model, the first binding constant K_1 can be expressed as;

$$K_1 = \left(\frac{\Theta_1}{(1-\Theta_1)[X]}\right) \tag{4.11}$$

The second binding constant can be expressed as;

$$K_2 = \left(\frac{\Theta_2}{(1-\Theta_2)[X]}\right) \tag{4.12}$$

And the concentration of the titrant at the n^{th} titration point (X_t) can be expressed as;

$$X_t = [X] + M_t(n_1\ \Theta_1\ + n_2\ \Theta_2) \tag{4.13}$$

The definition of terms is the same for all fitting models. Solving for Θ_1 and Θ_2 in Equations 4.11 and 4.12 and substituting them in Equation 4.12 yields;

$$X_t = [X] + \frac{n_1\ M_t[X]K_1}{1+[X]K_1} + \frac{n_2\ M_t[X]K_2}{1+[X]K_2} \tag{4.14}$$

Let

$$p = \frac{1}{K_1} + \frac{1}{K_2}\ (n_1\ + n_2\ )M_t - X_t$$

$$q = \left(\frac{n_1}{K_1} + \frac{n_2}{K_2}\right)M_t - \left(\frac{1}{K_1} + \frac{1}{K_2}\right)X_t\ + \frac{1}{K_1K_2}$$

And

$$r = \frac{-X_t}{K_1K_2} \tag{4.15}$$

Equation 4.14 can be expressed in terms of p, q and r;

$$[X]^3 + p[X]^3 + r[X] + r = 0 \tag{4.16}$$

Q can therefore be expressed as;

$$Q = M_t V_0 (n_1\ \Theta_1\ \Delta H_1 + n_2\ \Theta_2\ \Delta H_1) \tag{4.17}$$

Corrections for displaced heat can be expressed as;

$$\Delta Q_i = Q_i + \frac{dV_i}{V_0}\left[\frac{Q_i + Q_{i-1}}{2}\right] - Q_{i-1} \tag{4.18}$$

The thermodynamic parameters n_1, n_2, K_1, K_2, ΔH_1, ΔH_2, ΔS_1, ΔS_2 can then be optimised by Levenberg-Marquandt methods for nonlinear least squares [19, 20].

Complex formation titrations are mostly competitive. For two ligands A and B that compete for the third molecule P by;

$$P + A \overset{\Delta H_A}{\rightleftharpoons} PA$$

K_A can be expressed as;

$$K_A = \frac{[PA]}{[P][A]} \tag{4.19}$$

And for the reaction;

$$P + B \overset{\Delta H_A}{\rightleftharpoons} PB$$

K_B can be expressed as;

$$K_B = \frac{[PB]}{[P][B]} \tag{4.20}$$

Where [A] is the concentration of the compound A, [B] is the concentration of the compound B, [P] is he concentration of a compound P and [PA] is the concentration of the compound PA.

Sigurskjold [21] has described fully how the concentrations of each compound (A, B, P, PA, PB) can be calculated from titration point to titration point. From Sigurskjold's work [21] the corrected heat can be expressed as;[1]

$$\Delta Q_i = V_0(\Delta H_A \Delta[PA] + \Delta H_B \Delta[PB]) \tag{4.21}$$

4.3 EXPERIMENTAL

4.3.1 Sample preparation and calorimetric measurements

NaCl granules, NaOH and HCl ampoules were purchased from Merck. They were of analytical grade and were used without further purification. GLY, GLY-GLY, GLY-LEU, GLY-PHE, GLY-HIS and SAR were purchased from SIGMA-ALDRICH. SAR-GLY, SAR-LEU, SAR-PHE and SAR-HIS were purchased from GL Biochem (Shanghai). Microcal iTC_{200} calorimeter was used to measure the heats evolved/absorbed. The titration parameters were set as described in the iTC_{200} and Origin 7 user manual [1, 7]: the jacket temperature was set to 25^0C for all titrations, the cell temperature was also set to 25^0C, the number of injections ranged between 18 to 76 injections, the reference was set between 9 $\mu cal.mol^{-1}$ and 12 $\mu cal.mol^{-1}$, the initial delay ranged between 60 sec and 120 sec, the cell concentration ranged between 0.3 mM to 1 mM and the syringe concentration ranged between 5 mM and 10 mM, the stirring speed was set to 1000 RPM for all titrations.

Solutions of different concentrations of HCl were prepared and standardised as described [14-16]. For acid/base titrations, 0.5 mM NaOH solutions were prepared. All solutions were prepared in degassed/deionised water and were of 0.15 M ionic strength with NaCl. The reference cell was rinsed and filled with 0.15 M NaCl solution. The sample cell was rinsed and filled with 0.5 mM NaOH solution. The syringe was rinsed and filled with known concentrations of HCl. The syringe was purged twice to remove any air bubbles that could have been trapped into the solutions. The tip of the pipette was inserted into the sample cell and the titration was started. A control experiment was also run to measure background heats of dilution of NaOH.

[1] The theory section was extracted from Origin 7 user manual [1].

For ligand protonation titrations, 1 mM ligand solutions were prepared in dilute NaOH. The pH of the ligand solutions was adjusted such that it is very close to the pH that gives the first protonation/deprotonation constant. This was to avoid having excess OH^- in solution. All solutions were prepared in degassed/deionised water and were of 0.15 M ionic strength with NaCl. The reference cell was rinsed and filled with 0.15 M NaCl solution. The sample cell was rinsed and filled with the ligand solutions. The syringe was rinsed and filled with known concentrations of HCl. The syringe was purged twice to remove trapped air bubbles. The tip of the pipette was inserted into the sample cell and the titration was started. A control experiment was also run to measure heats of dilution of the ligand solutions.

For complex-formation titrations, 1:1 and 1:2 metal/ ligand solutions were prepared in degassed/deionised water. All solutions were of 0.15 M ionic strength with NaCl. The analyte solutions for complex formation titrations were adjusted to pH's below pH 7 with NaOH/NaCl. The sample cell was filled with metal/ligand solutions of known proportions and titrated against HCl. A control experiment for complex-formation titrations was also run to measure heats of dilution of the metal/ligand solutions.

4.3.2 Data handling

Data were analysed with Origin 7. Origin has five model fitting modes. The fitting mode that best describes the titration data was used. Data for the acid/base titrations was fit with one set of site model. One proton goes on OH^- to form water;

$$OH^-_{(aq)} + H^+_{(aq)} \rightleftharpoons H_2O_{(l)}$$

Data for ligand protonation titrations were fitted to a two site model. All ligands have two dissociable protons except for GLY-HIS that has three;

$$L + H \rightleftharpoons LH$$

$$LH + H \rightleftharpoons LH_2$$

$$LH_2 + H \rightleftharpoons LH_3$$

For complex formation titration, known ratios of metal/ligand were set to pH's below pH 7 and titrated with acid until metal/ligand solutions were completely saturated with acid. Control experiments were done for all protonation titrations and all complex formation to check if the background heats needed to be corrected or not.

4.4 RESULTS

4.4.1 Method validation

Water/water titrations and acid/base titrations were done to test whether the method is reliable or not. Water/water titrations were done basically to test the stability of the instrument. The sample cell was filled with distilled/deionised water, and the syringe was filled with distilled/deionised water. The titration parameters were set and the titration was started. As water in the syringe was being injected into the sample cell, power was measured. This power is the power that was used to maintain the temperature between the sample cell contents and the reference cell constant, T = 25 ^{0}C. Since the sample cell and the reference were both filled with distilled/deionised water, very little power was expected to maintain the temperature constant.

Acid/base titrations were done for two reasons. It is a well known system so it was used to test the reliability of the method and that of the operator. It was also used as a reference most importantly as a caution whenever there is excess OH^- since the titrations were started from high pH's to low pH's.

4.4.1.1 Water/water titrations

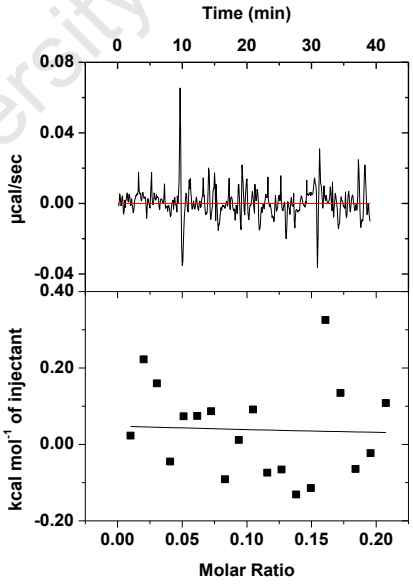

Figure 4.1: Isotherm for water titrated against water

Figure 4.1 shows an isotherm obtained when water was titrated against water at 25 ^{0}C at zero ionic strength. The upper panel shows the raw power signals in µcal.sec^{-1} plotted against

time in minutes. No signals were observed. This shows that the instrument is very stable. The lower panel shows the integrated heats. The black markers are the experimental points and the solid line is the optimal fit. The data were fit with a one set of site model. The heats ranged between -0.2 and 0.2 kcal.mol^{-1}. These heats are very small indicating the instrument is very stable.

4.4.1.2 Acid/base titrations

Figures 4.2A-D show the isotherms for different $[H^+]/[OH^-]$ titrations at 25 ^{0}C and 0.15 M ionic strength. The black signals are the power signals in μcal.sec^{-1} and the red solid lines are baselines. When a more concentrated acid solution was used, the power signals were bigger. The height of the power signals depends on the injection volumes and the concentration of the titrant. Injection volume = 1 μL per injection for all four titrations therefore the concentrations of the titrant are the ones that control the height of the power signals in this section. Power signals in Figure 4.2 D ($[H^+]$ = 20 mM) were the longest followed by power signal in Figure 4.2B ($[H^+]$ = 10 mM). The height of the power signals when 5 mM H^+ was used are more or less the same height, see Figure 4.2B and Figure 4.2C.

Figure 4.2 E shows integrated heats as a function of molar ratio $[H^+]/[OH^-]$. The one site model was used to fit the data. Integrated heats for 0.5 mM NaOH vs 10 mM HCl; 0.5 mM NaOH vs 5 mM HCl and 0.25 mM NaOH vs 5 mM HCl all have the same height. The height of the integrated heats is equivalent to ΔH of the reaction. The titration of 2 mM NaOH with 20 mM HCl however has a bigger height. This is because Microcal$_{200}$ has a dynamic range of 0-12.25 μcal.sec^{-1}. The heights of the power signals for the first three titrations were within 0-12.25 μcal.sec^{-1} range (Figures 4.2 A-C). The data that was obtained when 2 mM NaOH was titrated with 20 mM HCl is was outside the range of the instrument. Olive green markers in Figure 4.2 show the heats of dilution of NaOH. These were very small and therefore negligible.

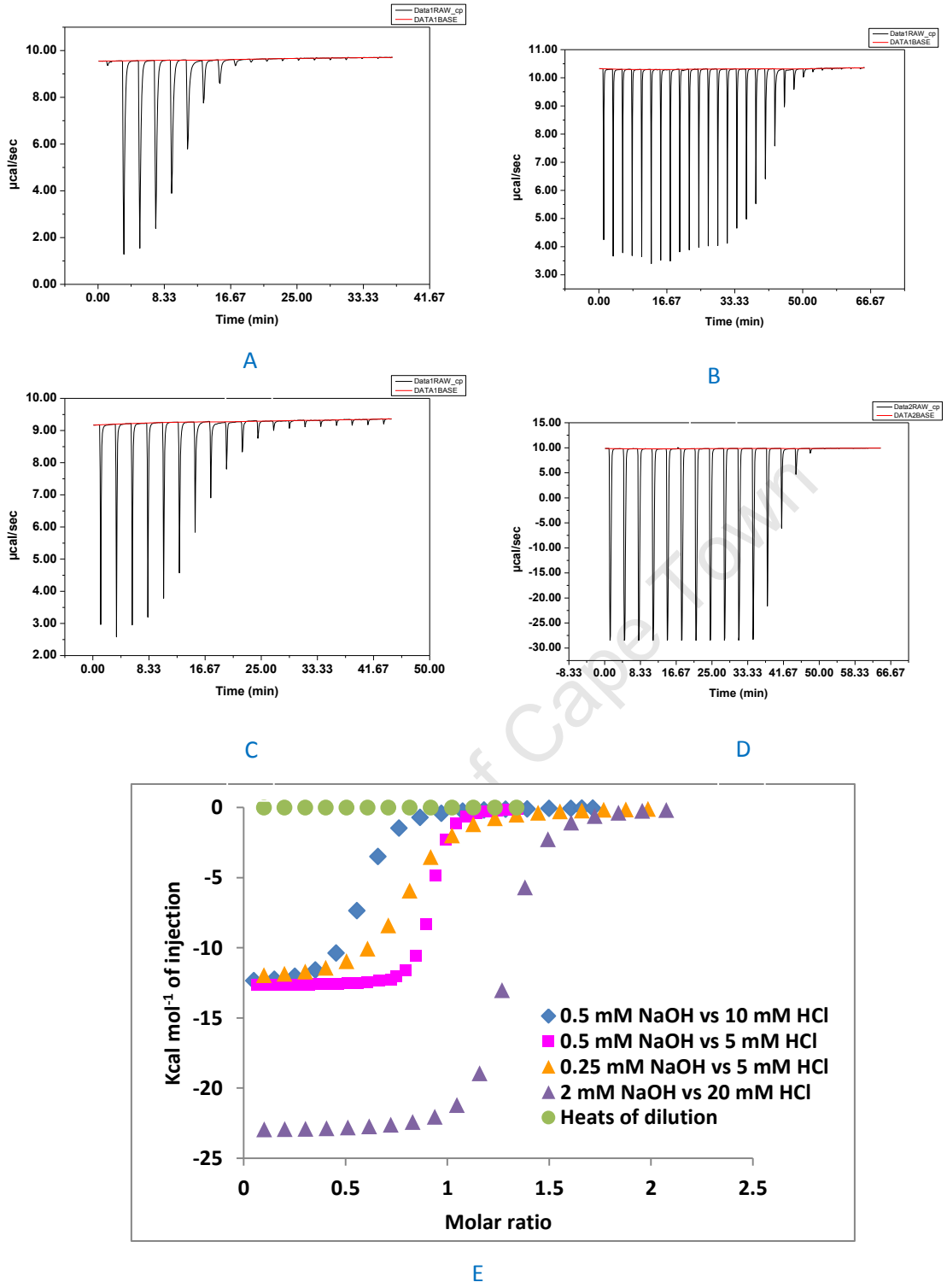

Figure 4.2: Isotherms for acid/base titrations. A: Raw isotherm for 0.5 mM NaOH vs 10 mM HCl; B: Raw isotherm for 0.5 mM NaOH vs 5 mM HCl; C: Raw isotherm for 0.25 mM NaOH vs 5 mM D: Raw isotherm for 2 mM NaOH vs 20 mM E: All four trials plus the control experiment

Thermodynamic parameters ΔH and ΔS were calculated by fitting data using Origin 7. These are given in Table 4.1.

Table 4.1: Thermodynamic parameters NaOH vs HCl titrations

Experiment	Log K	ΔH (Kcal.mol^{-1})	ΔS (Cal.mol^{-1}.^{0}C^{-1})
0.5 mM NaOH vs 10 mM HCl	5.32	-12.6 (±0.2)	-17.9
0.5 mM NaOH vs 5 mM HCl	6.06	-12.7 (±0.1)	-18.2
0.25 mM NaOH vs 5 mM HCl	5.37	-12.5 (±0.1)	-16.5
2 mM NaOH vs 20 mM HCl	5.11	-22.9 (±0.2)	-53.9

The equilibrium constant, log K, is different for all four titrations. All of them do not agree with the literature value of log K = 13.78 [2, 3, 4]. The equilibrium constants determined by ITC depend on the concentrations of the analyte [5, 6, 7]. Baranauskienė and co-workers [5] have described fully how the equilibrium constants for several titrations, including the acid/base titration determined by ITC differ from the literature values. Log K obtained by ITC defines the curvature of the isotherms [7], with an isotherm with the steepest slope (Figure 4.2E, plot for 0.5 mM NaOH vs 5 mM HCl) being the one with the highest log K value (Table 4.1).

ΔH for titrations 0.5 mM NaOH vs 10 mM HCl; 0.5 mM NaOH vs 5 mM HCl and 0.25 mM NaOH vs 5 mM HCl were reproducible. The power signals for all three titrations fall within the range 0-12.25 µcal.sec^{-1}, which is the range at which the instrument works. When all three plots were fit with Origin, an average of -12.6 kcal.mol^{-1} was calculated. This value agrees well with the literature value ΔH = -13.3 kcal.mol^{-1} [5, 8, 9, 10,]. ΔH for the titration 2 mM NaOH vs 20 mM HCl does not agree with the other three because the solutions were too concentrated and the power signals for this titration were not within 0-12.25 µcal.sec^{-1} and hence this titration has to be discarded.

The ΔS for the first three titrations are given in Table 4.1. They are reproducible but wrong because they are based on an incorrect logK as determined by the Origin software. For this reason these ΔS should be discarded and calculated from the know log K values determined independently by potentiometry. Gibbs's free energy, ΔG, was calculated from;

$$\Delta G = - \; T\ln K \tag{4.22}$$

Where R is the universal gas constant (R = 8.314 J. $K^{-1}.mol^{-1}$), T is the temperature and K is the protonation constant determined with glass electrode potentiometry. ΔS was calculated from the Gibb's free energy change ΔG, enthalpy change ΔH and temperature T.

$$\Delta G = \Delta H \quad T\Delta S \tag{4.23}$$

Equation 4.23 can be re-arranged;

$$\Delta S = \frac{\Delta H - \Delta G}{T} \tag{4.24}$$

ΔH was converted from $kcal.mol^{-1}$ to $kJ.mol^{-1}$. ΔG and ΔS were calculated. These are given in Table 4.2.

Table 4.2: Calculated enthalpy changes and entropy changes for the formation of water

Species	Log K	RTlnK ($kJ.mol^{-1}$)	ΔH_{exp} ($kJ.mol^{-1}$)	ΔS_{exp} ($J.K^{-1}.mol^{-1}$)	ΔH_{lit} [22] ($kJ.mol^{-1}$)	ΔS_{lit}[22] ($J.K^{-1}.mol^{-1}$)
LH	13.7	-78.2	-52.6 (±0.05)	85.6 (±20)	-55.8	80.7

ΔG is a large negative number therefore the reaction was spontaneous. ΔH is a large negative number and ΔS is a large negative value therefore the reaction driven by both the enthalpy change and the entropy change. ΔH and ΔS compare well with the literature values [5, 6] and the errors are relatively small which gives us confidence in the results.

4.4.2 Protonation titrations

4.4.2.1 Protonation of glycine

Glycine was titrated with acid from pH 9.13 until the height of the power signals reached zero, the baseline (pH ≈ 2). The results are shown in Figure 4.3. Figure 4.3A is the raw isotherm. The black signals are the power signals and the red solid line is the reference power. The reference power was set to 10 $\mu cal.sec^{-1}$ and it is very stable therefore the sample cell was clean and the ionic strength of the ligand solutions matched that of the acid solutions. The power signals are below the baseline therefore the heats were exothermic. The height of the isotherms is within 0 to 12.25 $\mu cal.sec^{-1}$.

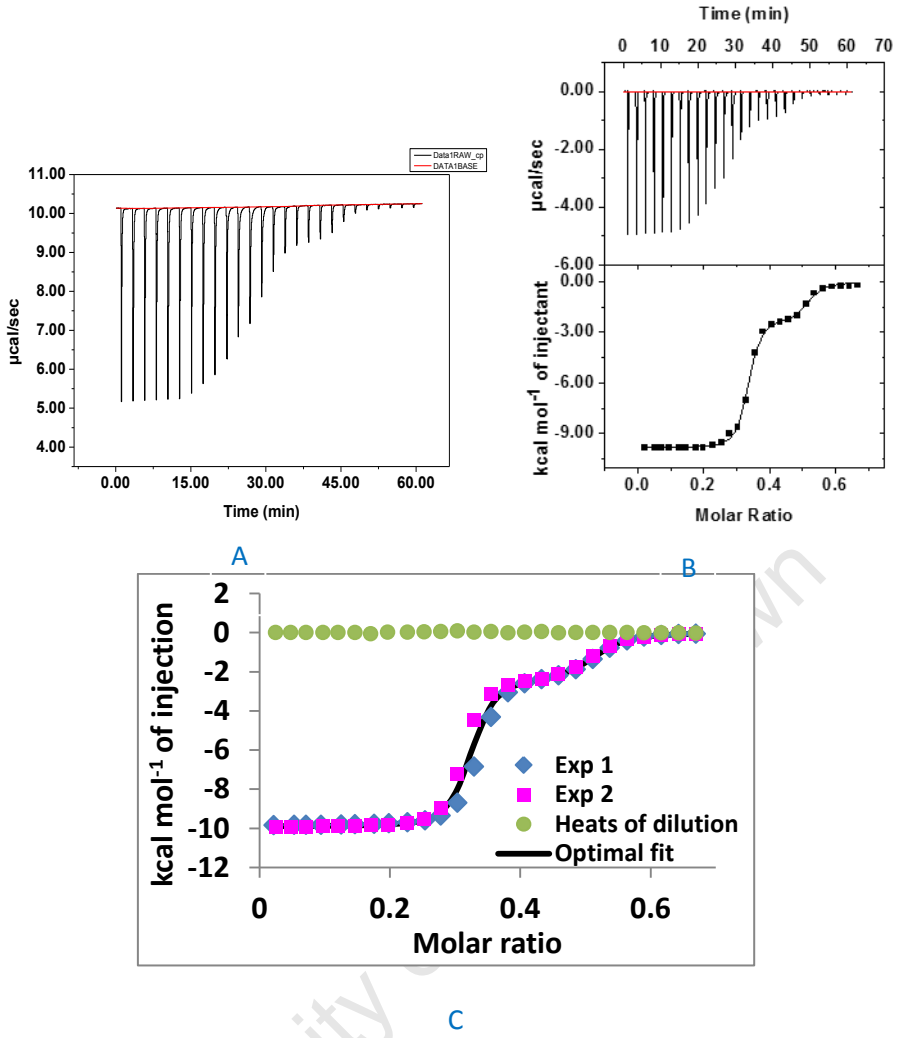

Figure 4.3: Isotherms for acid/base titrations. **A:** Raw isotherm for GLY Protonation **B:** Final isotherm for GLY protonation **C:** Molar ratio per mol of injection for the protonation of GLY ([H+]/[L]) as a function of dH

Figure 4.3B shows the final isotherm for glycine protonation. Data were fit with a two site model. The upper panel is the raw data (same as Figure 4.3A) except the baseline has been set to zero. The lower panel is the integrated data. The integrated data is the one that shows the actual heats evolved/absorbed. The black markers are the experimental data points and the solid line is the optimal fit. The isotherms are interpreted from left to right (small molar ratio to bigger molar ratio). The molar ratio describes the degree of saturation of the cell contents with the syringe contents. In this case the molar ratio = [H]/ [L]. The isotherm levels off at -9.94 Kcal.mol^{-1} of injection from molar ratio 0 to 0.25. In this range the reactants and the products were in thermal equilibrium; $L + H \rightleftharpoons LH$

The heat of formation of LH is therefore -9.94 kcal.mol^{-1}. The negative sign shows that the reaction was exothermic. The isotherm rises from molar ratio 0.25 to molar ratio 0.36. This indicates the formation of a new species. From molar ratio 0.36 to molar ratio 0.39 the isotherm levels off at -2.4 Kcal.mol^{-1} of injection. In this range LH_2 was at thermal equilibrium with LH and H; $LH + H \rightleftharpoons LH_2$

The heat accompanying this reaction was -2.35 kcal.mol^{-1}. The negative sign shows that the reaction was exothermic. From molar ratio 0.39 the graph rises until it reaches zero (the baseline). This indicates that LH_2 had finished forming and the acid that was being injected into the sample cell at this stage was just diluting the cell contents. To check if the results were reproducible, the same experiment was done twice. The results were put on the one graph (Figure 4.3 C). The solid line is the optimal fit of the two experimental plots. The olive green markers represent the heats of dilution of glycine. These were very small and thus negligible. The heats of protonation were converted to kJ.mol^{-1}. The values are shown in Table 4.3.

Table 4.3: Calculated enthalpy changes and entropy changes for protonation of glycine

Species	Log K	ΔG (kJ.mol^{-1})	ΔH_{exp} (kJ.mol^{-1})	ΔS_{exp} (J.K^{-1}.mol^{-1})	ΔH_{lit} [22] (kJ.mol^{-1})	ΔS_{lit} [22] (J.K^{-1}.mol^{-1})
LH	9.53	-54.4	-41.6 (±0.2)	42.9 (±10)	-44.4	39.3
LH_2	2.29	-13.1	-9.85 (±0.5)	10.8 (±3)	-4.10	31.2

ΔG for the protonation of the amine terminal is negative therefore the reaction was spontaneous. The heat accompanying the formation of LH was calculated to be -41.6 kcal.mol^{-1}. This value agrees well with the literature value [8, 11, 12]. ΔS for the formation of LH is a large positive value therefore the production of LH was favoured thermodynamically. Formation of LH_2 is also favored thermodynamically since ΔG is negative, ΔH is negative and ΔS is positive. The heat accompanying the formation of LH_2 is -9.85 kcal.mol^{-1}. This value is higher than the literature value (ΔH_{lit} = -4.40 kJ.mol^{-1}) [8, 11, 12].

4.4.2.2 Protonation of sarcosine

Sarcosine was titrated with acid from pH 9.28 until the height of the power signals reached zero, the baseline (pH ≈ 2). The results are shown in Figure 4.4.

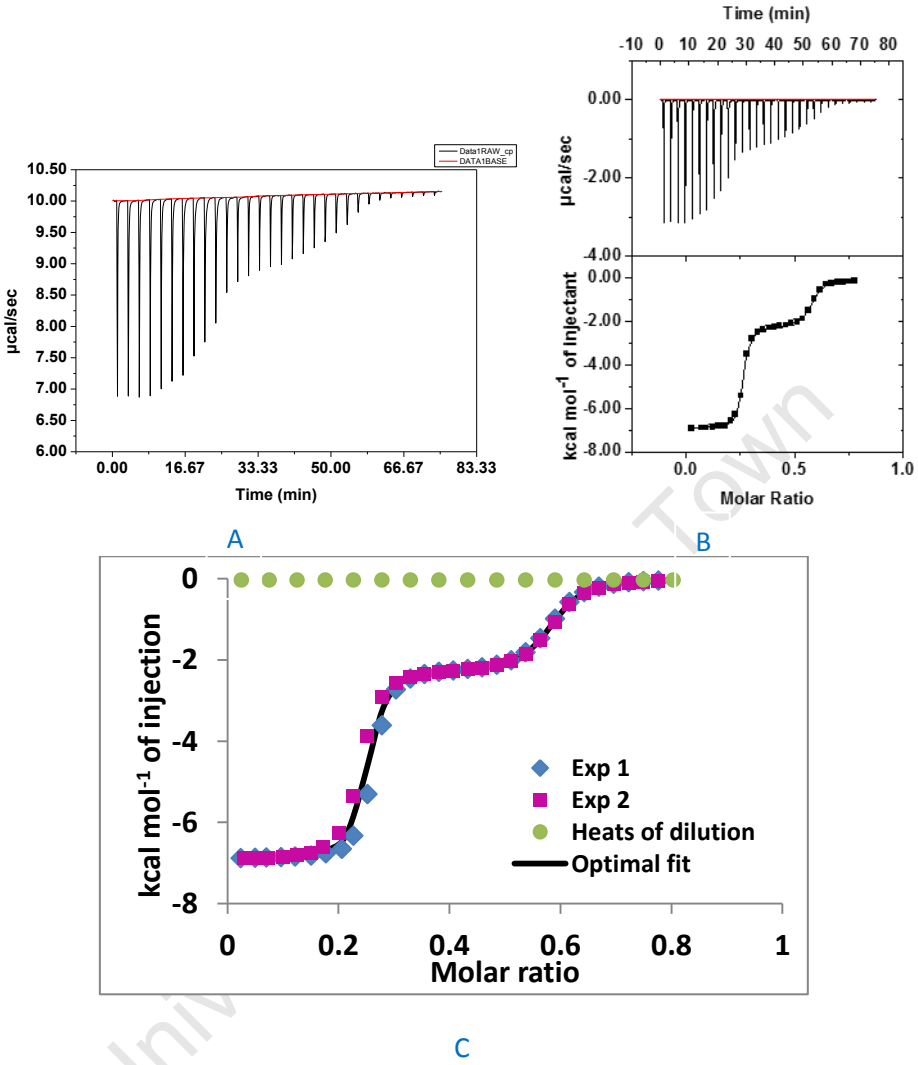

Figure 4.4: A: Raw isotherm for SAR Protonation B: Final isotherm for SAR protonation C: Molar ratio ([H+]/[L]) as a function of dH per mol of injection for the protonation of SAR

The heats of protonation were converted to kJ.mol^{-1}. The values are shown in Table 4.4.

Table 4.4: Calculated heats of protonation of sarcosine and the standard deviations

Species	Log K	ΔG (kJ.mol^{-1})	ΔH_{exp} (kJ.mol^{-1})	ΔS_{exp} (J.K^{-1}.mol^{-1})	ΔH_{lit} [22] (kJ.mol^{-1})	ΔS_{lit} [22] (J.K^{-1}.mol^{-1})
LH	10.0	-57.0	-28.9 (±0.1)	94.6 (±30)	-40.0	58.9
LH_2	2.11	-12.0	-9.51 (±0.1)	8.47 (±2)	-7.10	16.0

The heats accompanying the formation of LH were -28.9kJ.mol^{-1}. This value is significantly less than the literature value of -40.0 kJ.mol^{-1}. The results were reproducible and the

standard deviations are small which leads to confidence in the results. ΔG is a large negative value therefore the formation of LH was spontaneous. Formation of LH was thermodynamically favoured since ΔS is a large positive value. Formation of LH_2 was also spontaneous. Heats of formation of LH_2 were slightly larger than the literature value [8]. Protonation of sarcosine for both the acidic and the basic sites is driven by both entropy and enthalpy (Table 4.4).

4.4.2.3 Protonation of glycyl-glycine

The results for GLY-GLY protonation titrations are given in Figure 4.5. Two plateaus are observed for this titration. The height of the first plateau is equivalent to the heat of protonation of the basic end of the ligand, $\Delta H_1 = -10.6$ kCal.mol^{-1}. The height of the second plateau is equivalent to the heat evolved when the acidic end of the ligand was being protonated, $\Delta H_2 = -3.05$ kCal.mol^{-1}.

To test the reproducibility of the results, the same titration was done twice. The graphs are put together and shown in Figure 4.5C. The solid line is the optimal fit. The olive green markers are the heats of dilution. The heats of dilution are very small and thus negligible. The two experimental data sets run on top of each other and the optimal fit runs on top of the two experimental data sets therefore the results were reproducible.

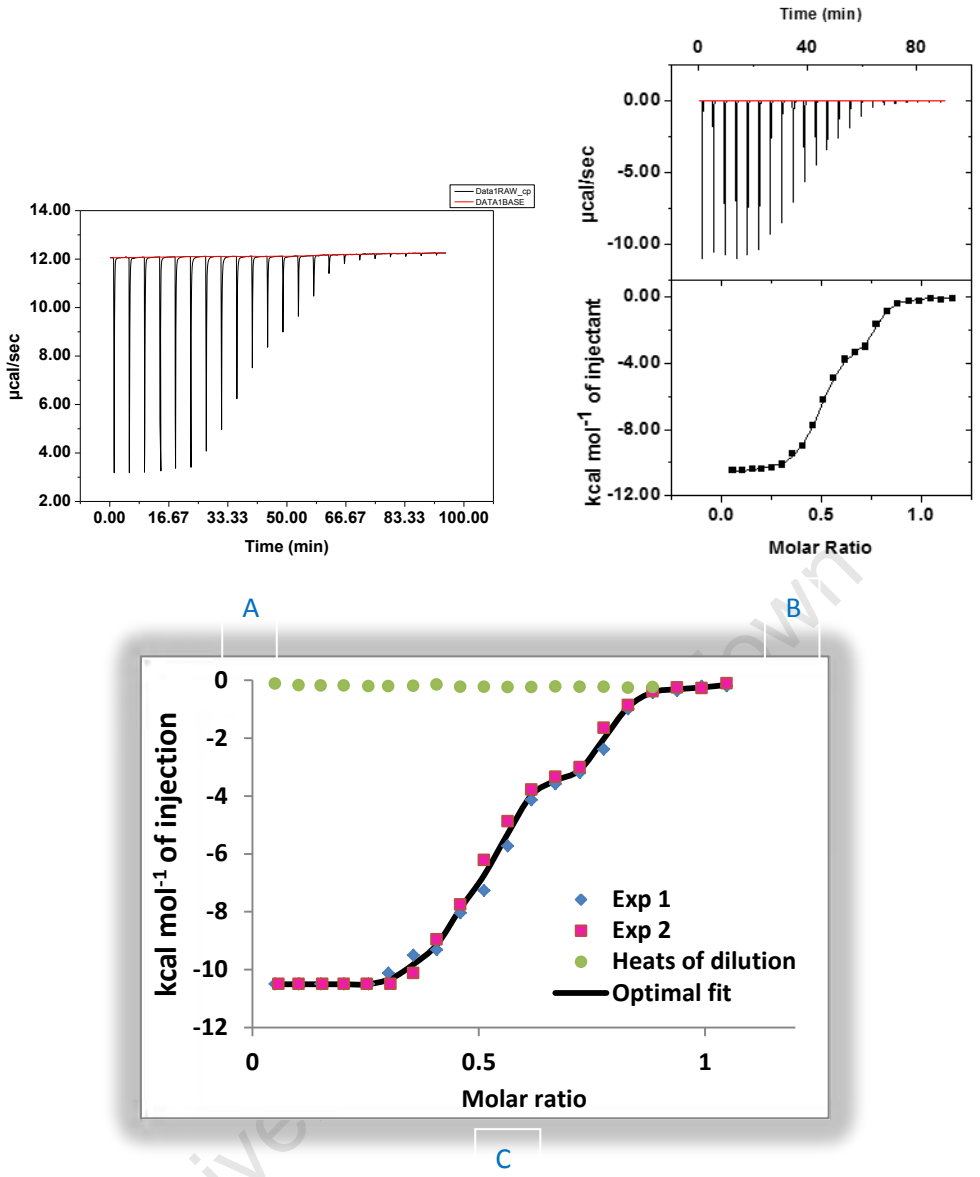

Figure 4.5: A: Raw isotherm for GLY-GLY Protonation B: Final isotherm for GLY-GLY protonation C: Molar ratio ([H+]/[L]) as a function of dH per mol of injection for the protonation of GLY-GLY

The thermodynamic parameters for the protonation of GLY-GLY are shown in Table 4.5. ΔG and ΔS for the protonation of the carboxylate end of GLY-GLY do not compare well with the literature [8].

Table 4.5: Calculated heats of protonation of glycyl-glycine and the standard deviations

Species	Log K	ΔG ($kJ.mol^{-1}$)	ΔH_{exp} ($kJ.mol^{-1}$)	ΔS_{exp} ($J.K^{-1}.mol^{-1}$)	ΔH_{lit} [22] ($kJ.mol^{-1}$)	ΔS_{lit} [22] ($J.K^{-1}.mol^{-1}$)
LH	8.16	-46.6	-44.6 (±0.08)	6.54 (±2)	-43.9	6.20
LH2	3.18	-18.1	-12.8 (±0.3)	18.0 (±5)	-1.00	55.6

4.4.2.4 Protonation of sarcosyl-glycine

The results for SAR-GLY protonation are given in Figure 4.6. ΔH_1 = -10.6 kCal.mol^{-1} and ΔH_2 = 2.51 kCal.mol^{-1}. The background heats of dilution are small and thus negligible. The graphs in Figure 4.6C are superimposable therefore the results were reproducible. This gives confidence in the results.

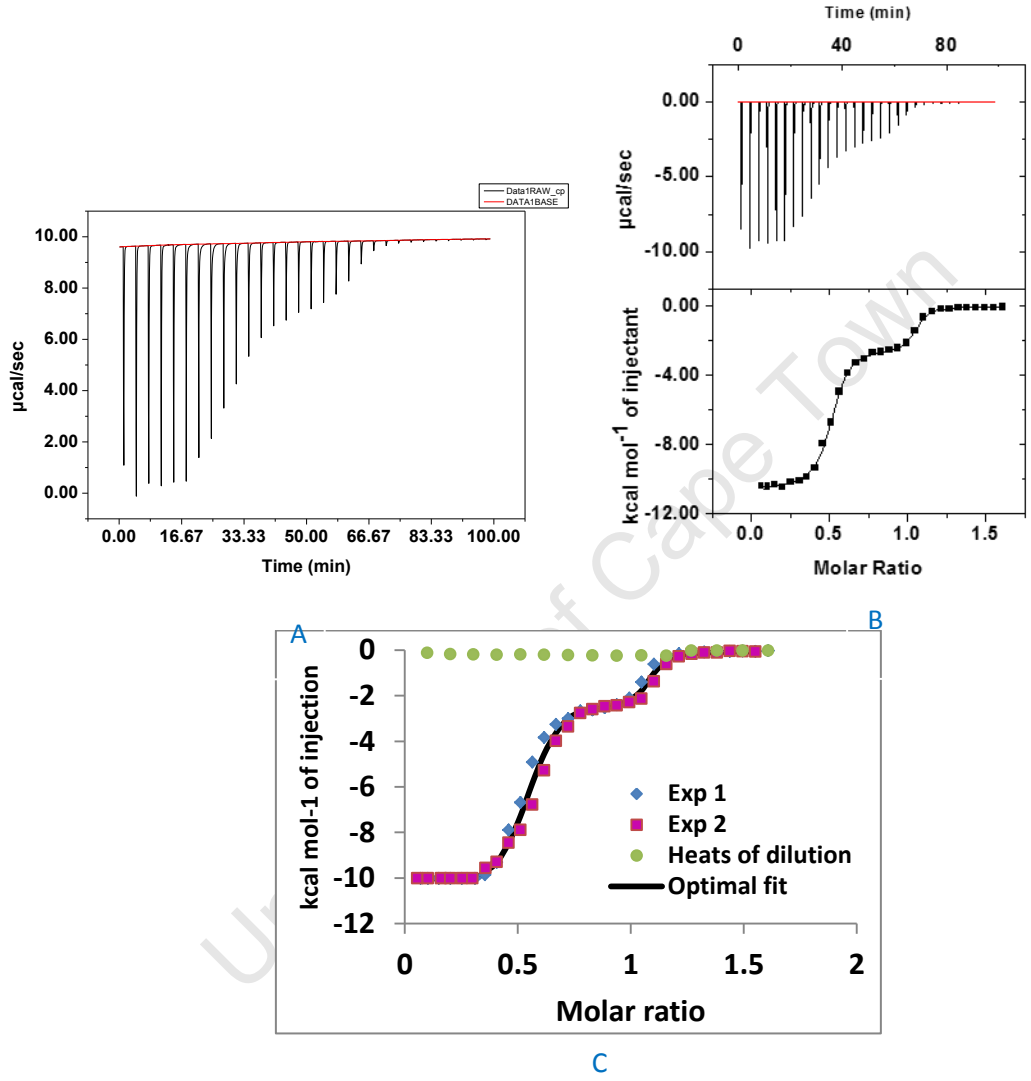

Figure 4.6: A: Raw isotherm for SAR-GLY Protonation B: Final isotherm for SAR-GLY protonation C: Molar ratio ([H+]/[L]) as a function of dH per mol of injection for the protonation of SAR-GLY

Table 4.6 shows the thermodynamic parameters for the protonation of SAR-GLY. The experimental results for SAR-GLY are comparable with the experimental results for GLY-GLY.

Table 4.6: Calculated heats of protonation of sarcosyl-glycine and the standard deviations

Species	Log K	RTlnK ($kJ.mol^{-1}$)	ΔH_{exp} ($kJ.mol^{-1}$)	ΔS_{exp} ($J.K^{-1}.mol^{-1}$)
LH	8.43	-48.1	-41.9 (±0.1)	20.8 (±6)
LH2	2.95	-16.8	-10.5 (±0.2)	21.2 (±6)

4.4.2.5 Protonation of glycyl-L-leucine

The results for the protonation of GLY-LEU are given in Figure 4.7. The heat at the end of the titration should be zero. At the end of the titration the ligand solution should be completely saturated with the acid solution therefore the heat observed at the end of the titration is the background heat of dilution [7, 17, 18]. The background heat for GLY-LEU is slightly higher than zero. Observation of the solution showed that slight foam had been generated by the stirring of this solution and this accounted for the small endothermic reaction. Kasimova [18] however, has suggests that the heat at the end of a titration may go above the baseline because the concentration of the solutions in the sample cell will have degassed significantly at the end of the titration.

For this titration ΔH_1 = - 10.7 $kCal.mol^{-1}$and ΔH_2 = -2.20 $kCal.mol^{-1}$. The graphs in Figure 4.7C are superimposable therefore the results were reproducible. The background heats of dilution cannot be ignored because they are non-zero. Data were corrected as described earlier [1, 6, 14].

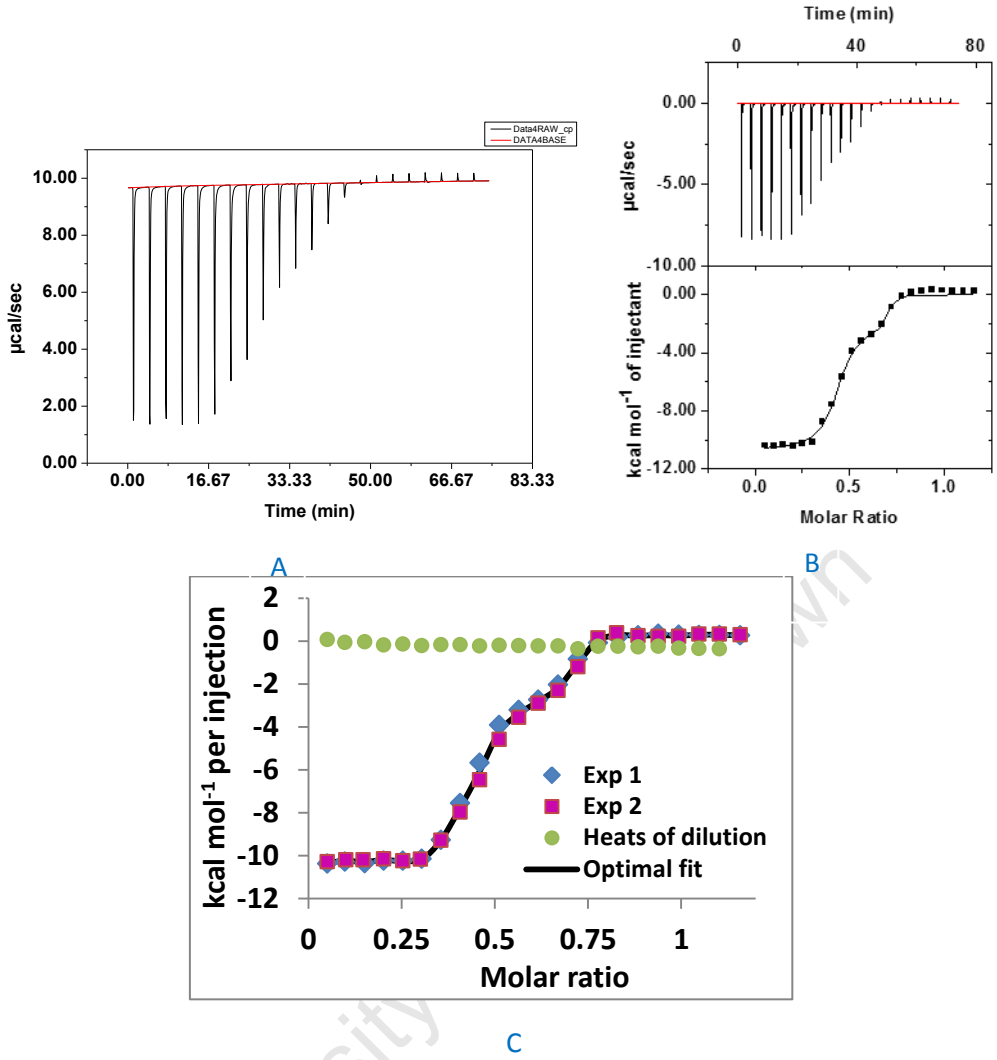

Figure 4.7: A: Raw isotherm for GLY-LEU Protonation B: Final isotherm for GLY-LEU protonation C: Molar ratio ([H+]/[L]) as a function of dH per mol of injection for the protonation of GLY-LEU

The corrected heats are shown in Table 4.7. ΔH for the formation of LH is comparable with the literature value [8]. ΔH for the formation of LH_2 is higher than the literature value [8], however all measures used to validate the method have been met.

Table 4.7: Calculated heats of protonation of glycyl-L-leucine and the standard deviations

Species	Log K	RTlnK (kJ.mol^{-1})	ΔH_{exp} (kJ.mol^{-1})	ΔS_{exp} (J.K^{-1}.mol^{-1})	ΔH_{lit} [22] (kJ.mol^{-1})	ΔS_{lit} [22] (J.K^{-1}.mol^{-1})
LH	8.20	-46.8	-44.8 (±0.2)	6.75 (±2)	-44.3	10.0
LH2	3.14	-17.9	-9.21 (±0.4)	29.2 (±9)	-3.00	49.7

4.4.2.6 Protonation of sarcosyl-L-leucine

Results for the protonation of SAR-LEU are given in Figure 4.8. The heat accompanying the first protonation of SAR-LEU is -9.19 kCal.mol^{-1} and the heat accompanying the second protonation of this ligand is -2.21 kCal.mol^{-1}. The graphs in Figure 4.8C are on top of each other. The results were therefore repeatable. This gives confidence in the results. Non-zero background heats were also observed with this ligand. These were corrected as described [1, 6, 14]. The corrected heats are given in Table 4.8.

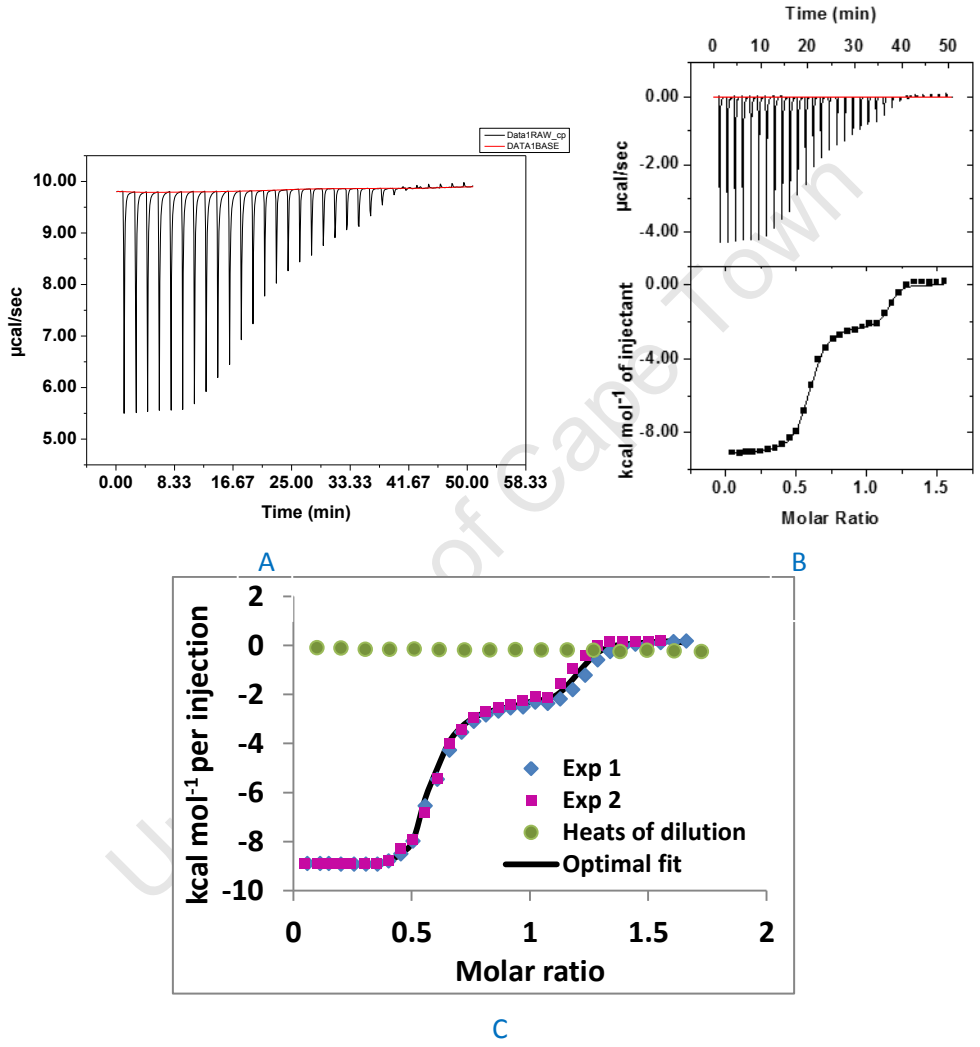

Figure 4.8: A: Raw isotherm for SAR-LEU Protonation B: Final isotherm for SAR-LEU protonation C: Molar ratio ([H+]/[L]) as a function of dH per mol of injection for the protonation of SAR-LEU

Formation of LH is therefore favoured thermodynamically and it does not depend on temperature. There is not published work on heats of protonation of SAR-LEU. The errors are small and the ΔH's compare well with GLY-LEU which is expected to have more or less the same chemical properties as SAR-LEU.

Table 4.8: Calculated heats of protonation of sarcosyl-L-leucine and the standard deviations

Species	Log K	RTlnK ($kJ.mol^{-1}$)	ΔH_{exp} ($kJ.mol^{-1}$)	ΔS_{exp} ($J.K^{-1}.mol^{-1}$)
LH	8.69	-49.6	-38.5 (±0.05)	37.3 (±11)
LH2	3.48	-19.9	-9.25 (±0.08)	35.6 (±11)

4.4.2.7 Protonation of glycyl-L-phenylalanine

The results for the protonation of GLY-PHE are given in Figure 4.9. The heat accompanying the first protonation of GLY-PHE is -10.7 $kCal.mol^{-1}$ and the heat accompanying the second protonation is -1.91 $kCal.mol^{-1}$. The results were reproducible since the graphs on Figure 4.9C are on top of each other. The background heats of dilution were very small and thus negligible.

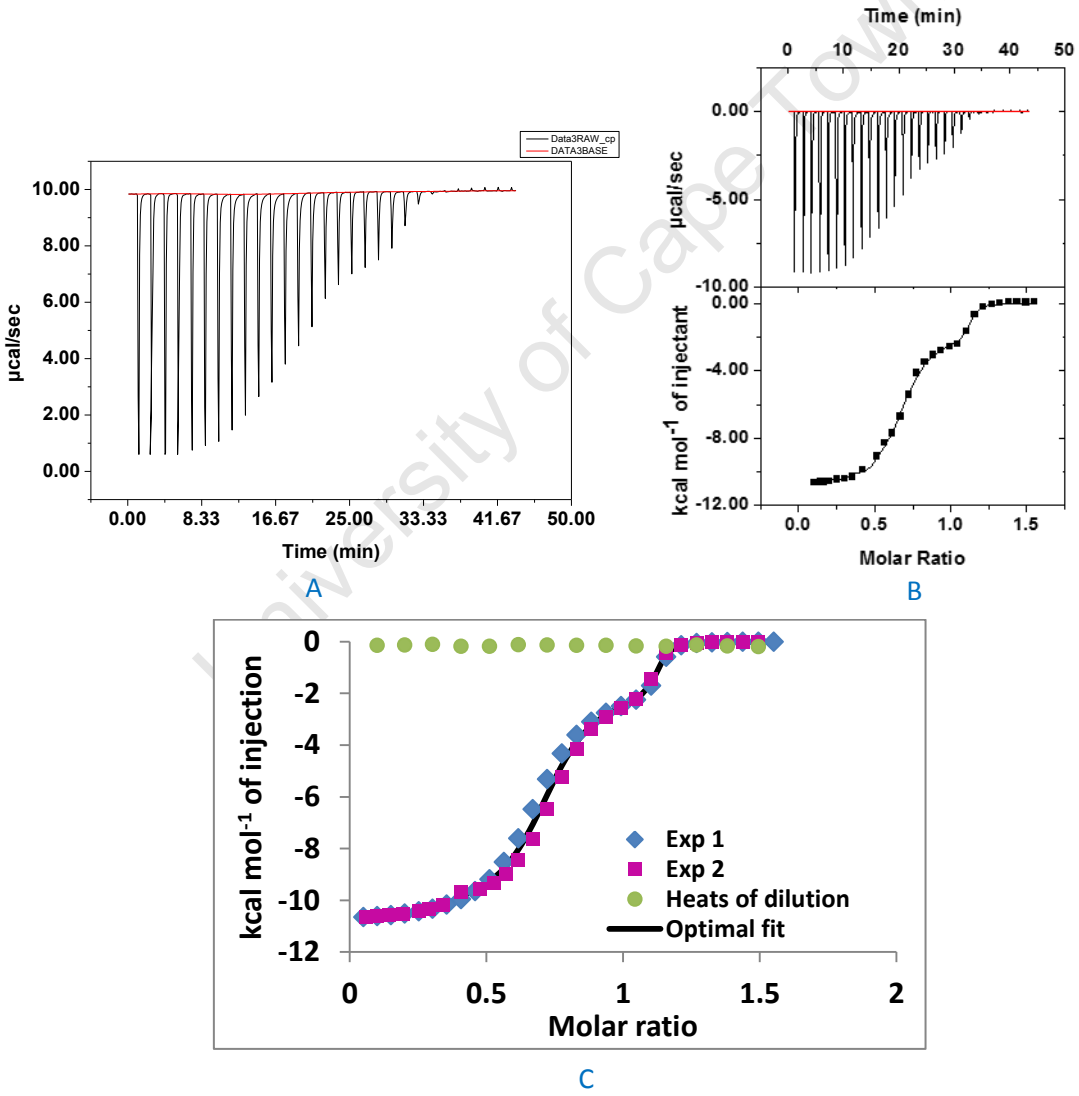

Figure 4.9: A: Raw isotherm for GLY-PHE Protonation B: Final isotherm for GLY-PHE protonation C: Molar ratio ([H+]/[L]) as a function of dH per mol of injection for the protonation of GLY-PHE

Table 4.9 shows thermodynamic parameters for the protonation of GLY-PHE. Formation of LH is favoured thermodynamically. ΔH and ΔS for the formation of LH agree well with the literature [8]. The spontaneity is mostly driven by enthalpy since ΔH = -44.6 kJ.mol^{-1} > -TΔS = -2.18 kJ.mol^{-1}. ΔH and ΔS for the formation of LH_2 is also favoured thermodynamically. The contribution of entropy and enthalpy is almost the ΔH = -8.00 kJ.mol^{-1} > -TΔS = -8.60 kJ.mol^{-1}.

Table 4.9: Calculated heats of protonation of glycyl-L-phenylalanine and the standard deviations

Species	Log K	RTlnK (kJ.mol^{-1})	ΔH_{exp} (kJ.mol^{-1})	ΔS_{exp} (J.K^{-1}.mol^{-1})	ΔH_{lit} [22] (kJ.mol^{-1})	ΔS_{lit} [22] (J.K^{-1}.mol^{-1})
LH	8.20	-46.8	-44.6 (±0.1)	7.31 (±2)	-43.9	7.90
LH_2	2.91	-16.6	-8.00 (±0.4)	28.8 (±9)	-1.00	52.3

4.4.2.8 Protonation of sarcosyl-L-phenylalanine

The results for the protonation of SAR-PHE are given in Figure 4.10. ΔH_1 = -9.77 kCal.mol^{-1} and ΔH_2 = -2.53 kCal.mol^{-1}. The graphs in Figure 4.10C are superimposable. The results were therefore reproducible. The background heats of dilution are very small and thus negligible.

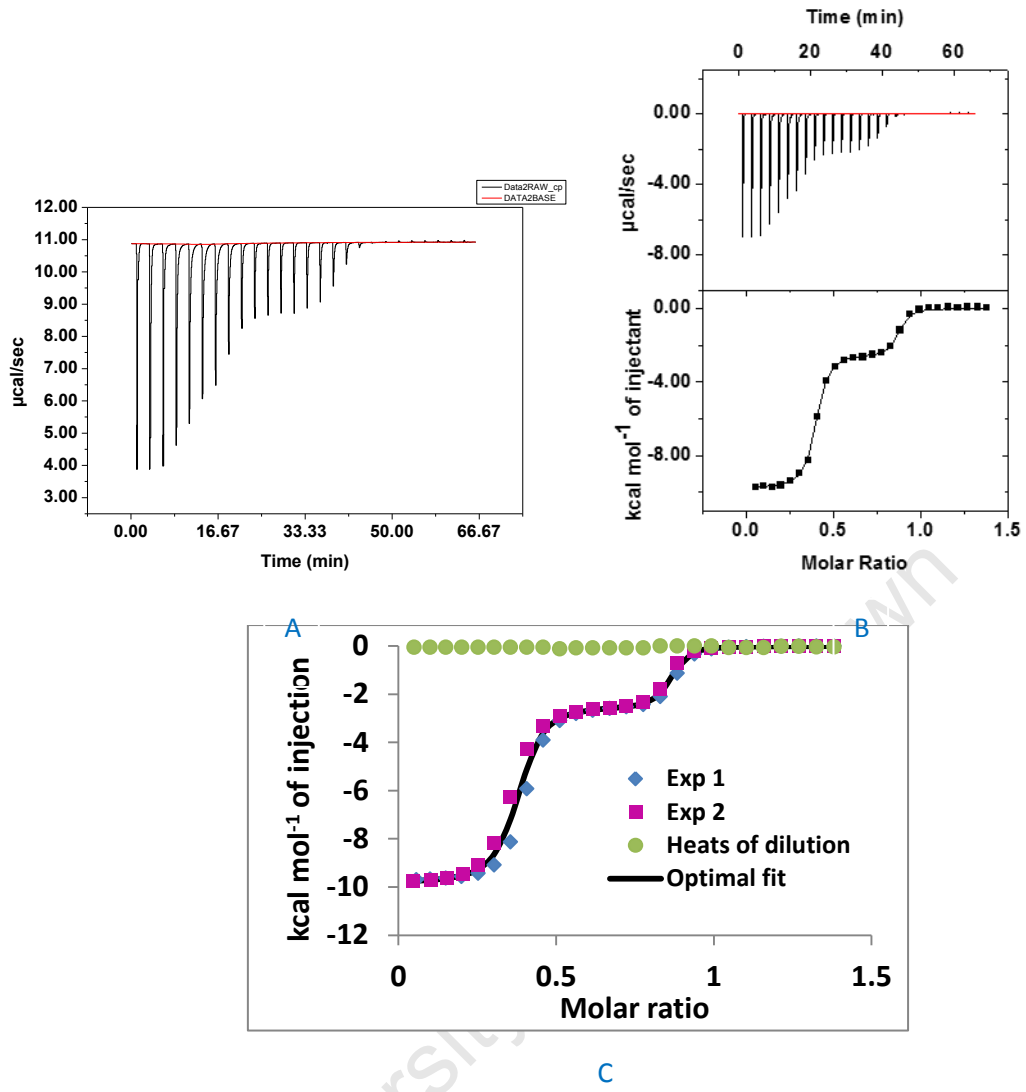

Figure 4.10: A: Raw isotherm for SAR-PHE Protonation B: Final isotherm for SAR-PHE protonation C: Molar ratio ([H+]/[L]) as a function of dH per mol of injection for the protonation of SAR-PHE.

Protonation heats of SAR-PHE are shown in Table 4.10. There is no literature for the protonation heats of SAR-PHE but the errors are small and the heats are comparable with the heats of protonation of GLY-PHE which is expected to have more or less the same chemical properties as SAR-PHE.

Table 4.10: Calculated heats of protonation of sarcosy-L-phenylalanine and the standard deviations

Species	Log K	RTlnK (kJ.mol^{-1})	ΔH_{exp} (kJ.mol^{-1})	ΔS_{exp} (J.K^{-1}.mol^{-1})
LH	8.48	-48.4	-40.9 (±0.03)	25.2 (±8)
LH_2	3.05	-17.4	-10.6 (±0.04)	22.9 (±7)

4.4.2.9 Protonation of glycyl-L-histidine

ITC data for the protonation of GLY-HIS is given in Figure 4.11. The heat accompanying the protonation of the amine terminal is -12.2 kCal.mol^{-1}. The heat accompanying the protonation of the imidazole N is -4.41 kCal.mol^{-1}. The heat accompanying the protonation of the carboxylate terminal is zero. The results are reproducible (Figure 4.11C) since the graphs are on top of each other. The background heats of dilution are very small and thus negligible

GLY-HIS has three dissociable protons [14, 18-20]. A total of three plateaus were expected. At the beginning to the titration (molar ratio = 0.05) the isotherms were expected to levels off indicating thermal equilibrium of L, H and LH for; $L + H \rightleftharpoons LH$

The second plateau was expected to be observed around pH 6 where the imidazole nitrogen is protonated. The third plateau was expected around pH 2 where the carboxylate terminal is protonated. Once the carboxylate was protonated, the graph was expected to rise until it reaches the baseline. However this was not observed because the amine terminal and the nitrogen of the imidazole are protonated at the same time (log K_{LH} = 8.14 and log K_{LH_2} = 6.61) [14, 18-20].

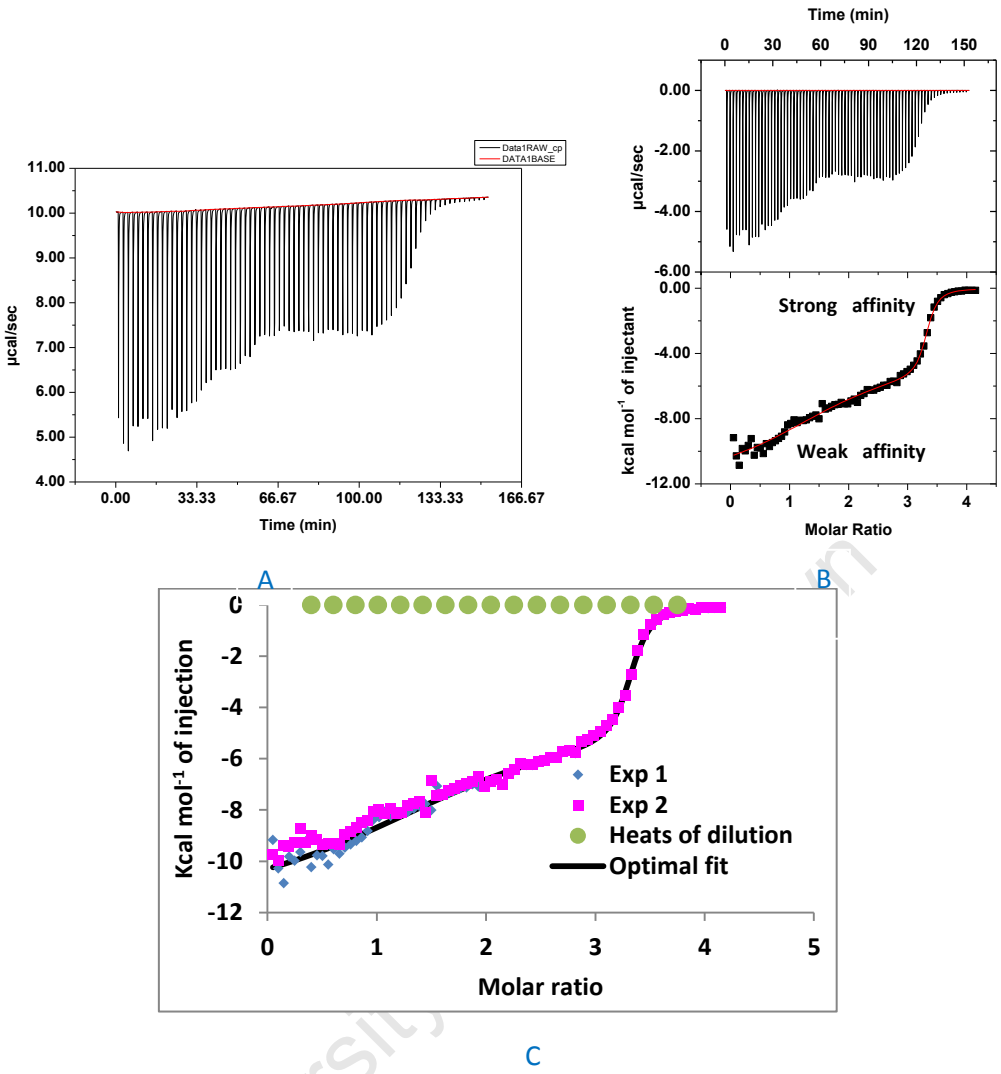

Figure 4.11: A: Raw isotherm for GLY-HIS Protonation B: Final isotherm for GLY-HIS protonation C: Molar ratio ([H+]/[L]) as a function of dH per mol of injection for the protonation of GLY-HIS

The data were analysed with a sequential 3 site model and the thermodynamic parameters for the protonation of GLY-HIS are given in Table 4.11. The spontaneity for the formation of LH is driven by enthalpy, the spontaneity for the formation of LH_2 is driven by both enthalpy and entropy, and the spontaneity for the formation of LH_3 is driven by entropy. There is no published work on the protonation heats of GLY-HIS but the results obtained here are comparable with all the other three glycine dipeptides (GLY-GLY, GLY-LEU and GLY-PHE).

Table 4.11: Calculated heats of protonation of glycyl-L-histidine and the standard deviations

Species	Log K	RTlnK ($kJ.mol^{-1}$)	ΔH_{exp} ($kJ.mol^{-1}$)	ΔS_{exp} ($J.K^{-1}.mol^{-1}$)
LH	8.34	-47.6	-50.9 (±1)	-11.2 (±30)
LH_2	6.61	-37.7	-18.5 (±0.8)	64.6 (±20)
LH_3	2.29	-13.1	0	43.8 (±10)

4.4.3 Complex formation titrations

All complex formation titrations were started from pH 7 or below. This was to avoid access OH- ions which may mask the results by; $OH^- + H^+ \rightleftharpoons H_2O$

The heats accompanying this reaction are huge and if the amount of OH- present in solution is not controlled the heat of formation of water may mask the results.

For all complex formation titrations, species form at different pH's and the complexes complete for Cu(II), the ligand and free H^+. This makes complex formation titrations more of a competitive reactions than the protonation titrations which are basically sequential. To check that the competitive model fitting mode of Origin is suitable for complex formation, solutions of two ligands that have different affinity for H^+ were put together in one sample cell and titrated with acid from pH 10.21 (the first protonation of these ligands occurs around this pH). 1:1 solutions of SAR (log K_{LH} = 10.0; log K_{LH2} = 2.11) and SAR-LEU (log K_{LH} = 8.69; log K_{LH2} = 3.48) were put in the sample cell and titrated with acid until the solutions were completely saturated with acid. Both the sample cell solutions and the pipette solutions were of 0.15 M ionic strength with NaCl. The results are shown in Figure 4.12.

From molar ratio 0.05 the graph levels off until it reached molar ratio 2.26 where it rises. The heat of this plateau is -7.08 $kcal.mol^{-1}$. This heat is comparable with the heat of protonation of the amine terminal of SAR (Section 4.4.2.2). From molar ratio 2.26 the graph rises until it reaches molar ratio 2.43 where is levels off. The height of this plateau is -2.3$kcal.mol^{-1}$. This value agrees well with the value obtained for the heat of protonation of the carboxylate terminal of SAR (Section 4.4.2.2). The graph rises again from molar ratio 3.51 until it touches the baseline at molar ratio between molar ratios 3.74 and 4.09.

Thermodynamic parameters for only one ligand could be calculated, not the average of the two or parameters for each ligand as anticipated. This shows that the competitive models does not work for this type of titrations.

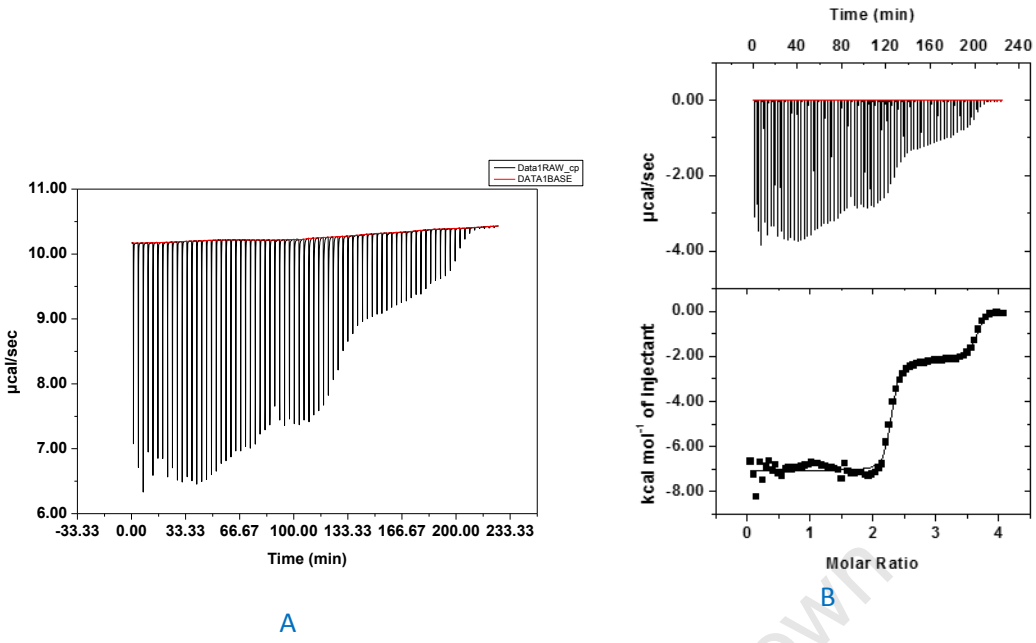

Figure 4.12: A: Raw isotherm for competitive protonation titrations of SAR and SAR-LEU B: Final isotherm for competitive protonation titrations of SAR and SAR-LEU

4.4.3.1 GLY / Cu(II)

1:1 Cu(II)/GLY at pH 7.02 was titrated with acid until the system was completely saturated with acid. The results are shown in Figure 4.13. Data were fit with a one site model. The isotherms are interpreted from lower molar ratio to higher molar ratio. The graph levels off from molar ratio 0.05 to molar ratio 0.45 where it rises until it touches the baseline. ΔH for only one species was observed, $\Delta H = -4.2$ kcal.mol^{-1}.

1:2 Cu(II)/GLY was titrated with acid from pH 6.15. The results are put together with the results for 1:1 Cu(II)/GLY. These are shown in Figure 4.13C. The height of the graphs ΔH for the two graphs is the same. The equivalence point N however is not the same. This is because the amount of complexes formed depends on the amount of OH^- present and the metal/ligand ratio. ΔH for only one species was observed. The olive green markers are the background heats of dilution. These were very small and thus negligible.

Cu(II) and GLY form only two species in solution [14-16]. These are ML and ML_2. The stability constant for ML is 1.07 log units greater than the stability constant of ML_2 (Chapter 3 Section 3.4.1.2). The height of the isotherms is -4.2 kcal.mol^{-1}. This is the heat accompanying the formation of ML since ML is more stable than ML_2 and Origin calculates

thermodynamic parameters of species that are the most stable in solution (Section 4.4.3), for systems that forms two or more species in solution and compete for starting materials.

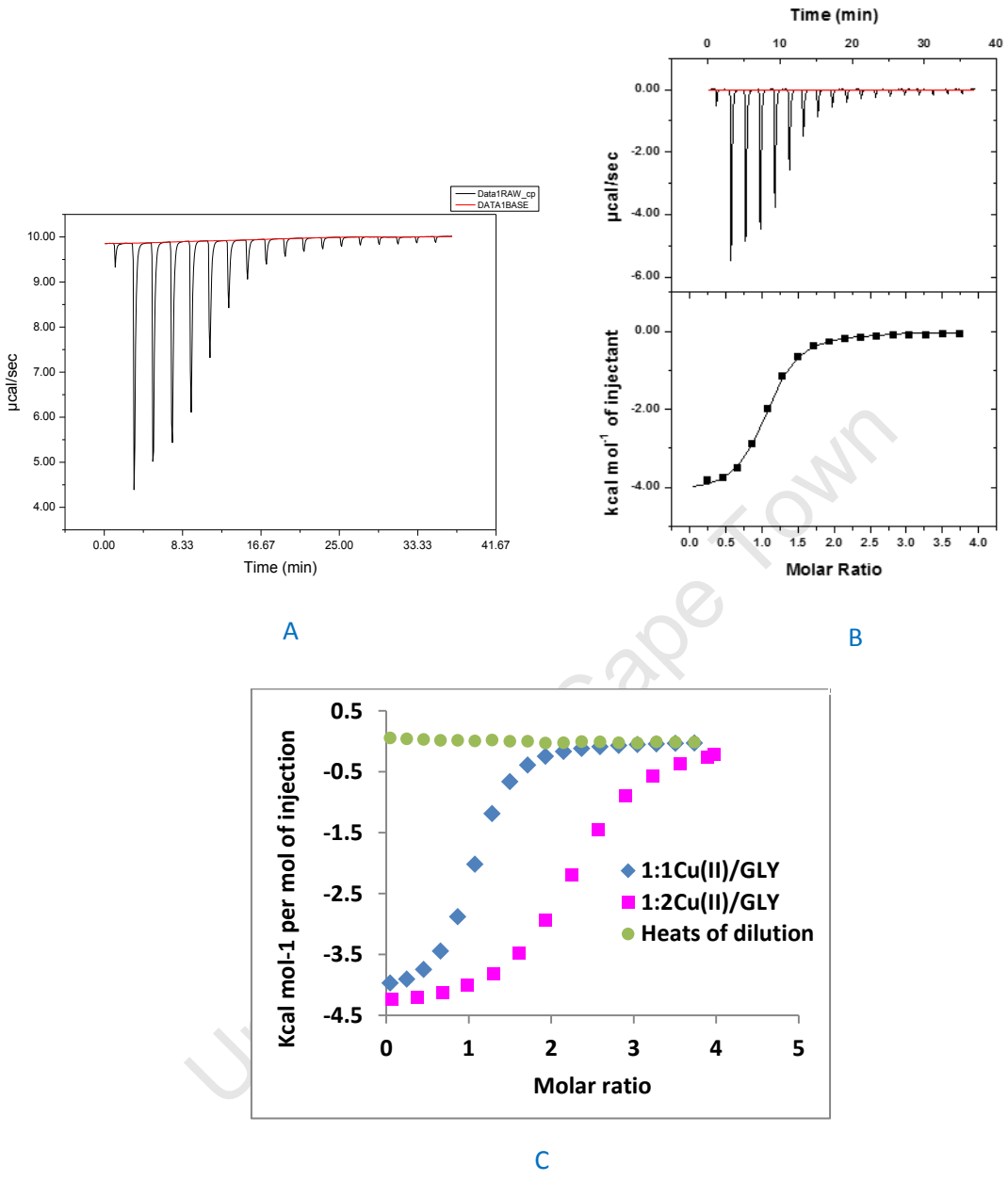

Figure 4.13: A: Raw isotherm for complexation of Cu(II) with GLY B: Final isotherm for the complexation of Cu(II) with GLY C: Molar ratio ($[H+]_{tot}/[L]_{tot}$) as a function of dH per mol of injection for the complexation of Cu(II) with GLY

The heats were converted to kJ.mol^{-1} and are giving in Table 4.12. The formation of ML is favoured thermodynamically.

Table 4.12: Calculated heats for complexation of Cu(II) with GLY and the standard deviations

Species	Log K	RTlnK (kJ.mol^{-1})	ΔH_{exp} (kJ.mol^{-1})	ΔS_{exp} (J.K^{-1}.mol^{-1})	ΔH_{lit} [22] (kJ.mol^{-1})	ΔS_{lit} [22] (J.K^{-1}.mol^{-1})
ML	8.09	-46.2	-17.5 (±0.05)	96.2 (±30)	-25.0	71.1
ML_2	7.02	-40.0	Not observed	-	-54.8	103

Complex formation titrations for Cu(II)/GLY have been done before [14]. A different experimental approach was used. Cu(II) and GLY solutions were prepared in buffer solutions. Ammonium acetate/acetic acid buffer was used for pH 5; 2-[N-morpholino] ethanesulfonic acid buffer was used for pH 6; 3-[N-morpholinino] propanesulfonic acid buffer was used for pH 7; and 3-[4,(2-hydroxyethyl)-1-piperazinyl] propanesulfonic acid buffer was used for pH 8. Cu(II) solutions were prepared in buffers and GLY solutions were also prepared in a matching buffer solution [14]. The sample cell was filled with Cu(II) solutions and titrated with GLY solutions [14]. The results differ significantly from pH to pH. At pH 5, the observed ΔH = 18.5 kJ.mol^{-1}; at pH6 ΔH = 3.36 kJ.mol^{-1}; at pH 7, ΔH = -13.2kJ.mol^{-1}; and at pH 8 ΔH = -11.8 kJ.mol^{-1} [14]. All these values do not agree with ΔH_{ML} = -25.0 kJ.mol-1 and ΔH_{ML2} = -54.8 kJ.mol^{-1}. This experimental design does not measure the true thermodynamic parameters but the conditional parameters (dependent on pH) for the completion between the ligand and the buffer for the metal ion. Hence one must be careful in comparing literature data which may be recorded using a different experimental approach.

4.4.3.2 SAR / Cu(II)

1:1 Cu(II)/SAR solutions were titrated with acid from pH 7.01 until the system was completely saturated with acid. The results are shown in Figure 4.14. The graph levels off from molar ratio 0.07 to molar ratio 0.23. The height of the plateau is -4.7kcal.mol^{-1}.

1:2 Cu(II)/SAR solutions were titrated with acid until the system was completely saturated with acid. The results are put together on one graph with the results for 1:1 Cu(II)/SAR titrations. These are given in Figure 4.14C. The height of the isotherms is reproducible regardless of the metal/ligand ratio used. N the equivalence point is however not reproducible since there is more free ligand in a 1:2 system than it is in a 1:1 system. N value for 1:2 Cu(II)/SAR titrations (N = 0.627) is twice the N value for 1:1Cu(II)/SAR titrations (N = 1.22). The olive green markers are the background heats of dilution. These are very small and thus negligible.

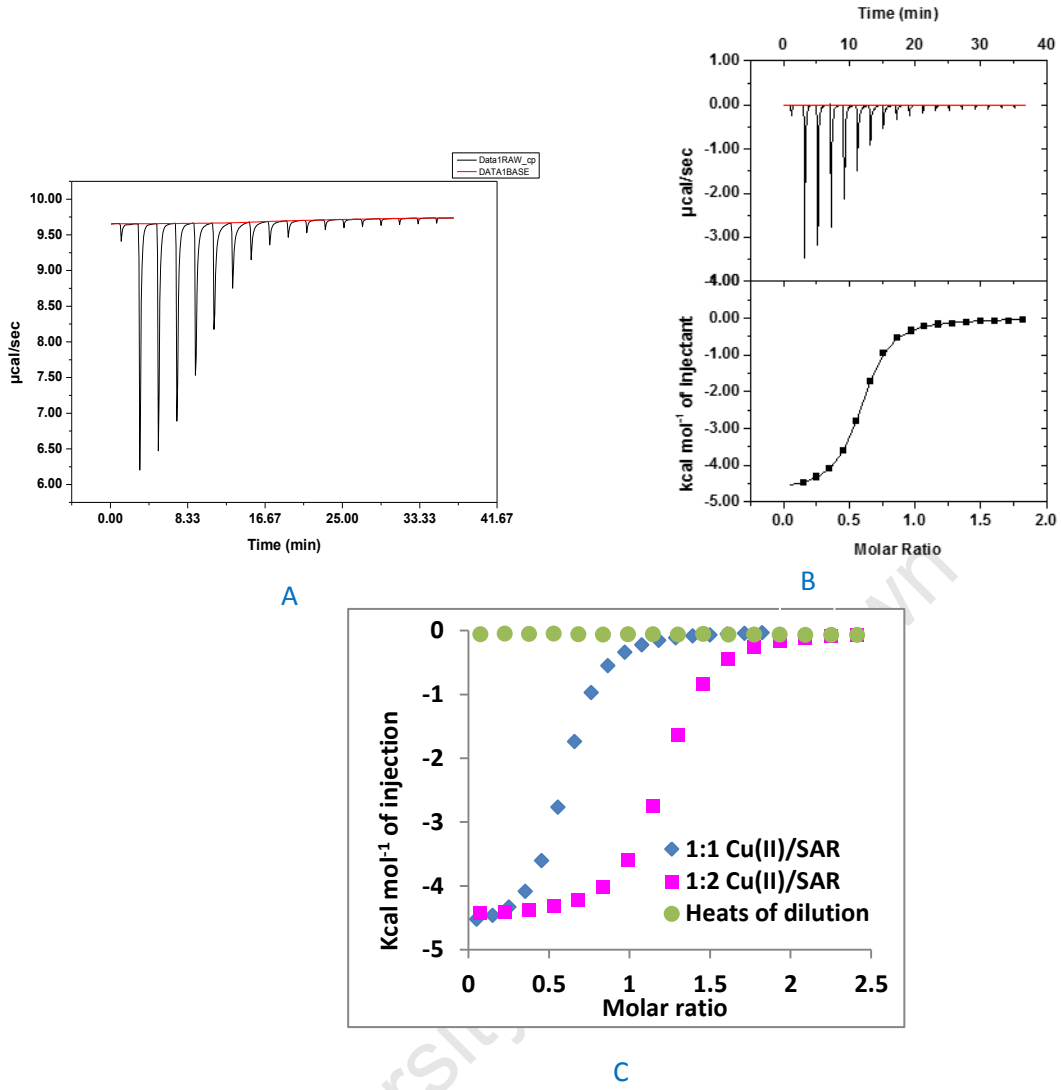

Figure 4.14: A: Raw isotherm for complexation of Cu(II) with SAR B: Final isotherm for the complexation of Cu(II) with SAR C: Molar ratio ($[H+]_{tot}/[L]_{tot}$) as a function of dH per mol of injection for the complexation of Cu(II) with SAR

Thermodynamic parameters of the complexation of Cu(II) with SAR are given in Table 4.13. Production of ML is spontaneous at all temperatures. The value of ΔH and ΔS for the formation of ML compares well with literature (ΔH = -19.0 kJ.mol^{-1}) [8]. Potentiometry revealed that several copper species are possible in this system, however, only one ΔH (ML) could be determined.

Table 4.13: Calculated heats for complexation of Cu(II) with SAR and the standard deviations

Species	Log K	RTlnK (kJ.mol^{-1})	ΔH_{exp} (kJ.mol^{-1})	ΔS_{exp} (J.K^{-1}.mol^{-1})	ΔH_{lit} [22] (kJ.mol^{-1})	ΔS_{lit} [22] (J.K^{-1}.mol^{-1})
ML	7.89	-45.0	-19.7 (±0.02)	84.9 (±30)	-19.0	91.2
ML_2	6.35	-36.2	Not observed	-	-41.8	146
MLH	4.09	-23.3	Not observed	-	-	-
ML_2H_{-1}	11.6	-66.1	Not observed	-	-	-

4.4.3.3 GLY-GLY / Cu(II)

The results for the complex formation titrations of Cu(II) with GLY-GLY are given in Figure 4.15. ΔH_{ML} = -6.10 kCal.mol^{-1}. The height of the graph for 1:1 Cu(II)/GLY-GLY is the same as the height of the graph for 1:2 Cu(II)/GLY-GLY. The background heats of dilution are very small and thus negligible.

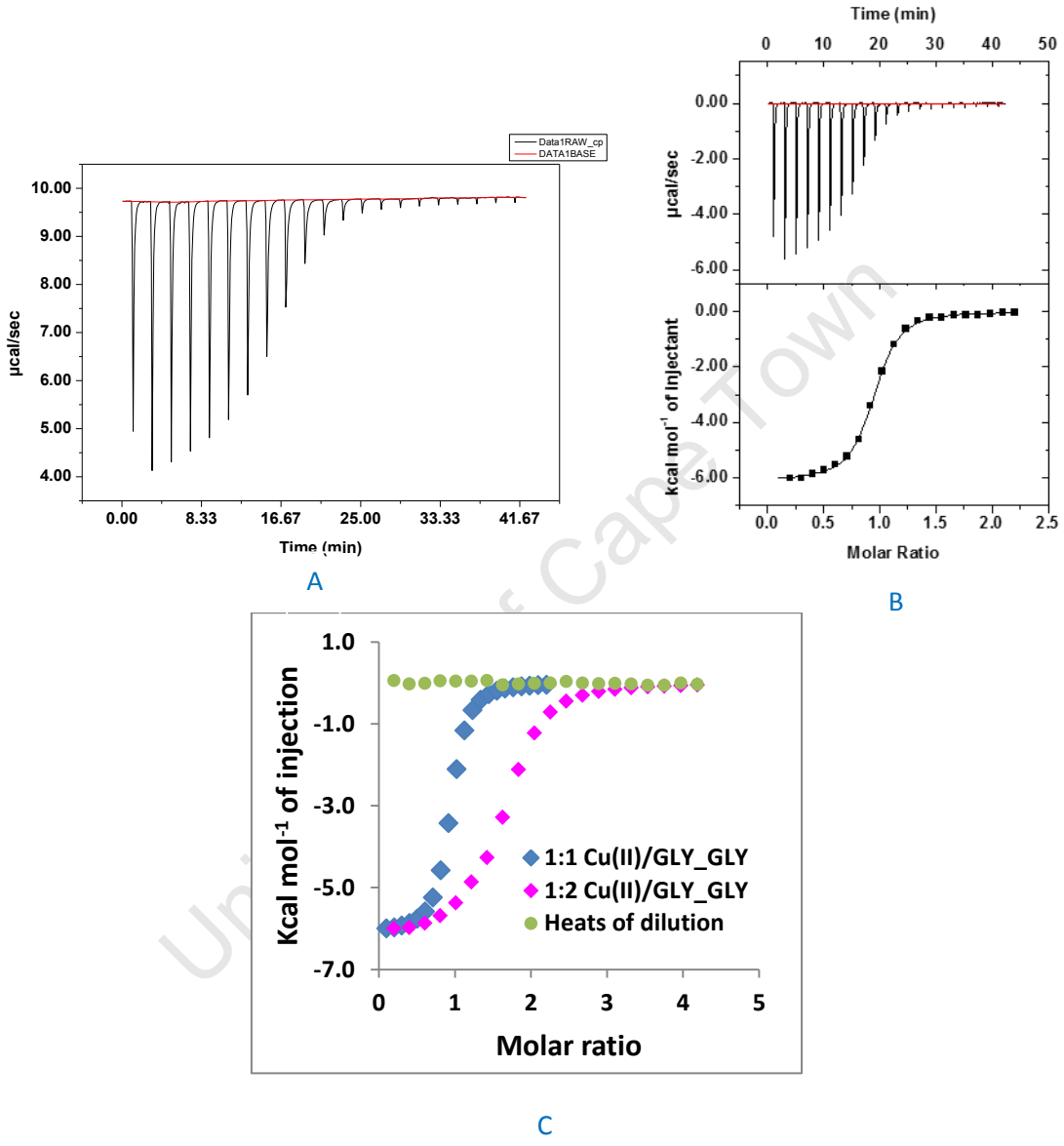

Figure 4.15: A: Raw isotherm for complexation of Cu(II) with GLY-GLY B: Final isotherm for the complexation of Cu(II) with GLY-GLY C: Molar ratio ($[H+]_{tot}/[L]_{tot}$) as a function of dH per mol of injection for the complexation of Cu(II) with GLY-GLY

Thermodynamic parameters for the complexation of Cu(II) with GLY-GLY are given in Table 4.14. ΔH compares well with the literature value (ΔH = -27.0 kJ.mol^{-1}). ΔH and ΔS could not be determined and there is no available data on ΔH and ΔS for the formation of ML_2 in the literature.

Table 4.14: Calculated heats for complexation of Cu(II) with GLY-GLY and the standard deviations

Species	Log K	RTlnK (kJ.mol^{-1})	ΔH_{exp} (kJ.mol^{-1})	ΔS_{exp} (J.K^{-1}.mol^{-1})	ΔH_{lit} [22] (kJ.mol^{-1})	ΔS_{lit} [22] (J.K^{-1}.mol^{-1})
ML	6.33	-36.1	-25.5(±0.03)	35.5 (±10)	-27.0	15.0
ML_2	4.68	-26.7	Not observed	-	-	-
MLH_{-1}	6.45	-36.8	Not observed	-	-30.3	-21.0
MLH_{-2}	10.5	-59.9	Not observed	-	-29.0	-38.0

4.4.3.4 SAR-GLY / Cu(II)

Complex formation titrations of Cu(II) with SAR-GLY are given in Figure 4.16. ΔH_{ML} = -6.00 kCal.mol^{-1}. The olive green markers are the background heats of dilution. These are very small and thus negligible.

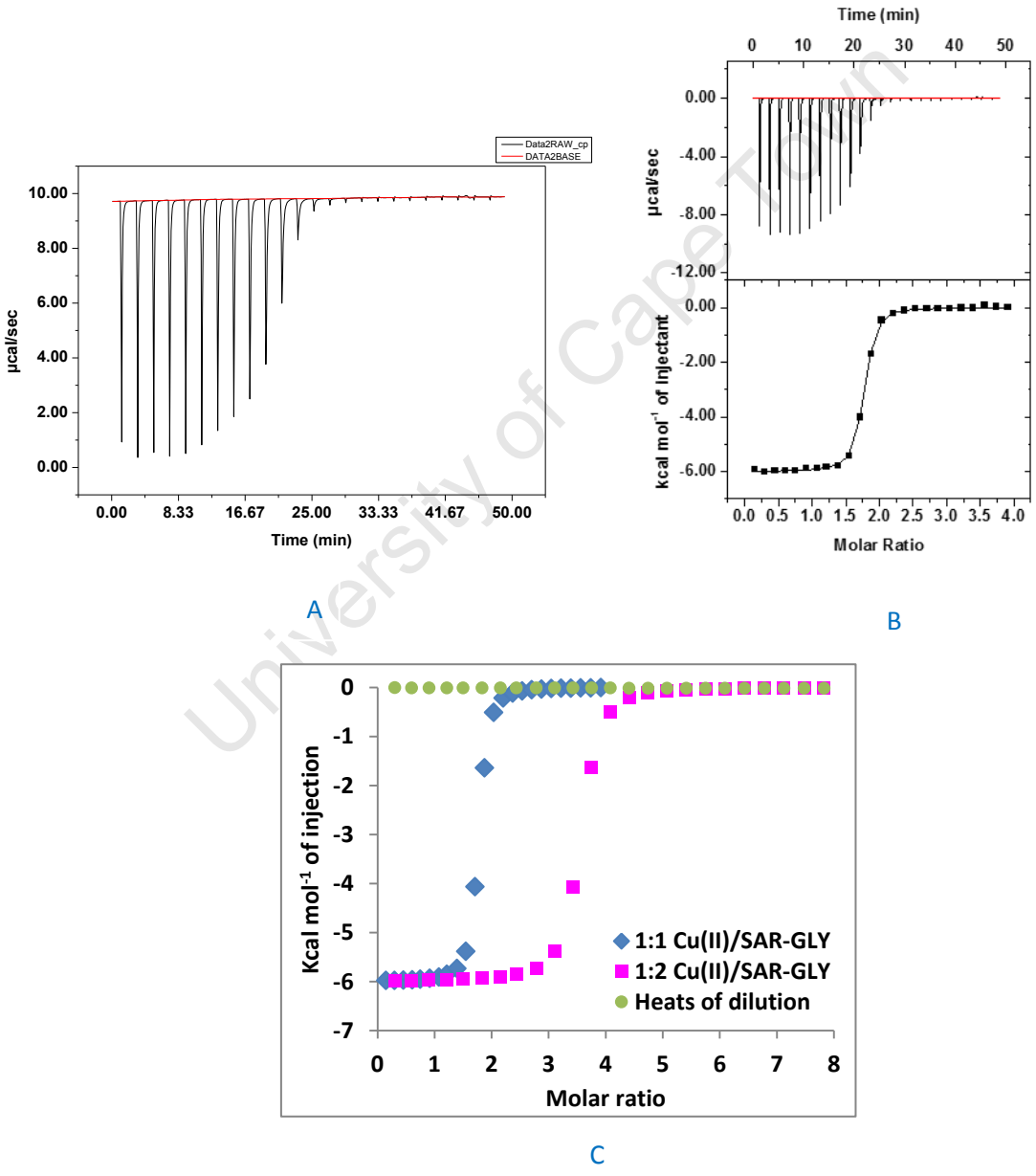

Figure 4.16: A: Raw isotherm for complexation of Cu(II) with SAR-GLY B: Final isotherm for the complexation of Cu(II) with SAR-GLY C: Molar ratio ($[H+]_{tot}/[L]_{tot}$) as a function of dH per mol of injection for the complexation of Cu(II) with SAR-GLY

Thermodynamic parameters for the complex formation titrations are shown in Table 4.15. ΔH observed in Figure 4.16 is the ΔH for the formation of ML. Even though ML_2H_{-1} (log K = 8.35) and ML_2H_{-2} (log K = 11.5) have higher log K values than ML (lig K = 6.15), these two species form at very high pH's (above pH 7). Since the titration were started below pH 7 to about pH 2 there were mainly two species in solution, ML and ML_2. ML (log K = 6.15) is more stable than ML_2 (log K = 4.19) and since only ΔH for the most stable species in solution is observed for competitive titrations, the -6.00 kcal.mol^{-1} observed in Figure 4.16 is the heat accompanying the formation of ML.

ΔH and ΔS for the complexation titrations of Cu(II) with SAR-GLY are not available in literature, however ΔH and ΔS for the formation of ML is comparable with ΔH and ΔS for the formation of ML for Cu(II)/GLY-GLY titrations.

Table 4.15: Calculated heats for complexation of Cu(II) with SAR-GLY and the standard deviations

Species	Log K	RTlnK (kJ.mol^{-1})	ΔH_{exp} (kJ.mol^{-1})	ΔS_{exp} (J.K^{-1}.mol^{-1})
ML	6.15	-35.1	-25.1 (±0.01)	33.6 (±10)
ML_2	4.91	-28.0	Not observed	-
ML_2H_{-1}	8.35	-47.6	Not observed	-
ML_2H_{-2}	11.5	-65.6	Not observed	-

4.4.3.5 GLY-LEU / Cu(II)

Figure 4.17 shows the results for complex formation titrations of Cu(II)/GLY-LEU. The heat accompanying the formation of ML for this titration is -6.61 kCal.mol^{-1}. The heights for 1:1 Cu(II)/GLY-LEU titration curve and that of a 1:2 Cu(II)/GLY-LEU titration are the same. ΔH_{ML} was therefore reproducible. The background heats of dilution are small and thus negligible.

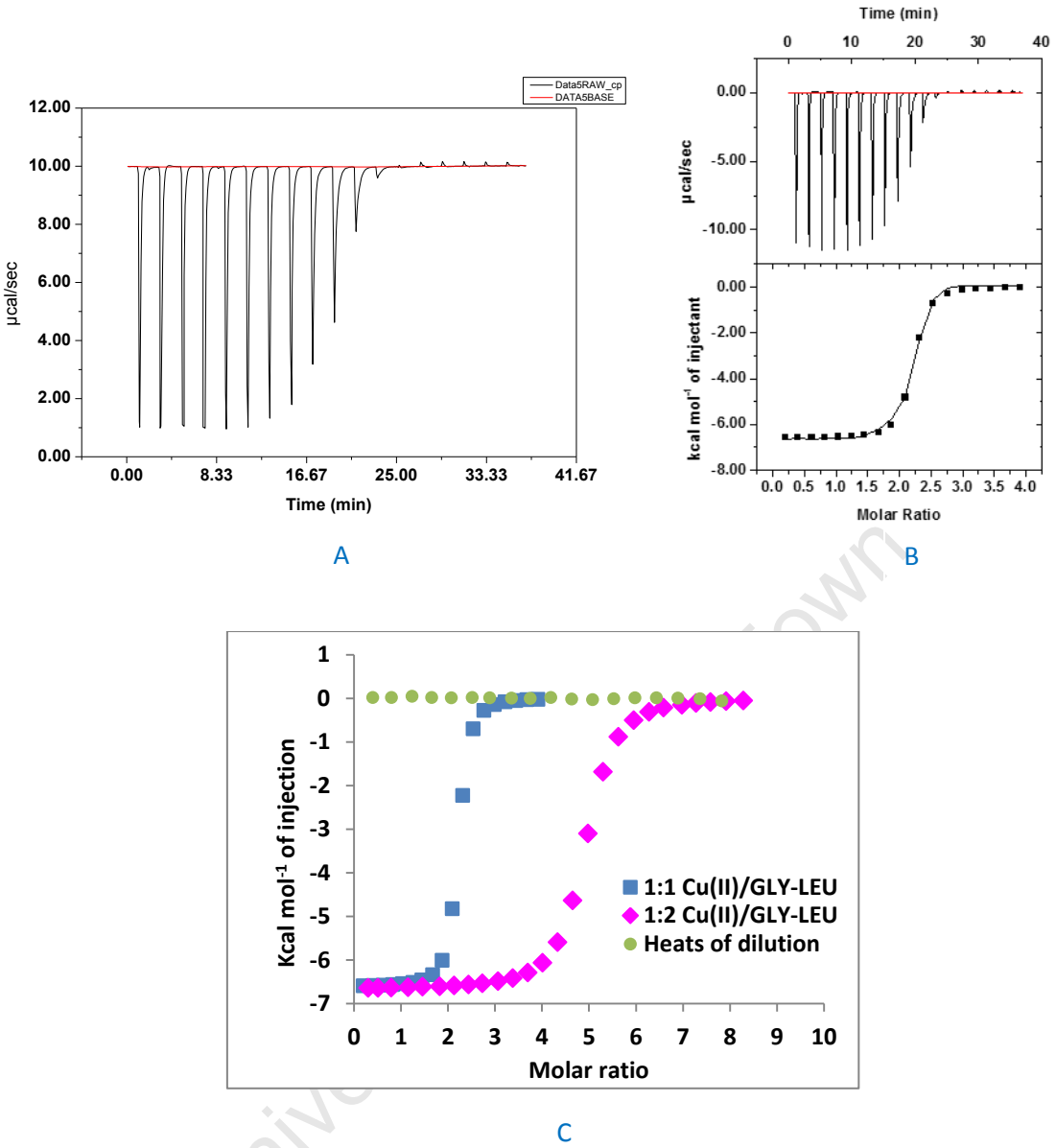

Figure 4.17: A: Raw isotherm for complexation of Cu(II) with GLY-LEU B: Final isotherm for the complexation of Cu(II) with GLY-LEU C: Molar ratio ($[H+]_{tot}/[L]_{tot}$) as a function of dH per mol of injection for the complexation of Cu(II) with GLY-LEU

Thermodynamic properties for the complexation of Cu(II) with GLY-LEU are given in Table 4.16. ΔH and ΔS for the formation of ML is not available in the literature therefore the results could not be compared with the values reported there.

Table 4.16: Calculated heats for complexation of Cu(II) with GLY-LEU and the standard deviations

Species	Log K	RTlnK (kJ.mol^{-1})	ΔH_{exp} (kJ.mol^{-1})	ΔS_{exp} (J.K^{-1}.mol^{-1})
ML	5.79	-33.0	-27.7 (±0.06)	18.0 (±5)
MLH_{-1}	4.71	-26.9	Not observed	-
ML_2H_{-1}	3.57	-20.4	Not observed	-
ML_2H_{-2}	1.78	-10.2	Not observed	-

4.4.3.6 SAR-LEU / Cu(II)

Results for Cu(II)/SAR-LEU are given in Figure 4.18. ΔH_{ML} = -5.23 kCal.mol^{-1}. ΔH_{ML} for 1:1 Cu(II)/SAR-LEU is the same as ΔH_{ML} for 1:2 Cu(II)/SAR-LEU. The background heats of dilution are very small and thus negligible.

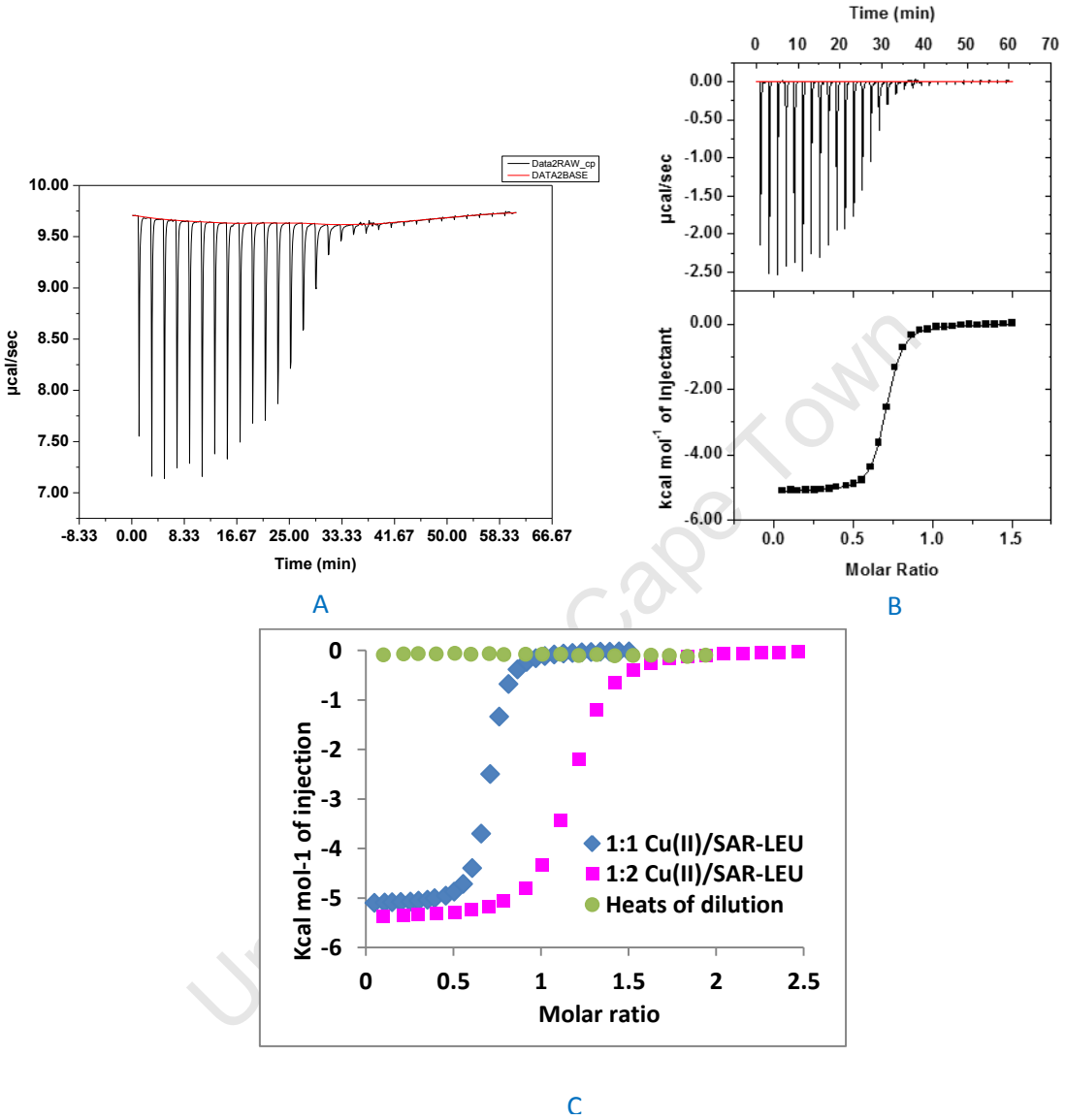

Figure 4.18: A: Raw isotherm for complexation of Cu(II) with SAR-LEU B: Final isotherm for the complexation of Cu(II) with SAR-LEU C: Molar ratio ($[H+]_{tot}/[L]_{tot}$) as a function of dH per mol of injection for the complexation of Cu(II) with SAR-LEU

ΔH for the formation of ML for Cu(II)/SAR-LEU titrations were converted to kJ.mol^{-1}. These are given in Table 4.17. There is no published work on calorimetry for Cu(II)/SAR-LEU however the errors were very small.

Table 4.17: Calculated heats for complexation of Cu(II) with SAR-LEU and the standard deviations

Species	Log K	RTlnK ($kJ.mol^{-1}$)	ΔH_{exp} ($kJ.mol^{-1}$)	ΔS_{exp} ($J.K^{-1}.mol^{-1}$)
ML	6.32	-36.1	-21.9 (±0.04)	47.5 (±10)
ML_2	4.01	-22.9	Not observed	-
MLH_{-1}	7.57	-43.2	Not observed	-
MLH_{-2}	10.3	-58.8	Not observed	-

4.4.3.7 GLY-PHE / Cu(II)

ΔH_{ML} for this titration is -4.96 $kCal.mol^{-1}$. The isotherms are given in Figure 4.19. The results were reproducible since the graph for 1:1 Cu(II)/GLY-PHE titrations have the same height as that of 1:2 Cu(II)/GLY-PHE titrations. The heats of dilution are very small and thus negligible.

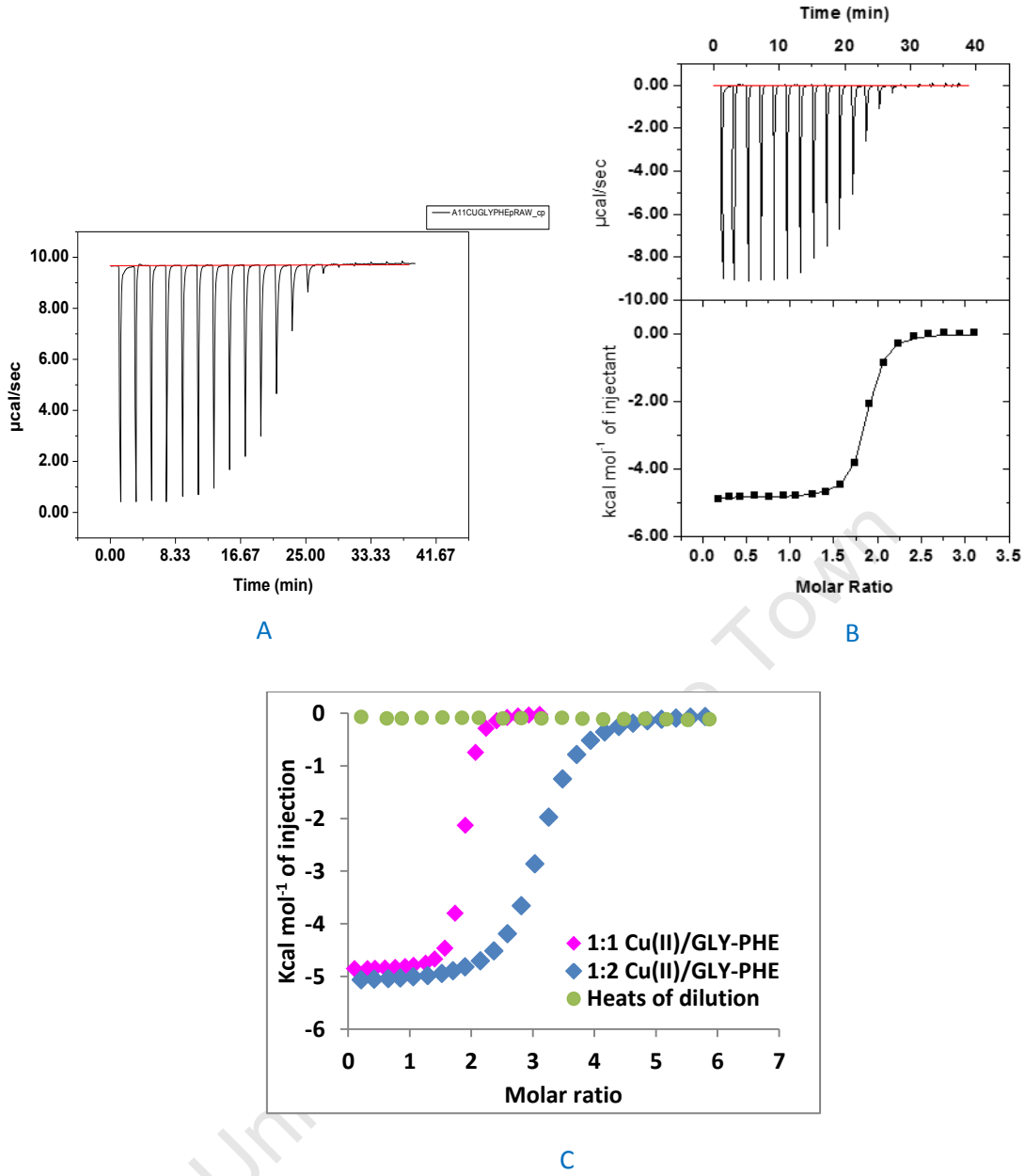

Figure 4.19: A: Raw isotherm for complexation of Cu(II) with GLY-PHE B: Final isotherm for the complexation of Cu(II) with GLY-PHE C: Molar ratio ($[H+]_{tot}/[L]_{tot}$) as a function of dH per mol of injection for the complexation of Cu(II) with GLY-PHE

Thermodynamic parameters for titrations of Cu(II)/GLY-PHE with acid were calculated and are given in Table 4.18. ΔH for the formation of ML slightly less than the literature value (Table 4.18), and ΔS is relatively higher than the literature value.

Table 4.18: Calculated heats for complexation of Cu(II) with GLY-PHE and the standard deviations

Species	Log K	RTlnK ($kJ.mol^{-1}$)	ΔH_{exp} ($kJ.mol^{-1}$)	ΔS_{exp} ($J.K^{-1}.mol^{-1}$)	ΔH_{lit} [22] ($kJ.mol^{-1}$)	ΔS_{lit} [22] ($J.K^{-1}.mol^{-1}$)
ML	6.37	-36.3	-20.8 (±0.08)	52.3 (±20)	-27.0	17.0
ML_2	5.16	-29.4	Not observed	-	-	-
ML_2H_{-1}	3.78	-21.6	Not observed	-	-16.0	5.40
ML_2H_{-2}	10.8	-61.6	Not observed	-	-	-

4.4.3.8 SAR-PHE / Cu(II)

ΔH_{ML} = -6.13 $kCal.mol^{-1}$. The isotherms are given in Figure 4.20. The results were reproducible. Olive green markers are the background heats of dilution. These are very small and thus negligible.

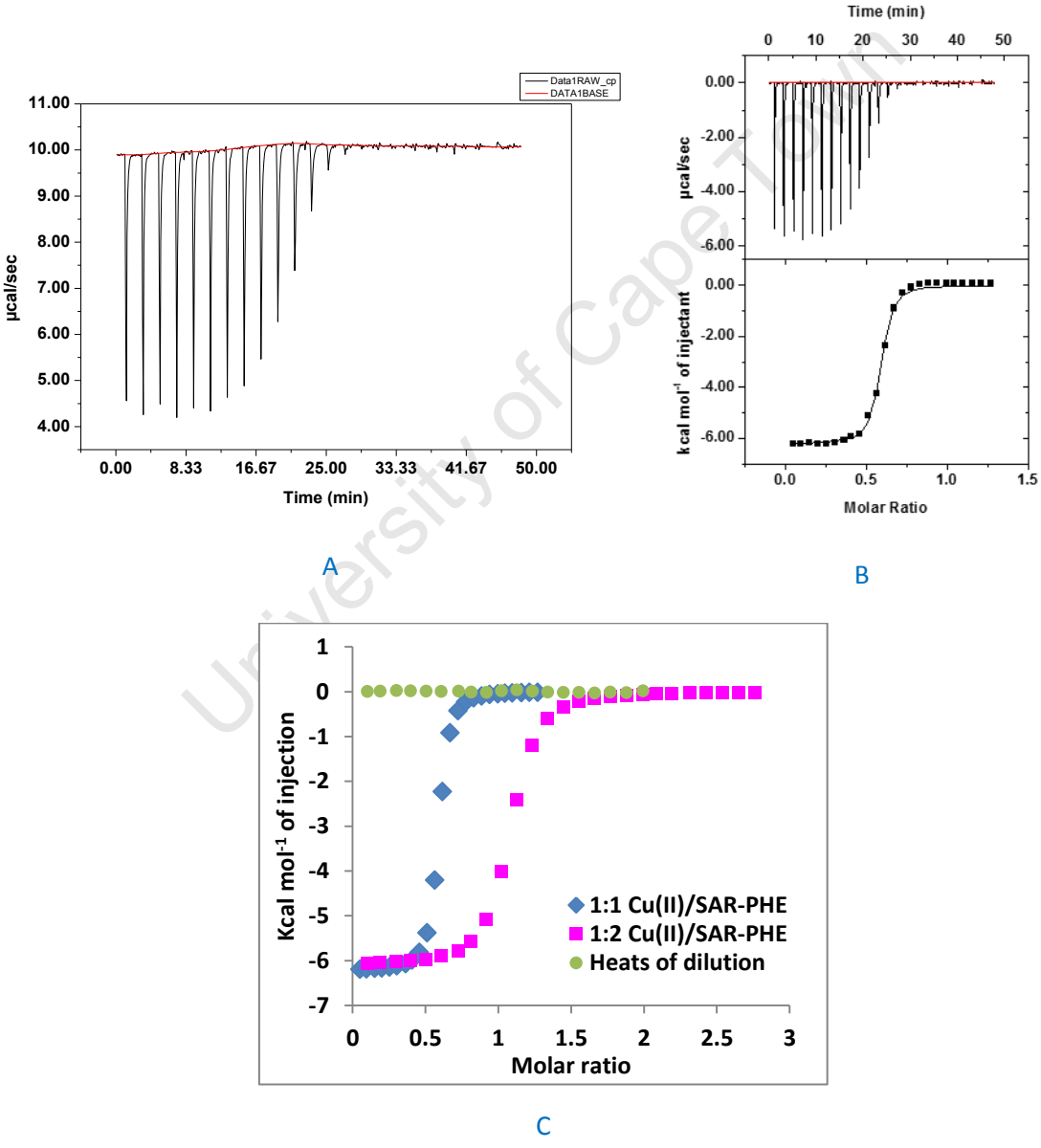

Figure 4.20: A: Raw isotherm for complexation of Cu(ii) with SAR-PHE B: Final isotherm for the complexation of Cu(II) with SAR-PHE C: Molar ratio ($[H+]_{tot}/[L]_{tot}$) as a function of dH per mol of injection for the complexation of Cu(II) with SAR-PHE

Thermodynamic parameters for Cu(II)/SAR-PHE titrations are given in Table 4.19. There is not published data to compare with. ΔH for the formation of MLH_{-1} and for the formation of MLH_{-2} could not be determined. ΔS's for these species could not be calculated either.

Table 4.19: Calculated heats for complexation of Cu(II) with SAR-PHE and the standard deviations

Species	Log K	RTlnK ($kJ.mol^{-1}$)	ΔH_{exp} ($kJ.mol^{-1}$)	ΔS_{exp} ($J.K^{-1}.mol^{-1}$)
ML	6.54	-37.3	-25.6 (±0.03)	39.1 (±10)
MLH_{-1}	5.51	-31.4	Not observed	-
MLH_{-2}	9.92	-56.6	Not observed	-

4.4.3.9 GLY-HIS / Cu(II)

Isotherms for Cu(II)/GLY-HIS complex formation titrations are given in Figure 4.21. The heat accompanying the formation of ML is -3.60 $kCal.mol^{-1}$. The height of isotherms for 1:1 Cu(II)/GLY-HIS is the same as the height for isotherms for 1:2 Cu(II)/GLY-HIS. ΔH_{ML} for this titration was therefore reproducible. The background heats of dilution are very small and thus negligible.

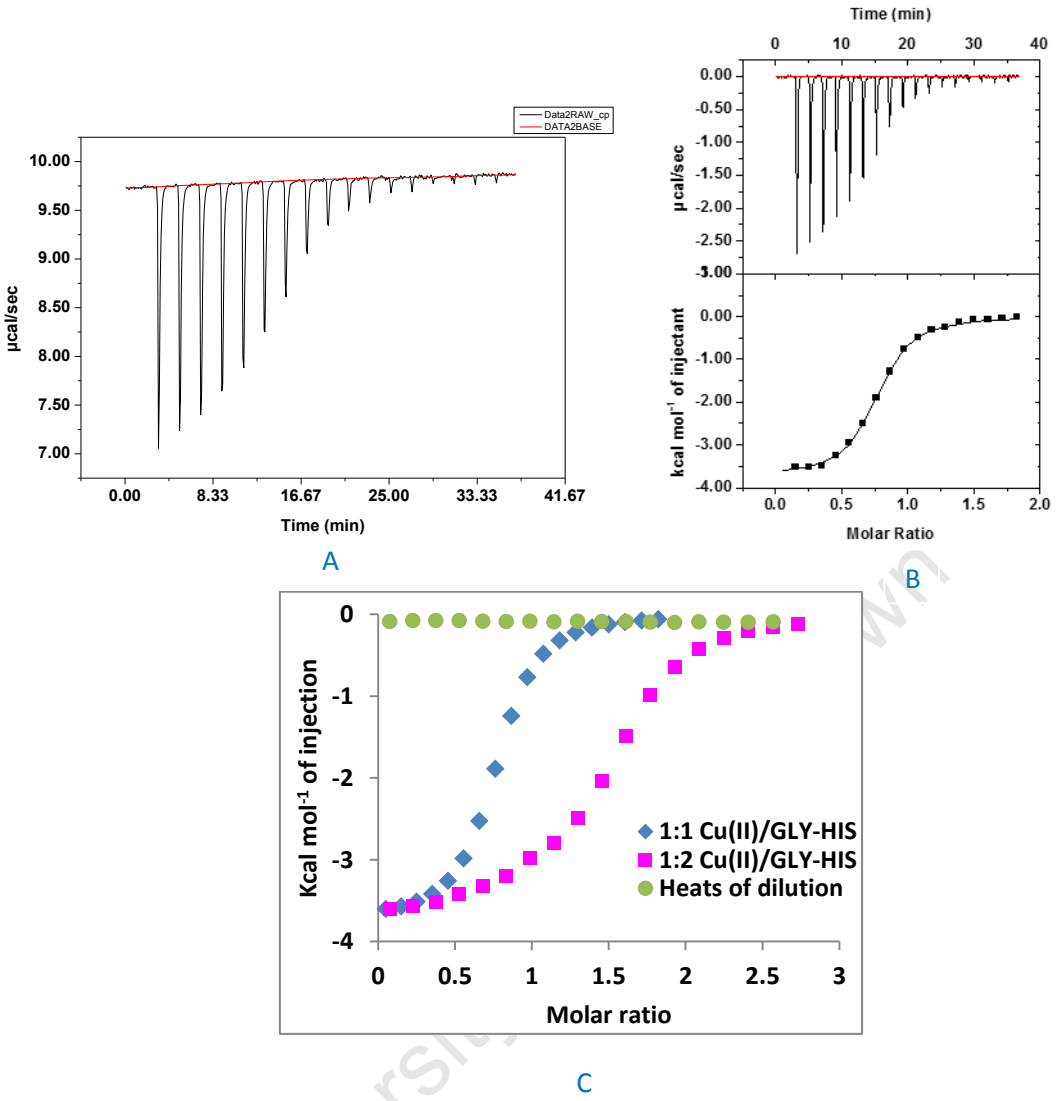

Figure 4.21: A: Raw isotherm for complexation of Cu(II) with GLY-HIS B: Final isotherm for the complexation of Cu(II) with GLY-HIS C: Molar ratio ($[H+]_{tot}/[L]_{tot}$) as a function of dH per mol of injection for the complexation of Cu(II) with GLY-HIS

Thermodynamic parameters for these titrations are given in Table 4.20. Complex formation titrations for Cu(II)/GLY-HIS have been done before but Cu(II) solutions and GLY-HIS solutions were prepared in buffers [14]. At pH 5, ΔH was 37.6 kJ.mol^{-1}; at pH 6, ΔH was -53.0 kJ.mol^{-1}; at pH 7, ΔH was -28.6 kJ.mol^{-1} and at pH 8, ΔH = -12.4 kJ.mol^{-1}. None of these four values agree with the -15.1 kJ.mol^{-1} (Table 4.20). Complex formation titrations depend on the amount of free acid as well as the amount of free metal/free ligand in solution. Titrations done at a fixed pH may restrict the amount of species formed as well as the distribution of species formed.

Table 4.20: Calculated heats for complexation of Cu(II) with GLY-HIS and the standard deviations

Species	Log K	RTlnK ($kJ.mol^{-1}$)	ΔH_{exp} ($kJ.mol^{-1}$)	ΔS_{exp} ($J.K^{-1}.mol^{-1}$)
ML	9.16	-52.3	-15.1 (±0.02)	125 (±40)
MLH_{-1}	4.84	-27.6	Not observed	-
MLH_{-2}	3.21	-18.3	Not observed	-
MLH_{-3}	2.00	-11.4	Not observed	-

4.5 DISCUSSIONS

All protonation equilibria are favoured thermodynamically even though the spontaneity of the formation of some species is more driven by entropy while some are driven by both entropy and enthalpy. A summary for thermodynamic parameters of the ligand protonation is given in Table 4.21. From potentiometric titrations, the first pKa of GLY (log K_{LH} = 9.53) was found to be less than the first pKa of SAR (log K_{LH} = 10.0). At this point the question was raised as to whether this was due to the inductive effect of the N-methyl group. From the calorimetry results, it is observed that ΔH_{LH} (GLY) is 12.7 kJ.mol^{-1} more than ΔH_{LH} (SAR). $T\Delta S_{LH}$ (GLY) is however 15.4 kJ,mol^{-1} less than $T\Delta S_{LH}$ (SAR). Thus the increased basicity of SAR is entropy driven rather than enthalpy driven. A similar effect is seen in the pKa of substituted amines, where the inductive effect of the methyl group results in a gas phase basicity order of $(CH_3)_3N > (CH_3)_2NH > (CH_3)NH_2 > NH_3$. However, in water the order is $(CH_3)_2NH > NH_3 > (CH_3)NH_2 > (CH_3)_3N$. This is the result of two competing effect, the inductive effect of the methyl group and the effect of H-bonding in solution [23].

As expected, the thermodynamic parameters for protonation of the carboxylic acid of GLY and SA are very similar. ΔH_{LH2} (GLY) is 0.34 kJ.mol^{-1} greater than ΔH_{LH2} (SAR), and $T\Delta S_{LH2}$ (GLY) is 0.69 kJ.mol^{-1} greater than $T\Delta S_{LH2}$ (SAR). The substantial decrease in ΔH_{LH2} compared to ΔH_{LH} is expected as the strength of the OH bond is much less than the NH bond. However, one might have expected ΔS to be large and positive because of decreased solvation of the neutral COOH as opposed to the charged COO^-. The LH form of both ligands is nonpolar and therefore the spontaneity of protonation of LH to LH_2 is mostly driven by enthalpy. Indeed, Li et al [24] obtained a value of 30.9 J.K^{-1}.mol^{-1} for protonation of the carboxyl group of glycine.

The effect of the peptide bond upon pKa can be seen by comparing GLY and GLY-GLY. The pKa_1 of GLY is 9.53 and that of GLY-GLY is 8.16, a decrease of 1.37 log units. The peptide bond decreases pKa_2 by 0.84 log units. Looking at the thermodynamic parameters for these two ligands, it is observed that the enthalpy values are very similar but that the entropy values are very different. Again one might have expected the electron withdrawing effect of the amide group to be reflected in the enthalpy and not the entropy.

With the exception of GLY-HIS, the pKa's and enthalpies of protonation of the dipeptides are all very similar. However, the entropies for the peptides (GLY-GLY, SAR-GLY, GLY-LEU, SAR-LEU, GLY-PHE and SAR-PHE) vary from 7 to 37 $J.K^{-1}mol^{-1}$. This is most likely due the error in the entropy measurement.

Table 4.21: Gibbs's free energy, enthalpy change and entropy change for the protonation of GLY ligands and SAR ligands.

Ligand	Species	ΔG ($kJ.mol^{-1}$)	ΔH_{exp} ($kJ.mol^{-1}$)	ΔS_{exp} ($J.K^{-1}.mol^{-1}$)	$-T\Delta S_{exp}$ ($kJ.mol^{-1}$)
GLY	LH	-54.4	-41.6	42.9	-12.8
	LH_2	-13.1	-9.85	10.8	-3.21
SAR	LH	-57.0	-28.9	94.6	-28.2
	LH_2	-12.0	-9.51	8.47	-2.52
GLY-GLY	LH	-46.6	-44.6	6.54	-1.95
	LH_2	-18.1	-12.8	18.0	-5.36
SAR-GLY	LH	-48.1	-41.9	20.8	-3.95
	LH_2	-16.8	-10.5	21.2	-6.32
GLY-LEU	LH	-46.8	-44.8	6.75	-2.01
	LH_2	-17.9	-9.21	29.2	-8.71
SAR-LEU	LH	-49.6	-38.5	37.3	-11.1
	LH_2	-19.9	-9.25	35.6	-10.6
GLY-PHE	LH	-46.8	-44.6	7.31	-2.18
	LH_2	-16.6	-8.00	28.8	-8.60
SAR-PHE	LH	-48.4	-40.9	25.2	-7.50
	LH_2	-17.4	-10.6	22.9	-6.81
GLY-HIS	LH	-47.6	-50.9	-11.2	3.34
	LH_2	-37.7	-18.5	64.6	-19.2
	LH_3	-13.1	0	43.8	-13.1

A summary of ITC results for complex formation titrations is given in Table 4.22. ΔH_{ML} (GLY) is 2.2 $kJ.mol^{-1}$ greater than ΔH_{ML} (SAR); ΔH_{ML} (GLY-GLY) is 1.0 $kJ.mol^{-1}$ greater than ΔH_{ML} (SAR-GLY); ΔH_{ML} (GLY-LEU) 5.8 $kJ.mol^{-1}$ greater than ΔH_{ML} (SAR-LEU); ΔH_{ML} (GLY-PHE) is 4.8 $kJ.mol^{-1}$ less than ΔH_{ML} (SAR-PHE) and ΔH_{ML} (GLY-HIS) is the least of all. The literature [16, 25, 36] shows that Cu(II) coordinates to the amine N-donor and to the carboxylate O-donor for Cu(II)/GLY and Cu(II)/SAR.

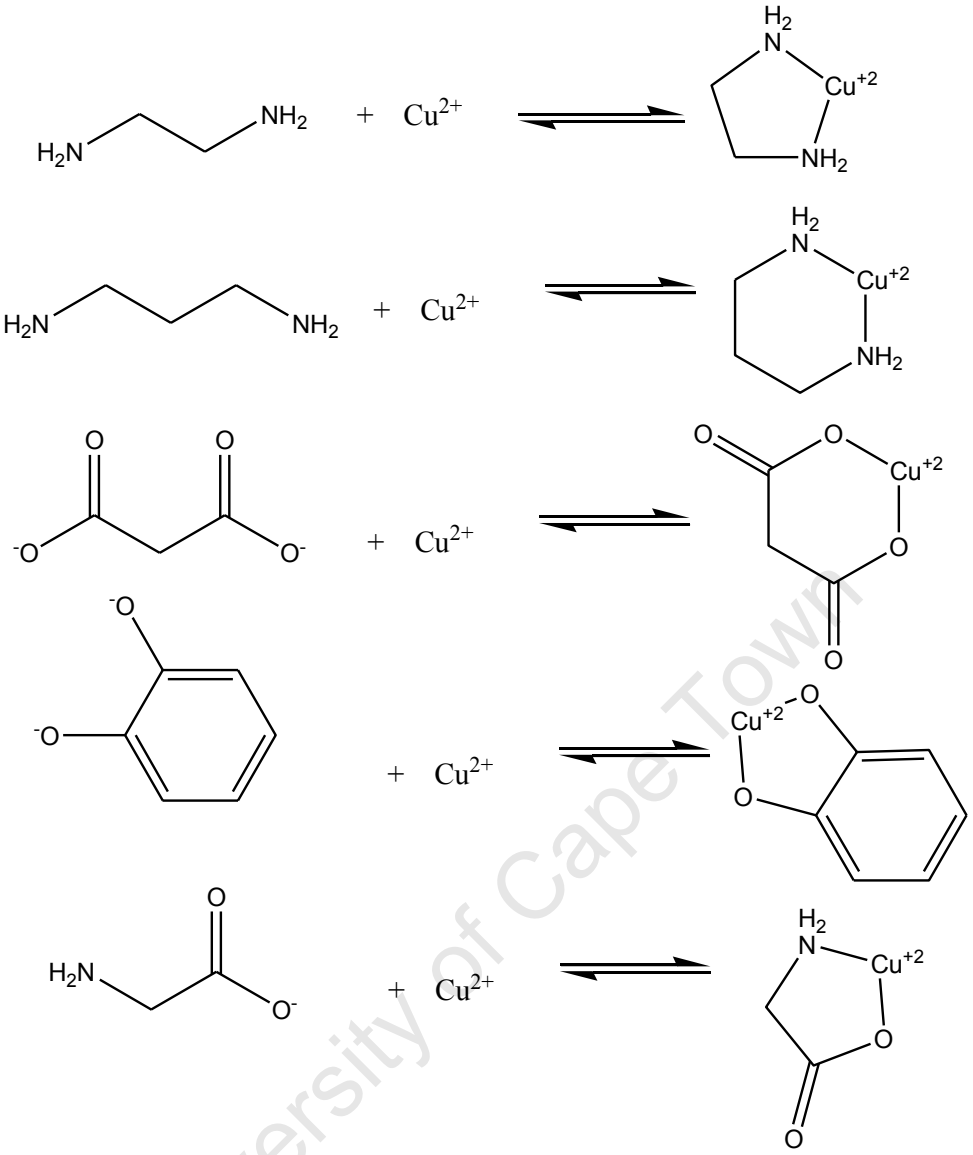

From Hancock's work [36], the heat accompanying the first reaction is -52.7 kJ,mol^{-1}, and the heat accompanying the second reaction is -47.7 kJ.mol^{-1}. The heat accompanying a single Cu-N bond (5-memebered chelate ring) is therefore -26.4 kJ.mol^{-1}, and the heat accompanying a single Cu-N bond (6-memebered chelate ring) is 23.9 kJ.mol^{-1}. Soli and co-workers [27], and other publishers [28, 29] have determined ΔH accompanying the formation of $CuCO_3$ = -10.4 kJ.mol^{-1}. From Mohan, Bancroft and Abbort's work [37], the heat accompanying the first reaction is -59.9 kJ.mol^{-1} (ΔH single (Cu-N) = -30.0 kJ.mol^{-1}), the heat accompanying the third reaction is +4.60 kJ.mol^{-1}(ΔH single (Cu-O) = +2.30 kJ.mol^{-1}), the heat accompanying the 4th reaction is -21.8 kJ.mol^{-1} (heat for a single Cu-O = -10.9 kJ.mol^{-1}), and the heat accompanying the 5th reaction is -27.6 kJ.mol^{-1}. ΔH_{ML} depends

on the ligand's affinity to bind with the metal ion (log K_{ML}). The heat accompanying a single Cu-N bond is almost the same for the first two reactions because the log K_{ML}'s for the first two ligands are similar; log K_{ML} (Cu-ethylene diamine) = 10.5 and log K_{ML} (Cu-propylene-1, 3-diamine) = 9.68 [36, 37]. Log K_{ML} (Cu-malonate) = 5.22, log K_{ML} (Cu-pyrocachol) = 13.8. The size of the chelate ring also affects ΔH's, with a single Cu-N (propylene-1, 3-diamine) being less than that of ethylene diamine. From this information the structure of Cu-peptides can be predicted. The peptides have four active binding sites; the terminal amine N, amide N, amide O and the carboxylate O. GLY-HIS has two additional N-donors on the imidazole side ring. All ΔH_{ML} (Cu-peptide) suggest that Cu(II) coordinates to one N donor atom and on one O donor atom since the experimental values are between -20.8 kJ.mol^{-1} and -27.7 kJ.mol^{-1}. These values are close to -31.1 kJ.mol^{-1} which is the sum of the average ΔH (Cu-N) and ΔH (Cu-O). ΔH_{ML} (Cu-GLY-HIS) is significantly less than -31.1 kJ.mol^{-1} therefore Cu(II) does not coordinate to the same electron donor groups as the other dipeptides when ML forms.

$-T\Delta S_{ML}$ (GLY) and $-T\Delta S_{ML}$ (SAR) are almost three times more than $-T\Delta S_{ML}$ (GLY-GLY), $-T\Delta S_{ML}$ (SAR-GLY) and $-T\Delta S_{ML}$ (SAR-PHE). This could mean that when Cu(II) coordinates to GLY-GLY, SAR-GLY and SAR-PHE very few water molecules were lost (almost a third of molecules that GLY and SAR) upon complexation with Cu(II). Some of the electron donor groups are still engaged in H-bonding with the water molecules. $-T\Delta S_{ML}$ (SAR-LEU) and $-T\Delta S_{ML}$ (GLY-PHE) are almost half $-T\Delta S_{ML}$ (GLY) and $-T\Delta S_{ML}$ (SAR). Very few water molecules were lost upon complexation of GLY-LEU with Cu(II). This could mean that terminal amine has not engaged in bonding.

Table 4.22: Gibbs's free energy, enthalpy change and entropy change for the complex formation titrations of Cu(II) with GLY ligands and SAR ligands

Ligand	Species	log K_{ML}	ΔG (kJ.mol^{-1})	ΔH_{exp} (kJ.mol^{-1})	ΔS_{exp} (J.K^{-1}.mol^{-1})	$-T\Delta S_{exp}$ (kJ.mol^{-1})
GLY	ML	8.09	-46.2	-17.5 (±0.05)	96.2	-28.7
SAR	ML	7.89	-45.0	-19.7 (±0.02)	84.9	-25.3
GLY-GLY	ML	6.33	-36.1	-25.5 (±0.03)	35.5	-10.6
SAR-GLY	ML	6.15	-35.1	-25.1 (±0.01)	33.6	-10.0
GLY-LEU	ML	5.79	-33.0	-27.7 (±0.06)	18.0	-5.37
SAR-LEU	ML	6.32	-36.1	-21.9 (±0.2)	47.5	-14.2
GLY-PHE	ML	6.37	-36.3	-20.8 (±0.08)	52.3	-15.6
SAR-PHE	ML	6.54	-37.3	-25.6 (±0.03)	39.1	-11.7
GLY-HIS	ML	9.16 [12]	-52.3	-15.1 (±0.02)	125	-37.2

4.6 CONCLUSIONS

The methyl substituent of sarcosine ligands does not affect the stability of ligands and subsequently does not affect the stability of complexes of these ligands with Cu(II) thermodynamically. Many authors [27-35] have used ITC to study thermodynamic properties of Cu(II) complexes but all of them have used buffers, which makes our experimental design the first of its kind and thus more studies have to be made to gather confidence in the method.

RERERENCES

[1] *ITC Data Analysis in Origin®*, MicroCal LLC. (**2004)**; 9-114.

[2] Noyes, K. and Sosman, R. B., *Journal of American Chemical Society*. (**1910**); 32, 159.

[3] Rossini, F. D. *Journal of Research of the National Bureau of Standards*. (**1931)**; 6: 847-856.

[4] Ollingson, E. O. *Journal of American Chemical Society*. (**1915);** 37(4): 699-709.

[5] Baranauskienė, L., Petrikatė, V., Matulienė, J. and Matulis, D. *International Journal of Molecular Sciences.* (**2009):** 10: 2752-2762.

[6] Schwarz, F. P., Reinisch, T., Hinz, H. and Surolia, A. *Pure and Applied Chemistry*. (**2008**); 80(9): 2025-2040.

[7] Gimeson, P. *Microcal™ iTC_{200} training manual*. G. E. Healthcare.

[8] Smith, R. M. and Martell, A. E. NIST Critically Selected Stability Constants of Metal Complexes Database. (**1994**). Version 8.0 for Windows.

[9] Dean, J. A. *Lange's Handbook of Chemistry.* (**1999);** 1174-1343.

[10] Christensen, J. J., Hansen, L. D., and Izatt, R. M. *Handbook of Proton Ionization heats*. (**1976):** 2505-2508.

[11] Izarr, R.M., Oscarson, J. L., Gillespi, S. E., Grimsrud, H., Renuncio, J. A. R., and Pando, C. *Biophysical Journal.* (**1992**); 61: 1394-1401.

[12] Branch, G. E. K. and Miyamoto, S. *Journal of American Chemical Society.* (**1930)**; 52(3): 863-868.

[13] Jameson, R. F. and Wilson, M. F. *Journal of Chemical Society.* (**1972)**; 23: 2617-2621.

[14] Mohajane, M. *MSc Thesis*. University of Cape Town. (**2010**).

[15] Suh, M., Lee, C., Sohn, S., Kim, J., Kim, W. and Eom, T. *Journal of Chemical and Analytical Science*. (**1999);** 12(3): 177-183.

[16] Odisitse, S. *PhD Thesis*. University of Cape Town. (**2007**).

[17] Freyer, M. W. and Lewis, E. A. *Methods in Cell Biology*. (**2008**); 84: 80-111.

[18] Kasimova, M. R (http://www.protein-solutions.dk/pdf/TroublwshootingITC.pdf).

[19] Marquardt, D. W. *Journal of Industrial and Applied Mathematics.* (**1963**); 11(2): 431-441.

[20] Budil, D. E., Lee, S.,Saxena., S and Freed, J. H. *Journal of Magnetic Resonance*. (**1996**); 120: 155-189.

[21] Sigurskjold, B. W. *Analytical Biochemistry*. (**2000**); 277(2): 260-266.

[22] Powell, K. J. The IUPAC Stability Constants Database. SC-Database. (**2000**).

[23] Perrin, C. L., Ohta, B. K. and Kuperman, J. *Journal of the American Chemical Society*. (**2003**); 125(49):15008-15019.

[24] Gang, L., Rui-Sen, L. and Han-Xing, Z. *Acta Physico-Chimica Sinica*. (**2000**); 16(2): 188-192.

[25] Colaneri, M. J., Vitali, J. and Peisach, *Journal of Physical Chemistry*. (**2009**); 113(19): 5700 5709.

[26] Temitayo, A., Issac, O. and Olugbenga, A. *International Journal of Chemistry*.(**2012**); 4(2): 49-59.

[27] Soli, A. L. and Byrne R. H. *American Society of Limnology and Oceanography*. (**1989**); 34(1): 239-244.

[28] Powell, K. J., Brown, P., Byrne, R. H, Gajda, T.,Helfter, G., Sjoberg, S. and Wanner, H. *Pure and Applied Chemistry*. (**2007**); 79(5): 895-950.

[29] Millero, F. J., -Casiano, M and -Davila, M. *Journal of Solution Chemistry*. (**2010**); 39(4): 543-558.

[30] Ababou, A. and Ladbur, J. E. *Journal of Molecular Recognition*. (**2007**); 20(1): 4 14,

[31] Thompsett, A. R., Abdelraheim, S. R., Daniels, M. and Brown, D. M. *The Journal of Biological Chemistry*. (**2005**); 280: 42750-42758.

[32] De Bruin, T. J. M., Marcelis, A. T. M. Zuilhof, H., and Sudhölter, E. J. R. *Journal of the American Chemical Society*. (**2000**); 16(22): 8270 8275

[33] Wilcox, D. E. *Inorganica Chimica Acta*. (**2008**); 261(4): 857 867.

[34] Saboury, A. A. *Journal of Thermal Analysis and Calorimetry*. (**2004**); 72(1): 93-103.

[35] Saboury, A. A. *Journal of the Iranian Chemical Society*. (**2006**); 3(1): 1-21.

[36] Hancock, R. D. *Pure and Applied Chemistry*. (**1986**); 58(11): 1445-1452.

[37] Mohan, M. S., Bancroft, D. and Abbort, E. H. Inorganic Chemistry. (**1979**); 18(2): 344-346.

5. STRUCTURAL STUDIES

5.1 ^{1}H NMR SPECTROSCOPY

5.1.1 INTRODUCTION

Proton magnetic resonance spectroscopy (^{1}H NMR) is a technique used to determine the structure of molecules. In the magnetic field, different protons resonate at different frequencies [15]. A spectrum for ^{1}H NMR is a plot of signal intensity against chemical shift. The choice a solvent used is critical when doing NMR experiments [4, 13]. Deuterated water is commonly used in ^{1}H NMR titrations and NaOD/DCl solutions are used to adjust the pD of the solutions [1-4].

The chemical shift depends on electron density which changes as the ligands changes from LH_2 to LH to L [5]. Thus a plot of chemical shift vs pD can be used to determine the site of protonation of a ligand [4, 5]. Many authors have used ^{1}H NMR to determine the sequence of protonation of the ligands, to estimate the protonation constants and to predict the structures of metal/ligand complexes [1-3, 8-12].

Due to its paramagnetic property, Cu(II) broadens spectra when it coordinates to the ligand. This broadening can be a "through bond effect" (Fermi contact interaction) or a "through space effect" which is dependent on the distance between the paramagnetic center and the observed nucleus. The differential effect of the metal ion on the ligand can then be used to determine the structure of the complex.

5.1.2 EXPERIMENTAL

All solutions were prepared in D_2O. Tertiary butyl alcohol was used as an internal reference. The pD of the solutions was adjusted with NaOD/DCl as described [1-3]. A CRISONmicro pH meter equipped with Ω Metrohm glass electrode was used to measure the pH. The spectra were recorded from pD 2 to pD 11 with a Bruker Avance 400 NMR spectrometer. Complex formation titrations were run as described [1]. Into the ligand solution, small aliquots of dilute Cu(II) solution were added. The pD of the ligands solutions was fixed at about pH 6 for the first six/seven titrations, and the pD was varied for the last three/four titrations. Since a pH electrode was used to measure pD, corrections are made as described [4, 6, 7];

$$pD = pH \text{ meter reading} + 0.44 \quad (5.1)$$

5.1.3 RESULTS

5.1.3.1 Protonation titrations

^{1}H NMR can be used as a probe to the site of protonation during a pH titration. In the case of the dipeptides studied, the site of protonation is known but the effect of protonation in terms of chemical shift change is not known. This information is needed when looking at the effect of metal ions upon the NMR spectrum. In water, the amine protons are in rapid chemical exchange and so are not seen in the NMR spectrum. At low pH it is possible to see the amide protons but they too are exchange broadened above pH ~6. For this reason the spectra were all run in D_2O, which is technically much easier and does not require solvent suppression.

5.1.3.1.1 Protonation of glycyl-leucine

^{1}H NMR results for the titration of GLY-LEU are given in Figure 5.1. Figure 5.1A is the raw spectra from pD 2.75 to pD 9.30. The signal labeled 'a' shifted significantly from pD 2.75 to pD 4.26. This signal is assigned to the proton of the α-carbon of the C-terminal (labeled 'a' on Figure 5.1C). This indicates that the protonation of the carboxylate terminal occurs at low pD's. A small change in chemical shift for the proton of the α-carbon 'a' was observed from pD 5.70 to pD 9.30. Form pD 2.75 to pD 7.95, signal 'b' did not shift significantly. A significant shift was observed between pD 7.95 and pD 9.30. This signal is assigned to the protons of the α-carbon of the N-terminal (carbon labeled 'b' on Figure 5.1B). This indicates that protonation of the amine terminal occurs at high pD's. Signals 'c' and 'd' did not shift significantly. Figure 5.1B shows the chemical shift as a function of pD. The protonation constants of GLY-LEU can be estimated from this graph. Log K_{LH} = 8.2. This is the mid-point of the steepest slope of 'a' on Figure 5.1B. Log K_{LH2} = 3.1. This is the mid-point of the steepest slope of 'b' on Figure 5.1B. These agree with the potentiometric results (Table 3.5).

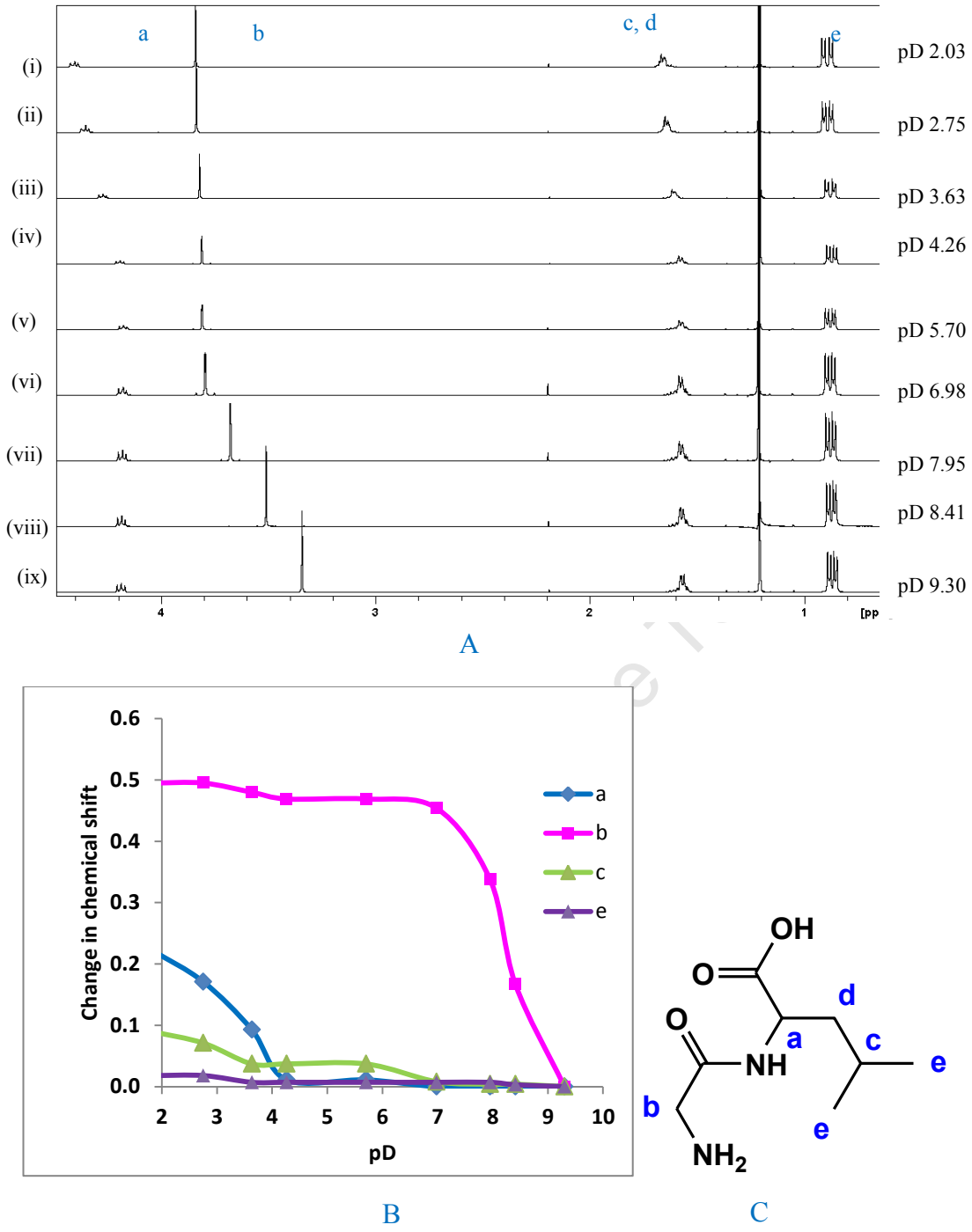

Figure 5.1: A: Raw ^{1}H NMR titration data from pD 2 to pD 10 for the protonation of GLY-LEU: **B:** Change in chemical shift for the protonation of GLY-LEU **C:** Assigned chemical shifts for GLY-LEU

5.1.3.1.2 Protonation of sarcosyl-leucine

Results for SAR-LEU protonation are given in Figure 5.2. Raw data is shown in Figure 5.2A, change in chemical shifts as a function of pD is given in Figure 5.2B and the assignments are given in Figure 5.2C. Protonation of the amine terminal occurs from pD 7.52 where signals 'a' and 'c' start shifting tremendously. Log K_{LH} = 8.7. This agrees with

the potentiometric results (Table 3.6). Protonation of the carboxylate terminal occurs at low pD's and it could not be estimated. Signals 'a' and 'e' however shifted at low pD's (pD 2.23 to pD 4.09). These two signals shifted due to the protonation of the carboxylate terminal.

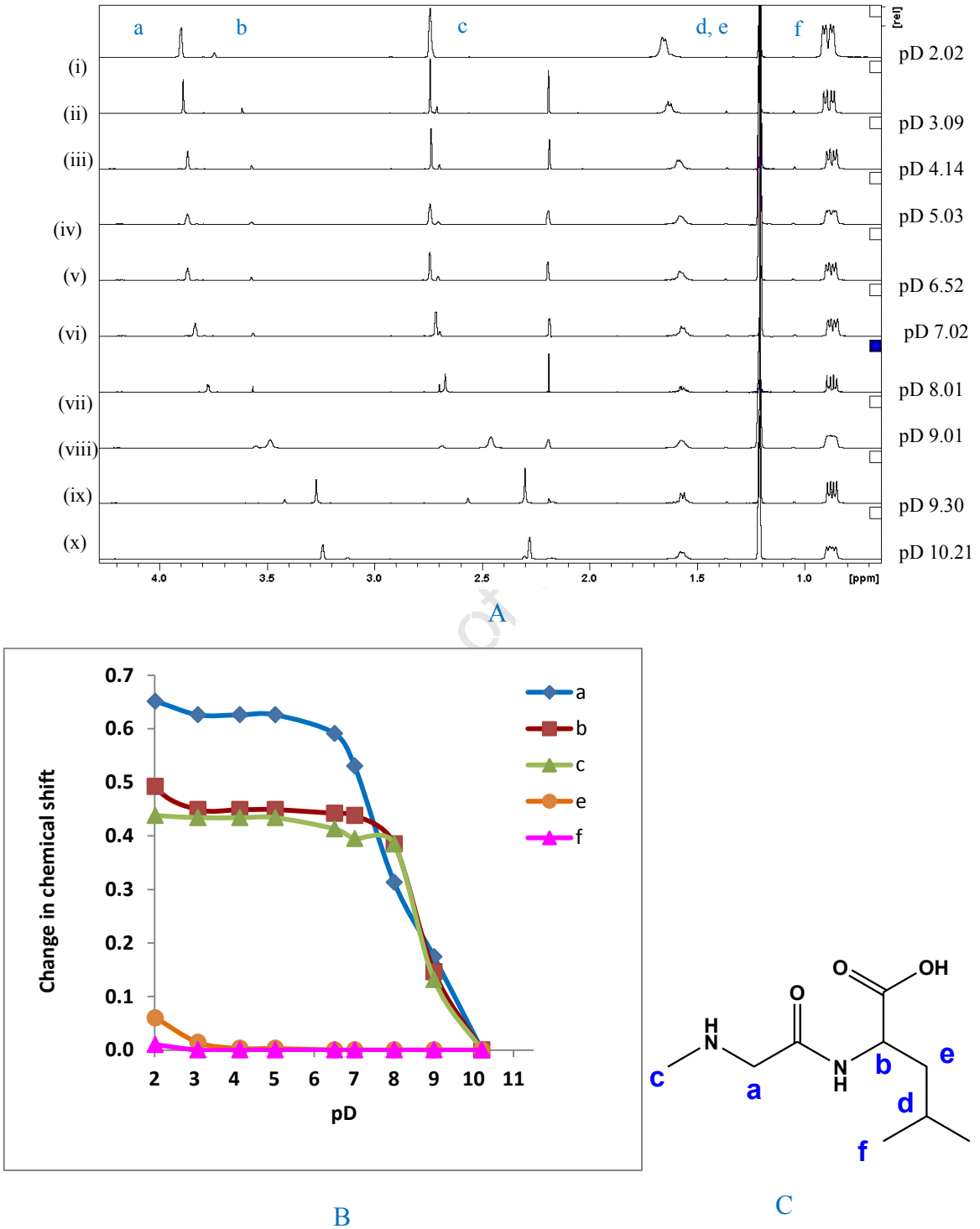

Figure 5.2: A: Raw ^{1}H NMR titration data from pD 2 to pD 10 for the protonation of SAR-LEU. **B:** Change in chemical shift for the protonation of SAR-LEU. **C:** Assigned chemical shifts for SAR-LEU

5.1.3.1.3 Protonation of glycyl-L-phenylalanine

Results for GLY-PHE protonation are given in Figure 5.3. Signal 'a' did not shift significantly throughout the titration, signal 'b' shifted from pD 7.44 to pD 11.17, signals 'c' and 'd' shifted between pD 2.22 and pD 4.07 and signal 'e' did not shift significantly and the change in this signal was not plotted against pD (Figure 5.3C). The first protonation occurs on the amine terminal and the second protonation occurs on the carboxylate terminal. Log K_{LH} = 8.3 and log K_{LH2} = 3.0. These agree with the potentiometric results.

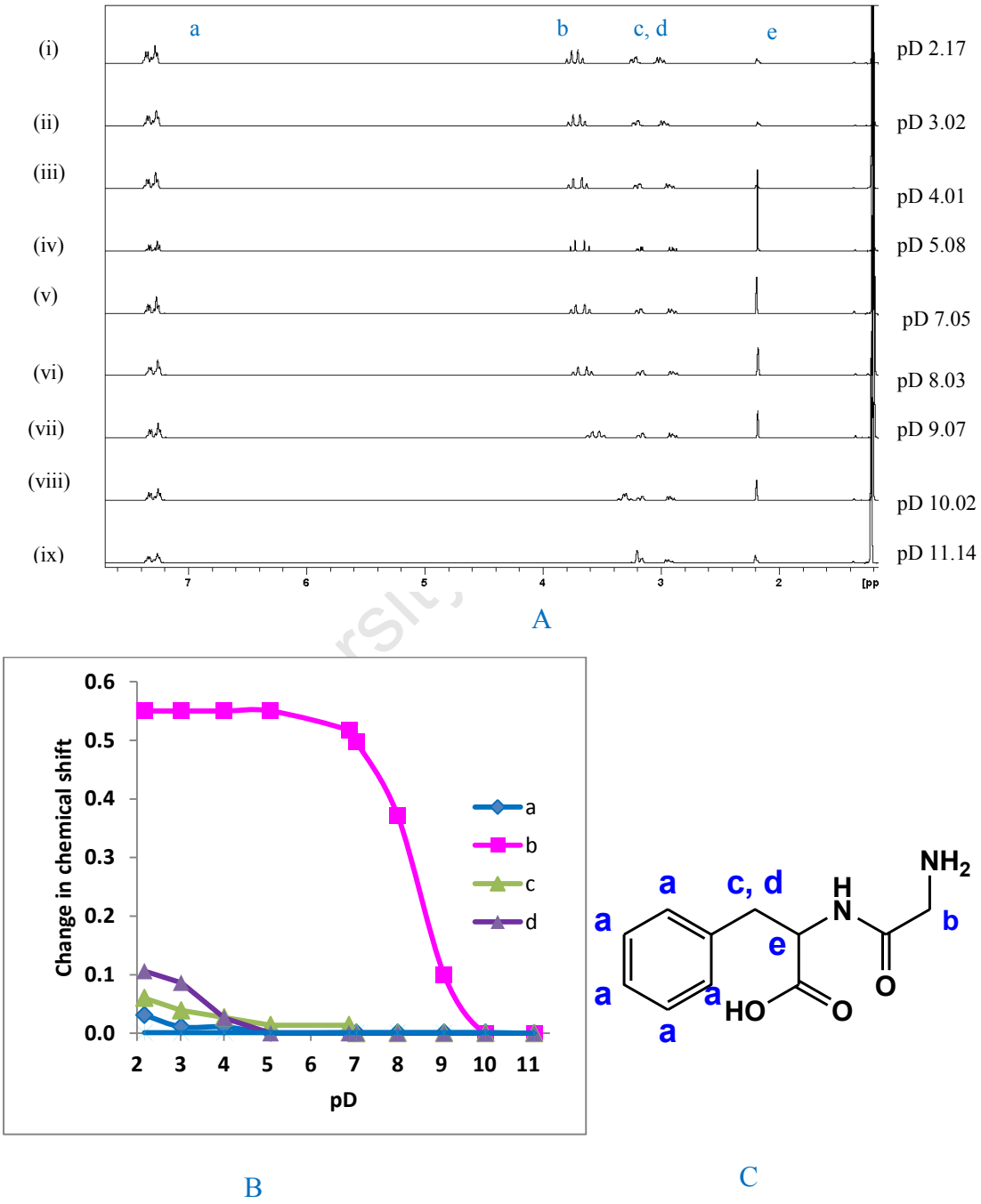

Figure 5.3: A: Raw ^{1}H NMR titration data from pD 2 to pD 11 for the protonation of GLY-PHE. **B:** Change in chemical shift for the protonation of GLY-PHE **C:** Assigned chemical shifts for GLY-PHE

5.1.3.1.4 Protonation of sarcosyl-L-phenylalanine

The results for the protonation of SAR-PHE are given in Figure 5.4. The signals that shift the most are signals 'b' and 'e' assigned to the protons of the α-carbon of the N-terminal and the protons of the methyl substituent respectively. These signals shift mostly from pD 6.91 to pD 11.17. Log K_{LH} = 8.5. This agrees with the potentiometric results (Table 3.8). This indicates the protonation of the amine terminal. Signal 'f' shifted the most between pD 2.22 and pD 4.01. Log K_{LH2} = 3.01.

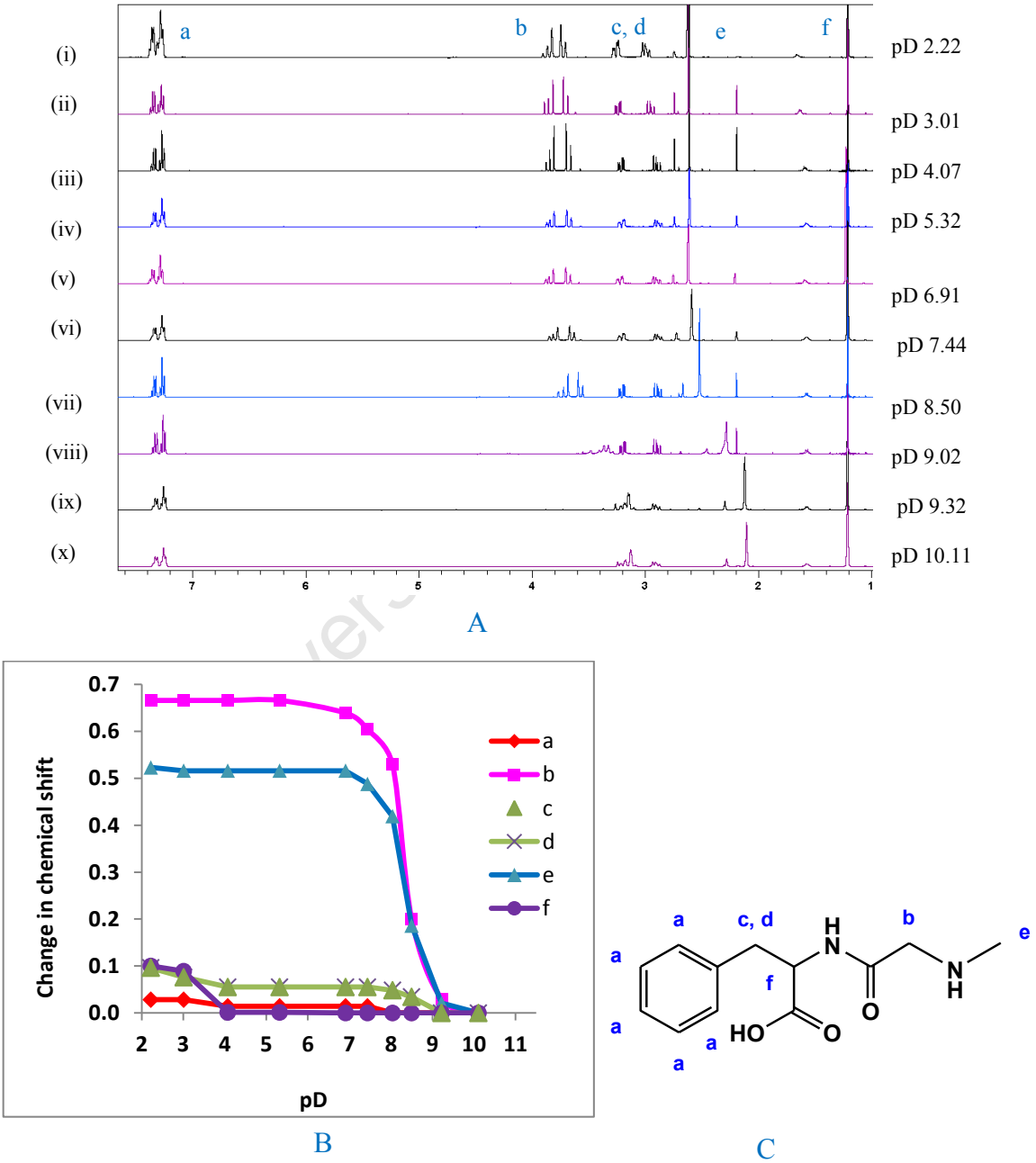

Figure 5.4: A: Raw ^{1}H NMR titration data from pD 2 to pD 10 for the protonation of SAR-PHE. **B:** Change in chemical shift for the protonation of SAR-PHE **C:** Assigned chemical shifts for SAR-PHE

5.1.3.2 Complex formation titrations

5.1.3.2.1 GLY-LEU / Cu(II)

^{1}H NMR results for complex formation titrations of GLY-LEU with Cu(II) are given in Figure 5.5. At pH 6.01, MLH_{-1} is the most predominant species. The 'a' and 'b' protons broaden significantly indicating that the metal is bound to sites near these protons. This must be the terminal amine and either the deprotonated amide nitrogen or the amide carbonyl. Since the stoichiometry of this complex is MLH_{-1}, binding to the amide nitrogen is indicated. When the pD was changed from pD 6.01 to pD 7.01 signal 'b' disappeared completely while 'a'was still visible. At this pH, ML_2H_{-1} is the predominant species and these NMR results are consistent with both amine nitrogens being coordinated but only one of the amide nitrogens.

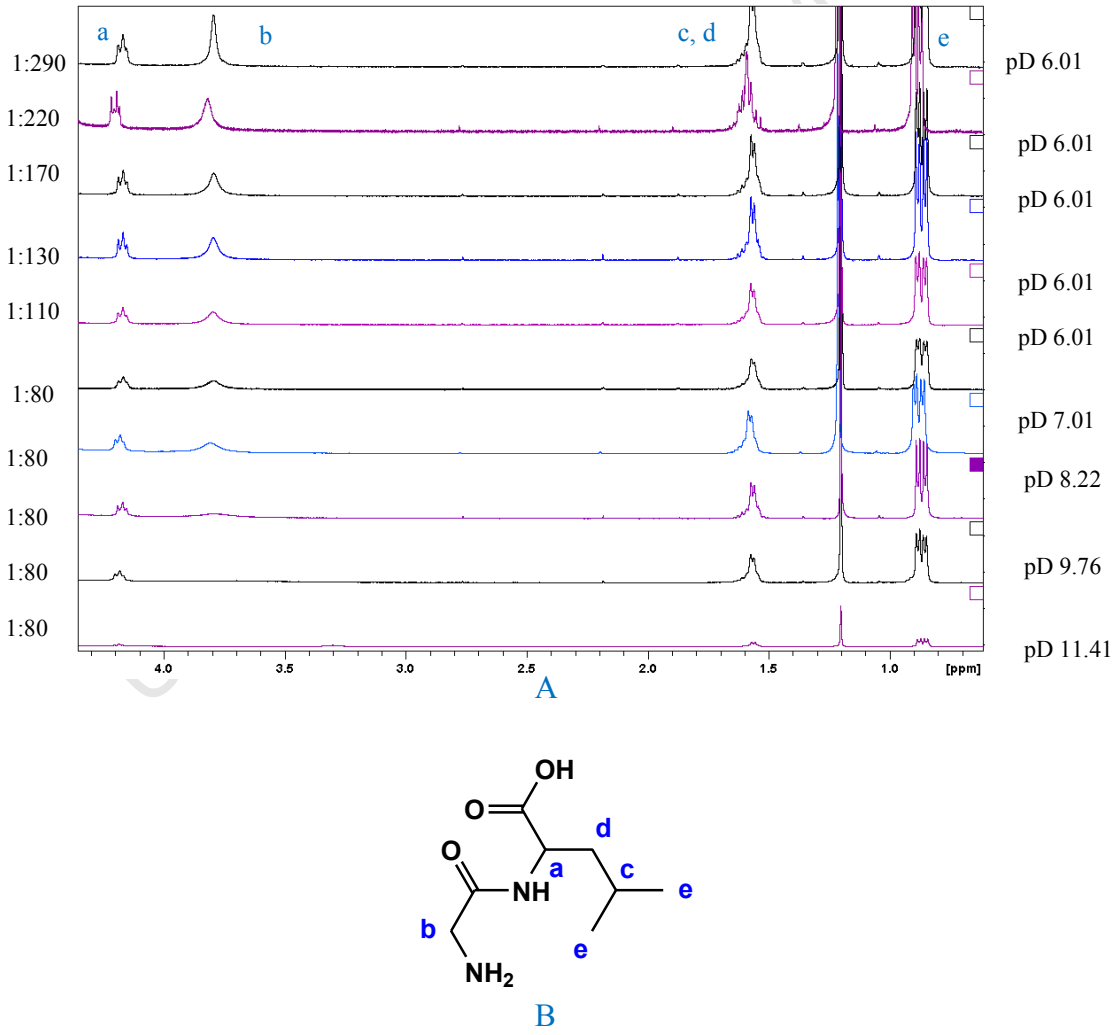

Figure 5.5: A: Raw ^{1}H NMR titration for the complexation of GLY-LEU with Cu(II). **B:** Assigned chemical shifts for GLY-LEU

5.1.3.2.2 SAR-LEU / Cu(II)

^{1}H NMR results for Cu(II)/SAR-LEU are given on Figure 5.6. ML species is the most predominant species at pH 5.65. Signals 'a', 'b', 'd' and 'e' were already broadened at the beginning of the Cu(II)/ligand titration. Signal 'c' broadened upon further titration with Cu(II). The broadening of signals 'a' and 'c' indicate coordination to the terminal N. The broadening of 'b', 'd' and 'e' indicate coordination to the amide N or the amide O. The stoichiometry supports coordination to the amine N and the amide O for this species. The second ligand molecule will arrange itself in the same manner when ML_2 forms (Cu(II) binds to the amine N and the amide O of both ligands). When the pH was increased from 5.65 to higher, signals 'a', 'b' and 'c' disappeared. The stoichiometry supports coordination to the amine N and the amide N when MLH_{-1} forms, and further coordination to the carboxylate O when MLH_{-2} forms.

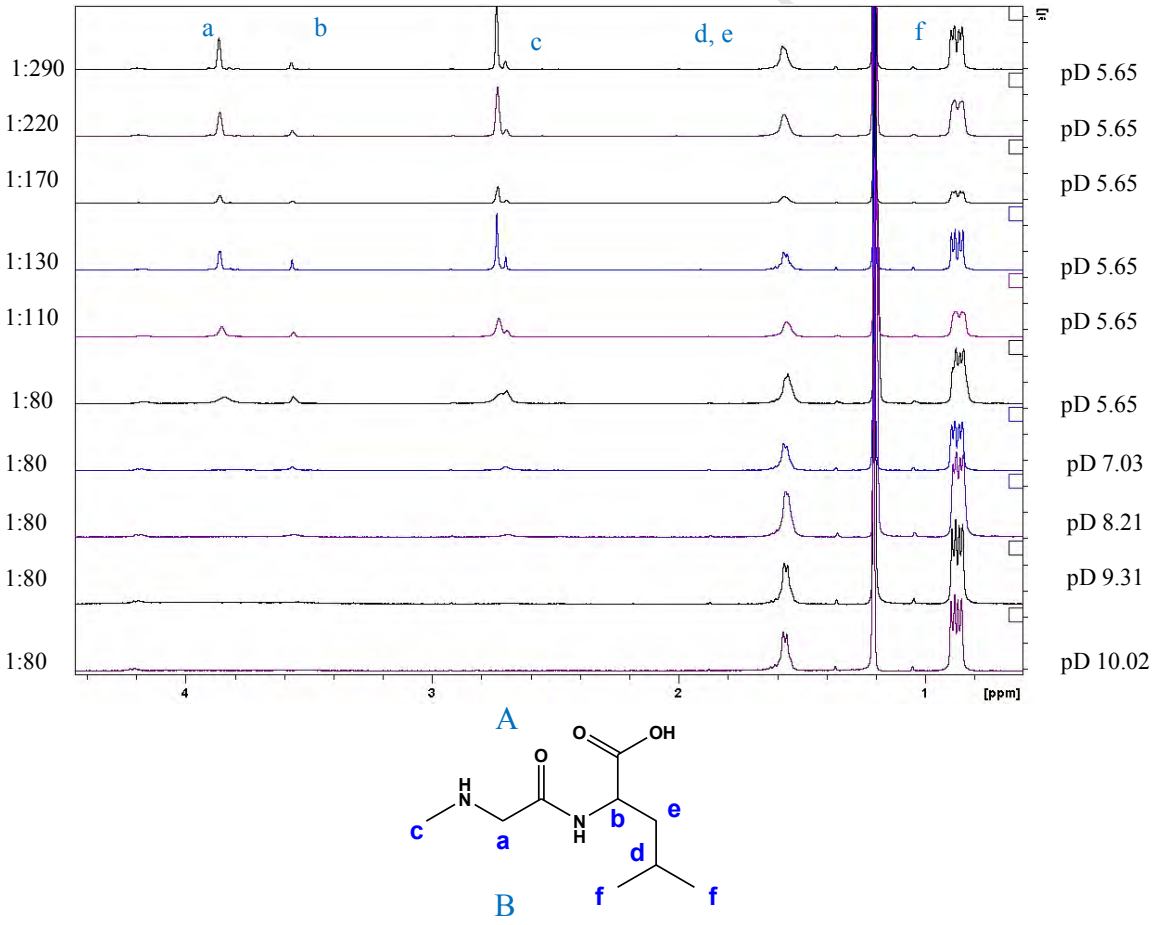

Figure 5.6: A: Raw ^{1}H NMR titration for the complexation of SAR-LEU: with Cu(II). **B:** Assigned chemical shifts for SAR-LEU

5.1.3.2.3 GLY-PHE / Cu(II)

^{1}H NMR results for the complexation of GLY-PHE with Cu(II) are given on Figure 5.7. At pD 6.32, ML is the most predominant species in solution. Signals 'b', 'c', 'd' and 'e' broadened when the concentration of Cu(II) was increased and the pH kept constant at pH 6.32. The broadening of signal 'b' indicates coordination of Cu(II) to the terminal amine. The broadening of 'c', 'd' and 'e' indicates coordination to the amide N or the amide O. Cu(II) binds to the amine N and the amide O when ML forms. When the pH was increased from 6.32 to 11.05, 'b', 'c', 'd' and 'e' disappeared completely. This indicates further coordination to the neighboring donors atoms; amine N, amide O and amide N. Cu(II) binds to the amine N and the amide O of both ligands when ML_2 forms. The stoichiometry supports coordination of Cu(II) to the amine N of both ligand molecules, coordination to the amide N of the first ligand molecule and coordination to the amide O of the second ligand molecule when ML_2H_{-1} forms, and coordination to amine N and amide N of both ligands when ML_2H_{-2} forms.

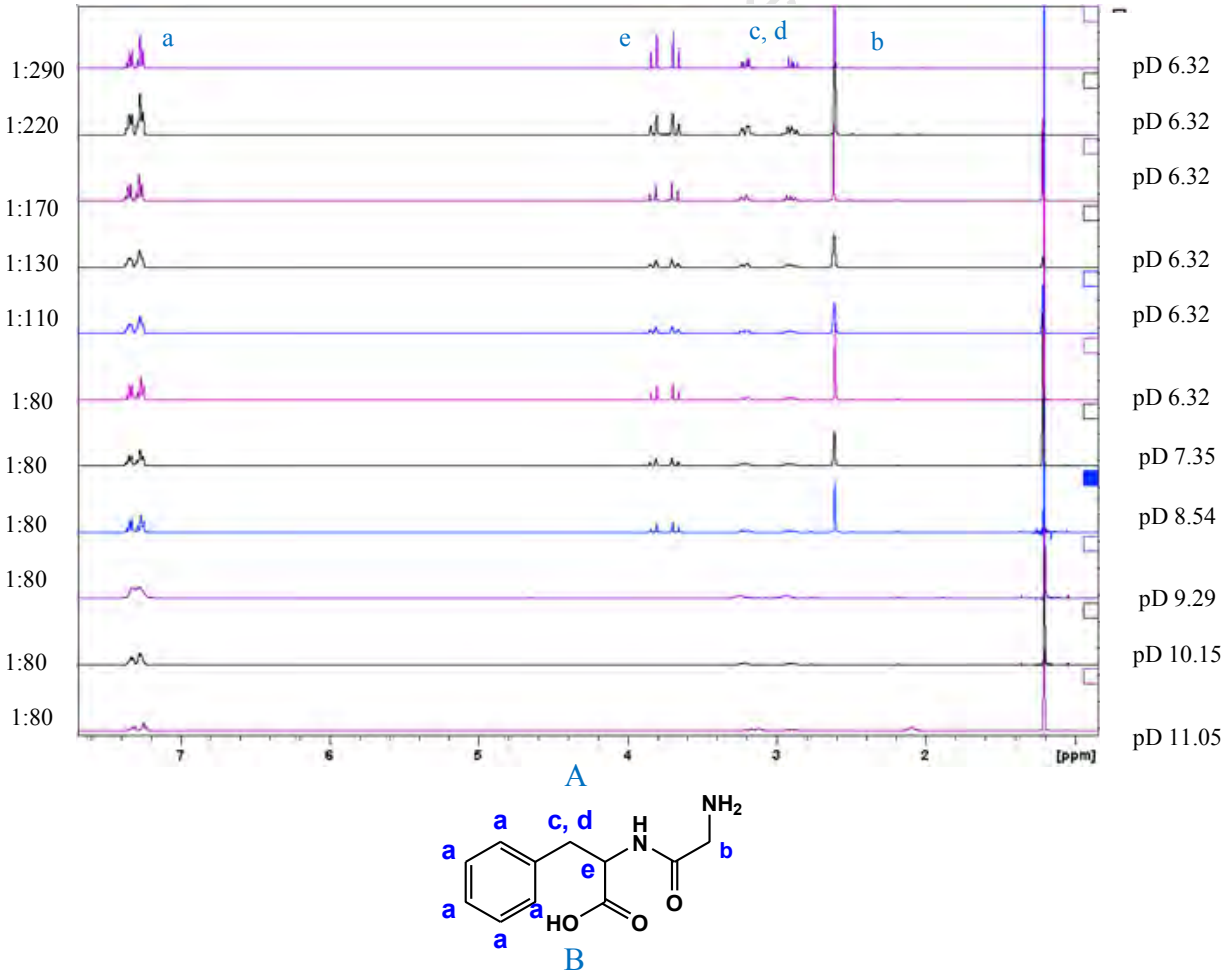

Figure 5.7: A: Raw ^{1}H NMR titration for the complexation of GLY-PHE: with Cu(II). **B:** Assigned chemical shifts for GLY-PHE

5.1.3.2.4 SAR-PHE / Cu(II)

Results for ^{1}H NMR titrations of SAR-PHE with Cu(II) are given in Figure 5.8. At pH 5.81, the most predominant species is the ML. When the Cu: ligand ratio was varied (from 1:290 to 1:80), signals 'b', 'c'. 'd' and 'f' broadened. The broadening of signal 'b' indicates coordination on the amine N. Broadening of signals 'b', 'c' and 'f' indicate coordination of the amide N or the amide O. Signal 'e' broadened from 1:110 Cu/ligand, at pH 5.81. The broadening of signal 'e' indicates coordination on the amine N.

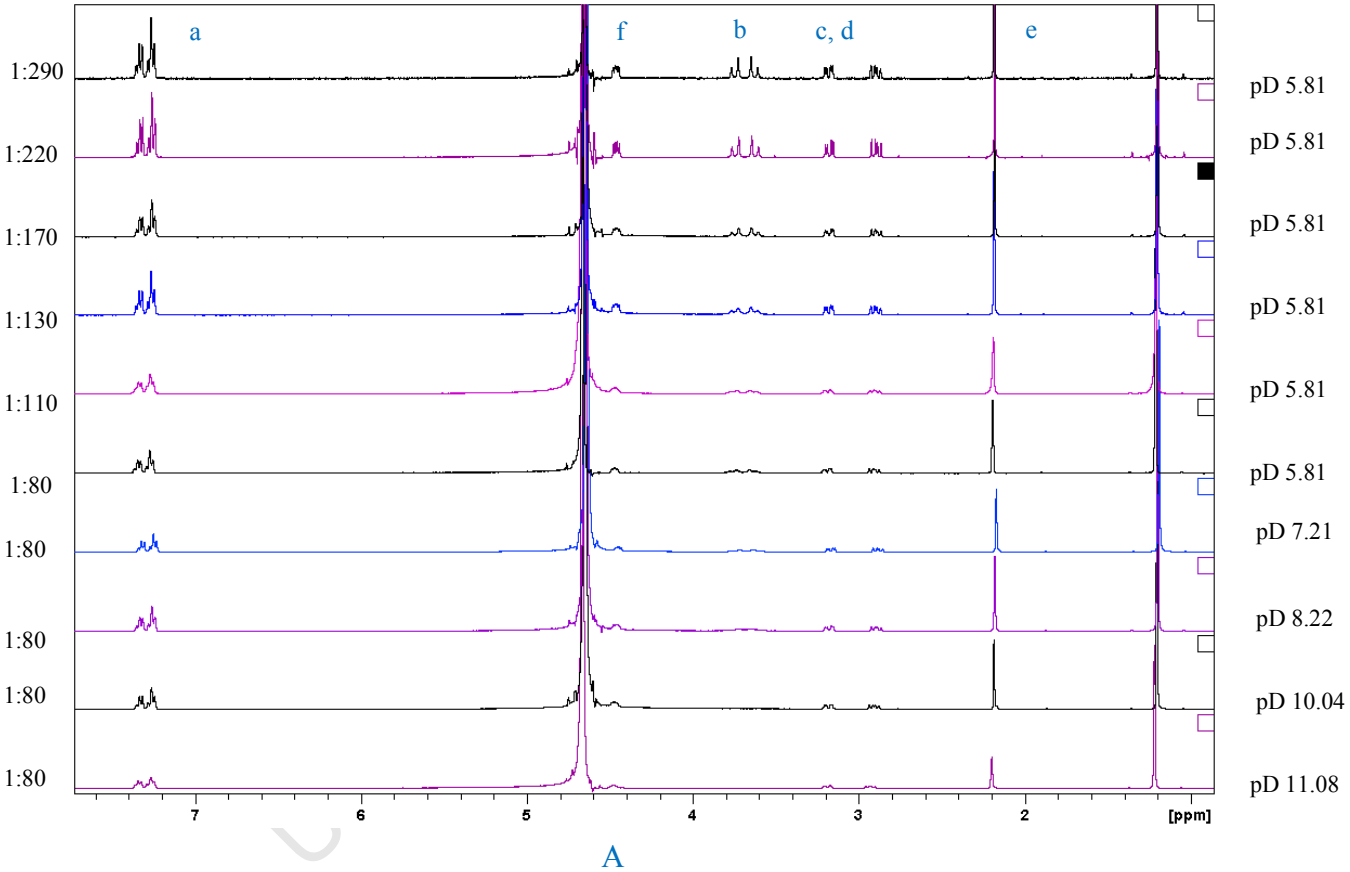

A

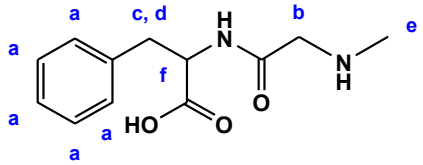

B

Figure 5.8: A: Raw ^{1}H NMR titration for the complexation of SAR-PHE: with Cu(II) **B:** Assigned chemical shifts for SAR-PHE

5.1.3.3 Discussions

The ligands have two dissociable protons, one on the terminal carboxylate and the other on the amine terminus. The first protonation occurs on the amine terminal and the second occurs on the carboxylate terminal. While this observation is trivial it does serve to illustrate that ^{1}H NMR can be used to assign protonation sites. The structure of LH_2 is represented as;

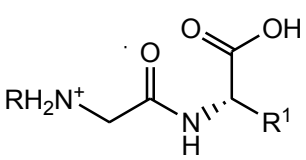

LH_2

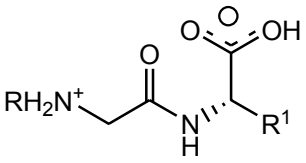

LH

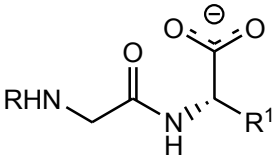

L

Where R = -H, and -CH_3

And R^1 = -H, 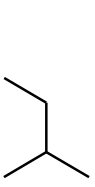 and 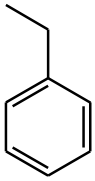

From ^{1}H NMR results it can be concluded that coordination occurs on the amine N and amide N or the amide O when ML forms. The stoichiometry however suggests that Cu(II) coordinates to the amine N and the amide O when ML forms, since coordination on the amide N will occur only if the amide proton is displaced. The latter represents the structure of species MLH_{-1}. For the same reasons, Cu(II) coordinates to the amine N and the amide O of both ligands when ML_2 forms. Cu(II) coordinates to the amine N of both ligands, on the amide O of the first ligand and on the amide N of the second ligand when ML_2H_{-1} forms. The structures are given below;

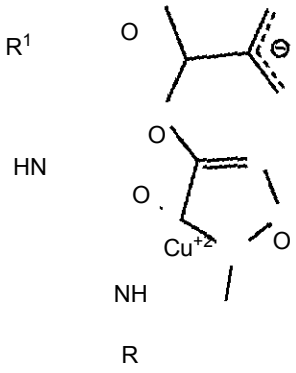

ML
(5-membered chelate)

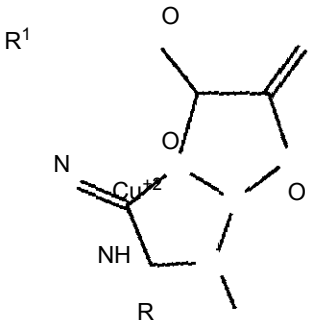

MLH_{-1}
(5, 5 chelate sequence)

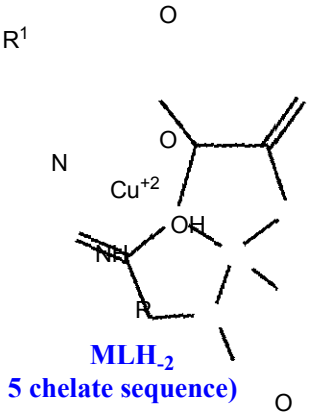

MLH_{-2}
(5, 5 chelate sequence)

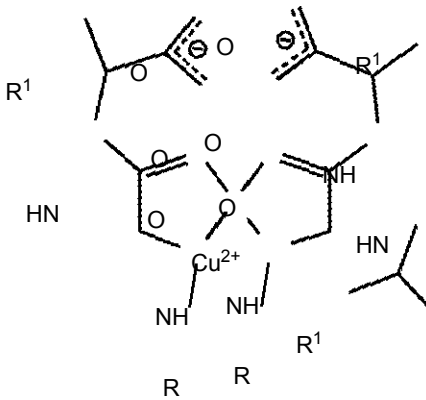

cis **ML_2**
(5, 5 chelate sequence)

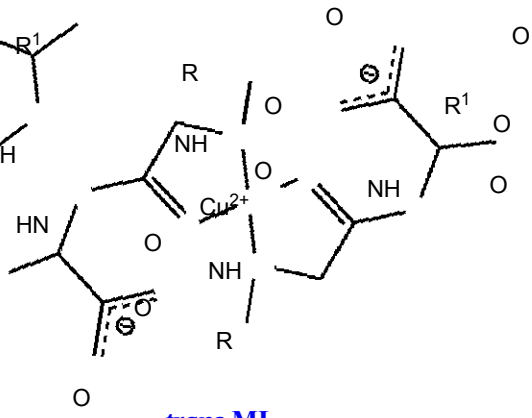

trans **ML_2**
(5, 5 chelate sequence)

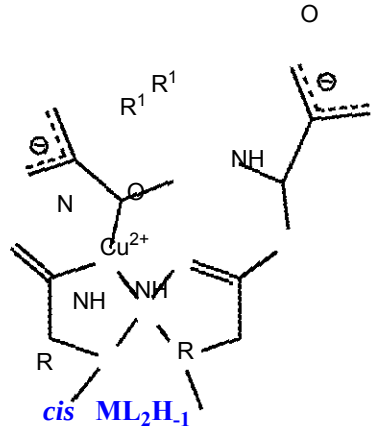

cis **ML_2H_{-1}**
(5, 5 chelate sequence)

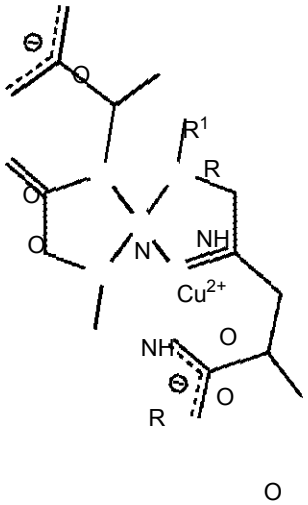

trans **ML_2H_{-1}**
(5, 5 chelate sequence)

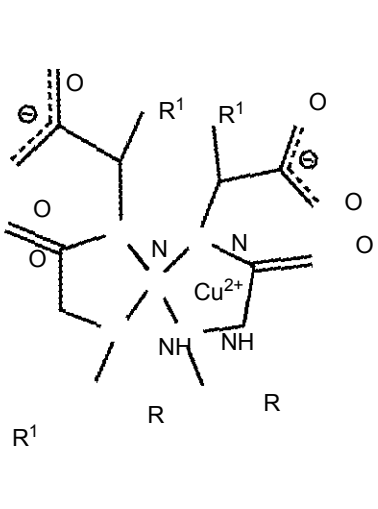

cis **ML_2H_{-2}**
(5, 5 chelate sequence)

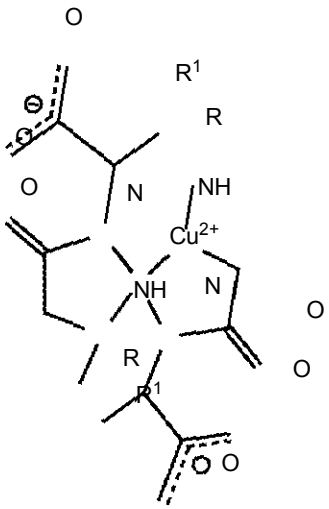

trans **ML_2H_{-2}**
(5, 5 chelate sequence)

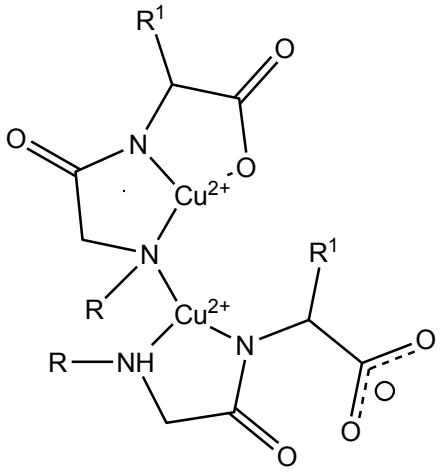

$M_2L_2H_{-3}$
(5, 5 chelate sequence) and a
5-membered chelate

Where R = -H, and $-CH_3$

And R^1 = -H, 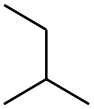 and 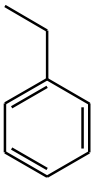

The charges on the electron donor groups that are engaged in coordination are omitted for simplicity. In each case the terminal carboxyl group could be coordinated. In some cases it would coordinate in an equatorial position but in others an axial position.

Electron paramagnetic resonance (EPR) measurements can be used to determine the number of water molecules that are involved in coordination. Unfortunately, EPR is not available in our laboratory.

5.2 UV-VIS SPECTROPHOTOMETRY

5.2.1 INTRODUCTION

Ultraviolet-visible absorption spectrophotometry (UV-Vis) is a spectroscopic technique which is used to gain insight into the structure of different metal species in solution [15-16]. When a beam of light is passed through an analyte solution, its intensity is reduced. This is because some of the light will have been absorbed by the analyte solution; some will have been reflected/ scattered [15-16]. The fraction of light absorbed by a species at a certain wavelength is its absorptivity (ε) at that wavelength. UV-Vis is used for quantitative analysis (Beer-Lambert's law);

$$A = \varepsilon bC \tag{5.2}$$

Where A is the absorbance, ε is the molar extinction coefficient, b is the path length of the sample cell and C is the molar concentration of the absorbing species. If the analyte solution is a mixture of different species, the total absorbance at a specific wavelength (A^{λ}) can be expressed as;

$$A^{\lambda} = b(\varepsilon_1{}^{\lambda}C_1 + \varepsilon_2{}^{\lambda}C_2 + \varepsilon_3{}^{\lambda}C_3 + \cdots \varepsilon_n{}^{\lambda}C_n) \tag{5.3}$$

Where the superscript λ is a parameter at a certain wavelength, subscripts 1, 2, 3…n are absorbing species. Equation 5.3 can be simplified;

$$A^{\lambda} = b\sum \varepsilon_i{}^{\lambda}C_i \tag{5.4}$$

If A, b and C are defined, then ε can be calculated. Different species absorb light at difference wavelengths and the maximum wavelengths of absorption can be correlated with the type of structure of a species. λ_{max}'s can therefore be used to predict structures of complexes. Billo's method [14] is one of the most popular methods of structure determination using λ_{max}'s. Calculated λ_{max} is expressed as;

$$\lambda_{max} = \frac{10^3}{n_i \nu_i} \tag{5.5}$$

Where n_i is the number of equatorial donor groups and ν_i is the ligand field of the complex. Ligands used in this study have four main electron donor atoms; N-donor of the amide, N-donor of the amine, O-donor of the carboxylate and O-donor of water. The electron donor groups and their corresponding ligand fields are given in Table 5.0.

Table 5.0: Electron donor groups and corresponding ligand field.

Electron donor group	Ligand field (υ_i in μm^{-1})
	0.353
	0.453
H_2O	0.296
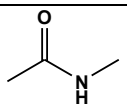	0.485
	0.343
^{-}OH	0.390

Many authors [18-22] have used UV-Vis to predict the structures of Cu(II) complexes.

5.2.2 EXPERIMENTAL

1:2 Cu(II)/ligands solutions were prepared in distilled-deionised water. The pH of these solutions was adjusted with NaOH/HCl from pH 2 to pH 11. CRISONmicro pH meter equipped with Ω Metrohm glass electrode was used to measure the pH. The exact amount of NaOH/HCl added was noted. The concentrations of the absorbing species were calculated at every pH. The absorbances of these solutions were measured with a Hewlette Parkard 8452A Diode Array spectrophotometer from 350 nm to 820 nm. A blank was used to correct the absorbance. Mixed species are formed at every pH and thus precise measurements of absorbance for individual species cannot be achieved and thus the molar extinction coefficients for individual species cannot be calculated directly form the spectra. A home-written computer program UV_spectra was used deconvolute the sectra and calculate the spectrum of individual species. This program uses essential Newton's method to solve Equation 5.3 for the molar extinction coefficient of each absorbing species at each

wavelength. The equilibrium model determined from potentiometry is used to calculate each species concentration at the different pH's. Since each the data, at each wavelength, are analysed independently there is no pre-condition that a smooth spectrum is obtained when the results are combined. Hence if the data can be deconvoluted (the set of simultaneous equations are non-singular) and smooth curves are obtained it lends confidence to the potentiometric model.

5.2.3 RESULTS

Table 5.1: Proposed electron donor groups and corresponding calculated λ_{max}'s for Cu(II)/dipeptide complexes.

Structure	Species	Involved electron-donor atoms/ groups						Calculated λ_{max} (nm)
		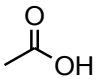			H_2O	OH^-	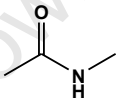	
A	ML	0	1	1	2	0	0	720
B	ML	1	1	1	1	0	0	692
C	MLH_{-1}	1	1	0	1	0	1	630
D	MLH_{-2}	1	1	0	0	1	1	595
E	ML_2	0	2	2	0	0	0	628
F	ML_2	2	2	0	0	0	0	620
G	ML_2	2	1	1	0	0	0	666
H	ML_2H_{-1}	0	2	1	0	0	1	577
I	ML_2H_{-1}	1	2	0	0	0	1	573
J	ML_2H_{-1}	2	1	0	0	0	1	608
K	ML_2H_{-1}	1	1	1	0	0	1	612
L	ML_2H_{-2}	0	2	0	0	0	2	533
M	$M_2L_2H_{-3}$	1	1	0	1	0	1	630 and
		0	2	0	0	1	1	561

Hypothetical structures for the copper dipeptides complexes are given below and the calculated maximum wavelengths for each structure given in Table 5.1. Koltun and co-workers [36], Gigel and Martin [37], Brookes and Pettit [38] suggest Structure A for ML, Structure C for MLH_{-1} and Structure H for ML_2H_{-1}. These structures, together with the

calculated maximum wavelengths, are used in the discussion of the results for the individual dipeptides.

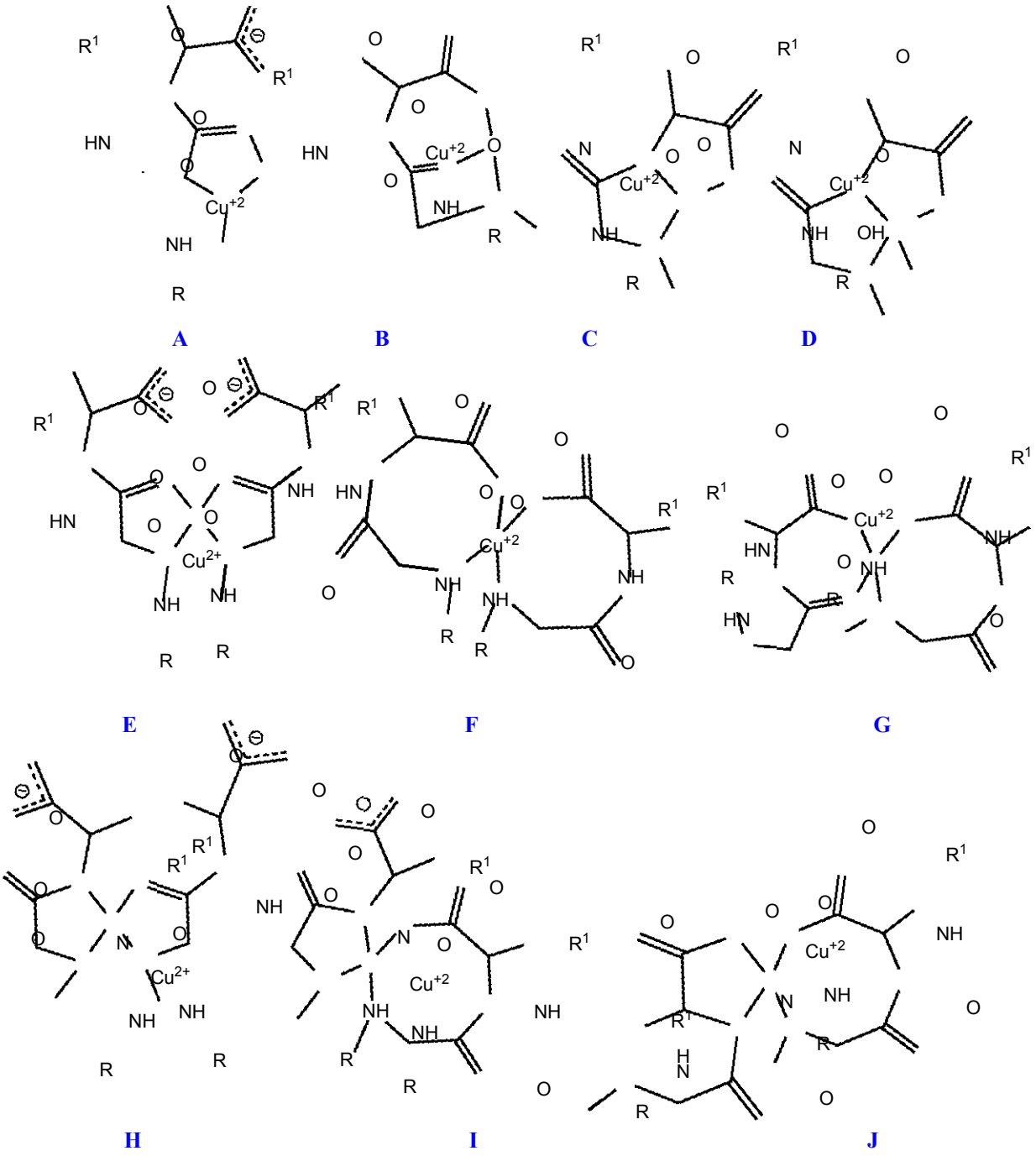

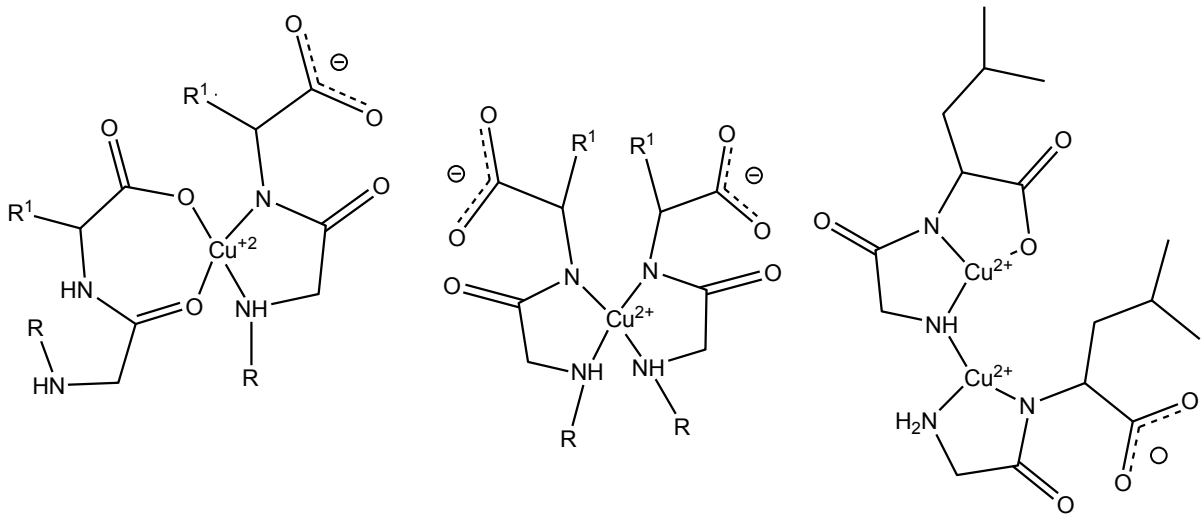

K **L** **M**

Where R = -H, and $-CH_3$

And R^1 = -H, 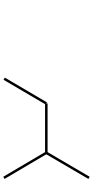 and 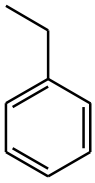

5.2.3.1 GLY-GLY / Cu(II)

UV-Vis results for Cu(II)/GLY-GLY are given in Figure 5.9. The smooth graphs indicate that the model is reasonable. A single absorption band was observed for each species. All the species absorb UV-Vis light between 450 nm and 800 nm. λ_{max} (ML) = 645 nm, (ε_{max} = 81.7 $dm^3.mol^{-1}.cm^{-1}$); λ_{max} (ML_2) = 635 nm, (ε_{max} = 15.5 $dm^3.mol^{-1}.cm^{-1}$); λ_{max} (MLH_{-1}) = 630 nm, (ε_{max} = 71.4 $dm^3.mol^{-1}.cm^{-1}$); and λ_{max} (MLH_{-2}) = 630 nm, (ε_{max} = 56.9 $dm^3.mol^{-1}.cm^{-1}$). The extinction coefficients are characteristic of LaPorte forbidden, spin allowed *d-d* transitions of a tetragonally distorted octahedral complex. GLY-GLY has four potential electron donor atoms; $N\text{-}_{amine}$, $N\text{-}_{amide}$, $O\text{-}_{amide}$, $O\text{-}_{carboxylate}$.

λ_{max} (ML) suggests that Cu(II) coordinates to the amine N-donor, on the amide O-donor, on the carboxylate O-donor and on one water molecule resulting in an 5,7 chelate sequence. When ML_2 forms, Cu(II) binds to the second ligand molecule through the amine N and the amide O, as a result, the band shifts to a shorter λ_{max}. λ_{max} shifts to a shorter wavelength when MLH_{-1} forms. This is a result of a $Cu\text{-}O_{amide}$ to $Cu\text{-}N_{amide}$ rearrangement. There is no observable change in λ_{max} when MLH_{-1} goes to MLH_{-2}, however the intensity of the band changes to lower ε_{max} indicating an increased symmetry.

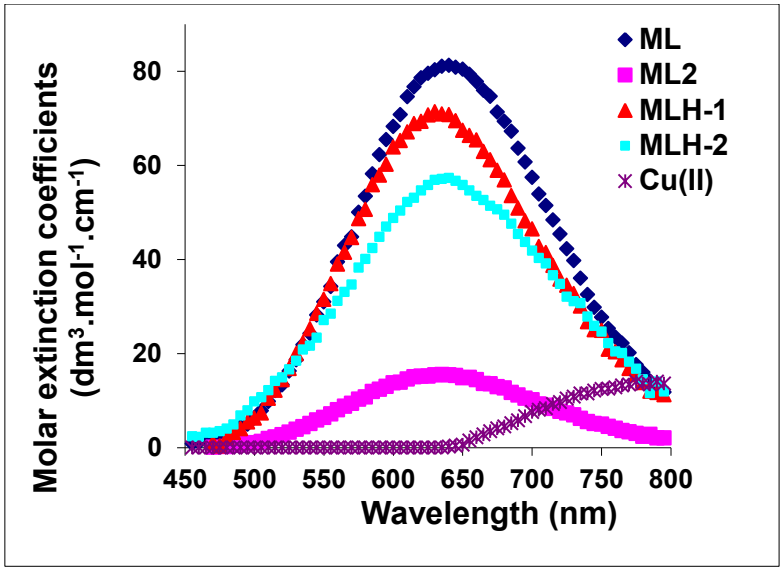

Figure 5.9: Molar extinction coefficients as a function of wavelength for Cu(II)/GLY-GLY complexes. The total ligand concentration = 0.005099 M and the total Cu(II) concentration = 0.005103 M.

Table 5.2 shows observed λ_{max}'s and calculated λ_{max}'s for Cu(II)/GLY-GLY system. Observed λ_{max} (ML) is 47 nm less than the calculated maximum wavelength. A difference of 47 nm between the calculated and the observed λ_{max} may be due the fact that coordination to the carboxylate O is axial while coordination to amide O, amine N and water O is equatorial. Billo's method [14] assumes no axial coordination. Coordination of Cu(II) to N-$_{amine}$ and O-$_{amide}$ when ML_2 forms is equatorial. The observed and calculated maximum wavelengths agree a slight difference of 7 nm falls within the experimental error and the accuracy of Billo's method. Some of the complex species form in very low concentrations which makes data analysis not as precise. Deprotonation of ML yields MLH_{-1}. The Cu-O_{amide} bond breaks and the Cu-N_{amide} bonds forms. There is a good agreement between the observed and the calculated λ_{max}'s for this species. Deprotonation of MLH_{-1} yields MLH_{-2}. The second proton is lost from a coordinated water molecule. A red shift was observed; calculated λ_{max} is 36 nm less than the observed λ_{max}. Axial Cu-$O_{hydroxide}$ has been reported to result in a red shift [39].

λ_{max} (ML) does not agree with the literature λ_{max} (ML) = 735 nm [36], however, λ_{max} (MLH_{-1}) and λ_{max} (MLH_{-2}) agree with the literature (λ_{max} (MLH_{-1}) = 635 nm and λ_{max} (MLH_{-2}) = 625 nm) [36]. The literature [36] suggests Cu(II) coordinates to the amine N, the amide O and two water molecules when ML forms. Proposed structures are given in Figure 5.10. For simplicity the charge on the electron donor groups to which Cu(II)

coordinated and the water molecules are not shown. The resonance structures are also not shown.

Table 5.2: Observed and calculated λ_{max}'s for Cu(II)/GLY-GLY complexes. Observed is abbreviated as obs and calculated as cal.

Species	Obs.λ_{max} (nm)	Obs. ε_{max} ($dm^3.mol^{-1}.cm^{-1}$)	Cal. λ_{max} (nm)	Involved electron-donor atoms/ groups					
							OH^-	H_2O	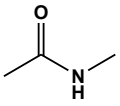
Cu(II)	>800	-	831	0	0	0	0	4	0
ML	645	81.7	692	1	1	1	0	1	0
ML_2	635	15.5	628	0	2	2	0	0	0
MLH_{-1}	630	71.4	630	1	1	0	0	1	1
MLH_{-2}	630	56.9	594	1	1	0	1	0	1

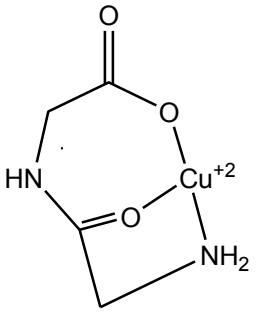

ML
(5, 7 chelate chelate sequence)

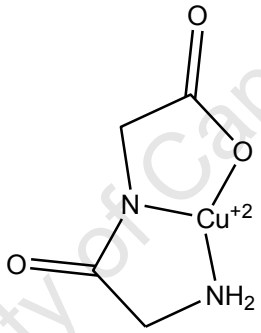

MLH_{-1}
(5, 5 chelate sequence)

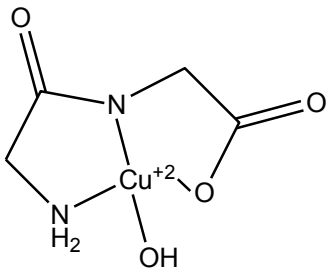

MLH_{-2}
(5, 5 chelate sequence)

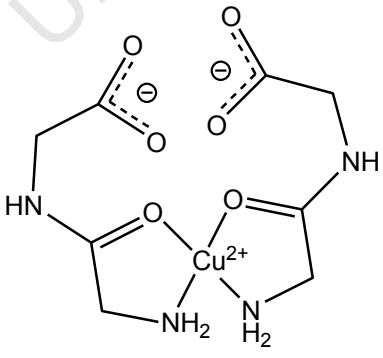

***cis* ML_2**
(5, 5 chelate sequence)

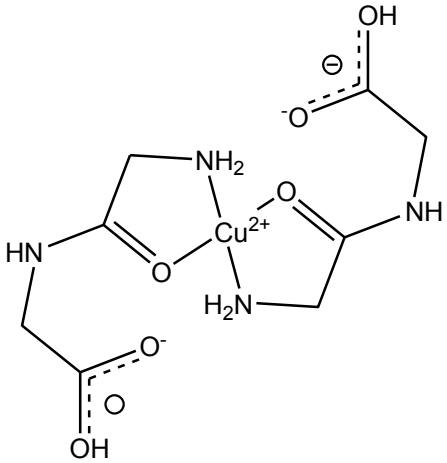

***trans* ML_2**
(5, 5 chelate sequence)

Figure 5.10: Structures of complexes formed between Cu(II) and GLY-GLY.

5.2.3.2 SAR-GLY / Cu(II)

The results for Cu(II)/SAR-GLY are given in Figure 5.11. λ_{max} (ML) = 640 nm. This suggests that Cu(II) coordinates to the amine N, amide O, carboxylate O and a water molecule yielding a 5, 7 chelate sequence. Cu-N_{amine}, Cu-O_{amide} and Cu-O_{water} are equatorial, Cu-$O_{carboxylate}$ is axial. The band shifts to a lower wavelength when ML_2 forms; λ_{max} (ML_2) = 635 nm. Equatorial Cu-O_{water} and axial Cu-$O_{carboxylate}$ break when ML_2 forms from ML, and Cu(II) coordinates to N_{amine} and O_{amide} of the second ligand molecule. There is no observable change when ML_2H_{-1} and ML_2H_{-2} form. The stoichiometry suggests ML_2H_{-1} forms when ML_2 is deprotonated. Cu(II) will therefore coordinate to amine N and the amide N of the first ligand, and to the amine N and the amide O of the second ligand when ML_2H_{-1}. The deprotonation of ML_2H_{-1} yields ML_2H_{-2}. The stoichiometry suggests Cu(II) coordinates to the amide N and the amine N of the first and of the second ligand molecule when ML_2H_{-2} forms.

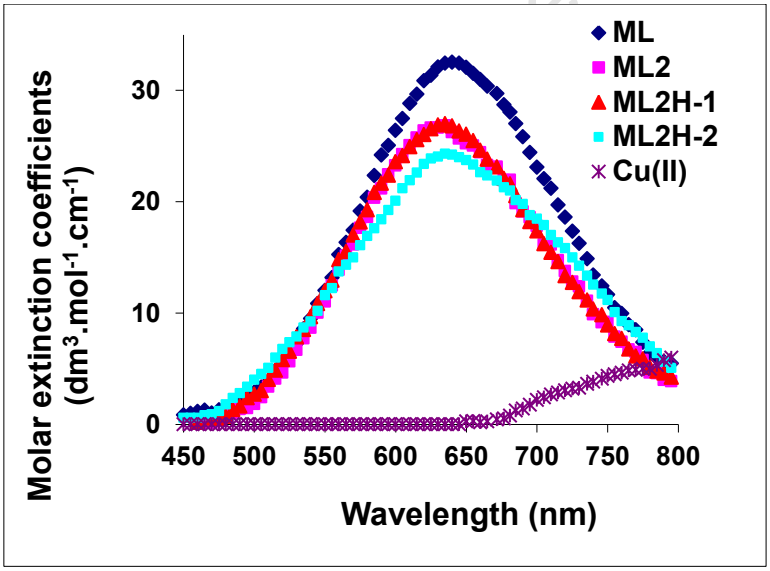

Figure 5.11: Molar extinction coefficients as a function of wavelength for Cu(II)/SAR-GLY complexes. The total ligand concentration = 0.005399 M and the total Cu(II) concentration = 0.005321 M.

Observed and calculated λ_{max}'s for Cu(II)/SAR-GLY titrations are given in Table 5.3. Predicted structures are given in Figure 5.12. Axial coordination of $O_{carboxylate}$ results in a blue shift (52 nm difference between the calculated maximum wavelength and the observed maximum wavelength). A slight red shift is observed with a neutral species ML_2. Gustiananda and co-workers [41] suspect an increase in H-bonding within peptides may result in a red shift. A larger red shift is observed with negatively charged species ML_2H_{-1}

and ML_2H_{-2}. Induced deprotonation of the amide nitrogen when a Cu-N_{amide} bond forms has been reported to be accompanied by a red shift of between 76 nm and 80 nm for some ligands [40].

Table 5.3: Observed and calculated λ_{max}'s for Cu(II)/SAR-GLY complexes. Observed is abbreviated as obs and calculated as cal.

Species	Obs. λ_{max} (nm)	Obs. ε_{max} ($dm^3.mol^{-1}.cm^{-1}$)	Cal. λ_{max} (nm)	Involved electron-donor atoms/ groups				
							H_2O	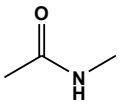
Cu(II)	>800	-	831	0	0	0	4	0
ML	640	32.5	692	1	1	1	1	0
ML_2	635	27.0	628	0	2	2	0	0
ML_2H_{-1}	635	27.0	577	0	2	1	0	1
ML_2H_{-2}	635	24.3	533	0	2	0	0	2

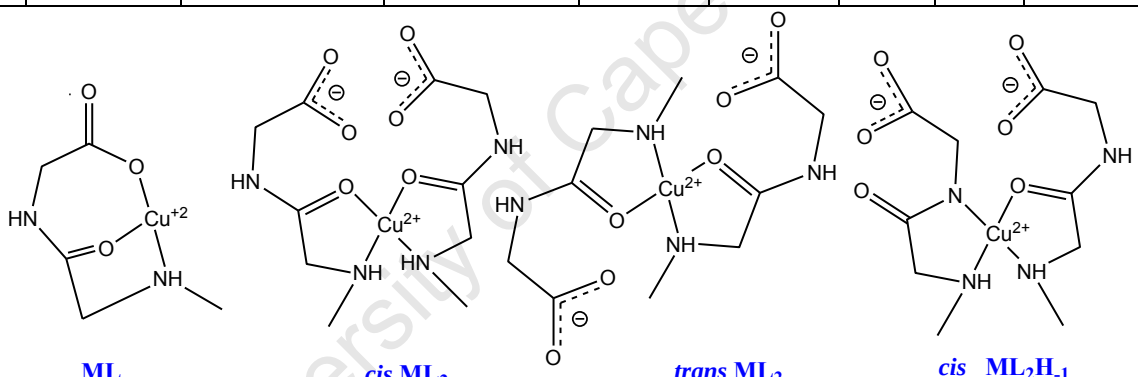

ML
(5, 7 chelate chelate sequence)

cis **ML_2**
(5, 5 chelate sequence)

trans **ML_2**
(5, 5 chelate sequence)

cis **ML_2H_{-1}**
(5, 5 chelate sequence)

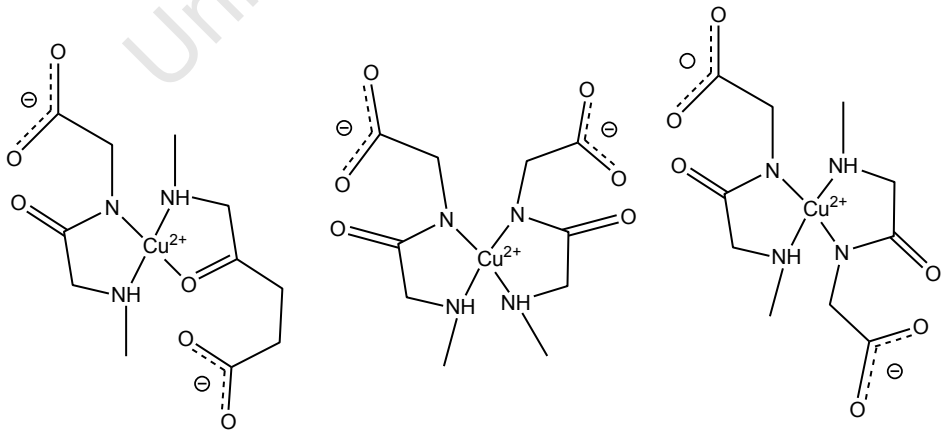

trans **ML_2H_{-1}**
(5, 5 chelate sequence)

cis **ML_2H_{-2}**
(5, 5 chelate sequence)

trans **ML_2H_{-2}**
(5, 5 chelate sequence)

Figure 5.12: Structures of complexes formed between Cu(II) and SAR-GLY. The total ligand concentration = 0.004897 M and the total Cu(II) concentration = 0.004789 M.

5.2.3.3 GLY-LEU / Cu(II)

Results for Cu(II)/GLY-LEU titrations are given in Figure 5.13. λ_{max} (ML) = 790 nm. This indicates that Cu(II) coordinates to the amine N and the amide O as suggested [36-38]. The band shifts to a lower wavelength when MLH_{-1} forms. This is a result of bond re-arrangements; Cu-O_{amide} bond breaks and Cu(II) coordinates to the N_{amide} and $O_{carboxylate}$ when MLH_{-1} forms. The band shifts to a much lower maximum wavelength when ML_2H_{-1} forms. λ_{max} (ML_2H_{-1}) = 605 nm. This suggest that Cu(II) coordinates to $O_{carboxylate}$ of the first and the second ligand molecule, to N_{amide} of the first ligand molecule and N_{amine} of the second ligand molecule. λ_{max} (MLH_{-1}) = λ_{max} ($M_2L_2H_{-3}$). This suggest that Cu(II) coordinates to the same electron donor groups when MLH_{-1} and $M_2L_2H_{-3}$ form.

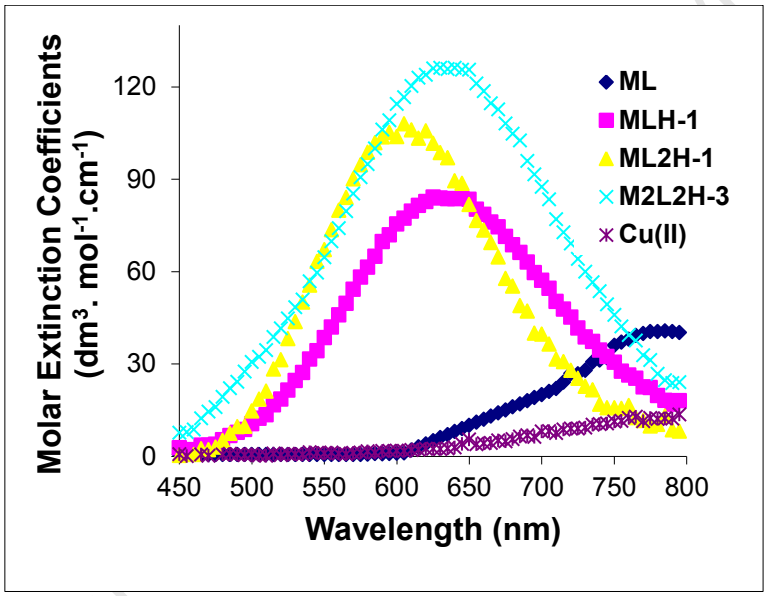

Figure 5.13: Molar extinction coefficients as a function of wavelength for Cu(II)/GLY-LEU complexes. The total ligand concentration = 0.005108 M and the total Cu(II) concentration = 0.004983 M.

Observed and calculated λ_{max}'s for the complex species are given in Table 5.4. The proposed structures are given in Figure 5.14. A red shift is observed for ML species. This might be a result of H-bonding between the non-coordinated COO^- and the solvent [41]. There is a good agreement between calculated and observed λ_{max}'s for other species. $M_2L_2H_{-3}$ has two λ_{max}'s. These are very close and thus overlapped, resulting in a broad band as shown in Figure 5.13.

Table 5.4: Observed and calculated λ_{max}'s for Cu(II)/GLY-LEU complexes. Observed is abbreviated as obs and calculated as cal.

Species	Obs.λ_{max} (nm)	Obs. ε_{max} ($dm^3.mol^{-1}.cm^{-1}$)	Cal. λ_{max} (nm)	Involved electron-donor atoms/ groups				
							H_2O	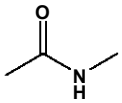
Cu(II)	>800	-	831	0	0	0	4	0
ML	790	40.5	720	0	1	1	2	0
MLH_{-1}	630	66.3	630	1	1	0	1	1
ML_2H_{-1}	605	78.9	608	2	1	0	0	1
$M_2L_2H_{-3}$	630	99.3	630 and	1	1	0	1	1
	-	-	593	0	2	0	1	1

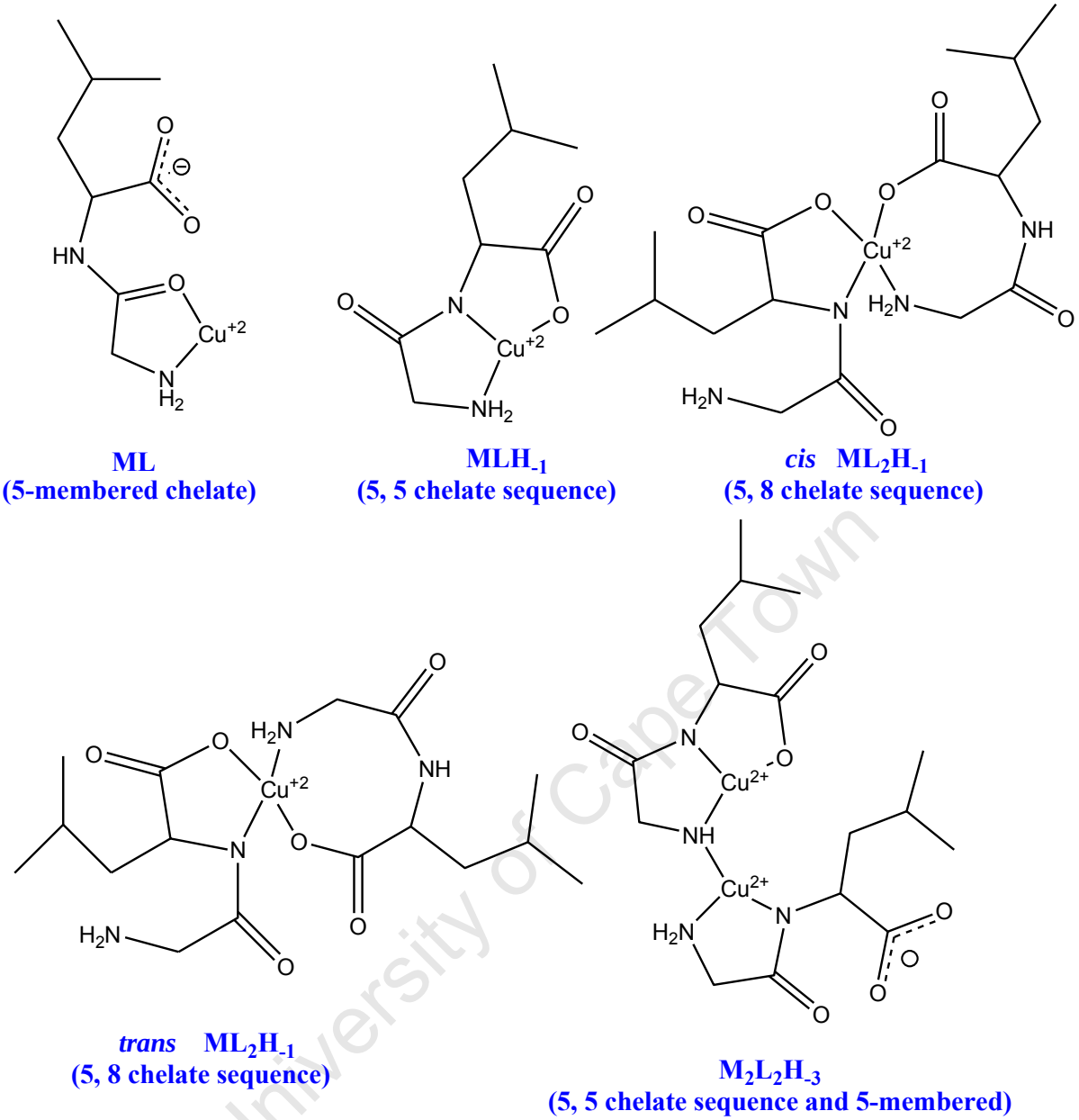

Figure 5.14: Structures of complexes formed between Cu(II) and GLY-LEU.

5.2.3.4 SAR-LEU / Cu(II)

Results for Cu(II)/SAR-LEU are given in Figure 5.15.

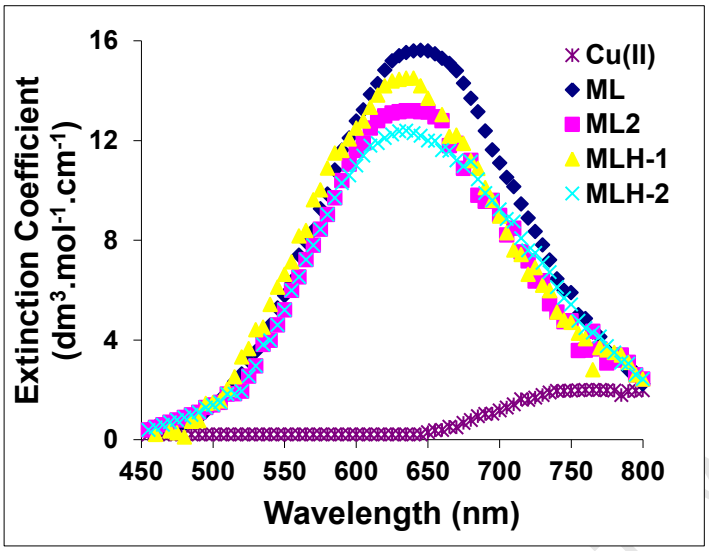

Figure 5.15: Molar extinction coefficients as a function of wavelength for Cu(II)/SAR-LEU complexes. The total ligand concentration = 0.005123 M and the total Cu(II) concentration = 0.004998 M.

Calculated and observed λ_{max}'s are given in Table 5.5. Predicted structures are given in Figure 5.16. Note that all the species had the same observed λ_{max} which was unexpected. However, the raw data for this ligand was different in that there was no shifting of the single absorption band during the titration.

Table 5.5: Observed and calculated λ_{max}'s for Cu(II)/SAR-LEU complexes. Observed is abbreviated as obs and calculated as cal.

Species	Obs.λ_{max} (nm)	Obs. ε max ($dm^3.mol^{-1}.cm^{-1}$)	Cal. λ max (nm)	Involved electron-donor atoms/ groups					
							OH^-	H_2O	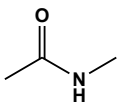
Cu(II)	>800	-	831	0	0	0	0	4	0
ML	645	15.6	692	1	1	1	0	1	0
ML_2	635	13.6	628	0	2	2	0	0	0
MLH_{-1}	635	14.7	630	1	1	0	0	1	1
MLH_{-2}	635	12.5	594	1	1	0	1	0	1

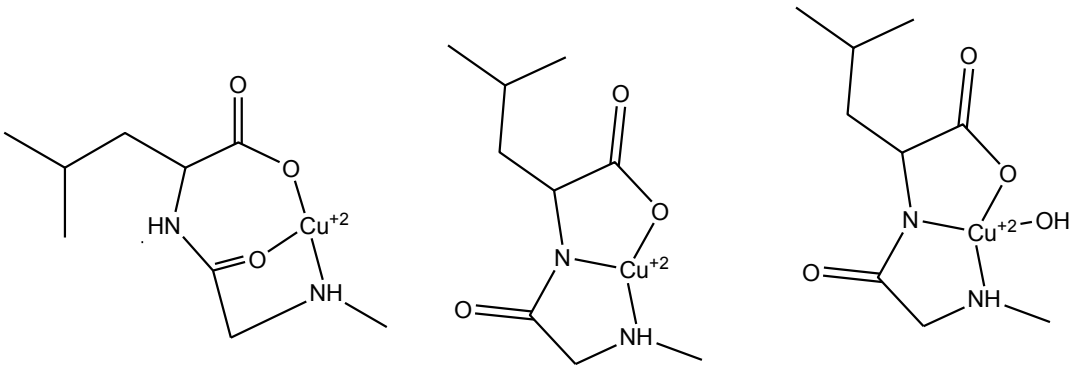

ML
(5, 7 chelate sequence)

MLH_{-1}
(5, 5 chelate sequence)

MLH_{-2}
(5, 5 chelate sequence)

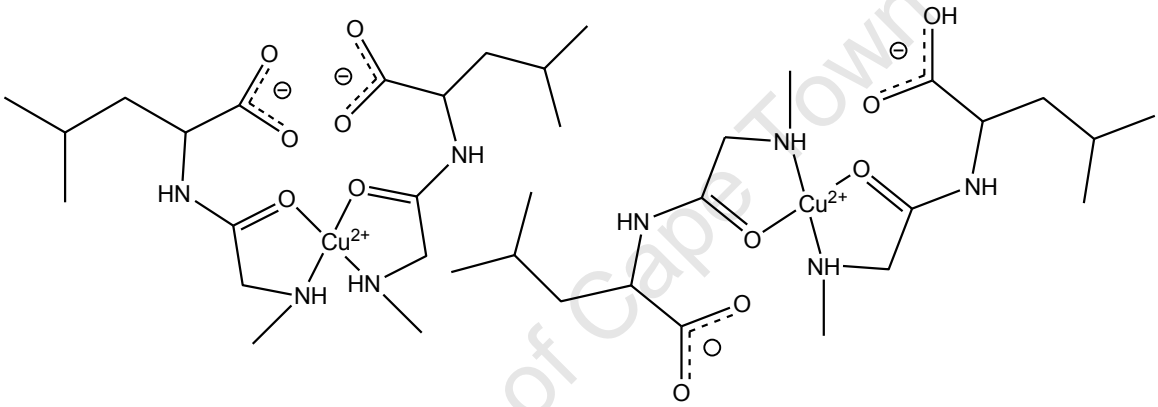

cis **ML_2**
(5, 5 chelate sequence)

trans **ML_2**
(5, 5 chelate sequence)

Figure 5.16: Structures of complexes formed between Cu(II) and SAR-LEU.

5.2.3.5 GLY-PHE / Cu(II)

Results for Cu(II)/GLY-PHE titrations are given in Figure 5.17

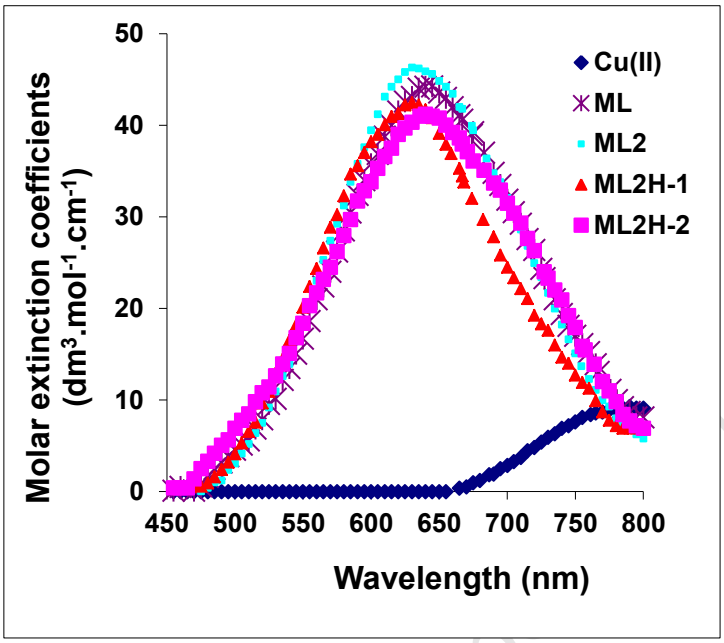

Figure 5.17: Molar extinction coefficients as a function of wavelength for Cu(II)/GLY-PHE complexes. The total ligand concentration = 0.005059 M and the total Cu(II) concentration = 0.005001 M.

Calculated λ_{max}'s, observed λ_{max}'s and corresponding electron donor groups and molar extinction coefficients are given in Table 5.6. The proposed structures are given in Figure 5.18.

Table 5.6: Observed and calculated λ_{max}'s for Cu(II)/GLY-PHE complexes. Observed is abbreviated as obs and calculated as cal.

Species	Obs.λ_{max} (nm)	Obs. ε_{max} ($dm^3.mol^{-1}.cm^{-1}$)	Cal. λ_{max} (nm)	Involved electron-donor atoms/ groups				
							H_2O	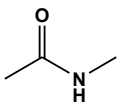
Cu(II)	>800	-	831	0	0	0	4	0
ML	645	44.2	720	0	1	1	2	0
ML_2	630	46.3	628	0	2	2	0	0
ML_2H_{-1}	630	42.5	577	1	1	1	0	1
ML_2H_{-2}	636	41.0	533	0	2	0	0	2

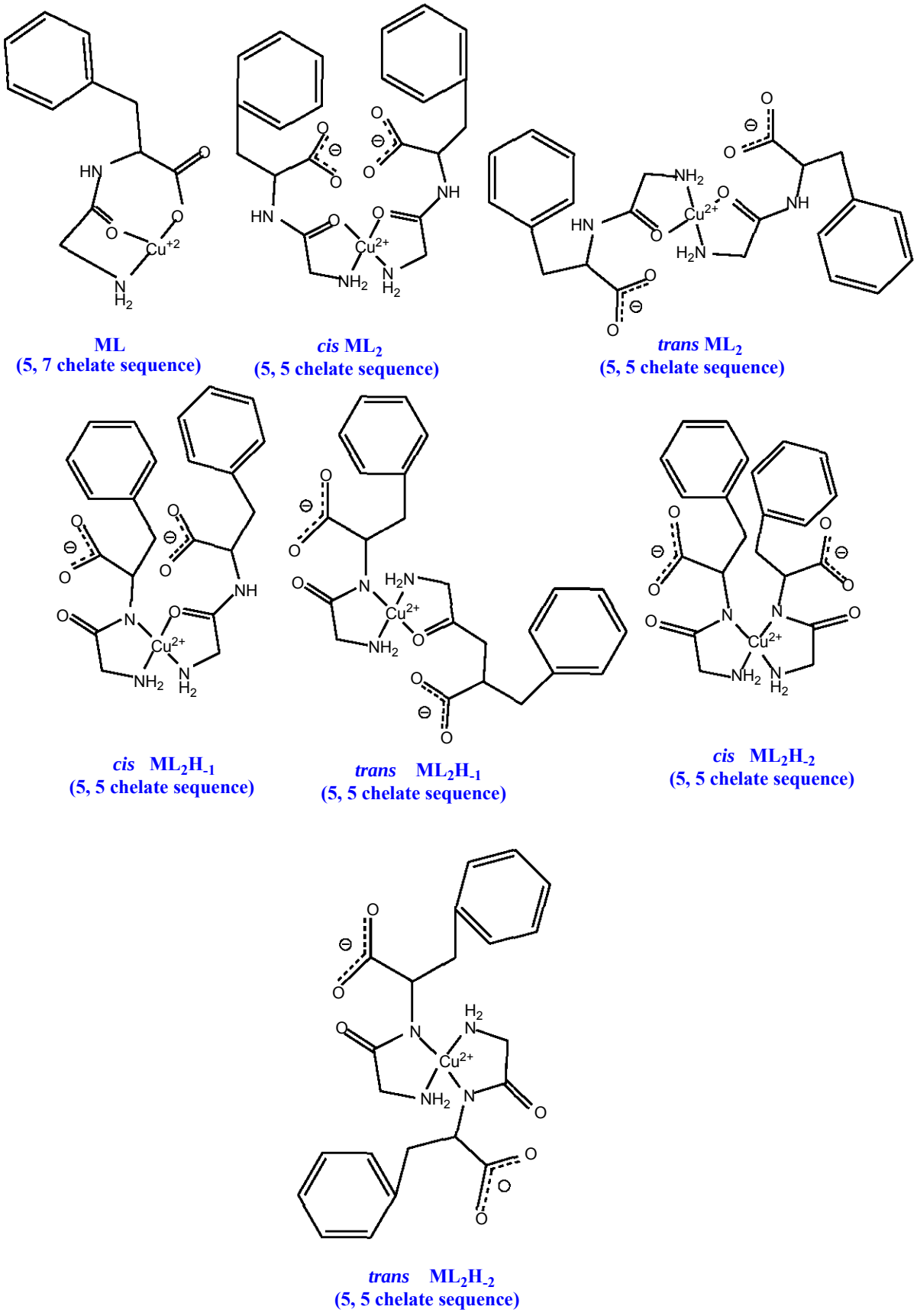

Figure 5.18: Structures of complexes formed between Cu(II) and GLY-PHE.

5.2.3.6 SAR-PHE / Cu(II)

Results for Cu(II)/SAR-PHE titrations are given in Figure 5.19.

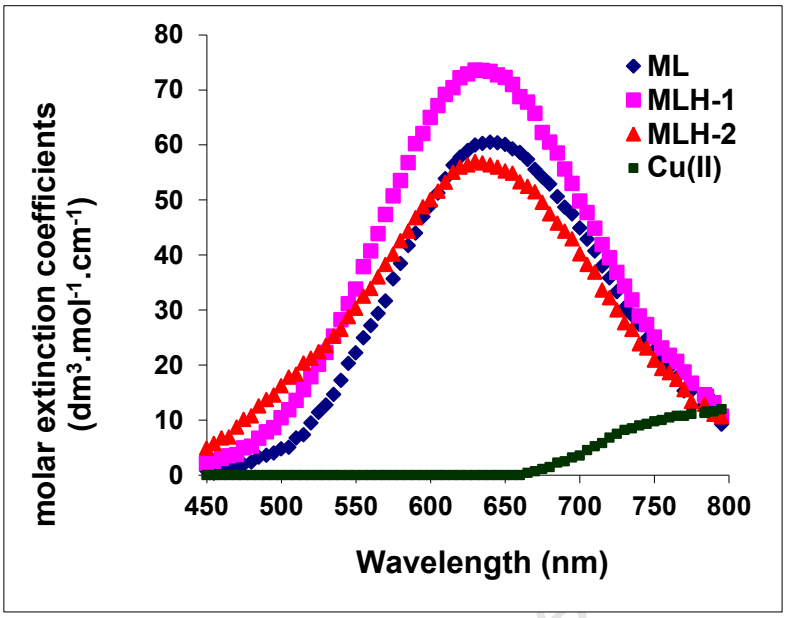

Figure 5.19: Molar extinction coefficients as a function of wavelength for Cu(II)/SAR-PHE complexes. The total ligand concentration = 0.004866 M and the total Cu(II) concentration = 0.004785 M.

Observed and calculated λ_{max}'s are given in Table 5.7. The proposed structures are given in Figure 5.20.

Table 5.7: Observed and calculated λ_{max}'s for Cu(II)/SAR-PHE complexes. Observed is abbreviated as obs and calculated as cal.

Species	Obs.λ_{max} (nm)	Obs. ε_{max} ($dm^3.mol^{-1}.cm^{-1}$)	Cal. λ_{max} (nm)	Involved electron-donor atoms/ groups					
						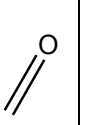	OH^-	H_2O	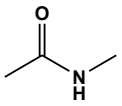
Cu(II)	>800	-	831	0	0	0	0	4	0
ML	650	60.1	692	1	1	1	0	1	0
MLH_{-1}	635	73.5	630	1	1	0	0	1	1
MLH_{-2}	635	56.7	594	1	1	0	1	0	1

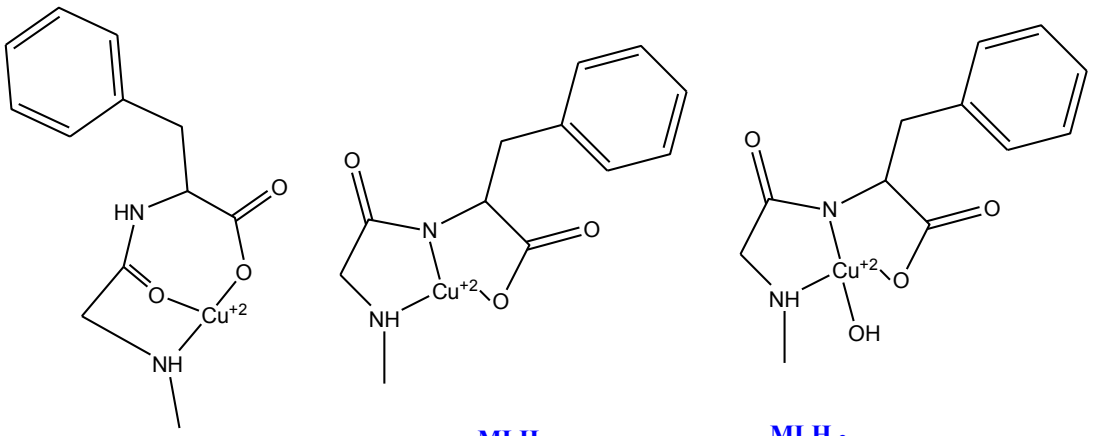

Figure 5.20: Structures of complexes formed between Cu(II) and SAR-PHE.

5.2.4 Discussions

At low pH's, where ML forms, Cu(II) coordinates to the N_{amine}, O_{amide}, $O_{carboxylate}$ and one water molecule for all the dipeptides except GLY-LEU. Cu-N_{amine}, Cu-O_{amide} and Cu-O_{water} are equatorial and Cu-$O_{carboxylate}$ is axial. Axial coordination results in a blue shift since Billo's method assumes the coordination is equatorial for all species. The deprotonation of ML yields MLH_{-1}. Cu(II) displaces the amide H when MLH_{-1} forms. Cu-O_{amide} to Cu-N_{amide} bond re-arrangement shifts the band to a lower wavelength. The second deprotonation occurs on the coordinated water molecule when MLH_{-2} forms.

The second route of complexation is from ML to ML_2 to ML_2H_{-1} to ML_2H_{-2}. The axial Cu-$O_{carboxylate}$ bond breaks when ML_2 forms and the second ligand molecule coordinates through the N_{amine} and O_{amide}. The deprotonation of ML_2 yields ML_2H_{-1}. H_{amide} is displaced by Cu(II) when ML_2H_{-1} forms. The second H_{amide} is also displaced when ML_2H_{-2} forms. The sequence of complexation of Cu-GLY-LEU differs significantly from that of other ligands (GLY-GLY, SAR-GLY, SAR-LEU, GLY-PHE and SAR-PHE): ML to ML_2 to MLH_{-1} to MLH_{-2} or ML to ML_2 to ML_2H_{-1} to ML_2H_{-2}. The sequence of complexation for Cu-GLY-LEU is ML to MLH_{-1} to ML_2H_{-1} to $M_2L_2H_{-3}$. Cu(II) coordinates to N_{amine}, O_{amide} and two water molecules when ML (Cu-GLY-LEU) forms. Log K_{ML} (Cu-GLY-LEU) is less than 6 log units (Chapter 3). Log K_{ML} for the other peptides is greater than 6 log units. The proposed structure for MLH_{-1} is the same as the other Cu-peptides. The structure of ML_2H_{-1} (Cu-GLY-LEU) differs significantly from the other Cu-peptides; Cu(II) coordinates to $O_{carboxylate}$ of the first and the second ligand molecules, to N_{amine} of the first ligand molecule and to O_{amide} of the second ligand molecule.

5.3 MOLECULAR MECHANICS

5.3.1 INTRODUCTION

Molecular mechanics is a method used to calculate the motion of atoms in a molecule using Newton's laws of motion [25]. The main task is to determine the most stable conformation of molecules at equilibrium using mathematical functions that best describe the total strain energy of a molecule [17, 23]. The structures are built using molecular orbital and valance bond theories, their conformation is optimised using force fields and the strain energy (U) of these structures is calculated. The geometry is optimised such that the total bond deformation strain (U_b), the total steric strain/van der Waals strain (U_s), the angle strain (U_a), and the torsional strain (U_t) are minimised. The total strain energy (U_{tot}) can therefore be expressed as;

$$U_{tot} = U_b + U_s + U_a + U_t \tag{5.6}$$

Bond deformation strain is energy the exerted on a bond between atoms, either by stretching the bond or compressing it. Due to a bond's ability to stretch/compress, the total bond deformation strain can be estimated using Hooke's law.

$$U_b = \sum_{bonds} \frac{1}{2} k_l (l - l_0)^2 \tag{5.7}$$

Where k_l is the force constant for a particular length, l is the bond length when the structure is deformed and l_0 is the length of the bond when the structure is at equilibrium. U_b can also be expressed in terms of Morse function;

$$U_b = \sum_{bonds} D_b \left(1 - e^{-a(l - l_0)}\right)^2 \tag{5.8}$$

The steric/van der Waals strain is the strain experienced by a molecule that has non-bonded electros from different substituents repel each other. This occurs when the distance between

these substituents is less than van der Waals radii [24]. Rappé and co-workers [24] have derived equations for calculating total steric strain;

$$U_s = \left[D_{IJ}\left(\frac{6}{\zeta - 6}\right)e^{\zeta}\right]e^{-\zeta\left(\frac{x}{x_{IJ}}\right)} - \left[D_{IJ}\left(\frac{\zeta}{\zeta - 6}\right)x_{IJ}{}^{6}\right] \tag{5.9}$$

Where D_{IJ} is the finite energy for breaking bonds, x_{IJ} is the van der Waals bond length, x is the atomic van der Waals distance, and ζ is the shape factor.

The angle deformations can also be estimated using Hooke's law.

$$U_a = \sum_{\text{angles}} \frac{1}{2} k_b (b - b_0)^2 \tag{5.10}$$

Where k_b is the force constant for a particular angle, b is the bond angle when the structure is deformed and b_0 is the bond angle when the structure is at equilibrium.

Torsional strain is experienced when a molecule undergoes a complete rotation around one bond.

$$U_t = \frac{V_1}{2}(1 + \cos(w)) + \frac{V_2}{2}(1 + \cos(2w)) + \frac{V_3}{2}(1 + \cos(3w)) \tag{5.11}$$

V_1 is a term assigned to van der Waals interactions/residual dipole-dipole interactions, V_2 is a term assigned to conjugation/hyper-conjugation and the term V_3 is assigned to steric or bonding/anti-bonding interactions.

Different force fields are used to optimise the geometry, the most common ones being the universal force filed (UFF). The mathematical expressions used when optimizing the structures differ from force field to force field. Many authors have stated which expressions are used in what force field [24, 26-28].

5.3.2 EXPERIMENTAL

Structures of the most probable complex species were built and minimization was carried out on a Windows Vista machine with Avogadro software [29-32]. The conformation of the structures was optimised with the universal force field (UFF) [24, 29, 33]. The results were verified with the steepest descent algorithm (gradient convergence).

5.3.3 RESULTS

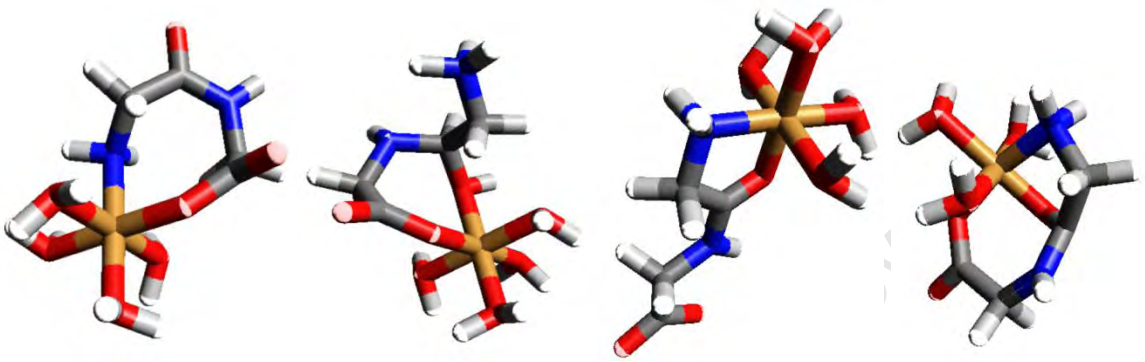

(a) ML **(b) ML** **(c) ML** **(d) ML-funny**

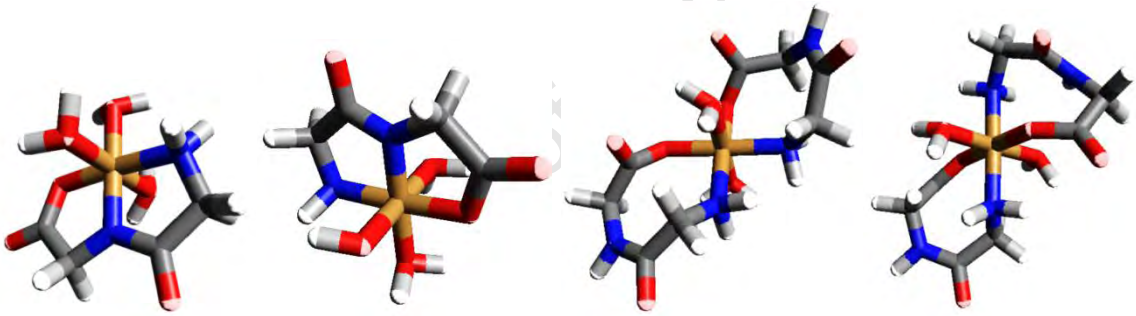

(e) MLH_{-1} **(f) MLH_{-2}** **(g) *cis* ML_2** **(h) *trans* ML_2**

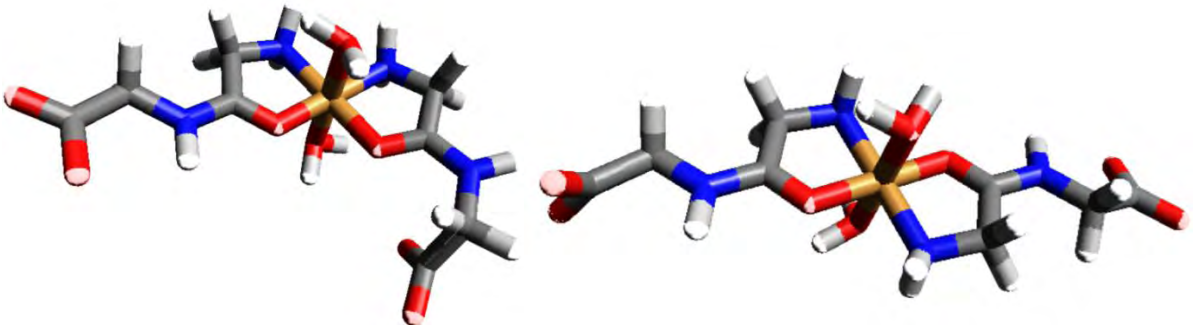

(i) *cis* ML_2 **(j) *trans* ML_2**

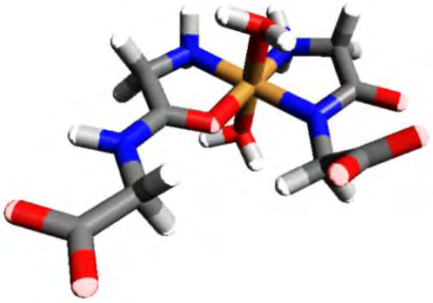

(k) ***cis*** ML_2H_{-1}

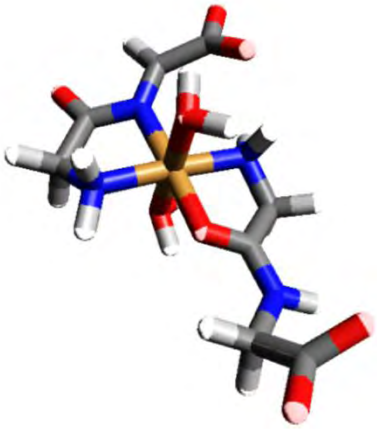

(l) ***trans*** ML_2H_{-1}

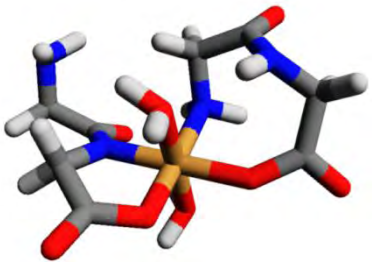

(m) ***cis*** ML_2H_{-1}

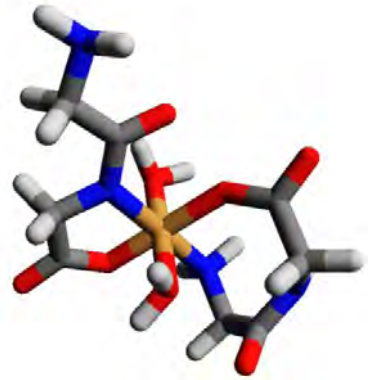

(n) ***trans*** ML_2H_{-1}

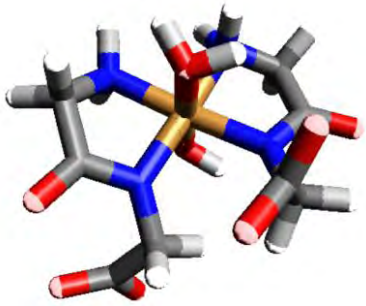

(o) ***trans*** ML_2H_{-2}

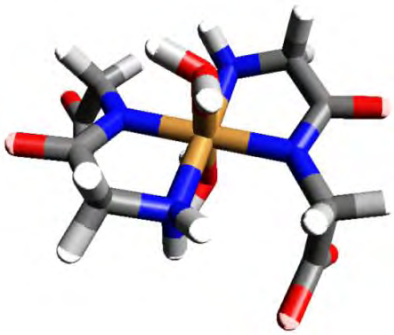

(p) ML_2H_{-2}

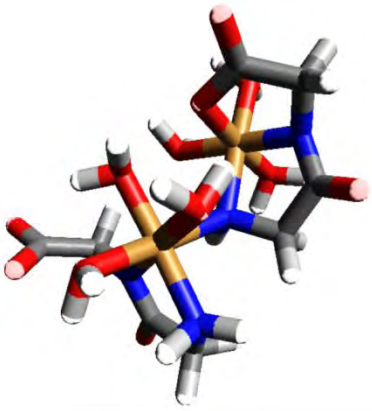

(q) $M_2L_2H_{-3}$

Cu(II) forms 6-coordinate complexes in an octahedral geometry. Structures (a) to (q) are different isomers of Cu(II) complexes. The calculated minimum energies are given in Table 5.7. In comparing these energies one must be careful to note that these are strain energies and not total enthalpies of formation. Thus it is only really meaningful to compare structures

with the same bonding. All Cu-glycine peptide complexes are more stable than Cu-sarcosine peptide complexes. The methyl substituent on the amine terminal adds more strain (steric strain) to the complexes. There are four possible conformations of ML: Structures (a) – (d). Structure (c) is the most stable of all, however uv-vis results show this conformation was only observed with Cu-GLY-LEU. Structures (a) and (b) were not observed with neither ^{1}H NMR nor uv-vis. It is not easy for Cu(II) to coordinate to both the terminal amine and the terminal carboxylate at the same time, nor is it easy for Cu(II) to coordinate to O_{amide} and $O_{carboxylate}$ without coordinating to N_{amine}. Cu-N bonds are stronger than Cu-O bonds. Conformation (d) was observed with all the peptides except for GLY-LEU. Of all the four probable ML conformations, this conformation is not favoured thermodynamically. Complexes that have equatorial Cu-ligand bonds and two axial Cu-water bonds are more stable than complexes that have one of the Cu-ligand bonds axial. The latter experience more angle and torsional strain.

MLH_{-2} is more stable than MLH_{-1}. The isomers (i) and (j) are more stable than isomers (g) and (h). Isomers (g) and (h) were not observed with ^{1}H NMR and uv-vis. The most stable conformation of ML_2H_{-1} is Structure (k). The *trans* form of ML_2H_{-2} is more stable than the *cis* form, except for Cu-SAR-GLY.

Table 5.7: Total minimum strain energies for structures (a) to (q)

Ligand	ML				MLH_{-1}	MLH_{-2}	ML_2				ML_2H_{-1}				ML_2H_{-2}		$M_2L_2H_{-3}$
	(a)	(b)	(c)	(d)	(e)	(f)	(g) *cis*	(h) *trans*	(i) *cis*	(j) *trans*	(k) *cis*	(l) *trans*	(m) *cis*	(n) *trans*	(o) *cis*	(p) *trans*	(q)
	U_{tot} (kJ.mol^{-1})																
GLY-GLY	184	233	121	487	150	140	608	476	181	370	192	244	446	372	319	261	518
SAR-GLY	240	274	134	508	175	161	499	580	272	404	225	435	486	445	531	354	618
GLY-LEU	238	233	134	565	228	189	578	593	369	480	284	384	770	533	565	448	620
SAR-LEU	300	321	171	591	287	221	807	540	380	553	366	463	856	593	732	525	872
GLY-PHE	252	366	193	569	292	233	817	730	407	512	346	394	709	633	650	545	717
SAR-PHE	310	368	222	580	256	266	862	707	417	573	386	471	744	591	810	680	844

5.4 GENERAL CONCLUSIONS

The first protonation occurs on amine terminal and the second one occurs on the carboxylate terminal. All *cis* isomers have lower total strain energies than their *trans* isomers except for ML_2H_{-2} whose *trans* forms are more stable than the *cis* forms. The *cis* form of ML_2H_{-2} (Cu-SAR-GLY) is however more stable than the *trans* form.

The sequence of protonation is as follows;

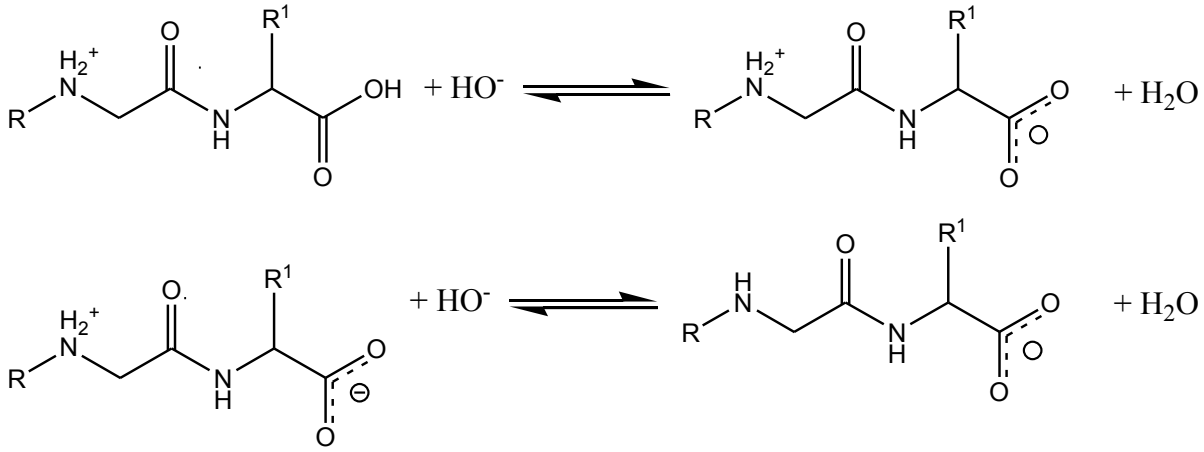

Molecular mechanics calculations suggest that a 5-memebered chelate (Cu-N_{amine}, Cu-O_{amide} and two Cu-O_{water} chelate system) is the most probable ML conformation. The complexation sequence is therefore drawn as;

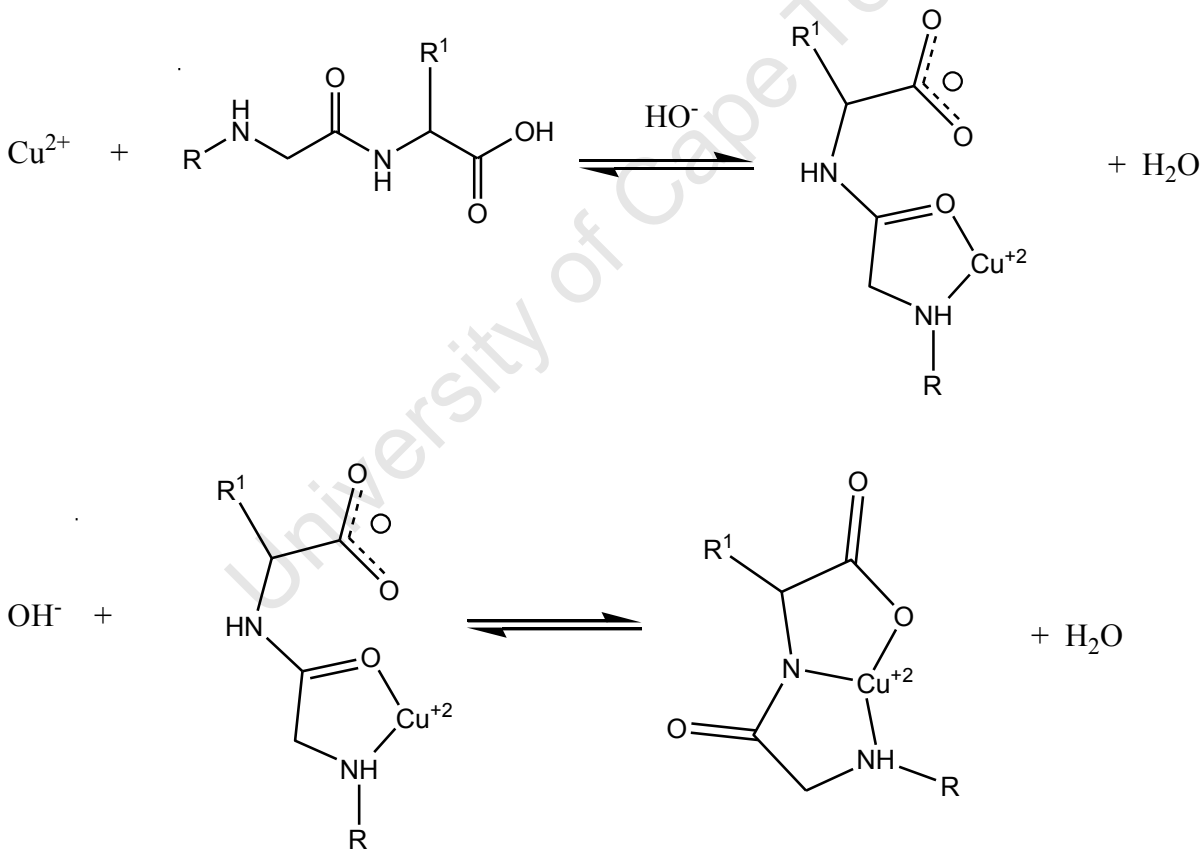

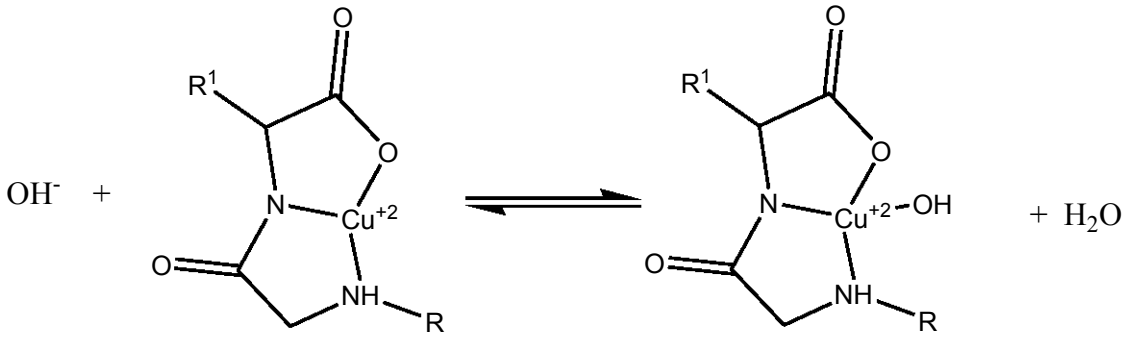

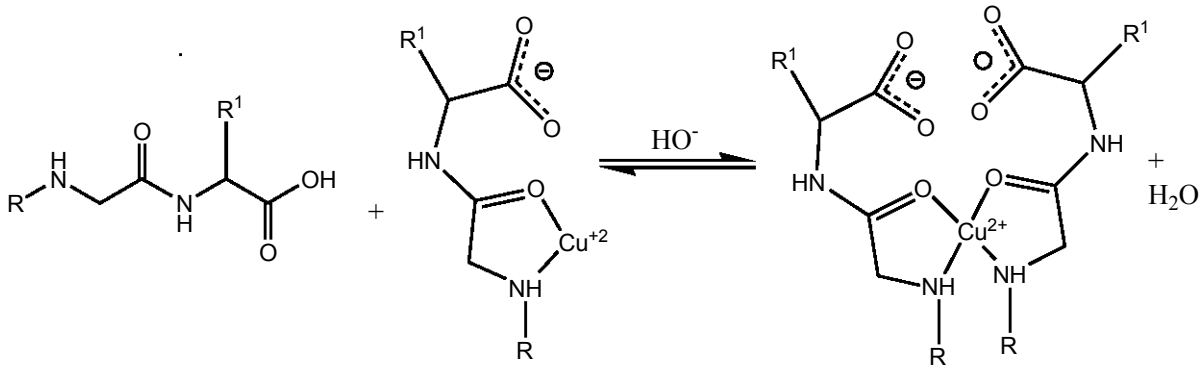

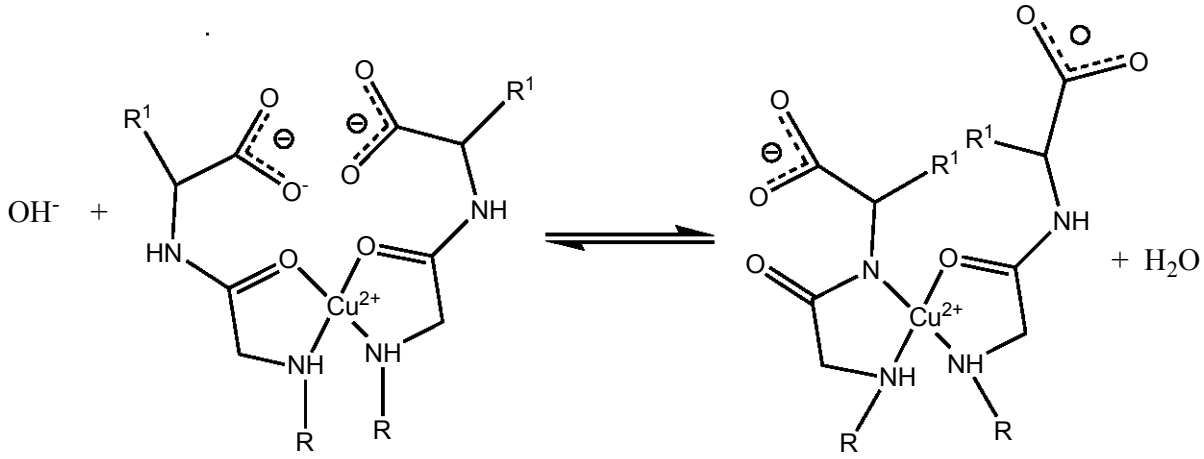

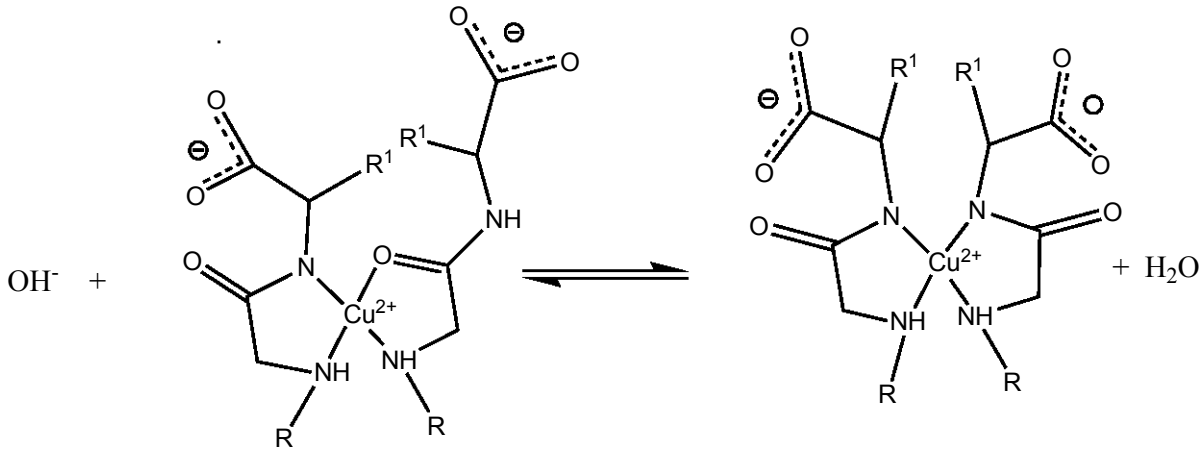

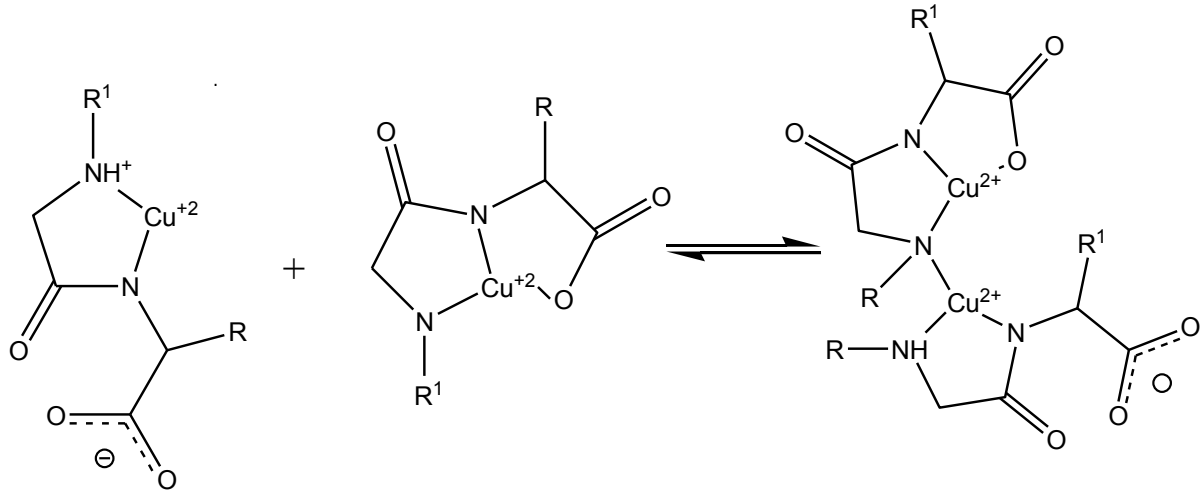

Where R = -H, and -CH_3

And R^1 = -H, 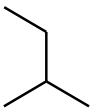 and 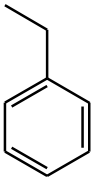

REFERENCES

[1] Mohajane, *M. MSc. Thesis*. University of Cape Town. (**2010**).

[2] Odisitse, S. *PhD Thesis*. University of Cape Town. (**2007**).

[3] Zvimba, J. N. *PhD Thesis*. University of Cape Town. (**2005**).

[4] Popov, K., Ronkkomaki, H. and Lajunen, L. H. *Pure and Applied Chemistry.***2006**, 78(3): 663–675

[5] Zvimba, J. N and Jackson, G. E. *Journal of Inorganic Chemistry*. (**2007**); 101: 1120-1128.

[6] Farkas, E., Kiss ,T. and Kurzak, B. *Journal of the Chemical Society*. (**1990**); 2: 1255–1257

[7] Glasoe, P. K. and Long, F. A. *Journal of Physical Chemistry.* (**1960**); 64:188–190

[8] Wells, A. M., Jelinska, C., Hosszu, L. L. P., Craven, C. J., Clarke, A. R., Collinge, J., Waltho, J. P. and Jackson. G. S. *Biochemical Journal*. (**2006**); 400: 501–510

[9] Martínez, J. M. L., Chattahb, A. K., Montib, G. A., Denisc, M. F. L., Buldaina, G. Y. and Orto, V. C. D. *Journal of Polymer Science*. (**2008**); 49(25): 5482–5489.

[10] Düggeli, M., Bonte, C. and Zelewsky, A. V. *Inorganica Chimica Acta*. (**2005**); 358(1) 41–49

[11] Sokolov, D. F., et al. *Journal of Royal Society of Chemistry*. (**2007**); 7(41): 4693-4700

[12] Zhao, X., Jiang, T., Wang, L., Yang, H., Zhang, S. and Zho, Ping. *Journal of Molecular Structure.* (**2010**); 984(3), 316–325

[13] Harrisi, R. K., Becker, E. D., De Menezes, S. M. C., Goodfellow, R. and Grangers, P. *Pure and Applied Chemistry*. (**2001**); 73(11): 1795–1818.

[14] Billo, E. J. *Inorganic and Nuclear Chemistry Letters.* (**1974**); 10(8): 613-617.

[15] Nuckolls, C et al. *Journal of the American Chemical Society*. (**1998);** 120: 8656-8660

[16] Upstone, S. L. *Encyclopedia of Analytical Chemistry*. (**2000**); 1699–1714

[17] Winkler, F. K. and Dunitz, J. D. *Journal of Molecular Biology*. (**1971**); 59(1): 169–182.

[18] Kitajima, N., Fujisawa, K., Fujimoto, C., Morooka, Y., Hashimoto,S., Kitagawa, T., Toriumi, K., Tatsumi, K. and Nakamura, A. *Journal of American Society.* (**1992**); 114(4): 1277–1291.

[19] Pessoa, J. C.., Correia, I., Kiss, T., Jakisch, T, Castro., M. M. C. A. and Gerades, C. F. G. C. *Journal* of the *Chemical Society*. (2002); 4440-4450.

[20] Jackson, G. E. and Nakani, B. S. *Journal of the Chemical Society*. (**1996**); 24(1): 1373-1377.

[21] Jackson., G. E., Linder, P. W. and Voyé, A. *Journal of the Chemical Society*. (**1996**); 24: 4605-4612.

[22] Nomkoko, T. E., Jackson., G. E., Nakani, B. S. and Hunter, R. *Journal of the Chemical Society* (**2006**); 33: 4029-4038.

[23] http://courses.chem.psu.edu/chem36/Chem36H/36H%20Web%20S%2705/ MolModThoe ry.pdf

[24] A. K. Rappi, A. K., Casewit, C. J., Colwell, K. S., Goddard III, W. A., and Skid, W. M. *Journal of the American Chemical Society*. (**1992**); 114**:** 10024-10039

[25] Turro, N. J. *Modern Molecular Photochemistry*. University Science Books. (**1991**).

[26] Halgren, T. A. *Journal of Computational Chemistry*. (**1996)**; 17(6): 490-519

[27] Brooks, B. R., Bruccoleri, R. E., Olafson, B. D., States, D. J., Swaminathan, S., Karplus, M. *Journal of Computational Chemistry*. (**1983**); 4(2): 187–217

[28] Cornell, W. D, Cieplak, P., Bayly, C. I., Gould, I. R., Merz, K. M. Jr, Ferguson, D. M., Spellmeyer, D. C., Fox, T., Caldwell, J. W. and Kollman, P. A. *Journal of Chemical Society.* (**1995**); 117: 5179–5197.

[29] Hanwell,, M. D., Curtis, D. E., Lonie, D. C., Vandermeersch, T., Zurek, E. and Hutchison, G. R. *Journal of Cheminformatics* (**2012**); 4(17): 1-17

[30] Temitayo, A., Issac, O. and Olugbenga, A. *International Journal of Chemistry.*(**2012**); 4(2): 49-59.

[31] http://avogadro.openmolecules.net/wiki/Main_Page

[32] Salciccioli, M., Yu, W., Barteau, M. A. Chen, J. G. and Vlachos, D. G. *Journal of American Society of Chemistry.* (**2011**); 133(20): 7996–8004

[33] Mera-Adasme, R., Mendizbal, F. Olea-Azar, C. Miranda-Rojas, S. and Fuentealba, P. The *Journal of Physical Chemistry*. (**2011**); 115(17): 4397–4405.

[34] Hancock, R. D. *Pure and Applied Chemistry*. (**1986**); 58(11): 1445-1452.

[35] Colaneri, M. J., Vitali, J. and Peisach, *Journal of Physical Chemistry*. (**2009**); 113(19): 5700–5709.

[36] Koltun, W. L., Fried, M and Gurd F. N. *Journal of the American Chemical Society.* (**1960**); 82: 233-241

[37] Sigel, H. and Martin B. R. *Chemical Reviews*. (**1982**); 82: 385-426

[38] Brookes, G. and Pettit, L. D. *Journal of Chemical Society*. (**1975**); 20: 2106-2112

[39] Odisitse, S., Jackson. G. E., Govender, T., Kruger, H. G. and Singh, A. *Journal of the Royal Society of Chemistry*. (**2007**); 1140-1149.

[40] Wu, S. –P., Du, K. –J. and Sung, Y. –M. *Journal of the Royal Society of Chemistry.* (**2010**); 39: 4363-4368.

[41] Gustianandaa, M., Harisb, P. I., Milburnc, P. J. and Greadya, J. E. *Federation of European Biochemical Societies Letters*. (**2002**); 512: 38-42

6. TISSUE PERMEABILITY AND BIO-DISTRIBUTION STUDIES

6.1 OCTANOL / WATER DISTRIBUTION COEFFICIENTS

6.1.1 INTRODUCTION

Octanol/water distribution coefficient is a technique used to measure the difference in solubility of compounds in two immiscible solvents. The degree of solubility in aqueous phase or in organic phase describes the hydrophilicity or lipophilicity of compounds. This is a powerful tool in estimating the tissue permeability of drugs. By definition, distribution coefficient (log D_{ow}) is described as;

$$\log D_{ow} = \log\left(\frac{[X]_{oct}}{[X]_{aq(i)} + [X]_{aq(n)}}\right) \tag{6.1}$$

Where $[X]_{oct}$ is the concentration of a solute X in octanol, $[X]_{aq(i)}$ is the concentration of a solute X that ionized in water, and $[X]_{aq(n)}$ is the concentration of a neutral (un-ionised) species of X in water.

Log D_{ow} is normally confused with log P_{ow} (partition coefficient). Log P_{ow} is defined as the ratio of un-ionised species between an organic phase and an aqueous phase. Log P_{ow} is expressed as;

$$\log P_{ow(acids)} = \log\left(\frac{[X]_{oct}}{[X]_{aq(n)}}\right) \tag{6.2}$$

The most common method is the shake-flask method [1-4]. A solution of a known concentration of an analyte is made in water. The analyte is then extracted into a known volume of an organic solvent (1-octanol for example). The amount of analyte left in the aqueous phase and the amount that went into the organic phase is measured. Depending on the nature of the analyte, some researchers use ultraviolet-visible spectrophotometry (UV-Vis) to measure the amount of the analyte [5, 6], some use atomic absorption spectroscopy (AAS) [7-9] and some use inductively coupled plasma mass spectrometry (ICP-MS) or inductively coupled atomic emission spectroscopy [10, 11].

Scherrer and Howard [12] have derived equations that correlate distribution coefficients of acids (log $D_{ow(acids)}$), partition coefficients (log $P_{ow(acids)}$), pKa's and pH.

$$\log D_{ow(acids)} = \log P_{ow(acids)} + \log\left(\frac{1}{1+10^{pH-pKa}}\right) \tag{6.3}$$

Where P_{ow} is defined as the ratio of un-ionised species between an organic phase and an aqueous phase. Log P_{ow} is expressed as;

$$\log P_{ow(acids)} = \log\left(\frac{[H]_{oct}}{[H]_{aq(n)}}\right) \tag{6.4}$$

Similarly, log $D_{ow(bases)}$ is expressed as;

$$\log D_{ow(bases)} = \log P_{ow(bases)} + \log\left(\frac{1}{1+10^{pKa-pH}}\right) \tag{6.5}$$

And,

$$\log P_{ow(bases)} = \log\left(\frac{[OH]_{oct}}{[OH]_{aq(n)}}\right) \tag{6.6}$$

If (pH – pKa) >> 1 then Equation 6.5 can be written as;

$$\log D_{ow(acids)} = \log P_{ow(acids)} + pKa - pH \tag{6.7}$$

And if (pKa-pH) >> 1 then,

$$\log D_{ow(bases)} = \log P_{ow(bases)} - pKa + pH \tag{6.8}$$

If the analyte is largely un-ionised in solution then;

$$\log D_{ow} = \log P_{ow} \tag{6.9}$$

For metal complexes the above definition of distribution or partition coefficient is not a really suitable measure of the lipophilicity/hydrophilicity of metal complexes and so log D_{ow} (or log P_{ow}) is defined as [7-9, 13];

$$\log D_{ow} = \log\left(\frac{[Cu(II)]_{oct}}{[Cu(II)]_{aq}}\right) \quad (6.10)$$

Where $[Cu(II)]_{oct}$ is the amount of Cu(II) extracted into the organic phase and [Cu(II)] is the amount of Cu(II) left in the aqueous phase.

6.1.2 EXPERIMENTAL

Standard solutions of Cu(II) were prepared as described [7-9] and calibration curves were constructed. 1:1 Cu(II)/ligand solutions were prepared in distilled/deionised water. Into ten different glass vials, 10 mL aliquots of 1:1 Cu(II)/ligand solutions were dispersed. Each glass vial contained 1:1 Cu(II)/ligands solutions at different pH's (from pH 2 to pH 11). Into the aliquots, 10 mL of 1-octanol (99 %) was added. The octanol had previously been saturated with water. The mixture was shaken for 2 min and left for 5 min for the two phases to separate. From each phase, 8 mL aliquots were withdrawn. Cu(II) in the organic phase was extracted back into an aqueous phase with 8 mL of 5 % HNO_3. 7 mL aliquots were withdrawn from this new aqueous phase (5 % HNO_3). The concentration of copper in each solution was determined using AAS (Varian SpectrAA Model 220FS). The octanol/water distribution coefficients were calculated using Equation 6.9.

6.1.3 RESULTS

6.1.3.1 GLY-GLY / Cu(II)

The results for Cu-GLY-GLY are given in Figure 6.1. Figure 6.1A is the log D_{ow} results and Figure 6.1B is the speciation graph for Cu(II)/GLY-GLY. Complexes of Cu(II) and GLY-GLY are more soluble in water than in 1-octanol since the log D_{ow}'s are negative (Figure 6.1A). The distribution coefficients do not change with pH (from pH 2 to pH 11). The distribution curves (Figure 6.1B) show that mixed species are observed at some pH's; log D_{ow}'s obtained here are therefore not for a single species. All four species (ML, ML_2, MLH_{-1} and MLH_{-2}) have about the same log D_{ow} value. ML_2 was formed in very small amounts due to the limited amount of ligand. Log D_{ow} at pH 7.4 (physiological pH) is -1.4.

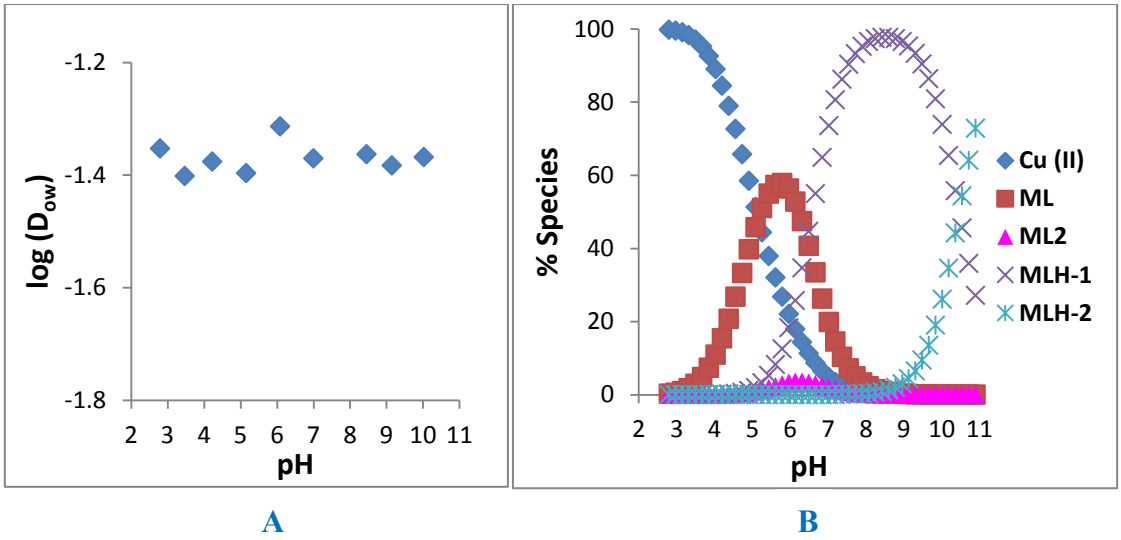

A B

Figure 6.1: A; Log (D_{ow}) as a function of pH for Cu(II)/GLY-GLY titrations B: Speciation graph for 1:1 Cu(II)/GLY-GLY. GLY-GLY total concentration = 0.01004 M.

6.1.3.2 SAR-GLY / Cu(II)

Distribution coefficient curve for Cu(II)/SAR-GLY is given in Figure 6.2A. The solubility in 1-octanol increases with increase in pH (from pH 5 to pH 11). In the pH range 2 – 5, the copper is predominantly present as the free ion or the ML species. Since log D_{ow} is constant in this pH range we conclude that both Cu(II) and ML have a distribution coefficient of -1.5. Log Dow = -1.3 at pH 8.5 where 97 % of the Cu(II) is present as ML_2H_{-1} and so the distribution coefficient is assigned to this value. The most predominant species at pH 7.4 is ML_2H_{-1}.

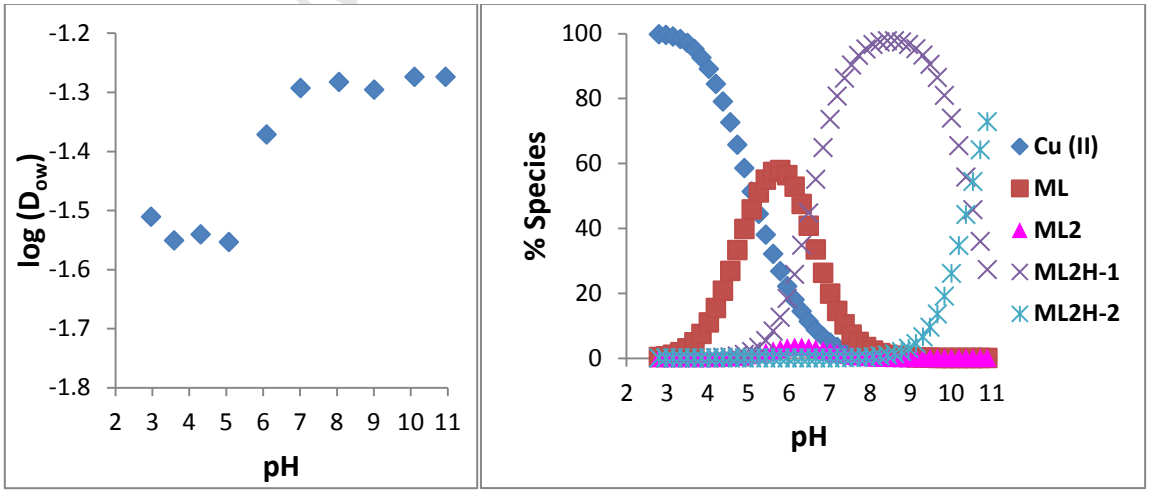

A B

Figure 6.2: A: Log (D_{ow}) as a function of pH for Cu(II)/SAR-GLY titrations B: Speciation graph for 1:1 Cu(II)/SAR-GLY. SAR-GLY total concentration = 0.01133 M.

6.1.3.3 GLY-LEU / Cu(II)

Results for Cu(II)/GLY-LEU are given in Figure 6.3. The solubility in 1-octanol increases from low pH's to high pH's. Log D_{ow} (ML_2H_{-1}) = -0.96. Log Dow = -0.96 at pH 9.1 where 95 % of the Cu(II) is present as ML_2H_{-1} and so the distribution coefficient is assigned to this value. This is the most predominant species at pH 7.4.

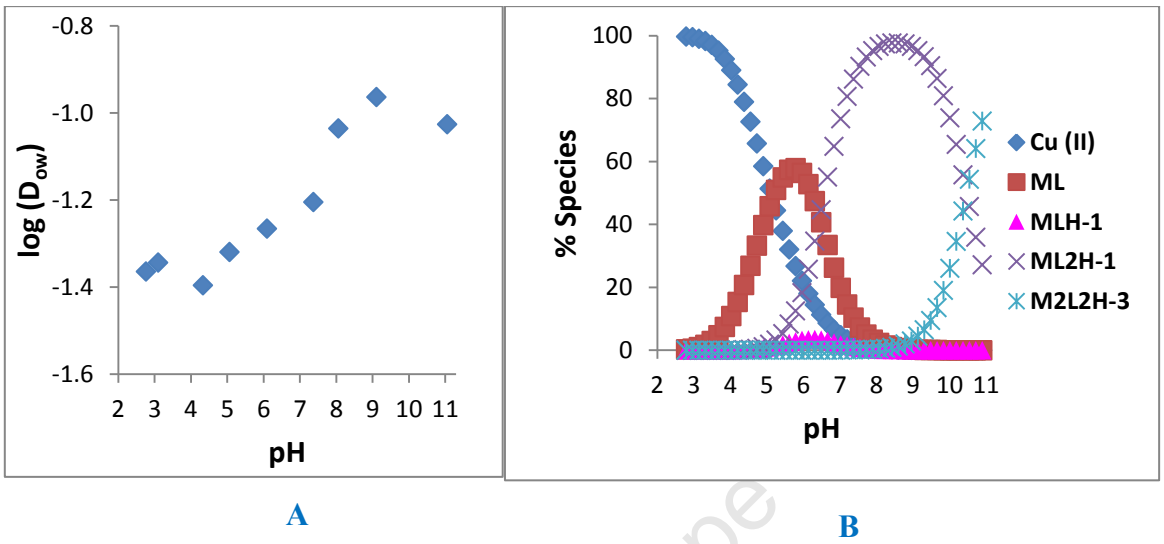

A B

Figure 6.3: A: Log (D_{ow}) as a function of pH for Cu(II)/GLY-LEU titrations B: Speciation graph for 1:1 Cu(II)/GLY-LEU. GLY-LEU total concentration = 0.01021 M.

6.1.3.4 SAR-LEU / Cu(II)

The distribution curves of complexes of Cu(II) and SAR-LEU in water and 1-octanol are given in Figure 6.4A. MLH_{-1} is the most predominant species at pH 7.4. Dow (MLH_{-1}) = -0.80. The log D_{ow} curve drops at pH's above pH 9.3. Cu(II) most likely precipitates out as $Cu(OH)_2$ at high pH's.

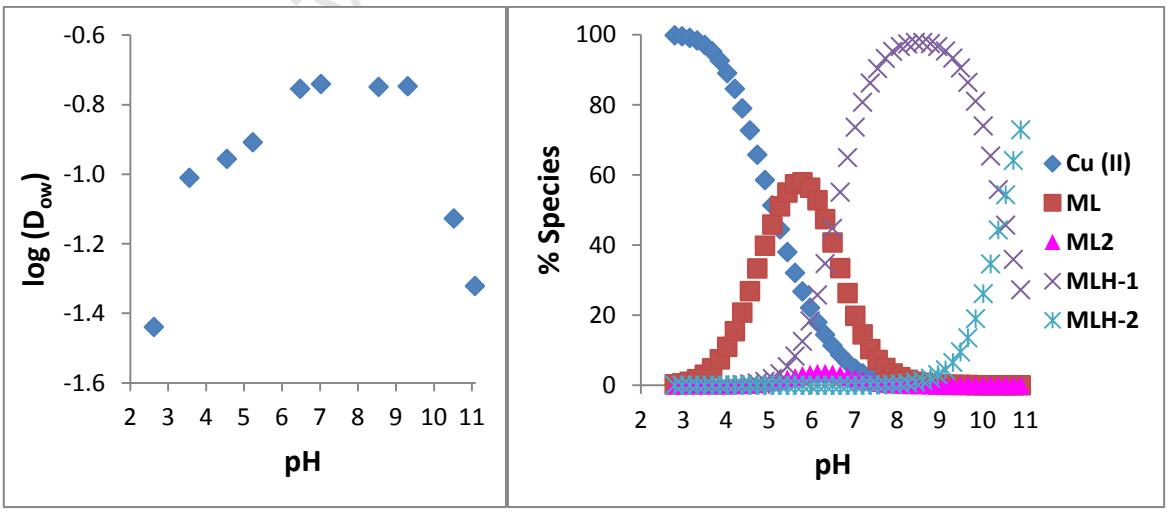

A B

Figure 6.4: A: Log (D_{ow}) as a function of pH for Cu(II)/SAR-LEU titrations B: Speciation graph for 1:1 Cu(II)/SAR-LEU. SAR-LEU total concentration = 0.01334 M.

6.1.3.5 GLY-PHE / Cu(II)

The results for Cu(II)/GLY-PHE are given in Figure 6.5. Log D_{ow} (pH 7.4) = -1.1. ML_2H_{-1} is most predominant at pH 7.4. At this pH there is a mixture of ML, ML_2 and ML_2H_{-1}. Log D_{ow} at pH 8.4 = -1.0 where about 97.8 % of ML_2H_{-1} forms. Log D_{ow} increases to -0.82 at pH 10 where a neutral (net charge = 0) species, ML_2H_{-2} forms.

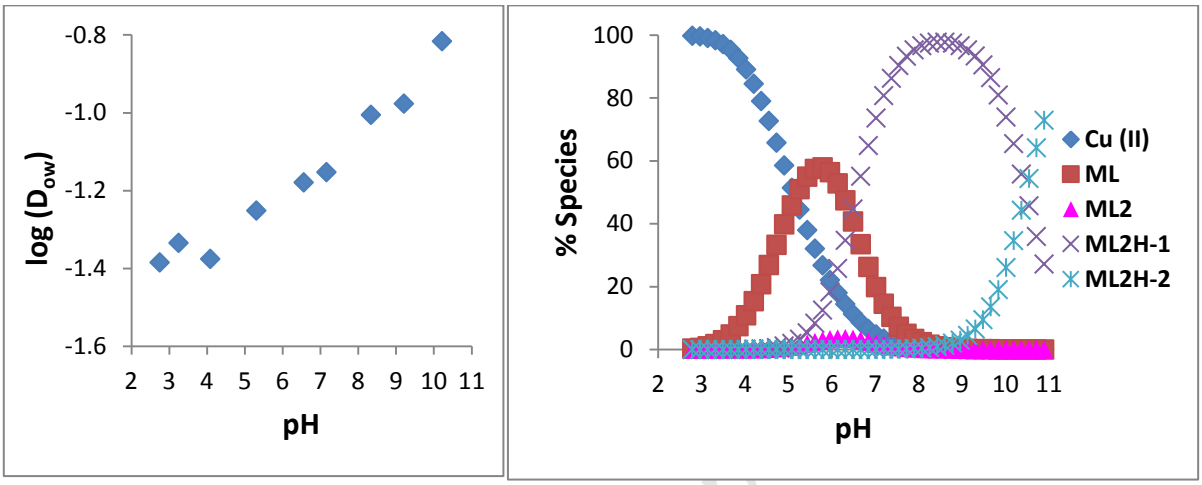

A B

Figure 6.5: A: Log (D_{ow}) as a function of pH for Cu(II)/GLY-PHE titrations B: Speciation graph for 1:1 Cu(II)/GLY-PHE. GLY-PHE total concentration = 0.01082 M.

6.1.3.6 SAR-PHE / Cu(II)

The results for Cu(II)/SAR-PHE are given in Figure 6.6. Log D_{ow} (pH 7.4) = -1.4. At this pH the most predominant species is the MLH_{-1}. Log Dow increases significantly from pH 9.3 to pH 10.9 where a neutral species (net charge = zero) MLH_{-2} forms.

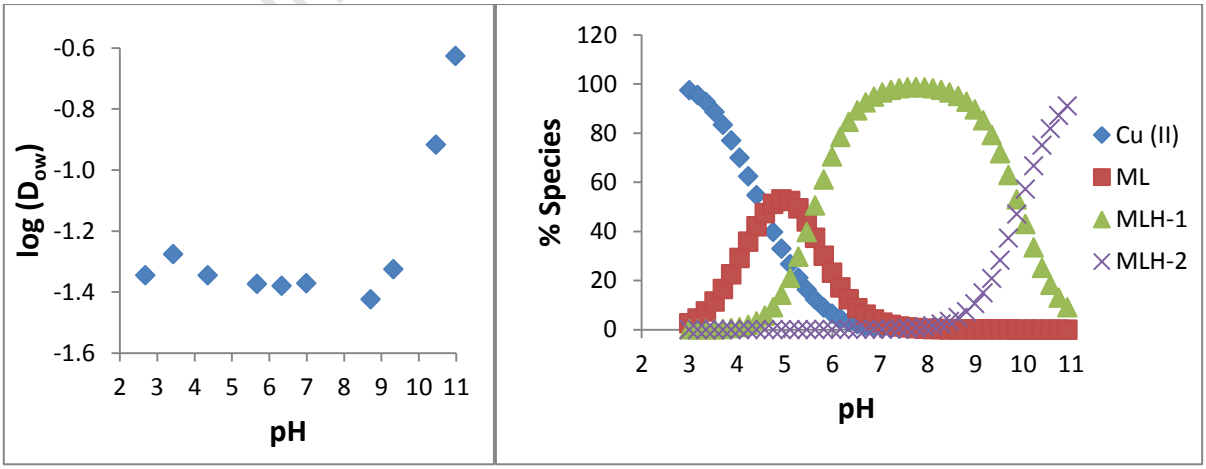

A B

Figure 6.6: A: Log (D_{ow}) as a function of pH for Cu(II)/SAR-PHE titrations B: Speciation graph for 1:1 Cu(II)/SAR-PHE. SAR-PHE total concentration = 0.01031 M.

6.1.3.7 GLY-HIS / Cu(II)

The results for Cu(II)/GLY-HIS are given in Figure 6.7. At pH 2.8, where the most predominant species is Cu(II), log D_{ow} = -1.4; at pH 7.4 where the most predominant species is the ML, log D_{ow} = -1.3; at pH 10.6 where the most predominant species is the MLH_{-1}, log D_{ow} = -1.3 and at pH's above pH 11, where MLH_{-3} is the most predominant species in solution, log D_{ow} = -0.69; at pH 11.

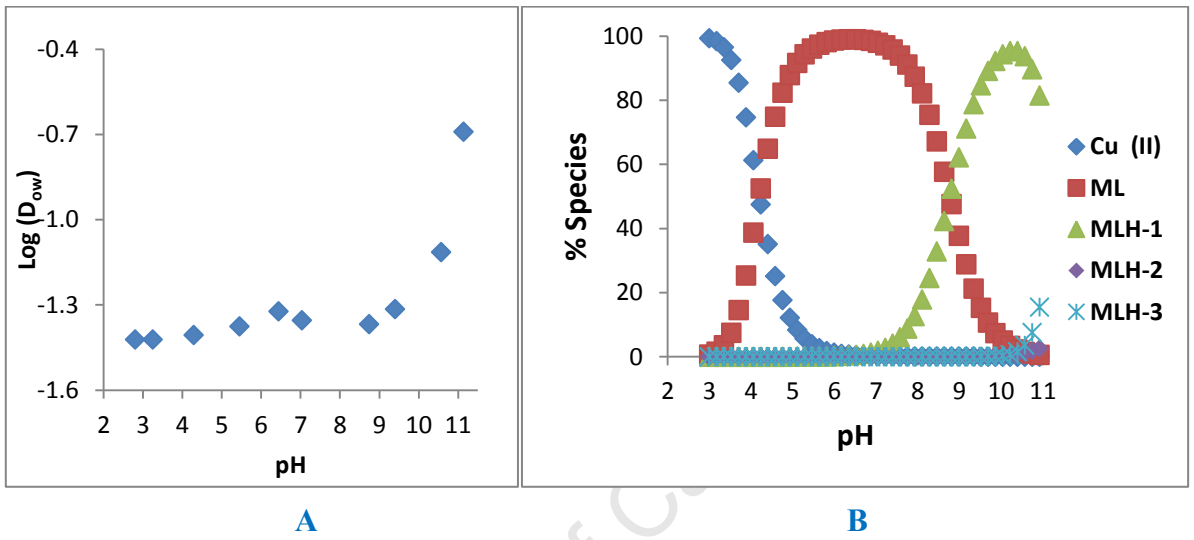

A B

Figure 6.7: A: Log (D_{ow}) as a function of pH for Cu(II)/GLY-HIS titrations B: Speciation graph for 1:1 Cu(II)/GLY-HIS. GLY-HIS total concentration = 0.01128 M.

6.1.5 DISCUSSIONS

The lipophilicity of complex species improves with an increase in pH, except in systems where Cu(II) precipitated out when excess amounts of NaOH were added. Complex species with a net charge of zero are the most lipophilic. The results are consistent with Zhu's work, [14], Jackson and co-workers [15-22, 25], ; complex species with a net charge of zero are more lipophilic than charged complex species. A summary table for log D_{ow}'s for complexes of Cu(II) with different ligands at pH 7.4 is given in Table 6.1.

Table 6.1: Log D_{ow}'s for Cu(II) complexes with different ligands at pH 7.4

Ligand	Species	Log D_{ow} (at pH 7.4)
GLY-GLY	MLH_{-1}	-1.4
SAR-GLY	ML_2H_{-1}	-1.3
GLY-LEU	ML_2H_{-1}	-0.96
SAR-LEU	MLH_{-1}	-0.80
GLY-PHE	ML_2H_{-1}	-1.0
SAR-PHE	MLH_{-1}	-1.4
GLY-HIS	ML	-1.3

The N-methyl substituent on the terminal amine enhances the lipophilicity of the copper complexes at pH 7.4 as anticipated. The lipophilicity of Cu-GLY-GLY and Cu-GLY-LEU is slightly increased but the lipophilicity of Cu-GLY-PHE decreases. However methylated terminal amine of SAR-PHE does increase the lipophilicity at higher pH, with a log D_{ow} (Cu-SAR-PHE) of -0.63 observed at pH 11.

All the complex species showed log D_{ow}'s below zero. Log $D_{ow} < 2.5$ is considered "low lipophilicity", log $D_{ow} > 5$ is considered "high lipophilicity" and log D_{ow} between 2.5 and 5 is considered "intermediate lipophilicity" [24]. Log D_{ow} (complexes) that fall within the range $2.5 <$ log Dow < 5 were aimed for. Zvimba and Jackson [25], however, suggest log D_{ow} of 0.60 is sufficient enough to allow trans-dermal transportation of drugs.

Not much work has been reported in the literature on the lipophilicity of Cu(II)-dipeptide complexes to compare with. However, novel Cu(II)-based anti-inflammatory drugs with log D_{ow}'s above zero at a physiological pH of 7.4 have been reported [18]. This ligand has two N-(2-aminoethyl) picolinamide moieties.

6.2 BLOOD PLASMA MODEL

6.2.1 INTRODUCTION

The chemical analysis of all the metal species present in a complex solution like blood plasma is not really possible. However, assuming the system is at equilibrium a computer model can be used to calculate this [18]. A typical model has a list of ligands and metals that are found at high concentrations in blood plasma. It also has a list of complex species that form between these ligands and metals together with their stability constants. This system can then be solved for the concentration of the individual species. Using this model it is possible to calculate the effect of an exogenous drug as long as its stability constants with the major metal ions, present in the model, are known [19-22]. This process is termed speciation modeling.

6.2.2 DATA HANDLING

Evaluation of Constituent Concentrations in Large Equilibrium Systems (ECCLES) was used to calculate the concentration of test drugs. The ECCLES has a list of species that are found in blood plasma and their cumulative stability constants [19-22]. The cumulative stability constants of species of interest are put into ECCLES and it simulates the speciation of species of interest at physiological pH of 7.4. Competition with other species is taken into account. This includes 7 metal ions and 40 ligands that generate 5000 complexes that are present in blood plasma [18-19]. ECCLES also calculates the plasma mobilizing index (p.m.i) [8-8, 18-19]. By definition;

$$\text{p.m.i} = \frac{\text{total concentration of low molecular weight metal complex species in the presence of a drug}}{\text{total concentration of low molecular weight metal complex species in normal plasma}} \tag{6.10}$$

The greater the ratio, the better the mobilizing capacity in blood plasma [15-22].

6.2.3 RESULTS

6.2.3.1 GLY-GLY

The blood plasma index of as a function of concentration is given in Figure 6.8. Despite the high *in vivo* concentration of Zn(II), GLY-GLY is able to mobilize Cu(II). However, at low ligand concentrations, between 0.001 M and 0.01 M, GLY-GLY mobilises Ni(II) more than Cu(II).

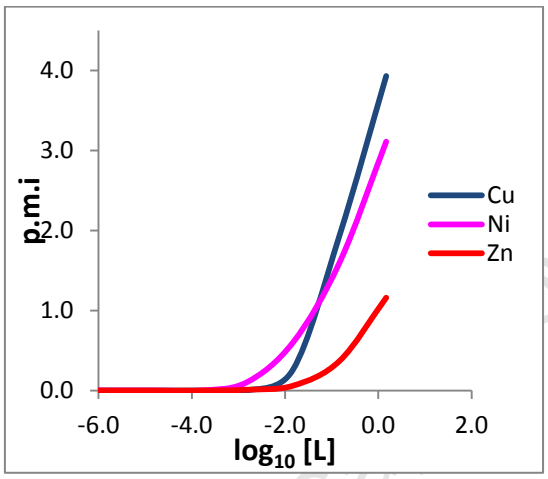

Figure 6.8: p.m.i as a function of $\log_{10}$ [L] for complexes of GLY-GLY and Cu(II), Ni(II) and Zn(II).

6.2.3.2 SAR-GLY

P.m.i curves for SAR-GLY are given in Figure 6.9. SAR-GLY mobilises Cu(II) more than Ni(II) and Zn(II).

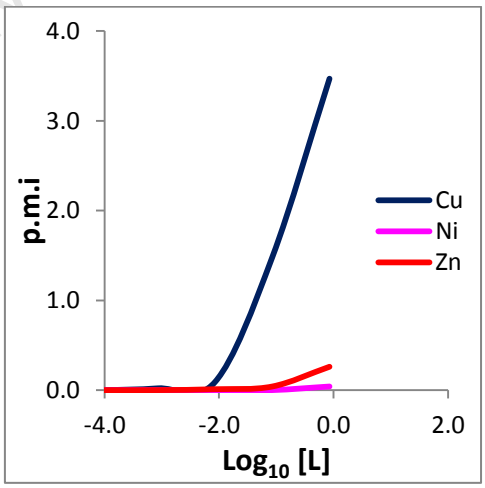

Figure 6.9: p.m.i as a function of $\log_{10}$ [L] for complexes of SAR-GLY and Cu(II), Ni(II) and Zn(II).

6.2.3.3 GLY-LEU

P.m.i curves for GLY-LEU are given in Figure 6.10. GLY-LEU mobilises Ni(II) than Cu(II).

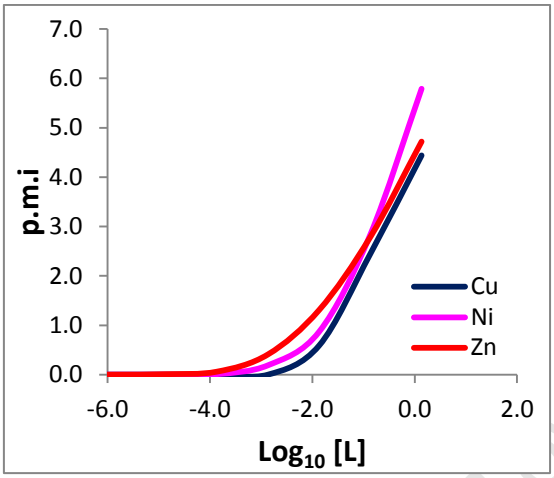

Figure 6.10: p.m.i as a function of $\log_{10}$ [L] for complexes of GLY-LEU and Cu(II), Ni(II) and Zn(II).

6.2.3.4 SAR-LEU

P.m.i curves for SAR-LEU are given in Figure 6.11. SAR-LEU mobilises Cu(II) than Ni(II) and Zn(II) at ligand concentrations above 0.1 M.

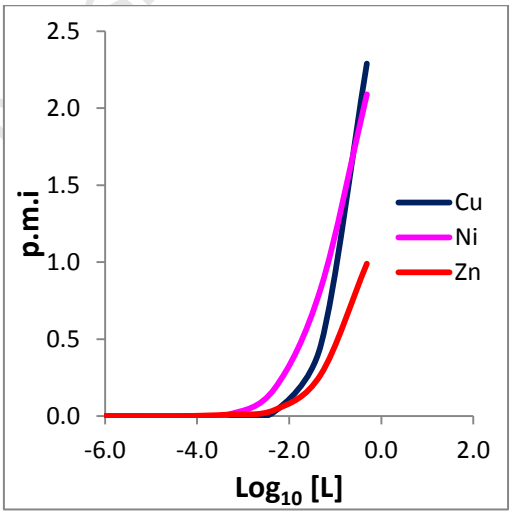

Figure 6.11: p.m.i as a function of $\log_{10}$ [L] for complexes of SAR-LEU and Cu(II), Ni(II) and Zn(II).

6.2.3.5 GLY-PHE

P.m.i curves for GLY-PHE are given in Figure 6.12. GLY-PHE mobilises Cu(II) than Ni(II) and Zn(II).

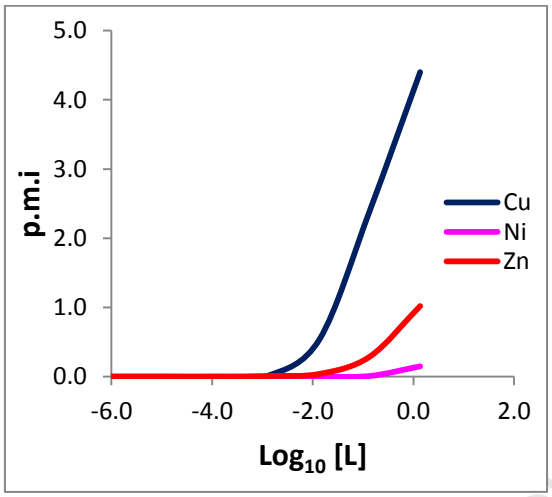

Figure 6.12: p.m.i as a function of $\log_{10}$ [L] for complexes of GLY-PHE and Cu(II), Ni(II) and Zn(II).

6.2.3.6 SAR-PHE

P.m.i curve for SAR-PHE is given in Figure 6.13. Cu(II) is mobilized at [SAR-PHE] above 0.01 M, Ni(II) is mobilized from lower ligand concentrations ([SAR-PHE] = 0.001 M). Zn(II) is mobilised at ligand concentrations about 1 M.

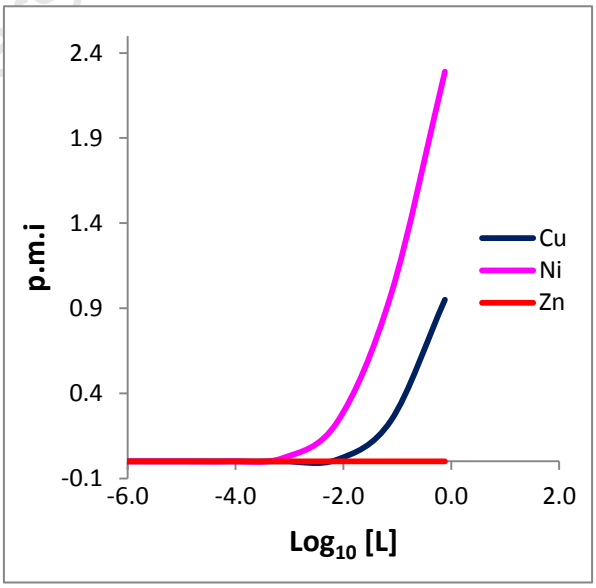

Figure 6.13: p.m.i as a function of $\log_{10}$ [L] for complexes of SAR-PHE and Cu(II), Ni(II) and Zn(II).

6.2.3.7 GLY-HIS

P.m.i's for complexes of GLY-HIS with Cu(II), Ni(II) and Zn(II) have been reported before [22]. GLY-HIS mobilized Ni(II) than it mobilizing Cu(II) in blood plasma.

6.2.4 DISCUSSIONS

Table 6.2 shows p.m.i values of different peptides with copper as a function -$\log_{10}$ peptide concentration. A graphic representation is given in Figure 6.2. GLY-LEU and GLY-PHE have the highest ability to mobilise copper *in vivo* from concentrations as low as 0.001M. Novel Cu(II)-based anti-inflammatory drugs with better copper mobilizing capacity have been reported [7, 20, 23, 25].

Table 6.2: Cu(II) mobilizing capacity of dipeptides at different ligand concentrations.

$\log_{10}$ [Ligand]	p.m.i GLY-GLY	p.m.i SAR-GLY	p.m.i GLY-LEU	p.m.i SAR-LEU	p.m.i GLY-PHE	p.m.i SAR-PHE	p.m.i GLY-HIS
-3.0	0	0	0	0	0	0	0
-2.0	0.15	0.15	0.46	0.06	0.40	0.01	0.02
-1.0	1.62	1.62	2.18	0.90	2.12	0.26	0.80
0	3.74	3.74	4.18	2.88	4.14	1.10	1.95

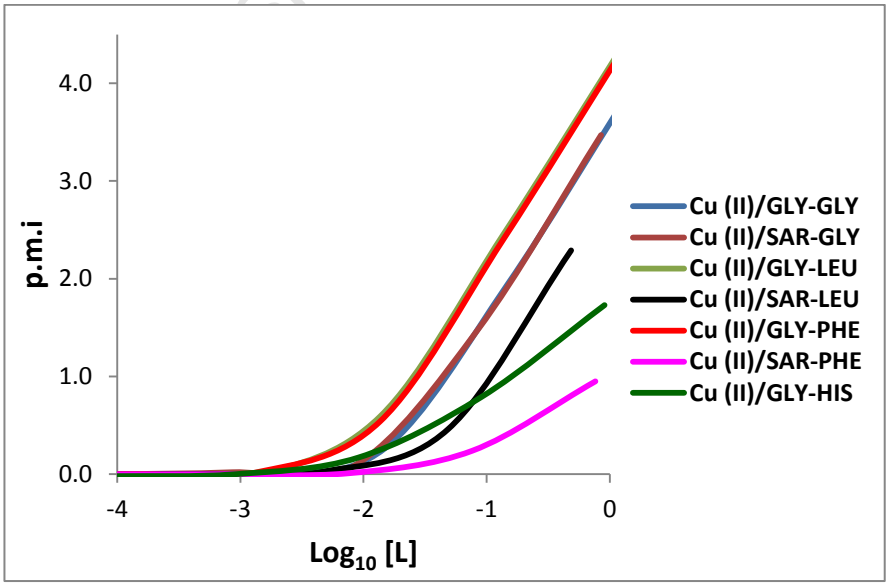

Figure 6.14: p.m.i as a function of $\log_{10}$ [L] for complexes of Cu(II) and GLY-GLY, SAR-GLY, GLY-LEU, SAR-LEU, GLY-PHE, SAR-PHE and GLY-HIS.

6.2 CONCLUSIONS

GLY-LEU and GLY-PHE are better Cu(II) chelaters *in vivo* than other dipeptides covered in this study. GLY-GLY and SAR-GLY have a better Cu(II) mobilizing capacity than SAR-LEU, SAR-PHE and GLY-HIS, however, their efficiency is only observed when the ligand concentration is about 0.01 M which is unrealistically high. GLY-LEU and GLY-PHE also form lipophilic complexes with Cu(II) and the physiological pH 7.4.

RERERENCES

[1] Takács-Novák, K. and Avdeel, A. *Journal of Pharmaceutical and Biomedical Analysis*. (**1996**); 14(11): 1405–1413.

[2] Teijeiroa, S.A., Moronia, G. N., Moturaa, M. I. and Briñónb, M. C. *Journal of Liquid Chromatography & Related Technologies*. (**2000**); 23(6): 855-872

[3] Harnisch, M., Möckel, H. J. and Schulze, G. *Journal of Chromatography A*. (**1983**); 282: 315–332.

[4] Glomme1, A., März1, J and Dressman, J. B. *Journal of Pharmaceutical Sciences*. (**2005**); 94(1); 1–16.

[5]. Araujo, M. C. U., Saldanha, T. C. B.,. Galva˜o, R. K. H. Yoneyama, T., Chame, H. C. and Visani, V. *Journal of Chemometrics and Intelligent Laboratory Systems*., (**2001**); 57(2): 65-146.

[6] Filho, H. A. D., Souza, E. S. O. N., Visani, V., Barros, S. R. R. C., Saldanha, T. C. B., Ara ujo, M. C. U. and Galva˜o, R. K. H. *Journal of the Brazilian Chemical Society*. (**2005**); 16: 58-62.

[7] Odisitse, O., Jackson, G. E., Govender, T., Krugerb, H. G. and Singhb, A. *Journal of the Royal Society of Chemistry*. (**2007**): 1140–1149.

[8] Odisitse, S. *PhD Thesis*. University of Cape Town. (**2003**).

[9] Zvimba, J. N. *PhD Thesis*. University of Cape Town. (**2005**).

[10] Enyedy, E. A., Hollender, D. and Kiss, T. *Journal of Pharmaceutical and Biomedical Analysis.* (**2011**); 54(5): 1073-1081

[11] Tsopelas, F. N., Ochsenku-Petropoulou, M. T., Tsantili-Kakoulidou, A. and Ochsenkuhn, K. –M. *Analytical and Bioanalytical Chemistry*. (**2005**); 381: 420–426

[12] Scherrer, R.A. and Howard, S. M. *Journal of Medicinal Chemistry*. (**1977**); 20(1):53–58.

[13] Mokalane, K. *MSc. Thesis*. University of Cape Town. (**2011**).

[14] Zhu, B. *Chemical Research in Toxicology*. (**2001**); 14: 222-227

[15] Zeevaart, J. R., Jarvis, N. V., Louw, W. K. and Jackson, G. E. *Journal of Inorganic*

Biochemistry. (**2001**); 83(1): 57-65.

[16] Jackson. G. E., Linder, P. W. and Voyé, A. *Journal of the Chemical Society*. (**1996**); 460-4612.

[17] Jackson, G. E. and Kelly, M. J. *Journal of the Chemical Society*. (**1990**); 1889-1893.

[18] Zvimba, J. N. and Jackson, G. E. *Journal of Inorganic Chemistry*. (**2007**); 1120-1128.

[19] Zeevaart, J. R., Jarvis, N. V. Louw, W. K. A., Jackson, G. E., Cukrowski, I and Mouton, C. J. *Journal of Inorganic Biochemistry*. (**1999**); 73: 265-272.

[20] Zvimba, J. N. and Jackson, G. E. *Journal of Inorganic Biochemistry*. (**2006**); 148-158.

[21] Zeevaart, J. R., Jansen, D. R., Botelho, M. F., Abrunhosa, A., Gomes. C., Metello, L., Kolar, Z. I., Krijger, G. C., Louw, W. K. and Dormehl, I. C. *Journal of Inorganic Biochemistry*. (**2004**); 98(9): 1521-1530.

[22] Mohajane, M. *MSc. Thesis*. University of Cape Town. (**2010**).

[23] Jackson, G. E. and Nakani, B. S. *Journal of the Chemical Society*. (**1996**); 1373-1377

[24] Gertz, M., Kilford, P. J., Houston, J. B. and Galein, A. *Drug Metabolism and Disposition.* (**2008**); 36(3): 535-542

[25] Zvimba, J. N. and Jackson, G. E. *Polyhedron*. (**2007**); 26(12): 2395-2404.

7. GENERAL DISCUSSIONS, CONCLUSIONS AND RECOMMENDATIONS

7.1 DISCUSSIONS

The main aim of this study was to develop drugs that will alleviate the inflammation associated with rheumatoid arthritis. These drugs should be dermally absorbable, copper complex that will elevate the bioavailable pool of copper *in vivo* without changing the composition of Ca(II), Ni(II) and Zn(II) *in vivo*. Four glycine dipeptides (GLY-GLY. GLY-LEU. GLY-PHE and GLY-HIS) and four sarcosine dipeptides (SAR-GLY, SAR-LEU, SAR-PHE and SAR-HIS) were developed. N-methylated compounds have been reported to be more lipophilic than their non-methylated analogues [1-3]. The N-methyl substituent however should not change the thermodynamic stability of complexes. Due to solubility problems studies on SAR-HIS could not be done.

Glass electrode potentiometry and isothermal titration calorimetry were used to study the thermodynamics of Cu-peptide complexes at 25 ^{0}C and 0.15 M ionic strength (NaCl). The methyl group does not compromise the thermodynamic stability of complexes. The stability of complexes however depends on the second amino acid residue of the peptide. ML (Cu-GLY-HIS) has the highest log K value. The side ring of GLY-HIS has two N-donor atoms (pKa = 6.6) [4-10]. Cu(II) coordinates to the N_{amine}, the O_{amide}, $N_{imidazole}$ and O_{water} when ML (Cu-GLY-HIS) forms [4, 7-10]. Cu-N bond is stronger than Cu-O bond, therefore ML (Cu-GLY-HIS) is more stable than ML (Cu-peptide covered in this study). Cu(II) coordinates to N_{amine}, the O_{amide}, $O_{carboxylate}$ and O_{water} when ML (Cu-peptide) forms (Chapter 5).

The lipophilicity of complexes was determined using octanol/water distribution coefficients. The N-methyl substituent does enhance the lipophilicity of peptide complexes. The second amino acid residue also affects the lipophilicity of the complexes. Of interest is the lipophilicity of the complex species that forms at physiological pH 7.4. The complexes of GLY-LEU and SAR-LEU with copper have the highest log D_{ow} values at this pH (-0.96 log units for Cu-GLY-LEU and -0.80 for Cu-SAR-LEU). ML_2H_{-1} is the most predominant species at pH 7.4 in a Cu-GLY-LEU system, and MLH_{-1} is the most predominant species at pH 7.4 in a Cu-SAR-LEU system. The proposed structures are given in Figure 7.1.

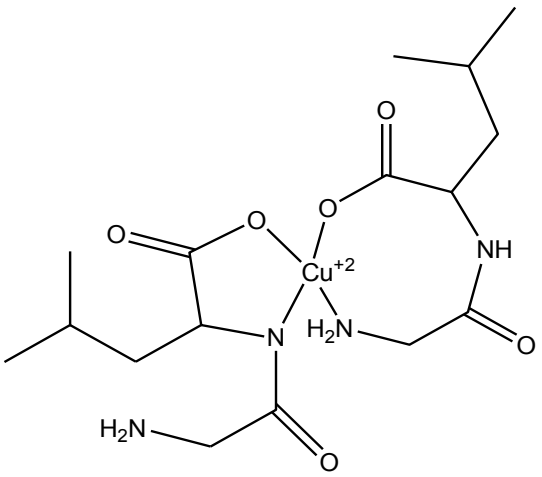

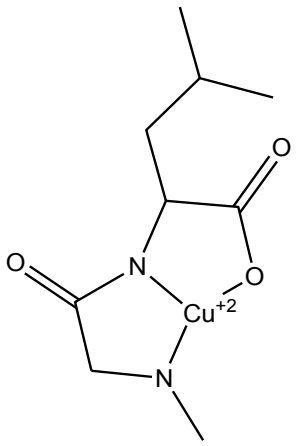

ML_2H_{-1}: D_{ow} = -0.96 **MLH_{-1}: D_{ow} = -0.80**

Figure 7.1: Structures of complex species of the highest log D_{ow} values.

Evaluation of Constituent Concentrations in Large Equilibrium Systems (ECCLES) was used determine the Cu(II)-mobilising capacity of peptides *in vivo* in the presence of other metal-ligand species that are found in high concentrations in blood plasma. Of interest are the three metal ions Ca(II), Ni(II) and Zn(II) which are competitors with Cu(II) in blood plasma. SAR-GLY and GLY-PHE mobilise Cu(II) more than Ca(II), Ni(II) and Zn(II) from very low concentrations. GLY-LEU and GLY-GLY also have a high mobilizing capacity but they mobilise Ni(II) and Zn(II) more at low ligand concentrations. A summary graph is given in Figure 7.2.

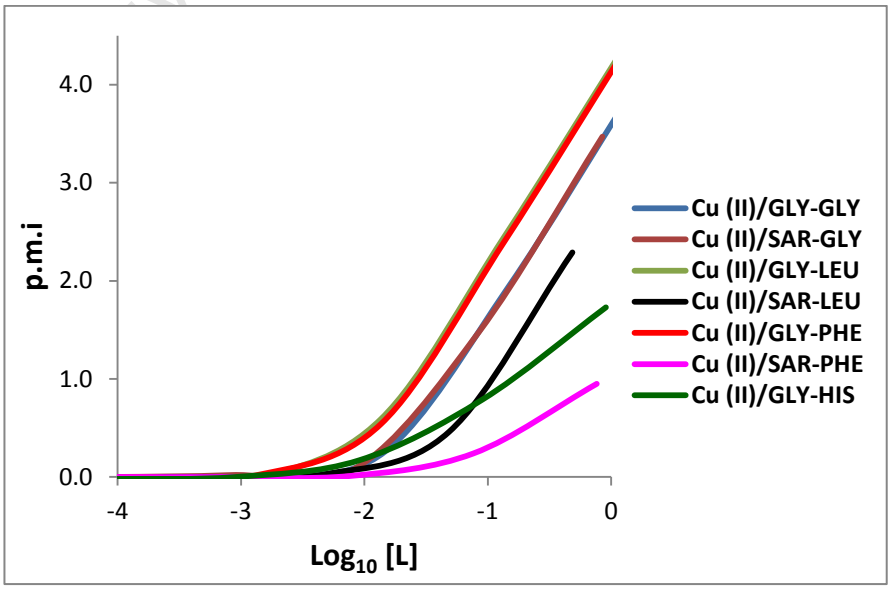

Figure 7.2: p.m.i as a function of $\log_{10}$ [L] for complexes of Cu (II) and GLY-GLY, SAR-GLY, GLY-LEU, SAR-LEU, GLY-PHE, SAR-PHE and GLY-HIS.

7.2 CONCLUSIONS AND RECOMMENDATIONS

The methylated terminal amines increase the lipophilicity of copper complexes without compromising their thermodynamic stability. However, log D_{ow}'s (Cu-peptides) are all negative and thus they are all very hydrophilic. Log $D_{ow} < 2.5$ is considered "low lipophilicity", log $D_{ow} > 5$ is considered "high lipophilicity" and log D_{ow} between 2.5 and 5 is considered "intermediate lipophilicity" [18]. Log D_{ow} (complexes) that fall within the range $2.5 < \log Dow < 5$ were aimed for. Since GLY-LEU and GLY-PHE have the highest mobilising capacity than all the other peptides. It will be interesting to see if a series of tripeptides that have a glycine residue, a leucine and a phenylalanine residue will compare with a series of tripeptides that have a sarcosine residue, a leucine and a phenylalanine residue. Proposed tripeptides are given in Figure 7.3.

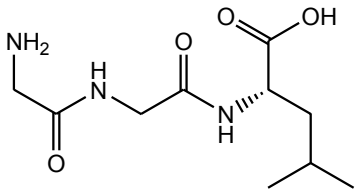

GLY-GLY-LEU

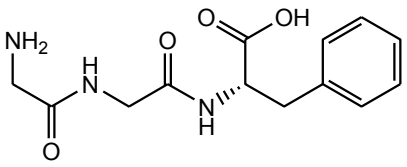

GLY-GLY-PHE

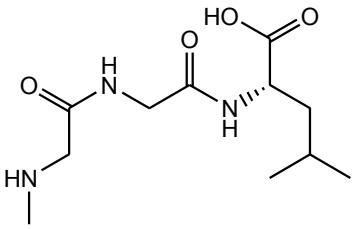

SAR-GLY-LEU

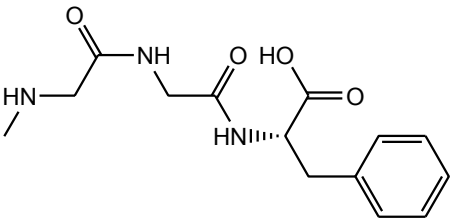

SAR-GLY-PHE

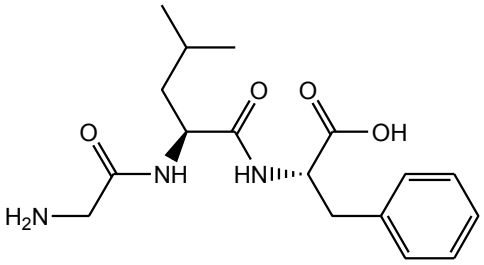

GLY-PHE-LEU

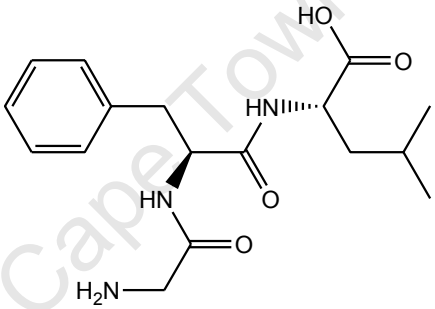

GLY-LEU-PHE

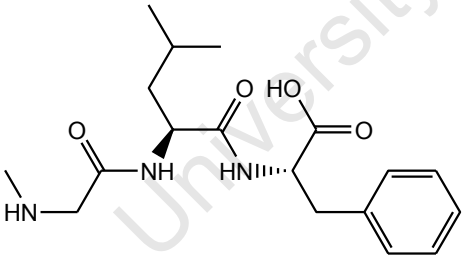

SAR-PHE-LEU

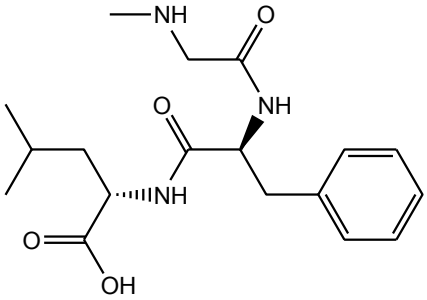

SAR-LEU-PHE

Figure 7.3: Proposed tripeptides.

REFERENCES

[1] Biron, E. et al. *Angewandte Chemie International Edition*. (**2008**); 47(14): 2595–2599.

[2] Hansch, C. *Drug Metabolism Reviews*. (**1972**); 1(1): 1-13

[3] Dechantsreiter, M. A., Planker, E., Mathä, B., Lohof, E., Hölzemann, G., Jonczyk, A., Goodman, S. L. and Kessler, H. *Journal of Medicinal Chemistry*. (**1999**); 42(16): 3033–3040

[4] Mohajane, M. *MSc. Thesis*. University of Cape Town. (**2010**).

[5] Smith, R. M. and Martell, A. E. NIST Critically Selected Stability Constants of Metal Complexes Database. (**1994**). Version 8.0 for Windows.

[6] Murray, K and May, M. P. Equilibrium Simulations for Titration Analysis. Version 3.0 for Windows. (**1989**).

[7] Surdy,P., Rubini, P., Buza´s, N., Henry, B., Pellerito, L. and Gajda, T. *Inorganic Chemistry*. (**1999**); 38: 346-352.

[8] Sóvágó, I., Farkas, E. and Gergely, A. *Journal of the Chemical Society*. (**1982**); 2159-2163

[9] Szabó-Plánkaa, T., Nagya, N., Rockenbauerb, A and Koreczb, L. *Polyhedron*. (**2000**); 19(19): 2049–2057

[10] Aiba, H., Yokoyama, A, and Takana, H. *Bulletin of the Chemical Society of Japan*. (**1974**); 47(6): 1437-1441.